Structural and Functional Studies on Vitamin B1-Dependent, Human and Bacterial Transketolases

Dissertation
for the award of the degree
"Doctor rerum naturalium"
of the Georg-August-Universität Göttingen

submitted by
Stefan Lüdtke
born in Haldensleben

Göttingen 2012

Members of the Thesis Committee:

Prof. Dr. Kai Tittmann (Reviewer)

Department of Bioanalytics
Albrecht-von-Haller-Institut für Pflanzenwissenschaften
Georg-August-Universität Göttingen

Prof. Dr. Ralf Ficner (Reviewer)

Department of Molecular and Structural Biology
Institut für Mikrobiologie und Genetik
Georg-August-Universität Göttingen

Prof. Dr. Christian Griesinger

Department of NMR based Structural Biology
Max Planck Institute for Biophysical Chemistry
(Karl Friedrich Bonhoeffer Institute)
Göttingen

Herewith I declare, that I prepared this thesis “Structural and Functional Studies on Vitamin B1-Dependent, Human and Bacterial Transketolases” independently and with no other sources and aids than quoted.

Göttingen, 12.04.2012

Stefan Lüdtke

Table of Content

List of Figures

Abbreviations

1desR5P	D-1desoxy ribose 5-phosphate
1desX5P	D-1desoxy xylulose 5-phosphate
3deazaThDP	1,2 dihydroxyethyl thiamin diphosphate
A_{260} or A_{280}	absorption at 260 or 280 nm
Ala	alanine
Amp	ampicillin
app	apparent
Apo	apoenzyme, enzyme without cofactor
Arg	arginine
Asn	asparagine
Asp	asparaginic acid
CD	circular dichroism
Da	dalton
DHEThDP	dihydroxyethyl thiamin diphosphate
DFT	density functional theory
ε	molar extinction coefficiant
E4P	D-erythrose 4-phosphate
E. coli	*escherichia coli*
*Ec*TK	transketolase A from *escherichia coli*
EDTA	ethylendiamintetraacetate
Θ	ellipticity
F6P	D-fructose 6-phosphate
GAP	D-glyceraldehyde 3-phosphate
G3P-DH	glycerol 3-phosphate dehydrogenase
GA	glycol aldehyde
Gln	glutamine
Glu	glutamic acid
Gly	glycine
His	histidine
HL-ThDP	hydroxylactyl thiamin diphosphate
HPA	β-hydroxypyruvate
*h*TK	human transketolase
Ile	isoleucine
IPTG	isopropyl-β-D-thiogalactoside
ITC	isothermal titration calorimetry
k	rate constant
K_D	dissociation constant
K	equilibrium constant
λ	wavelength
LB media	Luria-Bertani-Media
Leu	leucine
Lys	lysine

N3ThDP	N3´-pyridyl thiamin diphosphate
NADH/NAD^+	nicotinamide adenine dinucleotide (reduced form/oxidized form)
NMR	nuclear magnetic resonance
obs	observed
OD	optical density
pH	negative logarythm of H^+ concentration
Phe	phenylalanine
PEG	polyethylene glycol
PPP	pentose phosphate pathway
Pro	proline
PMSF	phenylmethylsulfonylfluorid
R5P	D-ribose 5-phosphate
Rib5P	D-ribitol 5-phosphate
rpm	revolutions per minute
S7P	D-sedoheptulose 7-phosphate
Ser	serine
SDS-PAGE	sodium dodecylsulfate polyacrylamide gelelektrophorese
SLS	swiss light source
σ	estimated standard error, standard deviation or standard uncertainty
σ_A	Sigma-A, variance-term accounting for error and incompleteness in structure models
TCA	trichloro acetic acid
ThDP	thiamin diphosphate
TIM	triosephosphate isomerase
Thr	threonine
Tris	tris (hydroxymethyl)-aminomethan
Trp	tryptophane
Tyr	tyrosine
U	unit
UV/Vis	ultraviolet and visible fraction of electromagnetic radiation
Val	valine
X5P	D-xylulose 5-phosphate

Acknowledgements

I would like to thank *Prof. Dr. Kai Tittmann* for the supervision of this thesis and for contribution of numerous valuable ideas, discussions and inspirations. I would also like to thank him for NMR data collection and for carrying out the quench-flow experiments. Furthermore I would like to thank him for teaching me fast kinetic methods.

I would like to thank *Prof. Dr. Ralf Ficner* for external co-supervision of this thesis and for taking part in the thesis committees. I would also like to thank him for the generous ability to use the instruments and facilities of his department.

I would like to thank *Prof. Dr. Christian Griesinger* for external co-supervision of this thesis, and for taking part in the thesis committees and for the possibility to perform NMR data collection in his department.

Furthermore I am grateful to *Jun. Prof. Dr. Heinz Neumann*, *Prof. Dr. Jörg Stülke* and *Prof. Dr. Holger Stark* for being members of my extended thesis committee.

I am deeply thankful to *Dr. Piotr Neumann* for his continuous support and teaching in theoretical and practical aspects of crystallography. Especially, I would like to thank him for carrying out the majority of the x-ray data processing work and refinement with Shelx. I would also like to thank him for suggestions and comments on structure refinement.

I extend my gratitude to *Prof. Dr. Christian Ducho* and *Anatol Spork* for the synthesis of R5P analogues and discussions about sugar chemistry in general.

I am thankful to *PD Dr. Ralph Golbik* and *Prof. Finian Leeper* for the synthesis of cofactor analogues.

I would like to thank all former and present members of the bioanalytics department for their help in the lab and the great working atmosphere. Especially previous work of *Ann-Kristin Diederich*, *Lars Mitschke* and *Dr. Peter Asztalos* contributed to the success of this thesis. I am grateful to *Dr. Danilo Meyer* for discussion on kinetic and thermodynamic problems. I would also like to thank *Dr. Kathrin Schröder-Tittmann* for cloning of human transketolase and support with the biofermenter. Thanks to my labmates *Dr. Anja Lehwess-Litzman, Stefan Schneider*, *Astrid Sitte*, *Alexander Piontek* for joining me at various synchrotron trips. I am thankful to *Cindy Wechsler* and *Elisabeth Koers* for carrying out NMR data collection.

Thanks to the Macromolecular Crystallography team at the Helmhotz Zentrum Berlin (HZB) for the outstanding technical support during x-ray data collection at HZB.

Thanks to the members of the Department of Molecular and Structural Biology for their help after the initial phase of our removal to Göttingen. In particular I would like to thank *Stephanie Schell, Daniel Weinrich* and *Dr. Achim Dickmanns*.

Thanks to all members of the Department of Plant Biochemistry for their help in setting up the laboratory. In particular I would like to thank *Dr. Florian Brodhun*, *Dr. Ellen Hornung*, *Dr. Kirstin Feussner*, *Pia Meyer*, *Gerd Mad*er and *Sabine Freitag*. Thanks to *Dr. Cornelia Herrfurth* and *Dr. Katharina Michels* for mass-spectrometric analysis of sugars and cofactors and *Prof. Dr. Ivo Feussner* for the generous ability to use the instruments of his department.

Thanks to *Dr. Michael John* for the generous ability to use the NMR-spectrometer of his department.

Thanks to *Dr. Christoph Parthier* for his help and all the good advice still in Halle.

Thanks to *Dr. Karin Kühnel* for support during x-ray data collection at SLS.

I am indebted to Göttingen Graduate School for Neuroscience, Biophysics and Molecular Bioscience (GGNB) office, particularly to *Kirstin Pöhlker*, *Christina Bach*, *Christin Fischer*, *Dr. Steffen Burkhard* and *Prof. Reinhard Jahn* for the organization of the graduate school and for the assistance through the administrative work that I went through. I am additional deeply thankful to the GGNB as recipient of junior group (recipient Prof. Kai Tittmann) and bridging stipends that enabled me to finish this thesis.

I like to acknowledge the Fond der Chemischen Industry as a recipient of a two-year Chemie-Fond Stipendium.

Thanks to *Dr. Piotr Neumann*, *Dr. Danilo Meyer*, *Dr. Florian Brodhun, Astrid Sitte* and *Stephanie Schell* for their friendship as well as *Piotr, Danilo, Astrid* and *Florian* for feedback and corrections of this manuscript.

Thanks to my family for their support and good advice.

And thanks to *Doris* for her love and support.

1. Introduction

1.1. Thiamin and its Biologically Active Derivatives

Thiamin (vitamin B1) and its derivatives are ubiquitously found and serve in numerous biological functions (Bettendorff and Wins, 2009). The triple ester (thiamin triphosphate) and the conjugate between triple ester and adenosin (adenosin thiamin triphosphate) could be shown to operate as signal molecules under amino acid- and carbon starvation conditions in prokaryotes (Bettendorff et al., 2007). These compounds were further shown to be continously formed and hydrolyzed in many multicellular organism and even in humans (Bettendorff, 1994 a; Bettendorff et al., 1994 b). However, a function as signal molecules in eukaryotes could yet not been presented. The by far most important thiamin derivative is the diphosphate ester thiamin diphosphate (ThDP, Fig. 1), that functions as organic catalyst in collaboration with the protein component of ThDP-dependent enzymes. Thiamin is neither synthesized nor stored to significant amounts in most vertebrates and thus required in their diets. In case of malnutrition humans can suffer from thiamin deficiency diseases beri-beri and wernicke-korsakoff syndrome (Zahr et al., 2011), which are both characterized by neurological complications, atrophy of limbs and edema (Voet, 2008).

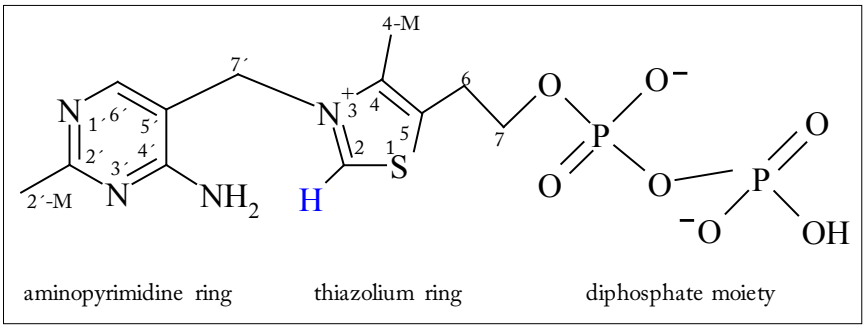

Fig. 1: Structure and nomenclature of thiamin diphosphate. The six-membered aminopyrimidine ring, the five-membered thiazolium ring and the diphosphate (or pyrophosphate) moiety are labeled. The diphosphate moiety is often called "anchor" originating from its function to facilitate binding to the individual ThDP-dependent enzyme. The acidic C2-H is shown in blue.

1.2. Reactivity of ThDP

The cofactor ThDP is supposed to be an early invention of evolution (Frank et al., 2007). This is not only explained by its ubiquitous distribution but also highlighted as it is required for central reactions of anabolic and catabolic metabolism. As an organic catalyst ThDP actively assists in forming and breaking bonds between carbon and sulfur, hydrogen, oxygen, nitrogen and, chemically demanding,

breaking and forming carbon-carbon bonds. ThDP-dependent enzymes exist in a big number and are involved in multiple metabolic pathways like the metabolism of amino acids and sugars or the biosynthesis of several vitamins, antibiotics and isoprenoids. Research focussing on this cofactor started very early and in the 1950s Breslow (Breslow, 1957) finally succeeded to indentify the reactive center. Breslow found that the C2 atom of ThDP, which must be activated by deprotonation to form a carbanion- or carbene state, is the nucleophile that performs catalysis (Fig. 2).

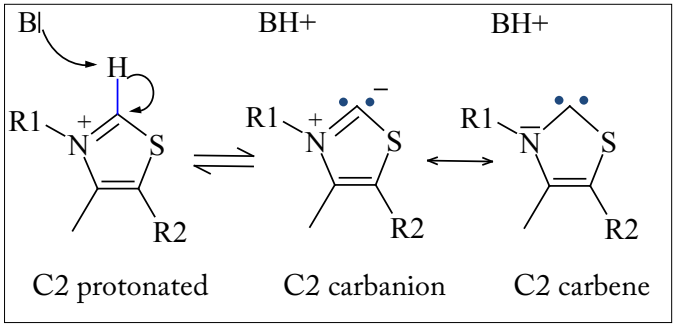

Fig. 2: Formation of the ThDP nucleophile after C2 deprotonation. Proton abstraction from C2 by a Brønsted base yields the catalytic nucleophile a carbanion (zwitterion) in resonance with a carbene structure (R1= aminopyrimidine ring, R2 = ethyldiphosphate).

Remarkably, ThDP on its own is a poor catalyst under physical conditions. This phenomenon mainly originates from its low C2-acidity (pK_A = 17-19)(Washabaugh and Jencks, 1988) and consequently the very small amount of reactive nucleophilic form under such conditions. However, binding of ThDP to the protein component of a ThDP-dependent enzyme was shown to dramatically accelerate C2-deprotonation (Hübner et al., 1998; Kern et al., 1997). While all yet described ThDP-dependent enzymes are considered to highly accelerate C2-deprotonation, stabilization of a significant amount of unprotonated species (Crosby and Lienhard, 1970) was excluded experimentally (Kern et al., 1997). However, the protonation state of enzyme-bound ThDP as well as its electronic structure are still subject of debate (Arduengo et al., 1997; Berkessel et al., 2011; Enders and Balensiefer, 2004; Enders et al., 2007; Nemeria et al., 2009). Hence, it remains to be further studied wether ThDP-dependend enzymes stabilize a zwittionic carbanion or a neutral carbene. Furthermore, recent NMR spectroscopical experiments (Paramasivam et al., 2011) support the presence of a significant fraction of deprotonated coenzyme at least for one representative ThDP-dependent enzyme.

While covalent catalysis is restricted to the C2-atom of the thiazolium ring, it was early postulated that the six-membered aminopyrimidine ring has co-catalytic function (Schellenberger, 1998). Pioneering work of Schellenbergers group that combined de-novo synthesis of cofactor analogues with functional, kinetic assays and later on NMR-based methods (Kern et al., 1997; Tittmann, 2000) clearly pointed out that nitrogen atoms N1´ and N4´ of the aminopyrimidine ring are pivotal components required for enzymatic ThDP catalysis. Upon incorporation into the active site of every ThDP dependent enzyme the cofactor is bound in V-conformation bringing the thiazolium C2 and

the 4´-amino function in close proximity (Muller et al., 1993). Based on this, the aminopyrimidine ring can act as a Brønsted acid/base catalyst in cofactor activation. According to the currently accepted mechanism ThDP first tautomerizes, initiated by a glutamate, into the imino form and the imino nitrogen acts as base to deprotonate C2. The six-membered ring thereby changes between three different protonation states (4´-aminopyrimidin AP, 1´-4´-iminopyrimidin IP and 4´-aminopyrimidinium APH$^+$, Fig. 3) (Jordan et al., 2003; Nemeria et al., 2004; Nemeria et al., 2009). The proton relay between C2-N4´-N1´and glutamate became a pradigm for the activation process until it was found that the ThDP-dependent enzyme glyoxylate-carboligase possess a substitution of glutamate by valine and thus a modification from this mechanism (Kaplun et al., 2008).

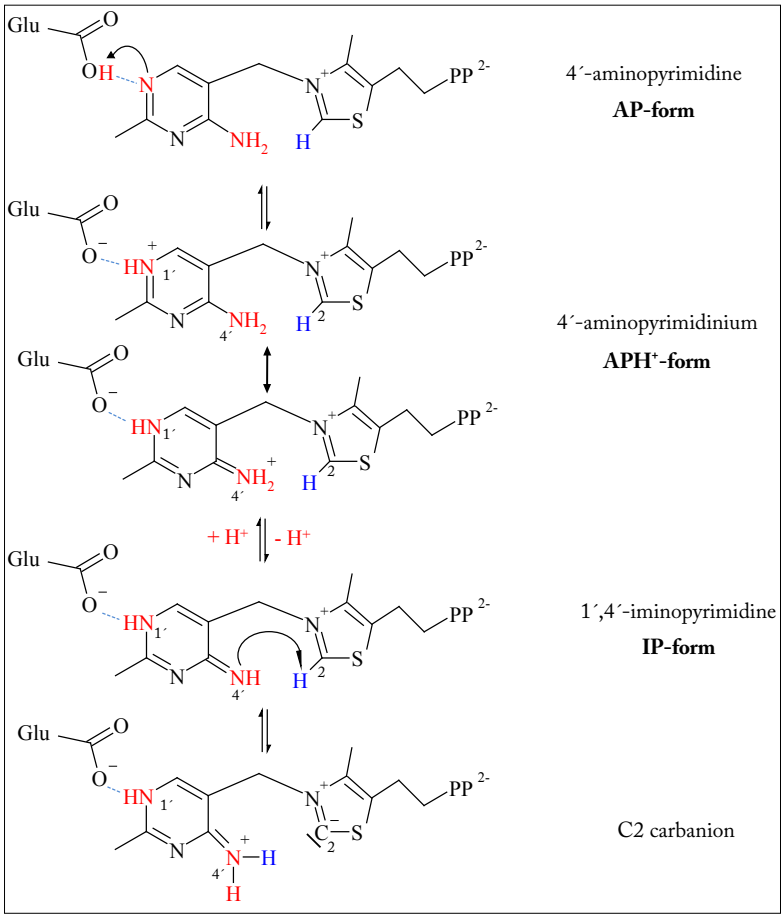

Fig. 3: Cofactor activation via different tautomeric states of the aminopyrimidine ring. The figure was prepared according to Kluger and Tittmann (2008) with minor modifications. For a detailed explanation see text. The three tautomeric states (AP, APH$^+$ and IP) of cofactors´ six-membered ring are indicated. Selected atoms are labeled. Hydrogen bonding interactions are indicated by blue dashed lines (PP = diphosphate moiety).

Beside its function in cofactor activation the aminopyrimidine ring is supposed to act as a Brønsted acid/base catalyst in multiple steps of catalysis (Nemeria et al., 2009). It was stated that the pK_A values of the three different tautomeric states of the cofactor are optimized for each ThDP-dependent enzyme (Nemeria et al., 2009). In consequence all three tautomeric forms should be accessible during catalysis to have a function either as acid or base. Noteworthy, the characteristic that both aromatic

systems contribute to catalysis in a fine balanced and dependent manner make ThDP unique among coenzymes. The group of Jordan spent a considerable time on assigning and monitoring those protonation states on different ThDP-dependent enzymes. By combination of model compound synthesis with absorbance- and circular dichroism (CD) spectroscopy spectral signatures were assigned for the AP- and the IP-form (Jordan et al., 2002; Nemeria et al., 2009) (Fig. 4). A negative CD band with a minimum at 320-330 nm is characteristic for the AP-form. The IP-form can be monitored using a positive CD- or a UV-signal between 300-310 nm. So far no signal assignment for the APH^+-form is reported. Based on those fundamentals, changes of cofactors´ protonation state as well as formation and interconversion of covalent intermediates can now be monitored and analyzed kinetically in solution (Nemeria et al., 2009).

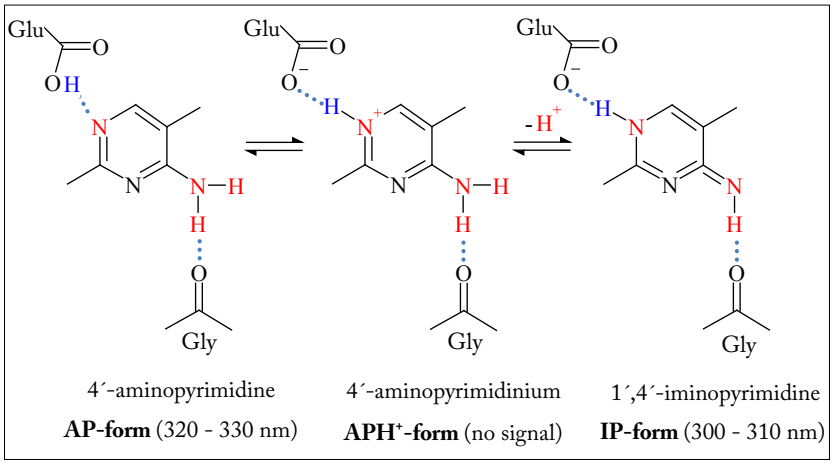

Fig. 4: Simplified scheme for stabilization of three postulated protonation states of the amino-pyrimidine ring of ThDP. Strictly conserved hydrogen bonding interactions to active site residues Glu (side chain) and Gly (backbone carbonyl) are indicated (blue dashed lines). Spectral signatures for AP- and IP-form are indicated.

1.3. Intermediates in ThDP Catalysis

As a potent nucleophile deprotonated ThDP adds covalently to the carbonyl group of a substrate resulting in an alteration of its electronic properties. Furthermore, the substrate is positioned precisely and can perform numerous biochemical reactions which all have in common that they require ThDP stabilized acyl carbanion equivalents (Kluger and Tittmann, 2008) formed after cleavage of the initial substrate-ThDP intermediate. Relying on the fact that the carbanion species are electronically stabilized by conjugation with the thiazolium moiety ThDP can be classified as an electrophilic catalyst as well. The assumption has always been that the positively charged thiazol nitrogen atom functions as electron sink to reduce the negative charge at C2. However, it was recently calculated that solely the thiazol sulphur atom (S1) can function as electron sink in contrast to the quaternary N3

atom which is typically drawn with one formal positive charge but possesses more than one full negative charge (DuPre and Wong, 2005, 2007).

Although a wide variety of different reactions is catalyzed by enzymes utilizing the organic cofactor ThDP those reactions proceed via analogous covalent intermediates (Frank et al., 2007; Kluger and Tittmann, 2008)(Fig. 5).

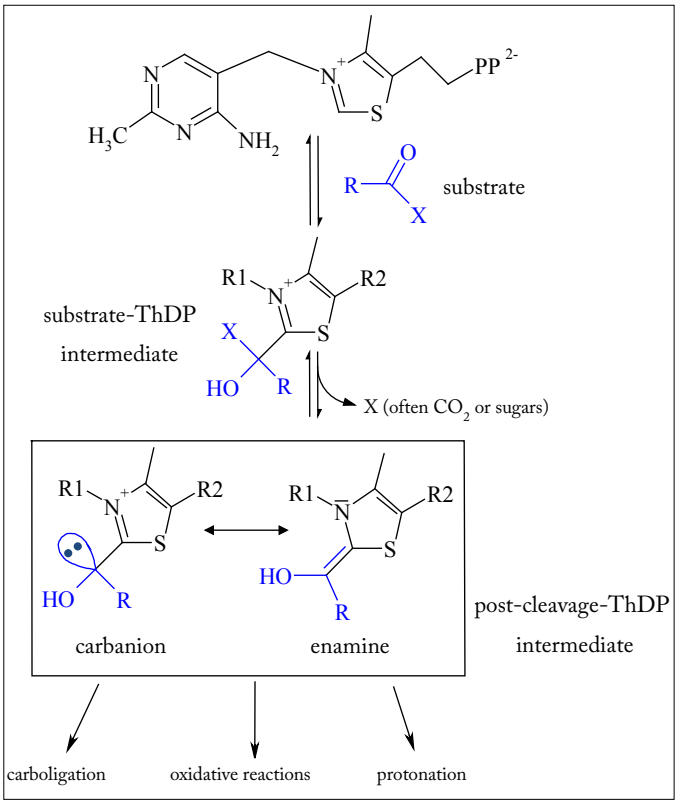

Fig. 5: Analogous intermediates but different fates of reaction in ThDP-dependent catalysis. General reaction mechanism of ThDP-dependent enzymes. Chemical structure of coenzyme thiamin diphosphate (ThDP) and of key covalent intermediates (R1= amino-pyrimidine ring, R2 = ethyldiphosphate).

The first covalent intermediate in all ThDP-dependent enzymes is the sp^3-hybridized substrate-ThDP adduct. A structural characterization of this intermediate or analogues thereof was so far successful for a limited number of ThDP-dependent enzymes (Asztalos et al., 2007; Bruning et al., 2009; Meyer et al., 2010; Tittmann and Wille, 2009; Wille et al., 2006) and enabled to delineate common mechanistical strategies for intermediate alignment which are in particular well understood for pyruvate converting enzymes (Kluger and Tittmann, 2008). The scissile substrate bond is directed perpendicular relative to the thiazolium ring allowing for an immediate conjugation of the transiently formed negative charge after bond cleavage. This maximum overlap mechanism (Turano et al., 1982) that was early postulated relying on a small molecule structure of a chemically synthesized intermediate was later shown to operate in numerous of those enzymes (Asztalos et al., 2007; Meyer et al., 2010; Wille et al., 2006). Another extraordinary structural observation was a strong deviation from planarity of up to 30° (Asztalos et al., 2007) for the C-C single bond connecting cofactor and substrate. The strain exerted on these high-energy intermediates is discussed to be a driving force for substrate cleavage yielding a more planar, unstrained carbanion/enamine post-cleavage intermediate (Tittmann and Wille, 2009).

The central branching point that determines the final reaction trajectory is the post-cleavage intermediate. This intermediate is supposed to be stabilized as a C2α carbanion (sp^3 hybridized) in

resonance with the corresponding enamine species (sp^2 hybridized) (Kluger and Tittmann, 2008). The fate of this central intermediate can be fairly classified into three subgroups:

- Protonation of the carbanion and release of an aldehyde found for ThDP-dependent decarboxylases.
- Oxidation by neighboring redox-active cofactors like flavins, lipoamid or iron-sulfur clusters. Typical examples for this class are α-ketoacid dehydrogenases, pyruvate oxidases and pyruvate-ferridoxin-oxidoreductases. Oxidation reactions can either proceed via one electron- (radical intermediates) or two electron-transfer (Tittmann, 2009).
- Carboligation to another carbonyl compound found e.g. in transketolases or acetohydroxy acid synthases.

The potential stabilization of the C2α carbanion with the enamine contributor is widely believed to lie on pathway for the reaction cycle. Furthermore, x-ray crystallographic snapshots of this reaction intermediate bound to different enzymes indeed revealed an accumulation of planar, enamine-like states in some but not all cases (Berthold et al., 2007; Fiedler et al., 2002; Machius et al., 2006; Suzuki et al., 2010; Wille et al., 2006). However, electronic stabilization of a planar, low-energy state dramatically decreases reactivity in general and especially lowers the nucleophilicity at C2α which is a prerequisite for the majority of following reactions. Noteworthy, the structural resolution of those intermediates (1.8-2.5 Å) doesn´t allow an assignment of their exact chemical state. Thus high-resolution crystallographic analysis of post-cleavage intermediates is highly desirable.

A recently implemented method to identify and quantify covalent reaction intermediates at defined time-points using ^{1}H-NMR spectroscopy represents another break-through in the mechanistical analysis of ThDP-dependent enzymes (Kluger and Tittmann, 2008; Tittmann et al., 2003). This method could already be adopted to numerous ThDP-dependent enzymes (Asztalos et al., 2007; Bruning et al., 2009; Kaplun et al., 2008; Schutz et al., 2005; Tittmann et al., 2005 a; Tittmann et al., 2005 b) and enabled the identification of rate-limiting steps or even more sophisticated the determination of microscopic rate constants of individual steps for multi-step reaction mechanisms.

Although those mechanistical studies are mostly of academic interest in some cases practical applications could be deduced. Meyer and colleagues demonstrated that favored reaction routes can be manipulated to accelerate desired side reactions enabling the synthesis of pharmaceutics (Meyer et al., 2011).

1.4. Biological Function of Transketolases

Transketolases (EC 2.2.1.1) are almost ubiquitous enzymes in cellular carbon metabolism and require ThDP and bivalent cations as cofactors for enzymatic activity (Schenk et al., 1998; Schneider and Lindqvist, 1998; Sprenger et al., 1995). TKs are involved in numerous metabolic pathways whereas the by far most important ones are the Calvin cycle and the pentose-phosphate pathway (PPP). In the

Calvin cycle of photosynthetic higher plants and algae, which is located in the chloroplast, TK is involved in recovering the CO_2 acceptor ribulose 1,5-bisphosphate. In addition TK has a central position in the cytosolic PPP which is conserved among all organisms with the exception of some archea (Soderberg, 2005).

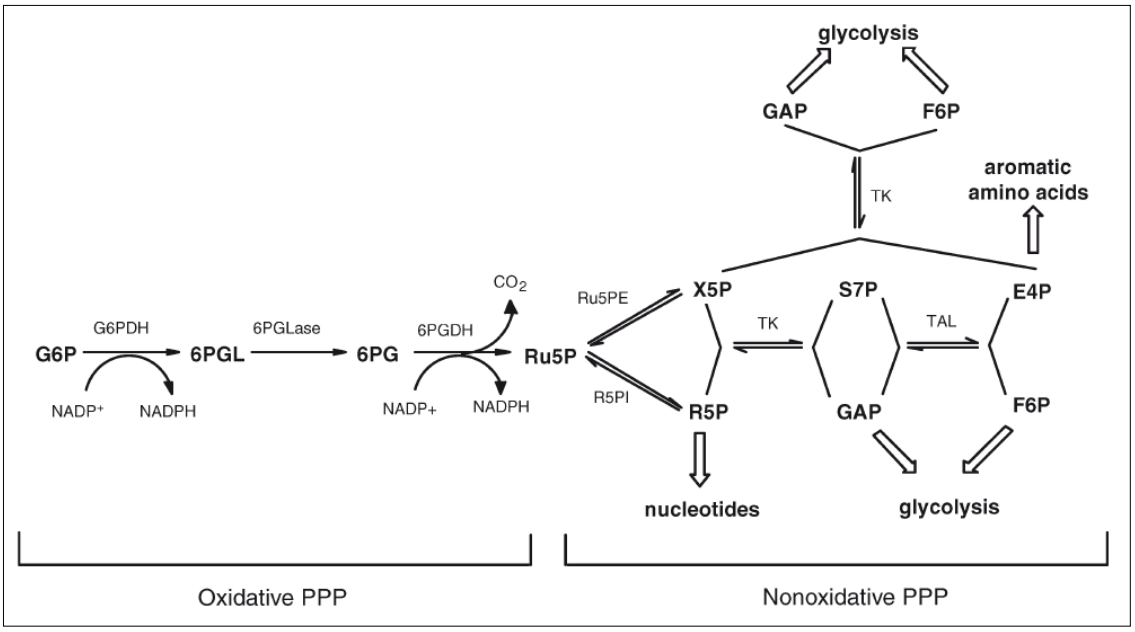

Fig. 6: Simplified, schematic view on the pentose phosphate pathway with major connections to other metabolic pathways. The figure is adapted from Soderberg (Soderberg, 2005). The oxidative part generates NADPH and finally leads to D-ribulose 5-phosphate (Ru5P). In the non-oxidative part a dynamic interconversion of sugar phosphates takes place which facilitates an adaption towards different metabolic needs. The reactions catalyzed by TK are identical to those in the Calvin cycle. Abbreviations: G6P = glucose 6-phosphate; G6PDH = glucose 6-phosphate dehydrogenase; 6PGL = 6-phosphoglucono-σ-lactone; 6GPLase = 6-phosphoglucono-σ-lactonase; 6PG = 6-phosphogluconate; 6PGDH = 6-phosphogluconate dehydrogenase, Ru5PE = ribulose 5-phosphate-3-epimerase; R5PI = ribose 5-phosphate isomerase; TAL = transaldolase

The PPP (Fig. 6) permits cells a flexible adaptation to different metabolic needs as it supplies intermediates for other metabolic pathways, generates precursors for biosynthesis of nucleotides, aromatic amino acids, and vitamins (later two ones not in animals). The PPP further produces the majority of cellular NADPH for sustaining the glutathione level and for reductive biosynthetic pathways of e.g. cholesterol and fatty acids. Tissues which are responsibly for lipid biosynthesis channel up to 30 % of the glucose into this shunt (Voet, 2008). Another important function of the PPP is located in erythrocytes. Since erythrocytes are mainly responsible for oxygen transfer they are confronted with high concentrations of reactive oxygen species. The detoxification of those molecules via gluthathione peroxidase depends on the regeneration of gluthathione which is catalyzed by gluthathione reductase (co-substrate NADPH).

Human TK (*h*TK) is expressed in all tissues highlighting its central metabolic function (Calingasan et al., 1995; Sax et al., 1996). An alteration of mammalian transketolase activity was reported for different disease states like diabetes, Alzheimer disease, Wernicke Korsakoff syndrome and numerous others (Hammes et al., 2003; Liu et al., 2008; Xu et al., 2002; Zhao et al., 2009). Unfortunately, none of these reports gave an explanation on a molecular level for the observed effects. It was stated (Boros et al., 1997) that 85 % of nucleic acid ribose in cancer cells is provided by the non-oxidative part of PPP through activity of transketolase and transaldolase making both enzymes interesting targets for anti-cancer drugs. While different research groups indeed showed independently that activity of *h*TK could be effectively decreased in vitro and in vivo by addition of small molecules inhibitors (Le Huerou et al., 2008; Thomas et al., 2008 a; Thomas et al., 2008 b), results concerning the influence of impaired *h*TK activity and cancer growth are conflicting (Boros et al., 1997). The human genome encodes for one transketolase (*h*TK) and two sequence-wise closely related proteins. Those transketolase-like proteins 1 and 2 (TKTL1 and 2)(Coy et al., 1996) show a high amino acid sequence identity of 61 % (TKTL1) and 66 % (TKTL2) (Mitschke et al., 2010) compared to *h*TK. While the cellular function and enzymatic activity of TKTL2 is unknown, over-expression of TKTL1 on RNA- and protein level was reported for different human cancers (Krockenberger et al., 2007; Xu et al., 2009) and linked to a poor survival of cancer patients (Volker et al., 2007; Xu et al., 2009). Contrary, a recent report (Mayer et al., 2010) suggests that previous studies on TKTL1 relying on real-time PCR and immuno-staining are probably unspecific or artefacts. This proposal is supported by sequence alignment (Mitschke et al., 2010) revealing that strictly conserved active site residues are missing in TKTL1 that were already shown to be pivotal for cofactor binding and catalysis in transketolase. Thus, it was concluded that TKTL1 presumably doesn´t exhibit TK activity (Mitschke et al., 2010).

For *E. coli* the existence of two functional transketolases is reported (Sprenger 1991) whose expression is regulated by an alternative sigma factor (RpoS) (Jung et al., 2005). Under exponential growing conditions TKTA is predominantly expressed whereas the second isoform TKTB shows highest expression in the stationary phase. So far functional and structural studies (Asztalos, 2007 b; Sprenger et al., 1995) were solely focused on TKTA which was also used for this study (naming here: *Ec*TK).

1.5. Three Dimensional Structure of Transketolase

Transketolases from all three kingdoms of live could be characterized structurally during the last two decades (Gerhardt et al., 2003; Lindqvist et al., 1992; Littlechild et al., 1995; Mitschke et al., 2010). Although the sequences of TKs are not strictly conserved (Schenk et al., 1998) their three dimensional structures reveal a remarkable resemblence. All described TKs are homo-dimeric enzymes with two active sites formed at the dimer interface (Fig. 7). Each bean-shaped monomer consists of three (α/β)-type domains: the N-terminal PP domain responsible for binding of the diphosphate “anchor” of the cofactor (residues 1 - 276 in *h*TK), the middle PYR domain binding the aminopyrimidine ring of ThDP (residues 316-472 in *h*TK) and a C-terminal domain (residues 492 - 623 in *h*TK). Importantly,

the PYR domain of one monomer and the PP domain of the other monomer form one active site. A nucleotide-binding function was postulated for the C-terminal domain (Schenk et al., 1998) relying on structural similarities with other nucleotide-binding domains but wasn´t verified by functional or biophysical studies.

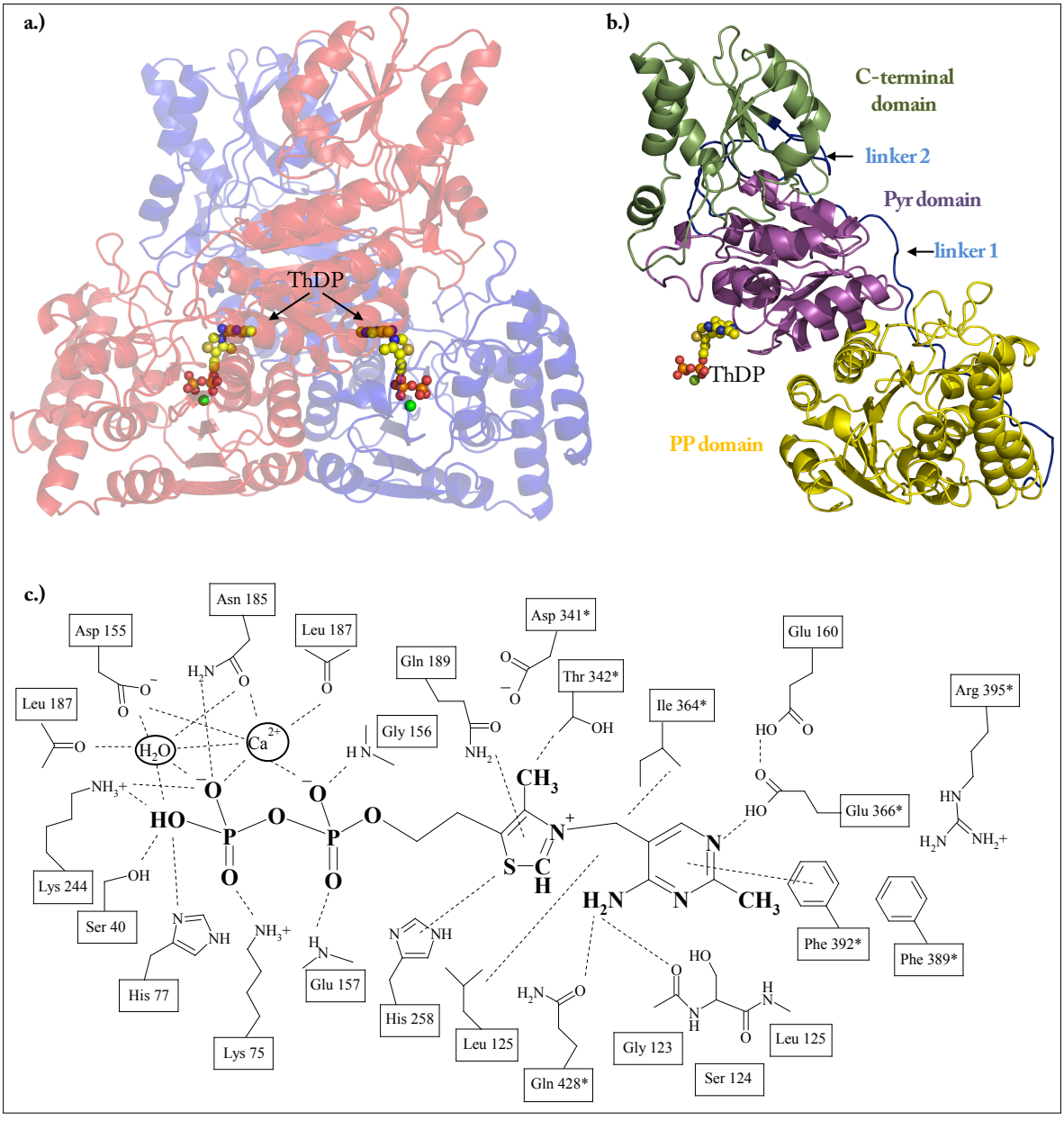

Fig. 7: Crystal structure of *b*TK. a.) Structure of the biologically functional dimer of *b*TK (Mitschke, 2010) in cartoon representation with bound cofactors ThDP (ball representations) and bivalent cation (green sphere). Individual monomers are shown in blue and red. **b.)** Domain structure of *b*TK in cartoon representation: N-terminal PP domain (yellow), middle Pyr domain (purple) and C-terminal domain (green). Flexible linker connecting PP and PYR (linker 1) as well as PYR and C-terminal domain (linker 2) are shown in blue. **c.)** Schematic diagram for the interactions of ThDP and Ca^{2+} with the active site of *b*TK. Interactions are indicated by dashed lines. Residues from the neighboring subunit are indicated by an asterisk.

Furthermore, the architecture of the active site is very similar among all structurally characterized TKs. At the entrance to the active site two positively charged arginines are located that function in positioning of the substrates´ and intermediates´ phosphate moiety (Asztalos et al., 2007; Nilsson et al., 1997; Schneider and Lindqvist, 1998). The substrate binding channel and the active site are mainly polar and offer multiple hydrogen bonding or electrostatic interactions (Fig. 7 c.) and Fig. 13)

1.6. Catalytic Mechanism of Transketolases

Transketolases are typical transferases that catalyze the reversible transfer reaction of C2-units (1,2-dihydroxyethyl) from ketose phosphates (donor substrate) to the C1 position of aldose phosphates (acceptor substrate). This two-substrate reaction can be classified kinetically as a ping-pong mechanism. TKs interconvert ketose phosphates (C5-C7 donors) and aldose phosphates (C3-C5 acceptors) of variable carbon chain length.

The overall reaction cycle (Fig. 8) can be subdivided into a donor half-reaction (donor ligation and -cleavage) and an acceptor half-reaction (acceptor ligation and product release). After activation the reactive, C2-deprotonated cofactor attacks the C2 of the donor in a nucleophilic manner to form the covalent donor-ThDP adduct. Ionization of C3α-OH and cleavage of the scissile C2α-C3α bond of the donor-ThDP intermediate results in the formation of an aldose phosphate, and of the 1,2-dihydroxylethyl-ThDP (DHEThDP) carbanion/enamine intermediate. This intermediate can then react with the previously eliminated aldose (reverse reaction) or with another acceptor substrate in competing equilibria. In the later case, C2α of DHEThDP attacks the C1 of the acceptor in a nucleophilic manner to form the covalent product-ThDP adduct. Liberation of product (ketose phosphate) finally completes the reaction cycle.

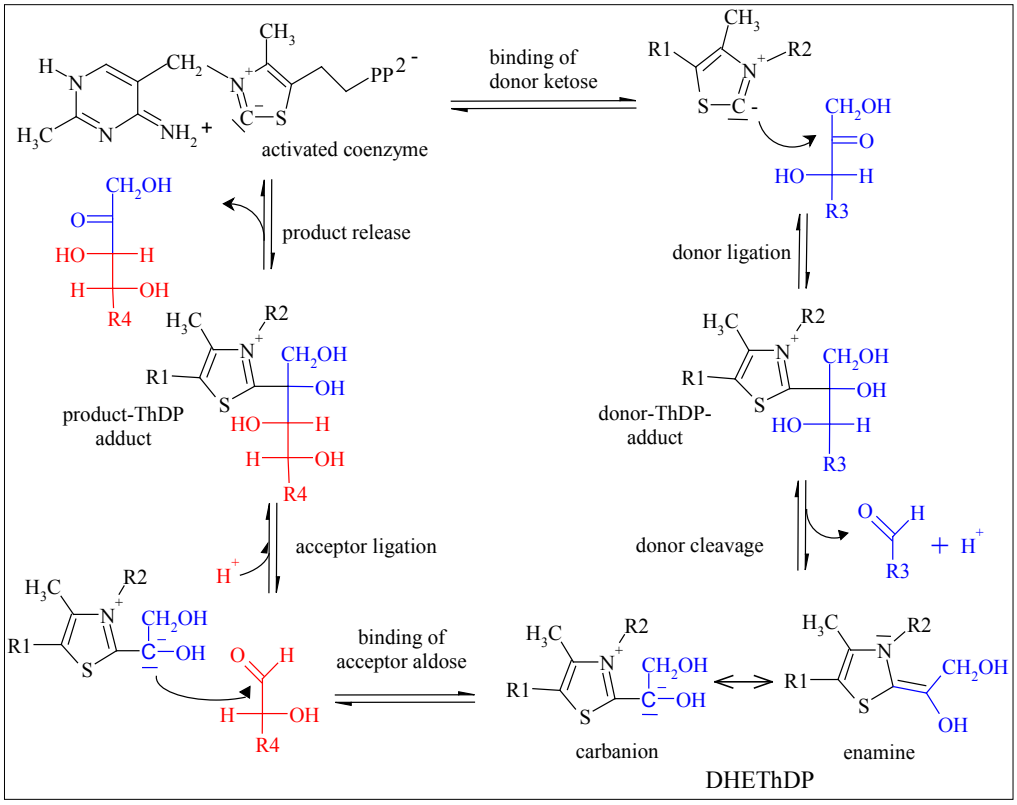

Fig. 8: Simplified, general reaction scheme of transketolase-catalyzed transfer of a dihydroxyethyl fragment from donor- to acceptor substrate. (R1 = ethyldiphosphate, R2= aminopyrimidine ring). Reaction steps and certain reaction intermediates (bold) are indicated. For explanation see text.

Studies on structure and mechanism of *Saccaromyces cerivisiea* TK (*Sc*TK) were carried out in great detail by Schneider, Lindqvist and co-workers (Nilsson et al., 1998; Nilsson et al., 1997; Schneider and Lindqvist, 1998; Wikner et al., 1995; Wikner et al., 1997). The x-ray structure analysis of covalent (Asztalos et al., 2007; Fiedler et al., 2002) and non-covalent (Asztalos et al., 2007; Nilsson et al., 1997) reaction intermediates allowed to delinate interactions of those intermediates with the protein. A very surprising and unexpected feature of the high-resolution structures of covalent D-xylulose 5-phosphate- and D-fructose 6-phosphate-ThDP adducts was significant strain in the tetrahedral cofactor-sugar adducts represented by a strong out-of-plane distortion (Asztalos et al., 2007) of the C2-C2α bond connecting substrates' carbonyl with the C2 of cofactor's thiazolium moiety. This is an extraordinary observation for a sp^2-hybridized carbon atom consequently implying a high-energetic state for those intermediates (Asztalos et al., 2007; Tittmann and Wille, 2009). In addition Fiedler and colleagues succeeded in determination of the x-ray structure of the DHEThDP intermediate and claimed a planar, resonance-stabilized enamine-like structure for this intermediate in transketolases (Fiedler et al., 2002).

1.7. A Short Introduction to the Energetics of Enzymatic Reactions

In contrast to uncatalyzed reactions the reaction coordinate of enzyme- or ribozyme-catalyzed reactions is mostly complex and contains different intermediate- and transition states (Fig. 9). The transition state is the highest point in free energy on the reaction pathway from substrate to product or substrate to a certain reaction intermediate (the top of a certain activation barrier). Transition states are experimentally not analyzable (life-time $\approx 10^{-15}$ s) and chemically represent species in which chemical bonds are made or be broken (Petsko, 2004; Voet, 2008). Intermediates are species that are transiently formed along the reaction coordinate from substrate to product. Those species are often short-lived but detectable and even structurally analyzable. The catalytic power of enzymes is represented by their ability to stabilize transition states on the one site and to destabilize the ground state and reactant states on the other site. Energetic terms that decrease the highest activation barrier (rate-limiting transition state) speed up the overall reaction. Notably, a balanced optimization of activation barriers during enzyme evolution is proposed (Albery and Knowles, 1976).

Enzymes are specific and efficient catalysts that can accelerate reactions by a factor of up to 10^{17} (Petsko, 2004) even at moderate reaction conditions. During the last decades experimental and theoretical approaches have contributed to elucidate underlying principles of transition state stabilization in enzyme catalysis. Those include electrostatic-, acid/base- or covalent catalysis, proximity of reacting groups, pre-alignment of reacting orbitals (orbital steering) and preclusion of solvent. It is widely accepted (Fersht, 1999; Petsko, 2004) that enzymes generally use more than one of the above mentioned mechanisms to perform catalysis rather than just for example electrostatic catalysis (Warshel et al., 2006). Ground state - and reactant state destabilization is considered to be achieved by forcing substrates or intermediates into high-energy conformations. However, their energetical affect on catalysis is discussed controversially. Although structures of enzyme-substrate or enzyme-inhibitor complexes contributed necessary structural insights of such mechanisms just in some rare cases a successful characterization of authentic reaction intermediates to atomic resolution could be achieved (Heine et al., 2001; Katona et al., 2002).

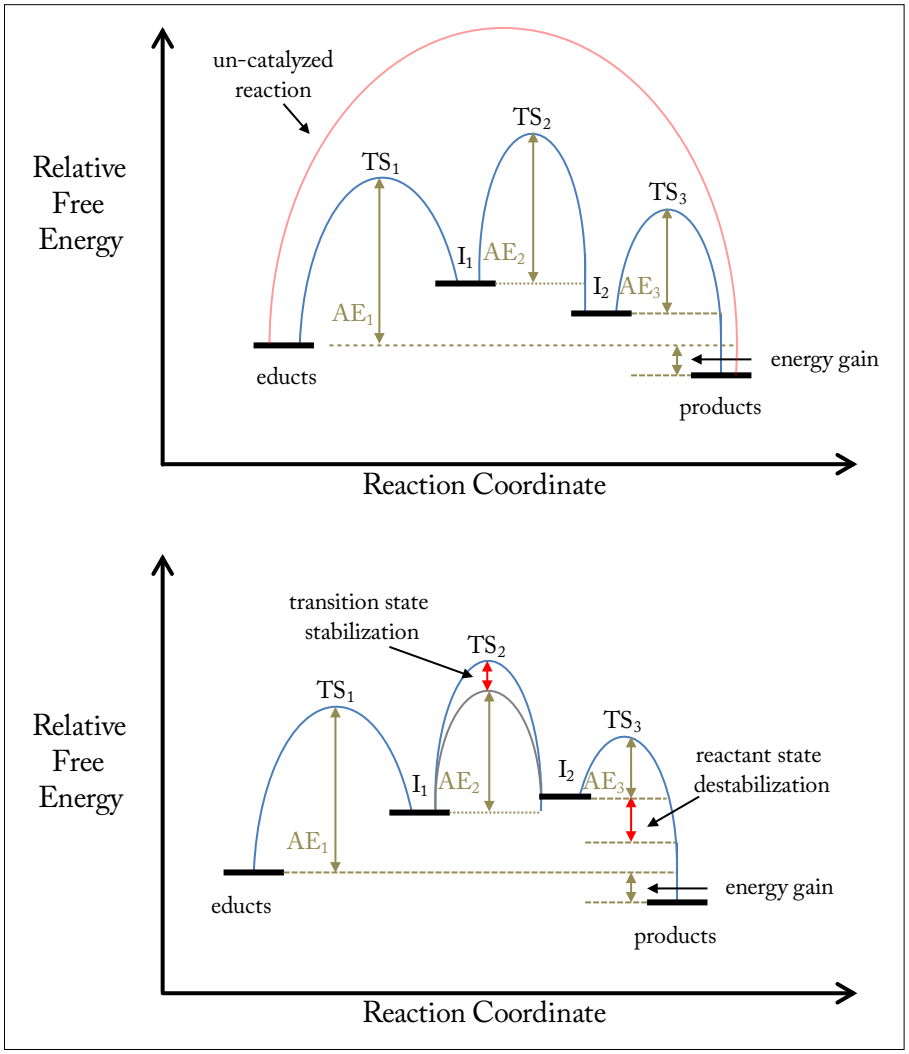

Fig. 9: Energy profile of an enzyme-catalyzed chemical reaction. Simplified reaction scheme for the relative free energy as a function of reaction progress for an uncatalyzed reaction (red) and an enzyme catalyzed reaction with two intermediates (I_1, I_2) and three transition states (TS_1, TS_2, TS_3). Individual activation energies or "barriers" (AE_1, AE_2, AE_3) have to over-come in elementary reaction step. Transition state stabilization as well as reactant state destabilization (lower profile) decrease activation energies and accelerate certain reaction steps. Because TS_2 is the highest transition states in the catalyzed reaction, the rate at which the reactants pass over this energy "hill" or "barrier" determines the overall rate of the reaction. TS_2 is therefore the rate-determining transition state and the conversion of I_1 to I_2 is the rate-determining step of this reaction (figure adapted from Petsko, 2004).

1.8. Impact of ThDP Research

While fungi, bacteria and plants posess numerous different ThDP-dependent enzymes, the number of human enzymes that require this organic cofactor is manageable. Besides cytosolic transketolase, the mitochondrial E1 components of pyruvate-, α-ketoglutarate- and branched chain α-keto acid-dehydrogenase multi-enzyme complexes as well as the peroxisomal 2-hydroxyacyl-CoA lyase are ThDP-dependent. Moreover, humans lack the ability to synthesize thiamin. Consequently, ThDP-dependent enzymes and in particular enzymes required for ThDP-synthesis came into the fore as potential drug targets. This tendency is reflected by the increasing number of determined three-dimensional structures of pathogen-derived ThDP-dependent enzymes during the last years, especially found for transketolases. The design of drugs that target pathogenic ThDP-dependent enzymes, especially those that base on ThDP analogues, requires detailed mechanistic knowledge about human enzymes using this coenzyme to estimate the impact of those compounds on humans.

Numerous ThDP-dependent enzymes are routinely used for stereospecific carboligation reactions (Fessner and Helaine, 2001; Muller et al., 2009; Pohl et al., 2004; Turner, 2000) and there is lively research to broader or change substrate specificities (Cazares et al., 2010; Galman et al., 2010; Hibbert et al., 2007). TKs possess a high specificity for donor substrates with *D*-threo configuration (*L*-C3, *D*-C4 configuration) and for acceptors that are hydroxylated at position 2 (*D*-C2 configuration) which is exploited for chemoenzymatic synthesis (Turner, 2000). Furthermore, the applicability of TK to function in bioreactors could be demonstrated recently (Matosevic et al., 2010, 2011). In consideration of the ongoing chemo-enzymatical research on TK it is rather contradictorily that mechanistic knowledge about the reactivity of intermediates (Asztalos, 2007 b) and the kinetics of microscopic reaction steps (Fiedler et al., 2001; Golbik et al., 2005) is limited.

1.9. Motivation

The main objective of this thesis is the complete structural description of the intermediates that are transiently formed along the reaction coordinate of the ThDP-dependent enzyme transketolase and to correlate structural properties of intermediates with chemical reactivity. By combining high-resolution x-ray crystallography with kinetic and thermodynamic analysis of microscopic catalytic steps a comprehensive picture of the entire enzymatic reaction cycle shall be presented.

Although previous functional and structural studies illuminated key issues of TKs´ catalytic cycles, numerous mechanistic questions regarding isolated catalytic steps remained unanswered. It is for example just partially understood how TK facilitates selection and convertion of substrates with different chain length. Furthermore some of TKs´ donor and acceptor substrates are predominantly cyclic in aqueous solution raising the question if and how TK actively assists their ring opening.

Another key objective of this thesis is the analysis of the participation of angular strain in catalysis of TK as an enzymatic tool for ground and reactant state destabilization. Numerous origins for the generation of strain, which were already suggested by Asztalos (Asztalos et al., 2007), shall be proven or weighted experimentally. Because angular strain is also reported for intermediates in other ThDP-dependent enzymes results on TK may have an impact for the entire ThDP-enzyme superfamily.

Enzymatic ThDP-dependent catalysis is achieved by an interplay of both aromatic cofactor ring systems. The six-membered aminopyrimidine ring, which participates in multiple steps of catalysis as Brønsted acid/base catalyst, adopts three different protonation states (IP, AP, APH^+) that are characteristic for certain, covalent intermermediate states (Nemeria et al., 2009). Spectroscopic and structural results presented in this thesis will be correlated with this concept of catalysis.

2. Materials & Methods

2.1. Materials

Compound	Supplier
1,2-dihydroxyethyl-3-deaza thiamin diphosphate	provided by Prof. Dr. Finian Leeper (University of Cambridge, UK)
5-phospho-D-ribose-diphosphate, sodium salt (purity 84 %)	Sigma-Aldrich Chemie GmbH, Deisenhofen
1-desoxy-D-ribose 5-phosphate, sodium salt	provided by Anatol Spork and Prof. Dr. Christian Ducho (Bioorganic and Medical Chemistry, University of Göttingen)
1-desoxy-D-xylulose 5-phosphate, sodium salt (purity 99 %)	Sigma-Aldrich Chemie GmbH, Deisenhofen
D-arabinose 5-phosphate, disodium salt trihydrate	Sigma-Aldrich Chemie GmbH, Deisenhofen
D-erythrose 4-phosphate, sodium salt (purity 72 %)	Sigma-Aldrich Chemie GmbH, Deisenhofen
D-fructose 6-phosphate, disodium salt hydrate	Sigma-Aldrich Chemie GmbH, Deisenhofen
D-ribose 5-phosphate, disodium salt hydrate	Sigma-Aldrich Chemie GmbH, Deisenhofen
D-ribitol 5-phosphate, sodium salt	provided by Anatol Spork and Prof. Dr. Christian Ducho (Bioorganic and Medical Chemistry, University of Göttingen)
D-sorbitol 6-phosphate, barium salt (purity 90 %)	Sigma-Aldrich Chemie GmbH, Deisenhofen
2,5-anhydro-D-mannitol-1-phosphate, barium salt hydrate	Carbosynth, Compton, UK
2,5-anhydro-D-glucitol-6-phosphate, barium salt hydrate	Carbosynth, Compton, UK
Acid sulphur	Carl Roth GmbH & Co KG, Karlsruhe
Acetic acid	Carl Roth GmbH & Co KG, Karlsruhe
Acrylamide	Carl Roth GmbH & Co KG, Karlsruhe
Agar	AppliChem GmbH, Darmstadt
Agarose	AppliChem GmbH, Darmstadt
Ammonium chloride	Carl Roth GmbH & Co KG, Karlsruhe
Ammonium sulfate	AppliChem GmbH, Darmstadt
Ampicillin	AppliChem GmbH, Darmstadt
Antifoam 204	Sigma-Aldrich Chemie GmbH, Deisenhofen

Barium chloride, dihydrate	AppliChem GmbH, Darmstadt
Baysilone paste	GE Bayer Silicones GmbH & Co. KG, Leverkusen
Benzylsulfonylfluoride (PMSF)	AppliChem GmbH, Darmstadt
Calcium chloride	Carl Roth GmbH & Co KG, Karlsruhe
Chloramphenicol	AppliChem GmbH, Darmstadt
Coomassie Brillant blue G-250	AppliChem GmbH, Darmstadt
Deuterium oxide 99.9%	Sigma-Aldrich Chemie GmbH, Deisenhofen
Diethyl ether	Carl Roth GmbH & Co KG, Karlsruhe
Dimethyldichlorsilane	AppliChem GmbH, Darmstadt
Dithioerythritol (DTE)	AppliChem GmbH, Darmstadt
Dithiothreitol (DTT)	AppliChem GmbH, Darmstadt
Dowex 50 Wx8 cation exchanger	AppliChem GmbH, Darmstadt
Ethylenediaminotetraacetic acid (EDTA)	AppliChem GmbH, Darmstadt
Ethanol	Carl Roth GmbH & Co KG, Karlsruhe
Ethylene glycol	AppliChem GmbH, Darmstadt
D-Glucose	AppliChem GmbH, Darmstadt
Glycerol (96 %)	Carl Roth GmbH & Co KG, Karlsruhe
Glycine	Carl Roth GmbH & Co KG, Karlsruhe
Glycylglycine	AppliChem GmbH, Darmstadt
Hydrochloric acid (37%)	Th. Geyer GmbH & Co. KG, Renningen
β-Hydroxypyruvate sodium salt (97 %)	Fluka Chemie GmbH, Switzerland
Imidazole	AppliChem GmbH, Darmstadt
Kanamycin sulfate	Carl Roth GmbH & Co KG, Karlsruhe
Magnesium chloride, hexahydrate	Carl Roth GmbH & Co KG, Karlsruhe
Magnesium sulfate	Carl Roth GmbH & Co KG, Karlsruhe
β-Mercaptoethanol	Carl Roth GmbH & Co KG, Karlsruhe
Methanol	Carl Roth GmbH & Co KG, Karlsruhe
Nicotinamide adenine dinucleotide, reduced (NADH)	Sigma-Aldrich Chemie GmbH, Deisenhofen
Phenylmethylsulfonyl fluoride	Sigma-Aldrich Chemie GmbH, Deisenhofen
N3´-Pyridyl-thiamin diphosphate (N3ThDP)	provided by PD Dr. Ralph Golbik (University of Halle/Wittenberg)
Phosphoric acid (85 %)	Carl Roth GmbH & Co KG, Karlsruhe

Potassium chloride	Fluka Chemie GmbH, Switzerland
Potassium dihydrogen phosphate	Carl Roth GmbH & Co KG, Karlsruhe
Potassium hydroxide	AppliChem GmbH, Darmstadt
Polyethylene glycol (PEG) 6000	Fluka Chemie AG, Buchs, Switzerland
Polypropylene glycol (PPG) 400	Fluka Chemie AG, Buchs, Switzerland
Pyruvate	Sigma-Aldrich Chemie GmbH, Deisenhofen
Sodium acetate, trihydrate	AppliChem GmbH, Darmstadt
Sodium chloride	AppliChem GmbH, Darmstadt
Sodium dodecylsulfate (SDS)	AppliChem GmbH, Darmstadt
Streptomycin sulfate	AppliChem GmbH, Darmstadt
SYPRO orange reagent	Sigma-Aldrich Chemie GmbH, Deisenhofen
N,N,N´,N´-Tetramethylethylendiamin (TEMED)	Carl Roth GmbH & Co KG, Karlsruhe
Thiamin	AppliChem GmbH, Darmstadt
Thiamin diphosphate (ThDP)	AppliChem GmbH, Darmstadt
Trichloroacetic acid	Sigma-Aldrich Chemie GmbH, Deisenhofen
3-(Trimethylsilyl) propionic-2,2,3,3- d_4 acid, sodium salt	Sigma-Aldrich Chemie GmbH, Deisenhofen
Tris-(hydroxymethyl)-aminomethane (Tris)	AppliChem GmbH, Darmstadt
Tryptone	AppliChem GmbH, Darmstadt
Yeast extract	AppliChem GmbH, Darmstadt
Yeast extract for high-density fermentation	Ohly GmbH, Hamburg
Enyzmes, Marker and Solutions	Supplier
DNase	AppliChem GmbH, Darmstadt
Plasmid prapartion QIAprep® Spin Miniprep kit (50)	Qiagen GmbH, Hilden
*Dpn*I (10 U/µl)	Fermentas GmbH, St.Leon-Rot
dNTP mix (10 mM)	Fermentas GmbH, St.Leon-Rot
Lysozyme	AppliChem GmbH, Darmstadt
Pfu Turbo DNA polymerase (2,5 U/µl)	Qiagen GmbH, Hilden or Fermentas GmbH, St.Leon-Rot
Phusion polymerase (2 U/µl)	Finnzymes, Finland
QuikChange site directed mutagenesis kit	Stratagene, USA

Sequencing mix BDT reaction mix Half-term buffer	Applied Biosystems, Darmstadt
Unstained protein molecular weight standard Gene Ruler™ 1 kb DNA ladder 0,5 µg/µl 6x DNA Loading Dye	Fermentas GmbH, St.Leon-Rot
Triosephosphate isomerase (TIM) + Glycerol 3-phosphate dehydrogenase (G3P-DH) Mix	Sigma-Aldrich Chemie GmbH, Deisenhofen
E. coli strains	Supplier
E. coli-JM109	Stratagene, USA
E. coli-BL21 Star (DE3)	Invitrogen
E. coli-Top10	Invitrogen
Plasmids	
pGSJ427 encodes for transketolase A from *E. coli* (*Ec*TK)	provided by Prof. Dr. Georg Sprenger (University of Stuttgart)
pET28a (+)	Novagen

Devices	Supplier
Biofermenter, Biostat C and C plus	Sartorius Stedim, Göttingen
Circular dichroism spectropolarimeter, Chirascan	Applied Photophysics Ltd., UK
Centrifuges, Universal 320R AvantiJ-30I AvantiJ-20XPI Biofuge Pico Optima LE-80K Ultracentrifuge	 Hettich AG, Bäch, Switzerland Beckmann Coulter GmbH, Krefeld Beckmann Coulter GmbH, Krefeld UniEquip GmbH, Martinsried Beckmann Coulter GmbH, Krefeld
Centrifuge tubes (50, 500, 1000 ml)	Beckmann Coulter GmbH, Krefeld
Chromatographic columns, Hi*Prep*™ 26/10 Desalting His*Prep* FF 16/10	GE Healthcare Bio-Sciences GmbH, Munich
Concentrator, Vivaspin 20 (30.000 and 50.000	Sartorius AG, Göttingen

MWCO)	
Cover plates, 18 mm	VWR International GmbH, Darmstadt
Crystallization plates (24 well), costar	Corning, Inc., USA
Electrophorese device, EV 231	Consort nv, Belgium
Electroporator, MicroPulser electroporator	Bio-Rad Laboratories GmbH, Munich
Filters for NMR samples, 0.45 µm	GE Water & Process Technologies
FPLC-Systems ÄKTA*prime* plus ÄKTA*purifier*	GE Healthcare Europe
Gel documentation chamber, Raytest Ida	Herolab, Wiesloch
Inkubation shaker, Unitron	Infors AG, Bottmingen, Switzerland
ITC-System, ITC_{200} and VP-ITC	GE Healthcare
Microfluidizer, M-110S Small Volume Pneumatic	Microfluidics (Division of MFIC Corp.), USA
NMR-Spectrometer, ARX 400 MHz Avance (Institute for Organic and Supramolekulare Chemistry, Göttingen University) 700 MHz (Department for NMR Based Structural Biology, MPI for Biophysical Chemistry, Göttingen)	Bruker Biospin GmbH, Karlsruhe
pH electrode	Hettler Toledo, Gießen
Precission cuvettes, suprasil	Hellma GmbH & Co. KG, Mühlheim
Stopped-flow system, SX.18 MV and SX.20 MV	Applied Photophysics Ltd., UK
Steril filters, 0.20µm	VWR International GmbH, Darmstadt
Superloop (10 ml, 50 ml, 150 ml)	GE Healthcare Europe GmbH, Freiburg
Thermoblock, Digital Dry Bath 3721D	Fisher Bioblock Scientific, UK
Thermocycler, TProfessional Standard 96 well Gradient	Whatman Biometra®, Göttingen
UV-Vis Spectrometer, V-650	Jasco GmbH, Groß-Umstadt
X-ray MM-007 rotating-anode generator, Micromax 007-HF X-stream 2000, R-AXIS IV++ imaging-plate system	Rikagu Corp., USA
<u>Software</u>	
Gene runner V.3.05	Hastings Software, Inc.

SigmaPlot Version 11.0	Systat Software, Inc
Origin-7	OriginLab Corporation, USA
CHIMERA	http://www.cgl.ucsf.edu/chimera/
Phenix suite	(Adams et al., 2010 a)
PROPKA	(Bas et al., 2008)
PYMOL	*DeLano Scientific LLC*
CCP4 suite	(Bailey, 1994)
SHELXL-11	(Sheldrick, 2008)
Kaleidagraph	Synergy Software, USA
MestreNova	Mestrelab Research, Spain
ClustalW2	http://www.ebi.ac.uk/Tools/msa/clustalw2/ (Larkin et al., 2007)
ESPript 2.2	http://espript.ibcp.fr/ESPript/ESPript/index.php (Gouet et al., 1999)
Anomalous Scattering Coefficients	http://skuld .bmsc.washington. edu/scatter/AS_form.html
Dali Search	http://ekhidna.biocenter.helsinki.fi/dali_server/
ExPasy, ProtParam	http://web.expasy.org/protparam/
MESPEUS-database	http://mespeus.bch.ed.ac.uk/MESPEUS/ (Hsin et al., 2008)
PRODRG server	http://davapc1.bioch.dundee.ac.uk/prodrg/ (Schuttelkopf and van Aalten, 2004)
MOLPROBITY	http://molprobity.biochem.duke.edu/ (Davis et al., 2007)

Media, buffers and solutions

Media, buffers, and solutions were prepared with deionized water and autoclaved if necessary (121 °C, 20 min). Solutions with heat-labile components were sterilized (steril filters, 0.22 µm). The pH of the solutions was adjusted by the addition of NaOH or HCl if not otherwise stated.

2.2. Methods

2.2.1. Molecular Biology

The gene of *h*TK in the pET 28a vector was cloned and kindly provided by Dr. Kathrin Schröder-Tittmann. This expression construct encodes for *h*TK with a C-terminal thrombin cleavage site followed by a hexa-histidine tag. The C-terminal tag extends *h*TK by 14 amino acids (*h*TK-Leu-Val-

Pro-Arg-Gly-Ser-Leu-Glu-His-His-His-His-His-His). Active site variants were generated based on this construct using standard molecular methods. The utilized primers are depicted in Tab. 1.

The gene of *Ec*TK in the pGSJ427 vector was kindly provided by Prof. Dr. Georg Sprenger (University of Stuttgart). The active site variants *Ec*TK $His^{100}Ala$ and $His^{473}Ala$ were generated and kindly provided by Ann-Kristin Diederich and Dr. Peter Asztalos. This expression construct encodes for EcTK with a C-terminal hexa-histidine tag. The gene of *Ec*TK is under control of a constitutively active promoter and requires no induction of the protein expression.

Tab. 1: List of utilized, specific primer.

Primer	Nucleotide sequence (5'-3')
*h*TKGln^{189}Ala forward	5' –GATATTAACCGTCTGGGCGCGAGCGATCCGGC-3‘
*h*TKGln^{189}Ala reverse	5‘-GCCGGATCGCTCGCGCCCAGACGGTTAATATC-3‘
*h*TKHis^{37}Gln forward	5‘-CGGGTAGCGGTCAGCCGACCAGCTG-3‘
*h*TKHis^{37}Gln reverse	5‘-CAGCTGGTCGGCTGACCGCTACCCG-3‘
*h*TKHis^{258}Gln forward	5‘-GATAAAGAAAGCTGGCAGGGCAAACCGCTG-3‘
*h*TKHis^{258}Gln reverse	5‘-CAGCGGTTTGCCCTGCCAGCTTTCTTTATC-3‘
sequencing primer 1	5‘-GGCATGGCGTATACCGGCAA-3‘
sequencing primer 2	5‘-CAGGAAATCTATAGCCAGATC-3‘
sequencing primer 3	5‘-ACCCGTGCGTTGATCAGAT-3‘
sequencing primer 4	5‘-TAATACGACTCACTATAGGG-3‘
sequencing primer 5	5‘-TATGCTAGTTATTGCTCAG-3‘

2.2.1.1. Concentration Determination of DNA

DNA concentrations were determined spectroscopically using the absoption at 260 nm. The following correlation was used to determine the concentrations:

1 A_{260} = 50 µg/ml doubled stranded DNA = 0.15 mM (in nucleotides)

2.2.1.2. Agarose Gelelectrophorese

Agarose gelelectrophoresis was used for analysis of DNA molecules after PCR reactions. Samples were supplemented with DNA loading dye (6 x DNA loading dye: 30 % (v/v) glycerol, 0.25 % (w/v) bromophenol blue), and were separated using a horizontal electrophoresis. Gels typically contained 1-2 % agarose and 1 x TAE buffer (40 mM Tris, 1 mM EDTA, 20 mM acetate, pH 8.5). After separation of the DNA fragments the gel was transferred into a solution containing 2 µg/ml ethidium

bromide and incubated for 5-10 min. The visualization of bands under UV light was carried out in a gel documentation system.

2.2.1.3. Polymerase Chain Reaction (PCR)

PCR was used for the amplification of gene fragments as well as for site directed mutagenesis. A standard PCR reaction of a total volume of 25 µl contained 5 µl 5x Pfu buffer, 0.5 µl dNTP mix (10 mM of each nucleotide-5'-triphosphate), 5-50 ng template DNA, 125 pmol sense and antisense primer, and 0.3 µl Phusion DNA Polymerase (2 U/µl). The temperature protocol included an initial denaturation step (step 1; 95 °C, 1 min), another denaturation step (step 2; 95 °C, 30 sec), a primer annealing step (step 3; 2-5 °C below the melting temperature of the complementary primer sequences, 30 sec), an elongation step (step 4; 72 °C, 30 s per kilobase product), and a final step (step 5; 72 °C, 5 min). Steps 2-4 were repeated 25 times. In case of PCR reactions for site-directed mutagenesis the mixture was supplemented with *Dpn*1 after the PCR to digest maternal DNA according to protocol (QuikChange site-directed mutagenesis kit).

2.2.1.4. DNA Sequencing

All DNA constructs used during this work were analyzed for the correct sequence of the respective inserts by DNA sequencing. A standard DNA sequencing reaction of a total volume of 10 µl contained 1 µl plasmid (200-300 ng), 1 µl sequencing primer (500 nM), 1.5 µl BDT ready reaction mix, 1.5 µl half term buffer and 5 µl steril water. The temperature protocol included an initial denaturation step (step 1; 96 °C, 1 min), another denaturation step (step 2; 95 °C, 5 sec), a primer annealing step (step 3; 55 °C, 15 sec) and an elongation step (step 4; 60 °C, 4 min). Steps 2-4 were repeated 25 times. After the sequencing reaction the mixture was supplemented with 2 µl 3 M Na-acetate, 2 µl 125 mM EDTA and 50 µl EtOH (96 % v/v) resulting in a precipitation of the DNA. DNA was pelletized by centrifugation (20000 x g, 20 min), washed with 70 µl ethanol (70 % v/v) and finally dried at 70 °C for 3 min. The DNA pellet was then diluted in formamide and stored at -20 °C. The final sequencing step was performed by Alexander Nolte (Department of Developmental Biochemistry, University of Göttingen).

2.2.1.5. Plasmid Transformation

To transfer plasmid DNA into different *E. coli* strains, electroporation or chemo transformation was used following standard protocols. Chemical- and electro-competent cells were prepared according to Inoue et al. and Tung et al. (Inoue et al., 1990; Tung and Chow, 1995). All competent cells were stored in 50 µl aliquots at -80°C. In a standard approach, 1 µl of extracted plasmid was mixed with 50 µl of chemically competent or chemo-competent *E. coli* cells and the cells were incubated for 10 min on ice. For transformation the chemically competent bacteria were heat-shocked for 40 s at 42 °C and subsequently cooled on ice for 2 min. In contrast the electro-competent bacteria were transferred into

an electro transformation cuvette and electricity (1.8 kV, 25 mF, 200 Ω) was applied. In both cases 900 µl of SOC medium (2 % (w/v) trypton, 0.5 % (w/v) yeast extract, 0.05 % (w/v) NaCl, 2.5 mM KCl, 10 mM $MgCl_2$, 2 % (w/v) glucose) was added and the bacteria were incubated for further 45 min at 37 °C. Successfully transformed cells were selected on LB-agar plates supplemented with appropriate antibiotics. Final antibiotic concentrations in media were 50 µg/ml kanamycin, 34 µg/ml chloramphenicol or 100 µg/ml ampicillin.

2.2.2. Protein Chemistry

2.2.2.1. Concentration Determination of Proteins

The concentration of proteins without a chromophoric cofactor was determined spectroscopically. For that purpose the absorbance at 280 nm was determined. Molar extinctions coefficients for proteins under study were calculated (ProtParam). Additionally, the coefficiant A_{280}/A_{260} was calculated to check each protein preparations for contaminations with nucleic acids. The concentration of proteins with chromophoric cofactors was determined in a colorimetric assay relying on a lab-specific protocol based on the method of Bradford (Bradford, 1976).

2.2.2.2. Sodium Dodecyl Sulfate - Polyacrylamide Gel Electrophoresis (SDS-PAGE)

For analysis of purified or stored proteins SDS-PAGE was performed relying on a protocol of Laemmli and Weber (Laemmli, 1970; Weber et al., 1972). SDS gels contained a stacking part, cast of 5 % acrylamid, 125 mM Tris (pH 6.8) polymerized with 0.3 % w/v APS and 0.03 % TEMED. Proteins were resolved on the lower gel, containing 12-15 % acrylamide, 375 mM Tris (pH 8.8) polymerized with 0.3 % APS and 0.3 % TEMED. Protein samples were mixed with SDS loading buffer (4 % (w/v) glycerol, 80 mM SDS, 150 mM Tris, pH 6.8), heated to 96 °C for 5 min and loaded on the stacking part of the gel. Gels (thickness 1 mm) were run at 1 mA/cm² in SDS running buffer (25 mM Tris, 200 mM glycine und 3.5 mM SDS, pH 8.3) until the front of the loading dye reached the bottom of the gel. After protein separation the gels were stained with 0,25 % (w/v) Coomassie Brilliant Blue in 30 % methanol and 6 % acetic acid for 30 min and bleached first in 30 % methanol, 10 % acetic acid and finally in water.

2.2.2.3. Proteinexpression

Expression in Shaking-Flask

A single colony was used to inoculate 8 ml culture which was used after 12 h of growth to further inoculate a 300 ml overnight culture for cell cultivation at 37 °C. This overnight culture was used to inoculate 12 x 500 ml main culture supplemented with 70 µg/ml thiamin in baffled shaking flasks (all cultures: LB medium, 50 g/ml kanamycin for *h*TK and 100 µg/ml ampicillin for *Ec*TK). In case of expression of *h*TK or variants thereof the temperature was rapidly decreased to 16 °C when an OD of approx. 1 was reached and gene expression was induced by the addition of 100 µM IPTG. The cells

were harvested after 12 h at 12 °C. Bacteria expressing *Ec*TK or variants thereof were cultivated at 37 °C for 12-16 h. In all cases the cells were pelletized by centrifugation (4800 rpm, 30 min, 4 °C) and stored at – 80 °C until usage.

High-Density Fermentation

In order to produce high amounts of transketolase for NMR methods and crystallographic studies high-density fermentation was applied using a biofermenter.

A single colony was used to inoculate 8 ml culture which was used after 12 h of growth to further inoculate a 300 ml overnight culture (both cultures: LB medium, 50 µg/ml kanamycin for *h*TK or 100 µg/ml ampicillin for *Ec*TK) for cell cultivation at 37 °C. This overnight culture was used to inoculate 6 liters of fermentation medium (300 g fermentation yeast extract, 3 g NH_4Cl, 30 g glucose, 4 g $MgSO_4$, 66 g K_2HPO_4, 1 ml antifoam, 70 µg/ml thiamin) supplemented with appropriate antibiotics. The culture was stirred with 400–1500 rpm at a constant saturation with air of 30 % at 37 °C. After depletion of the glucose, feeding was started using a glucose feeding solution (2 liters containing 600 g of fermentation yeast extract and 600 g of glucose). The air flow was gradually increased during cultivation from 3 to 24 liters/min. A pH of 7 was maintained by automatic titration of 10 % NaOH or 10 % H_3PO_4.

For fermentation of *h*TK or variants thereof the temperature was rapidly decreased to 18 °C when an OD of approx. 50 was reached and gene expression was induced by the addition of 100 µM IPTG. Cells were harvested after 4 h growth at 18 °C. Bacteria expressing *Ec*TK or variants thereof were cultivated at 37 °C until an OD of 80-100 was reached and were subsequently harvested.

In all cases the cells were pelletized by centrifugation (4800 rpm, 30 min, 4 °C) and stored at –80 °C until usage. The wet weight of the cells differed between 0.6 to 1.2 kg per fermentation.

2.2.2.4. Protein Purification of *Ec*TK

For a standard purification (Asztalos, 2007 b) 20 g cell pellet were resuspended in 125 ml buffer (20 mM Tris, 300 mM NaCl, 1 mM DTE, 1 mM EDTA, 20 mM imidazole, 10 µg/ml lysozyme, pH 8.0) and disrupted by three passages through a microfluidizer. After removal of cell debris by centrifugation (45 min, 20000 rpm, 4 °C) the nucleic acids were precipitated by stepwise addition of 2 % streptomycin sulfate. The DNA was then pelletized by centrifugation (45 min, 20000 rpm, 4 °C) and the solution was supplemented with 2 mM $CaCl_2$. The supernatant was loaded onto an equilibrated Ni-NTA column. After a washing step with 100 ml buffer (20 mM Tris, 300 mM NaCl, 20 mM imidazole, pH 8.0) the protein was eluted with a linear gradient over 100 ml reaching 100 % elution buffer (20 mM Tris, 300 mM NaCl, 200 mM imidazole, pH 8.0).

2.2.2.5. Protein Purification of *h*TK

For a standard purification 100 g cell pellet were resuspended in 400 ml buffer (20 mM Tris, 300 mM NaCl, 100 µM ThDP, 5 mM $CaCl_2$, 20 mM imidazole, 0.5 mM phenylmethylsulfonyl fluoride, 10 µg/ml lysozyme, 50 ng/ml DNase1, pH 8.0), and disrupted by three passages through a microfluidizer. Cell debris was pelletized by centrifugation (45 min, 20000 rpm, 4 °C) and the supernatant was loaded onto an equilibrated Ni-NTA column. After a washing step with 100 ml buffer (50 mM Tris, 300 mM NaCl, 20 mM imidazole, pH 8.0) the protein was eluted with a linear gradient over 100 ml reaching 100 % elution buffer (25 mM Tris, 300 mM NaCl, 200 mM imidazole, pH 8.0).

2.2.2.6. Preparation of apo *h*TK

For several biophysical methods ThDP had to be removed from the enzyme facing the problem, that *h*TK binds its cofactors in an irreversible manner. The applied protocol for the preparation of apo enzyme relies on a protocol by Wang et al. (Wang et al., 1997) but contains several modifications. The whole preparation was carried out on ice with solutions at 2-4 °C. One ml *h*TK 10–20 mg/ml in 20 mM Tris, 300 mM NaCl, 200 mM imidazole, pH 8.0 was transferred into 4.1 ml 1M EDTA, 10 mM Tris, pH 8.0 and incubated for 15 min. After addition of 3 ml 45 % (w/v) $(NH_4)SO_4$ and 4 % glycerol the reaction mixture was stirred gently and incubated for further 20 min. The pH was then adjusted to 3.5 by addition of diluted H_2SO_4. The *h*TK $(NH_4)_2SO_4$ pellet generated by centrifugation (45 min, 40000 rpm, 4 °C) was subsequently diluted in 50 mM glycylglycine, 2 % glycerol, pH 7.9. The pH of this solution was immediately adjusted to 7.6 (for functional studies) or 7.9 (for crystallization). Residual protein aggregates were removed by centrifugation (45 min, 15000 rpm, 4 °C). The quality of each preparation and the ability of the apo enzyme to be reactivated were tested by activity assay. In all cases ThDP could be removed totally but traces of the bivalent cation were still present.

2.2.2.7. Size Exclusion Chromatography - Desalting

To transfer proteins into a desired buffer condition for different applications size exclusion chromatography was applied. We used HighPrep-Desalting columns following the manufacturer instructions for this purpose.

2.2.3. Substrates and Substrate Analogues

Substrates used for functional assays and for crystallization were purchased from Sigma Aldrich, Toronto Research Chemicals or Carbosynth. Purity of those compounds and contamination with other potentially interfering compounds was confirmed by nano electrospray ionization mass spectrometry performed by Dr. Cornelia Herrfurth or Dr. Katharina Michels (Plant Biochemistry,

University of Göttingen). Ribitol 5-phosphate and 1-desoxy-ribose 5-phosphate were synthesized by Anatol Spork and Prof. Dr. Christian Ducho (Bioorganic and Medical Chemistry, University of Göttingen). Purity of the compounds was verified by ^{1}H NMR and ^{13}C NMR-spectroscopy performed by Anatol Spork.

2.2.3.1. Concentration Determination of Cofactors and Analogues thereof

N3´-pyridyl thiamin diphosphate (N3ThDP) was synthesized and kindly provided by PD Dr. Ralph Golbik (University of Halle/Wittenberg). 1,2-dihydroxyethyl-3-deaza thiamin diphosphate was synthesized and kindly provided by Prof. Finian Leeper (University of Cambridge, UK). The concentration of ThDP and the cofactor analogues was determined spectroscopically using molecular absorbance coefficients listed in Tab. 2.

Tab. 2: Structure and spectroscopic properties of ThDP and selected analogues (PP = diphosphate moiety). Selected atoms are labeled.

Cofactor	Spectroscopic characteristics	Structure
ThDP	isosbestic point at 273.5 nm, $\varepsilon_{273.5\ nm}$ = 7757 $M^{-1} * cm^{-1}$	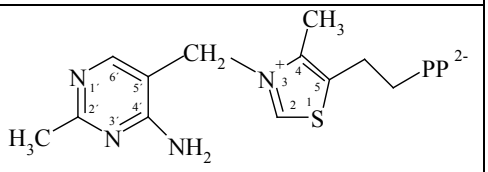
N3´-Pyridyl ThDP	isosbestic point at 297.6 nm, $\varepsilon_{297.6\ nm}$ = 5900 $M^{-1} * cm^{-1}$	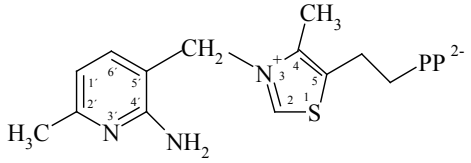
1,2-Dihydroxy-3deaza ThDP	isosbestic point at 245nm, $\varepsilon_{245\ nm}$ = 10280 $M^{-1} * cm^{-1}$	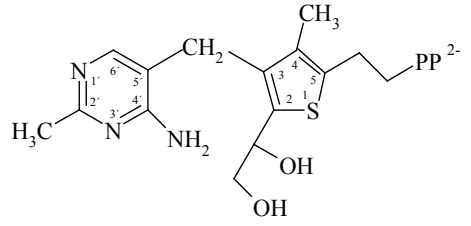

2.2.3.2. Synthesis of Sedoheptulose 7-Phosphate

The native TK substrate S7P is not commercially available and was synthesized relying on a protocol of Charmantray et al. (Charmantray et al., 2009) with some modifications. Ribose 5-phosphate (1.375 mmol) was diluted in 2.875 ml 50 mM glycylglycine, 2 mM ThDP, 6 mM $CaCl_2$, pH 7.6 containing 84 U *Ec*TK. Every 6 min 100 µl of a solution containing 27.5 µmol β-hydroxypyruvate, 2 mM ThDP, 6 mM $CaCl_2$, 50 mM glycyl-glycine (pH 7.6) was titrated into the R5P solution. The reaction was stirred slowly at 22 °C. After 6 h the sample was cooled on ice and 3 volumes of methanol were added slowly while the reaction was stirred. The enzyme was pelletized by centrifugation (15 min, 4 °C, 4500 rpm) and the supernatant was supplemented with 1.875 mmol $BaCl_2$ diluted in 1.25 ml H_2O

(pH 6.0). After 15 min incubation on ice the sample was centrifuged (15 min, 4 °C, 4500 rpm) and the pellet was discarded. The supernatant was mixed with 5 volumes ethanol and incubated for 90 min on ice. The barium salt of S7P was then pelletized by centrifugation (20 min, 4 °C, 11000 x g) and washed twice with 40 ml ethanol and finally with 40 ml diethylether.

For usage in enzymatic assays and for crystallization studies the S7P barium salt had to be converted into a disodium salt using a cation exchanger. For this purpose 50 to 100 mg of the barium salt were diluted in H_2O and loaded onto a self packed cation exchange column consisting of approx. 2 g Dowex 50 x 8 H^+. The column was previously equilibrated with diluted NaOH solution (pH 8-9). After mixing of the barium salt with the column material and incubation for 10 min at RT, S7P was finally eluted with 8 ml of NaOH solution (pH 8-9). The pH of the eluted fractions was then adjusted to 7. After lyophyllization, S7P sodium salt was stored at –20 °C until usage.

2.2.4. Kinetic Methods

2.2.4.1. Steady-State Activity Assay

The enzymatic activity of *h*TK and *Ec*TK for conversion of the native substrates xylulose 5-phosphate (X5P) and ribose 5-phosphate (R5P) into sedoheptulose 7-phosphate (S7P) and glyceraldehydes 3-phosphate (G3P) was monitored spectrophotometrically in a steady state assay using the auxiliary enzymes triose-phosphate isomerase (TIM) and *sn*-glycerol-3-phosphate: NAD^+ 2-oxidoreductase (G3P-DH) to detect formation of G3P (Fig. 10). The concomitant oxidation of NADH was followed at 340 nm in 50 mM glycylglycine, pH 7.6, at 30 °C (*h*TK) or 25 °C (*Ec*TK). The assay was performed in a total volume of 200 µl and further contained 0.22 mM NADH, 3.6 units of *sn*-glycerol-3-phosphate: NAD^+ 2-oxidoreductase/triose-phosphate isomerase, 100 µM ThDP, 5 mM $CaCl_2$, 0.1–2 mg/ml *h*TK or 0.05-0.5 mg/ml *Ec*TK, and variable concentrations of X5P and R5P. One unit is defined as the formation of 1 µmol of G3P per min. In order to determine the K_M values for X5P and R5P, the concentration of one substrate was kept constant at 1 mM X5P or 5 mM R5P.

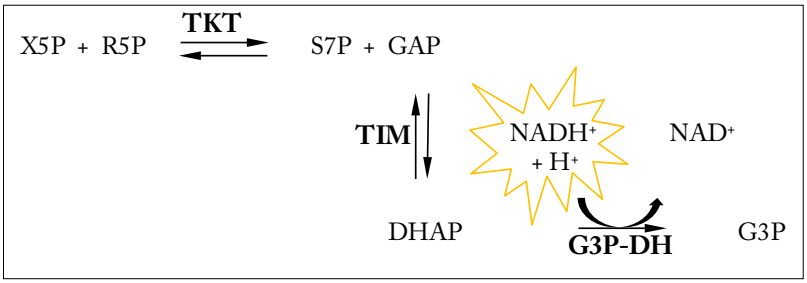

Fig. 10: Schematic presentation of the spectrophotometric activity assay for transketolase. TK-dependent production of glyceraldehyd 3-phosphate (GAP) is linked to the formation of glycerol 3-phosphate (G3P) using two auxiliary enzymes; TIM and G3P-DH (see text).

The dependency of the initial rates on the substrate concentration was analyzed according to eq. 1.

$$v = \frac{Vmax * [S]}{K_M + [S]}$$

Vmax = maximal velocity

K_M = Michaelis constant

eq. 1: Michaelis-Menten equation.

2.2.4.2. Steady-State Activity Assay – Inhibiton by Substrate Analogues

The capability of substrate analogues to act as competitive inhibitors was analyzed quantitatively using the coupled activity assay described above. The concentrations of R5P and X5P were adjusted to 0.2 mM and the concentration of the individual analogues was varied. For measurements with analogues present as barium salts the auxiliary enzymes, which are stored as a 4.8 M ammonium sulfate suspension, had to be dialyzed against 50 mM glycylglycine, pH 7.6 before usage.

2.2.4.3. Fast Kinetics-Stopped Flow Absorbance Spectroscopy

The stopped-flow technique is a rapid mixing method with a dead time of approx. 1.5 ms enabling the visualization of fast kinetic events. The stopped-flow and sequential stopped-flow measurements with *Ec*TK were performed with a stopped-flow spectrophotometer SX.18 MV or SX.20 MV at single wavelength. Furthermore, the formation of enzyme-bound DHEThDP intermediate was monitored using diode array detection. Time-resolved spectra were collected in equidistant time intervals. Experiments were generally performed at 25 °C with an optical path length of 1 cm. The absorption at any wavelength was generally normalized with water.

Single mixing experiments

Single wavelength measurements were performed at a wavelength between 295-325 nm. Enzyme and substrates were mixed in all cases in a 1 to 1 ratio. The final concentrations of enzymes, cofactors and substrates after mixing are shown in the figures in the results part.

Sequential mixing experiments

Sequential mixing experiments were performed to study the reaction of enzyme-bound dihydroxyethyl thiamin diphosphate intermediate (DHEThDP) with acceptor substrates. Therefore the DHEThDP formed in a first mixing experiment of enzyme and β-hydroxypyruvate (both at the same concentration) was mixed after an optimal time interval with the acceptor substrate. Optimal time points for the second mixing step, which is the time of highest concentration of enzyme-bound DHEThDP intermediate, were obtained from single mixing experiments. For *Ec*TK wt this interval was 10 s and *Ec*TK $His^{473}Ala$ 100 s. The final concentrations of enzymes, cofactors and substrates after the second mixing step are shown in the figures in the results part.

2.2.5. Biophysical Methods

2.2.5.1. Isothermal Titration Calorimetry

Isothermal titration calorimetry (ITC) allows the direct and quantitative characterization of the thermodynamics of binding events. From one optimal ITC experiment the association constant, the binding enthalpy, the binding entropy and the stoichiometry of a binding event can be calculated. For our studies we utilized the VP-ITC system or the ITC_{200} system both using the power compensation method. ITC was used to investigate the interaction between *Ec*TK or variants thereof with donor or acceptor substrates. Due to the fact, that acceptor sugars are just bound and not converted by holo *Ec*TK we could use the native cofactor ThDP. For all ITC experiments with the donor sugars ThDP was replaced with the analogue N3´-Pyridyl-ThDP. *Ec*TK reconstituted with this analogue is able to bind but not to convert donor substrates.

The enzyme (10 mg/ml) was dialyzed twice for 12 h at 8 °C against 300 ml 50 mM glycylglycine, 5 mM $CaCl_2$, pH 7.6. In case the samples were used for measurements with acceptor substrates or analogues thereof the dialysis buffer contained 1mM ThDP. The substrates were dissolved in the second dialysis buffer. If necessary the pH was adjusted to pH 7.6. The ITC cell was filled with 7.2 mg/ml *Ec*TK (100 µM active sites), 300 µM N3´-Pyridyl-ThDP (for experiments with donor substrates) or 1 mM ThDP (for experiments with acceptor substrates), 50 mM glycylglycine, pH 7.6. The injection syringe was filled with 10 to 15 mM of the individual substrate, 300 µM N3´-Pyridyl-ThDP (for experiments with donor substrates) or 1 mM ThDP (for experiments with acceptor substrates), 5 mM $CaCl_2$, 50 mM glycylglycine, pH 7.6. Measurements were generally performed at 8 °C with a stirring speed of 300 min^{-1} (VP-ITC) or 1000 min^{-1} (ITC_{200}). To check for artificial heat effects due to dilution, substrates were titrated into the cell just containing 300 µM N3´-Pyridyl-ThDP (for experiments with donor substrates) or 1 mM ThDP (for experiments with acceptor substrates), 50 mM glycylgycine, pH 7.6. The heat produced or consumed in those experiments was subtracted from the real titration experiment during data analysis with the integrated software. The final amounts of heat per injection were fitted according to a 1:1 binding model. The stoichiometry was set to 1 because of the very low affinity of the interaction and the resultant hyperbolic shape of the thermograms. Since the concentration determination of the titrant is accurate this restrain is acceptable and fitting of the binding curve benefits thereof (Freyer and Lewis, 2008).

ITC was also used to determine the enthalphy for the carboligation reaction of donor substrate xylulose 5-phosphate (X5P) with *Ec*TK (reconstituted with ThDP). For those experiments the ITC cell was filled with 1.8 mg/ml *Ec*TK (25 µM active sites), 300 µM ThDP, 1 mM $CaCl_2$, 50 mM glycylglycine, pH 7.6. The injection syringe was filled with 375 µM X5P, 300 µM ThDP, 1 mM $CaCl_2$, 50 mM glycylglycine, pH 7.6. After one single injection the experiment was analyzed and the

enthalpy was determined by integration. Since a small part of the overall enthalpy is generated by X5P binding this part, that was determined in an independent experiment, was subtracted.

2.2.5.2. Circular Dichroism Spectroscopy

Circular dichroism spectra were recorded for *h*TK, *Ec*TK and active site variants of both enzymes in the far UV and in the near UV/Vis range with a Chirascan CD-spectropolarimeter to quantify secondary structure elements as well as to analyze binding of cofactors. Spectra in the far UV range were collected from 180-260 nm with a path length of 1 mm at different temperatures in 50 mM sodium phosphate buffer. Spectra in the near UV/Vis range were collected from 280-450 nm with a path length of 1 cm. A detailed description of sample ingredients can be found in the individual figure legend. Thermal stability of transketolase was analyzed by circular dichroism performing heat induced transitions from 20 °C to 94 °C with the following parameters:

- detection at 222 nm
- step 0.5, rate 2.0 °C min
- tolerance 0.2 °C
- time per point 12 s
- duration of scan 17 s

The midpoint of the thermal transition was determined according to eq. 2. This equation holds true for reversibly unfolding proteins. For irreversibly unfolding proteins like TK the thermal transitions are dependent on the heat rate and on the duration at a certain temperature. The transition midpoint of unfolding is therefore an apparent value which can be used to compare different protein measured under the same parameterization.

$$y = \frac{(yf + mf * T) + (yu + mu * T)\ \exp\left[\frac{\Delta Hm}{R * T}\right] * \left[\frac{T - Tm}{T}\right]}{\left[\frac{\Delta Hm}{R * T}\right] * \left[\frac{T - Tm}{T}\right]}$$

eq. 2: Determination of the apparent midpoint for thermal unfolding (Pace et al., 1998).

y	=	CD signal at 222 nm
T	=	temperature (K)
Tm	=	midpoint of the thermal transition
R	=	ideal gas constant
ΔHm	=	enthalpy change of unfolding of Tm
yf, mf	=	baseline parameter of the folded protein
yu, mu	=	baseline parameter of the unfolded protein

2.2.5.3. Fluorescence-Based Thermal Stability Assay

The influence of different ions on the stability of holo *h*TK was analyzed by thermal induced unfolding. This method makes use of a fluorophore that exhibits a stronger fluorescence emission upon intercalation into the hydrophobic core of an unfolding or unfolded protein relative to folded and native protein. Since detection is fluorescence-based and will be performed in 96 well plates it is a powerful tool to screen with small amounts of protein for conditions of highest protein stability

(Ericsson et al., 2006). Given that *h*TK contains a structural sodium ion (Mitschke et al., 2010) we tested different concentrations of sodium chloride. In addition potassium chloride, magnesium chloride, imidazol and ThDP were tested for a putative, positive effect on thermal stability of *h*TK. Fluorescence-based thermal stability measurements were performed from 20 to 95 °C in 1 °C steps using a real-time PCR instrument (Department for Molecular Structural Biology, excitation 490 nm and emission 575 nm) and a 96 well plate. The total sample volume of 20 µl contained 9 µl of *h*TK stock solution (2 µM active sites in 50 mM glycylglycine, pH 7.6), 2 µl sypro orange (100 x) and 9 µl of additive solution. Samples were tested with this assay in doublets. All additives were tested alone and in combination with each other. The unfolding curves were normalized and the apparent unfolding temperature was determined with the integrated software.

2.2.5.4. Analysis of Covalent Reaction Intermediates by Acidic Quench ^{1}H-NMR-Spectroscopy

The NMR-based identification of covalent reaction intermediates is a powerful tool to analyze microscopic steps of catalysis of ThDP-dependent enzymes (Kluger and Tittmann, 2008; Tittmann et al., 2003). For that purpose enzymes will be incubated with substrates under steady state or pre steady state conditions, and the reaction will be quenched by addition of acid. After removal of the denatured enzyme the acid-stable reaction intermediates present in the supernatant can be analyzed by ^{1}H-NMR spectroscopy. For the TK reaction this approach enables quantitative analysis of different microscopic equilibria like the formation of the Michaelis complex, the formation and cleavage of the covalent donor intermediate, and in case for the overall reaction the ligation of an acceptor aldose with the first cleavage product.

We used this method to analyze the donor-half reaction (just donor present) or the overall-reaction (donor and acceptor present) of TK. Due to the fact that free ThDP falsifies the results of this approach, enzymes were purified as holo enzyme (*h*TK) or as apo form and reconstituted in equimolar amounts of ThDP (*Ec*TK). In a standard experiment 200 µl of 15 mg/ml enzyme (219 µM active sites *h*TK or 208 µM acitve sites *Ec*TK) were mixed with 200 µl of 50 mM substrate and generally incubated for 1 min at 8 °C if not mentioned elsewhere. The reaction was stopped by addition of 200 µl of 12.5 % (w/v) trichloroacetic acid, 3.7 % (v/v) HCl in D_2O, pH 0.75. Faster reactions were initiated and stopped in a quench-flow apparatus (performed by Prof. Dr. Kai Tittmann). Denatured samples were incubated for 5 min at 8 °C and the precipitated enzyme was pelletized by centrifugation (5 min, 14000 rpm, 4 °C). The supernatant containing the acid-stable cofactor and substrate-cofactor adducts was filtered and then analyzed in a NMR spectrometer. NMR data collection was performed by Elisabeth Koers, Cindy Wechsler or Prof. Dr. Kai Tittmann (internal standard 3-(trimethylsilyl) propionic-2,2,3,3-d_4 acid) using optimized, dedicated parameters (Tittmann, 2000). Data analysis was performed with *MestreNova* and *SigmaPlot*.

2.2.5.5. Determination of the Protonation State of Enzyme-bound ThDP by a pH/Solvent Jump ^{1}H-NMR Spectroscopy Method

Apo *Ec*TK was transferred into 50 mM glycylglycine in D_2O, pD 7.6 by 6 cycles of ultrafiltration. Highly concentrated apo *Ec*TK (100 µl of 1 or 2 mM active sites apo *Ec*TK (72 or 144 mg/ml)) was reconstituted with equimolar amounts of ThDP (in D_2O), 10 mM $CaCl_2$ in 50 mM glycylglycine (pH 7.6) and incubated for 20 min on ice. The pH/solvent jump was performed by manual addition of 10 ml 20 % (w/v) formic acid in H_2O (Fig. 11).

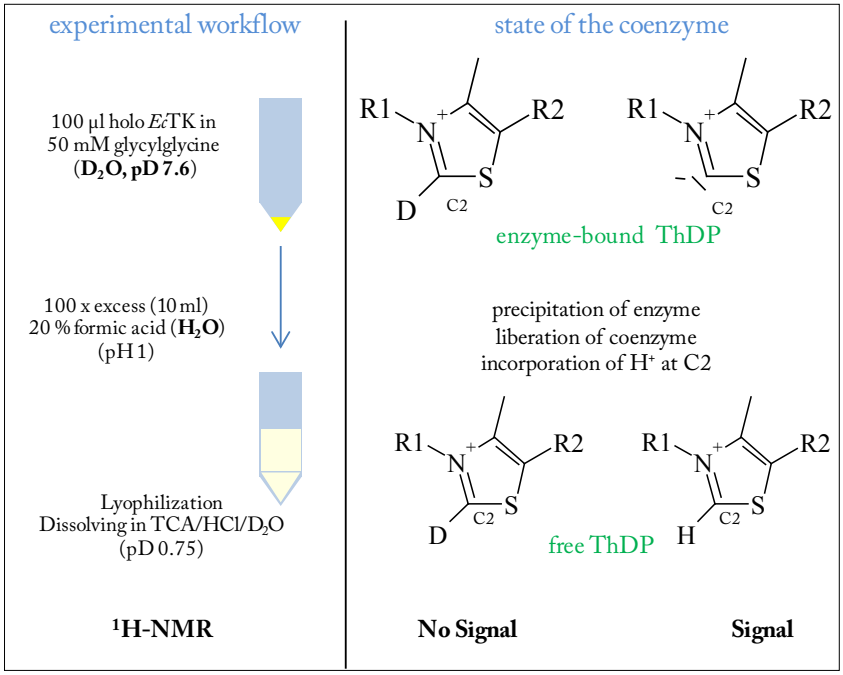

Fig. 11: Scheme for a pH/solvent jump approach. Left side: experimental workflow including sample preparation followed by signal detection by ^{1}H-NMR spectroscopy. For detailed explanation see text. **Right side:** protonation state of ThDP before (top, enzyme-bound) and after (bottom, free) the pH/solvent jump. Please note that solely protonated ThDP possesses a ^{1}H NMR signal.

Therefore the 100 µl sample was transferred to the bottom of a 50 ml tube and the 10 ml quench solution was added quickly. The samples were shock cooled in liquid N_2, lyophilized at -54 °C and 0.1 mbar for approximately 30-35 h and then stored until usage at -80 °C. Lyophyllized samples were dissolved in 900 µl of 4.16 % (w/v) TCA, 1.23 % (v/v) DCl in D_2O and vortexed intensively for 3 min. The protein was pelletized by centrifugation (5 min, 14000 rpm, 4 °C) and the filtrated supernatant was analyzed by ^{1}H NMR spectroscopy. NMR-data collection was performed by Cindy Wechsler. Previously enzyme-bound cofactor that was undeuterated at C2 will show a signal in this ^{1}H-NMR spectra due to incorporation of a proton whereas deuterated C2 will be spectroscopically

silent. Given that the pH of the NMR sample is 0.75 an undesired, later D/H exchange is very unlikely. The experiments rely on a protocol established by Elisabeth Koers (Koers, 2010).

The pK_A of enzyme bound ThDP C2 was calculated according to the eq.3.

$$pH = pK_A + \log 10 \left[\frac{A^-}{HA} \right]$$

A^- = concentration of conjugated base
HA = concentration of conjugated acid

eq. 3: Handerson-Hasselbalch equation.

2.2.5.6. X-ray Crystallography

X-ray diffraction datasets, which were collected in-house or at different synchrotron radiation facilities (EZB, ESRF, SLS), were processed with *XDS* (Kabsch, 2010). Protein models were iteratively refined and improved with *REFMAC 5* (Murshudov et al., 1997), *PHENIX* (Adams et al., 2010 a) or *SHELXL-11* (Sheldrick, 2008) and finally validated with *MOLPROBITY* (Davis et al., 2007). Data collection- and structure refinement statistics can be found in the appendix.

2.2.5.6.1. *Crystallization*

Crystals were grown using the vapor diffusion method in hanging drops relying on crystallization conditions reported by Asztalos *et al.* (*Ec*TK) and Mitschke *et al.* (*b*TK) (Asztalos, 2007 b; Mitschke et al., 2010). In both cases the quality of crystals could be significantly improved by macroseeding.

*H*TK, purified as holo enzyme, was concentrated to 14-18 mg/ml in 50 mM glycylglycine (pH 7.9), supplemented with 1 mM ThDP and 5 mM $CaCl_2$ and incubated for 20 min on ice. 3 µl of protein solution was mixed in a 1:1 ratio with a reservoir solution containing 13-15.5 % (w/v) PEG 6000, 4 % PPG 400, 2 % glycerol, 50 mM glycylglycine at pH 7.9. Apo *b*TK was crystallized after incubation for 20 min on ice with cofactor analogues at a concentration of 0.3–1 mM and 5 mM $CaCl_2$.

*Ec*TK, purified as apo enzyme, was concentrated to 16-20 mg/ml in 50 mM glycylglycine (pH 7.9), supplemented with 5 mM ThDP or 0.3-1 mM N3ThDP and 5 mM $CaCl_2$ and incubated for 20 min on ice. 3 µl of protein solution was mixed in a 1:1 ratio with a reservoir solution containing 17-22 % (w/v) PEG 6000, 2 % glycerol, 50 mM glycylglycine at pH 7.9.

Macroseeding was performed for both TKs 24 h after initial preparation of the crystallization drops at 6-8 °C. For that purpose previously obtained crystals were transferred into a 5 µl crystallization drop and crushed with a fine needle. Traces of such seeds were transferred into each new crystallization drop. Seeding-induced crystal growth occurred within 3-5 days at 6-8 °C. Prior flash-cooling in liquid nitrogen the crystals were incubated for 5-10 s in cryo-solution containing 20 % (w/v) PEG 6000 and

30 % (v/v) ethylene glycol in 50 mM glycylglycine, 0.3-1 mM ThDP analogue or 5 mM ThDP, 10 mM $CaCl_2$ (pH 7.9).

2.2.5.6.2. *Substrate Soaking*

For substrate soaking experiments (Fig. 12 and Tab. 3) the cryo solution was additionally supplemented with substrate and single crystals were transferred into the soaking solution for a defined time at 8 °C. If necessary the pH of the soaking solution had to be adjusted to 7.9. In order to trap the dihydroxyethyl-ThDP intermediate in *h*TK and *Ec*TK single crystals of each enzyme were soaked in 20 mM β-hydroxypyruvate resolved in cryo solution 2 (Cryo2: 10 % (w/v) PEG 6000, 15 % (v/v) ethylene glycol in 50 mM glycylglycine, pH 7.9) for 3 to 20 min and were then transferred into another cryo-solution (Cryo1: 20% (w/v) PEG 6000, 30% (v/v) ethylene glycol, 5 mM ThDP, 10 mM $CaCl_2$ in 50 mM glycylglycine, pH 7.9) for 5-10 s before flash-cooling. Individual soaking conditions for all structures presented in this manuscript are listed in Tab. 3. All crystals were stored in liquid nitrogen until measurement.

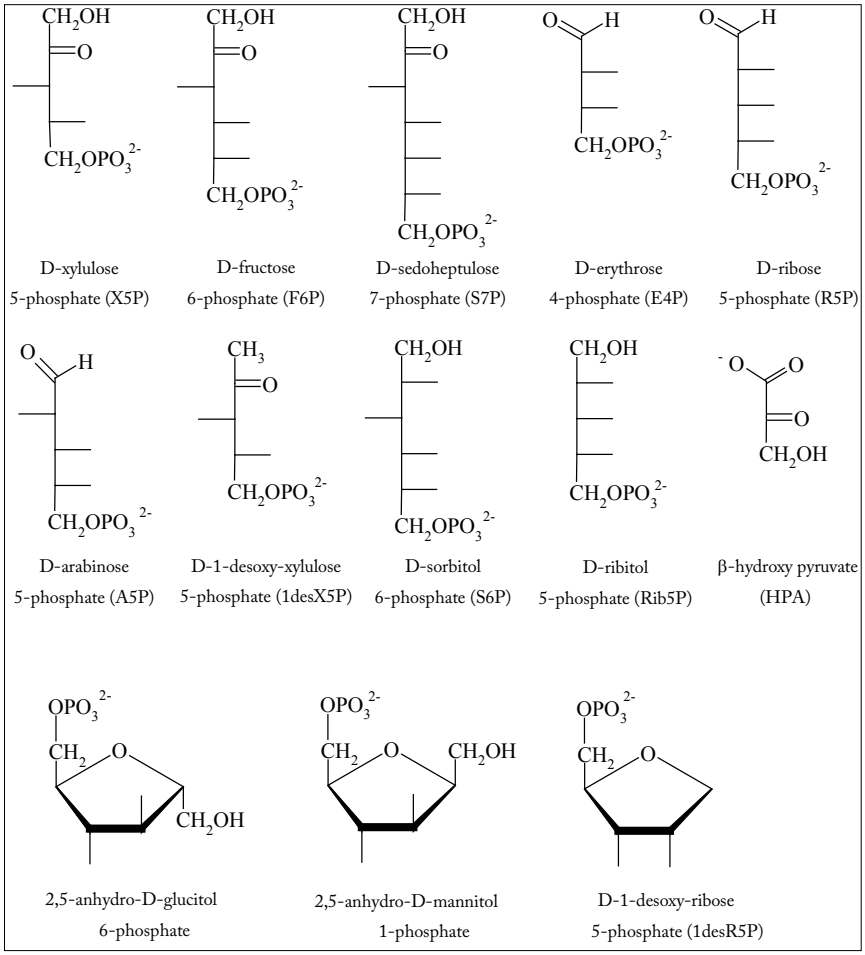

Fig. 12: Substrates and substrate analogues used for substrate soaking experiments. All sugar phosphates are depicted in Fischer projection except 2,5 anhydro-D-glucitol 6-phosphate, 2,5 anhydro-D-mannitol 1-phosphate and D-1-desoxy ribose 5-phosphate (Harworth projection). Note that D-fructose 6-phosphate, D-sedoheptulose 7-phosphate, D-ribose 5-phosphate and D-arabinose 5-phosphate can also adopt different cyclic semiacetal forms not depicted here. All substrates which harbor a free aldehyde or keto functionality could in principle be hydrated in aqueous solution.

2.2.5.6.3. *Data Collection In-House*

A highly redundant dataset of *h*TK determined to 1.717 Å was collected from a single crystal in-house in a nitrogen cryostream (130-140 K, XSTREAM2000, Rigaku/MSC, Japan) with an R-AXIS IV++ imaging-plate system (Rigaku/MSC, Japan) using CuKα radiation (wavelength 1.5418 Å) generated by a Rigaku MM-007 rotating-anode generator. All crystals measured at synchrotrons were tested for diffracting properties and overall quality (mosaicity, twinning etc.) first on an in-house generator.

2.2.5.6.4.*Data Collection at the Synchrotron*

High-resolution datasets were collected at different synchrotron sources (Swiss Light Source (SLS) in Villingen, European Synchrotron Radiation Facility (ESRF) in Grenoble, Helmholtz-Zentrum Berlin für Materialien und Energie (HZB)) at cryogenic temperatures.

In order to obtain complete datasets for the high and low resolution part of well defracting crystals (better than 1.2 Å) we collected at least one low resolution dataset with short exposure times and a weak total dose to a maximum resolution of 1.4–1.6 Å. In addition to that high resolution datasets were collected from the same piece with longer exposure times to collect the high resolution part. High and low resolution datasets were afterwards merged with *XDS* (Kabsch, 2010). For *ß*TK (crystal size: 0.2 mm * 0.1 mm * 0.1 mm) and *Ec*TK (crystal size: 1.0 mm * 0.3 mm * 0.3 mm) multiple high-resolution datasets (40-100°) from one single crystal were collected. Care has been taken to choose the size of the translation which had to be long enough in order to prevent effects of radiation damage resulting from previous x-ray exposition. Datasets showing best resolution and statistics were merged afterwards and used for structure refinement. All datasets revealed no signs of detectable radiation damage as evidenced by low R_{merge} (analysis of R_{merge} vs batch plot).

Tab. 3: Substrate soaking conditions and data collection information for all presented crystal structures.

Structure	Beamline	Soaking Conditions	Resolution (Å)
*ß*TK	SLS PXII	10 s (Cryo1)	1.16
*ß*TK	in-house	10 s (Cryo1)	1.717
*ß*TK + N3ThDP	SLS PXII	10 s (Cryo1 + 0.3 mM N3ThDP instead of ThDP)	1.3
*ß*TK + N3ThDP + xylulose 5-phosphate	HZB14.1	4 min, 100 mM X5P (Cryo1, 0.3 mM N3ThDP instead of ThDP)	1.15
*ß*TK + N3ThDP + fructose 6-phosphate	HZB14.1	6 min, 100 mM F6P (Cryo 1, 0.3 mM N3ThDP instead of ThDP)	1.2
*ß*TK + ThDP + sedoheptulose 7-phosphate	SLS PXII	6 min, 100 mM S7P (Cryo 1, 0.3 mM N3ThDP instead of ThDP)	1.37
*ß*TK + 2,5-anhydro-glucitol 6-phosphate	HZB 14.1	2min, 100 mM 2,5-anhydro-glucitol 6-phosphate (Cryo1)	1.09
*ß*TK + 2,5-anhydro-mannitol 1-phosphate	HZB 14.1	2min, 100 mM 2,5-anhydro-mannitol 1-phosphate (Cryo1)	1.14
*ß*TK +sorbitol 6-phosphate	HZB14.1	3 min, 100 mM S6P (Cryo1)	1.45
*ß*TK + xylulose 5-phosphate	ESRF ID 14.3	1min, 100 mM X5P (Cryo1)	0.97
*ß*TK + fructose 6-phosphate	ESRF ID 14.3	1min, 100 mM F6P (Cryo1)	0.98
*ß*TK + sedoheptulose 7-phosphate	HZB14.1	3 min, 100 mM S7P (Cryo1)	1.03

*h*TK + arabinose 5-phosphate	HZB14.1	3 min, 100 mM A5P (Cryo1)	0.99
*h*TK + 1desoxy-xylulose 5-phosphate	ESRF ID 14.3	3min, 100 mM 1desX5P (Cryo1)	1.09
*h*TK + β-hydroxypyruvate	HZB14.1	3 min, 20 mM HPA (Cryo2)	1.45
*h*TK + 1,2dihydroxy-3-deaza ThDP	HZB 14.1	10 s (Cryo1)	1.26
*h*TK + erythrose 4-phosphate	HZB 14.1	1 min, 100 mM E4P (Cryo1)	1.14
*h*TK + ribose 5-phosphate	HZB 14.1	1 min, 100 mM R5P (Cryo1)	1.2
*h*TK + ribitol 5-phosphate	HZB 14.1	12 min, 100 mM ribitol 5-phosphate (Cryo1)	1.18
*h*TK + 1desoxy-ribose 5-phosphate	ESRF ID 14.3	17 min, 100 mM 1desR5P (Cryo1)	1.15
*h*TK +β-hydroxypyruvate	HZB14.1	3 min, 20 mM HPA (Cryo2)	1.45
*Ec*TK	SLS PXII	10 s (Cryo1)	1.048
*Ec*TK +β-hydroxypyruvate, 20 min	ESRF ID 14.3	20 min, 20 mM HPA (Cryo2)	0.97
*Ec*TK + N3ThDP	SLS PXII	10 s (Cryo1)	0.97
*Ec*TK + N3ThDP + xylulose 5-phosphate	SLS PXII	4 min, 100 mM X5P (Cryo1, 0.3 mM N3ThDP instead of ThDP)	1.4
*Ec*TK + ribitol 5-phosphate	ESRF ID 14.3	5 min, 100 mM ribitol 5-phosphate (Cryo1)	0.974
*Ec*TK + 1desoxy-ribose 5-phosphate	HZB14.1	10 min, 100 mM 1desoxy-ribose 5-phosphate (Cryo1)	1.028
*Ec*TK + E4P	HZB14.1	3 min (Cryo1)	1.4
*Ec*TK $His^{473}Ala$ + R5P	in-house	10 min (Cryo1)	1.8

2.2.5.6.5.*Data Processing*

Datasets were generally processed with *XDS*. Friedel pairs have been always merged despite for the high redundant dataset of *h*TK measured in-house to 1.717 Å. This dataset was collected to detect a weak anomalous signal that was used to confirm the presence of enzyme-bound ions. In case that several datasets were collected from one single crystal all datasets were processed and if possible best parts were merged with *XDS*. Data processing was mainly accomplished by Dr. Piotr Neumann (Department for Molecular Structural Biology, University of Göttingen).

2.2.5.6.6.*Molecular Replacement*

Molecular replacement was carried out for the three newly found polymorphic crystal forms of *h*TK in monoclinic space group $P2_1$ with *MOLREP* (Vagin and Teplyakov, 1997) or *PHASER* (McCoy, 2007).

As a result of different arrangements of *h*TK molecules in the crystalline state the enzyme was already found to be present either in monoclinic space group C2 (Mitschke et al., 2010) or in the hexagonal space group $P6_1$ (Structure deposited 2009 by Krojer and coworkers, structural genomics consortium,

SGC). In addition we could crystallize *h*TK in monoclinic space group $P2_1$ and found three different unit cells for this space group all significantly differing in cell length (Tab. 4). Noteworthy, the observed packing polymorphism doesn´t originate from different crystallization conditions since we found crystals with different unit cell parameters within one crystallization drop.

Tab. 4: Polymorphism of *h*TK in the crystalline state. Space groups found for *h*TK crystals and properties thereof. Matthew coefficients (Matthews, 1968) were calculated with matthews-coef program from CCP4 suite (Bailey, 1994).

	C2	$P6_1$**	$P2_1$ Form C	$P2_1$ Form B	$P2_1$ Form A
a (Å)	113.7	117.2	109.6	73.2	73.5
b(Å)	86	117.2	78.3	85.6	77.9
c (Å)	73	176.8	146.9	92.6	112.1
α (°)	90	90	90	90	90
β (°)	125.3	90	94	94.1	92.3
γ (°)	90	120	90	90	90
monomers per asymmetric unit	1	2	4	2	2
matthews coefficient	2.16	2.03	2.36	2.17	2.4
solvent content (%)	43.0	39.4	47.8	43.3	48.8
best resolution (Å)	0.97	2.05	1.37	1.259	1.15

The structure of *h*TK crystallized in $P2_1$ Form A was solved using the 1.75 Å resolution structure of *h*TK crystallized in C2 (Mitschke et al., 2010) as search model. The biological unit of *h*TK is a dimer. The structure reported by Mittschke et al. crystallized with a monomer in the asymmetric unit and as a crystallographic dimer. Initial Matthew coefficient calculation suggested the presence of a dimer in the asymmetric unit for two polymorphic crystal forms. Hence, a dimeric search model was generated in *PYMOL* and successful utilized for structure solution of Form A by molecular replacement. Form A was then used as search model for the two other polymorphic crystal forms of *h*TK crystallized in space group $P2_1$. Analysis of the dataset of $P2_1$ Form C with 4 *h*TK monomers in the asymmetric unit revealed the presence of pseudo-translation. The position of the first dimer has been automatically found by the molecular replacement software. To complete the structure the second dimer was placed in the asymmetric unit applying the pseudo translation vector to the first dimer.

While the solvent content of those different crystal forms is very similar the best resolved structures were determined for space group C2. A structural alignment of *h*TK crystallized in space group C2 and $P2_1$ revealed just minor differences of less than in total 10-15 amino acids in the N- and C-termini. Aside from those few residues all main chains and side chains adopt very similar or even identical positions. Even the positions of numerous solvent molecules are identical. A closer inspection

further revealed no shielding of the active site entrance suggesting that all crystal forms can be used for substrate soaking experiments to trap reaction intermediates of the *h*TK reaction cycle.

2.2.5.6.7. *Model Building, Refinement and Validation*

Structure refinement was carried out using *PHENIX* (Adams et al., 2010 a) employing the maximum-likelihood method, with 1.5 to 5% of randomly chosen data for validation by the R_{free} factor (Brunger, 1992). After a first rigid body refinement against medium resolution (2-2.5 Å) using the until then best available model, water picking and refinement cycles against higher resolution data was performed in steps of 0.2 Å automatically in *PHENIX*. At a resolution of 1.4–1.2 Å the model was inspected manually with *COOT* (Emsley et al., 2010). Here, the conformation of side chains and the position of water molecules or other ligands were checked. For the atomic resolution datasets data in steps of 0.02 Å was included starting from 1.05 Å resolution. After each refinement cycle the model was checked and alternative conformations of side chains or solvent molecules were added in *COOT*. Starting from 1.4 Å atoms were generally refined with anisotropic B-factors. The positions of hydrogen atoms were added with *PHENIX.REDUCE* (Adams et al., 2010 a) starting from a resolution of 1.2 Å and refined using the riding model. Thereby no additional refinable parameters are generated but the contribution of hydrogens for x-ray scattering is taken into account.

Other refinement programs like *REFMAC 5* (Murshudov et al., 1997) or *SHELXL*-11 (Sheldrick, 2008) were used during the determination process of some structures. Refinement in *SHELXL-11* was carried out by conjugate-gradient least-squares methods on F2, with 1.5 -5 % randomly chosen data for validation by the R_{free} factor (Brunger, 1992). Restraints for bond distances in the proteins were used as provided by *SHELXPRO*. Bulk solvent correction and anisotropic scaling have been applied. Estimation of standard deviations (esd) of bond lengths and bond angles was carried out by full-matrix refinement using a pre-release version of *SHELXL*-11 that was kindly provided by Prof. George Sheldrick (Structural Chemistry, University of Göttingen). *SHELXL* refinements were predominantly performed by Dr. Piotr Neumann.
Restraints for ligands (buffer molecules, substrates and cofactors) for refinement with *PHENIX* were generated with the *PRODRG* server (Schuttelkopf and van Aalten, 2004). Bond lengths are discussed and compared relying on standard bond length derived from small molecule crystallography (Allen et al., 1987; Pletcher et al., 1979). Validation of the refined models was carried out using *COOT* and *MOLPROBITY*. Anomalous difference density map ((F+) - (F-)) was generated with *SIGMA A*, *CAD* and *FFT* (Bailey, 1994) using a final refined model as source of phases which were used to phase the calculated anomalous differences. Sigma A-weighted electron density maps (2mFo-DFc, mFo-DFc) were generated with *PHENIX* or *FFT*. Preparation of figures was carried out with *PYMOL*.

3. Results & Discussion

3.1. Structural and Functional Differences between human and *E. coli* Transketolase

*H*TK and *Ec*TK reveal unique structural (Mitschke et al., 2010) and functional characteristics (Schenk et al., 1998). Since those differences are important for a mechanistic understanding the most important ones are described here.

Both TKs share a high amino acid sequence similarity of 48 % (26 % sequence identity). The monomers of *h*TK (pdb-code: 3MOS) and *Ec*TK (pdb-code: 1QGD) can be superimposed with a root mean square deviation value of 2.3 Å and a high Dali Z score of 38.2 (586 C atoms were aligned) using the DaliLite v. 3 program (Holm and Rosenstrom, 2010) demonstrating a high structural similarity. While the overall fold of the dimeric enzyme and the topology of subunits or domains doesn´t deviate significantly between *h*TK and *Ec*TK a remarkably structural difference is detectable for the linker region (Linker 1 in Fig. 13) between the PP and Pyr domain. Whereas this region is unstructured in *h*TK, the corresponding segment in *Ec*TK is significantly longer (approx. 20 amino acids) and folds into a helix-turn-helix motif. Furthermore, several loops in *h*TK are shorter or completely missing which is a consequence of the smaller number of amino acid residues in *h*TK (623) in comparison to *Ec*TK (663) (for detail see Fig.75).

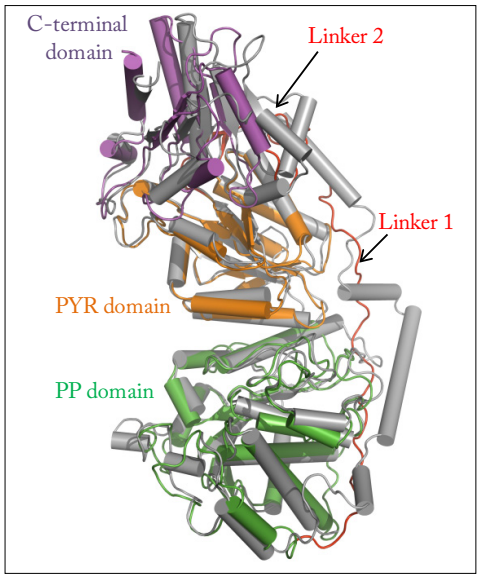

Fig. 13: Superposition of *h*TK and *Ec*TK monomers. The domain structure of bothTKs (*Ec*TK grey, pdb code: 1QGD; *h*TK colored, pdb code: 3MOS) is shown in cartoon presentation with α-helices as barrels, β-sheets as arrows and loops or unstructured parts as wires. The three domains of *h*TK are shown in different color code: N-terminal PP domain in green, middle PYR domain in orange and C-terminal domain in purple. Flexible linker of *h*TK are shown in red.

The active sites of both transketolases are well superimposable (Fig. 14). Aside from two amino acid exchanges all other residues necessary for substrate binding and catalysis are identical in both enzymes. Most importantly, a histidine residue (His473 in *Ec*TK) that is strictly conserved in non-mammalian TKs is replaced by a glutamine (Gln428 in *h*TK) (Schenk et al., 1997). Hence, a function of this residue as acid/base catalyst in mammalian TKs has to be excluded (Schneider and Lindqvist, 1998). The second amino acid exchange is that of an unpolar

isoleucine sitting atop of the cofactor thiazolium ring (Ile189 in *Ec*TK) that is replaced by polar glutamine in *h*TK (Gln189). Because this residue is always a hydrophobic residue in non-mammalian TKs that spans into the substrate binding site suggest a function for Gln189 in substrate binding and orientation in reactant states (Mitschke et al., 2010).

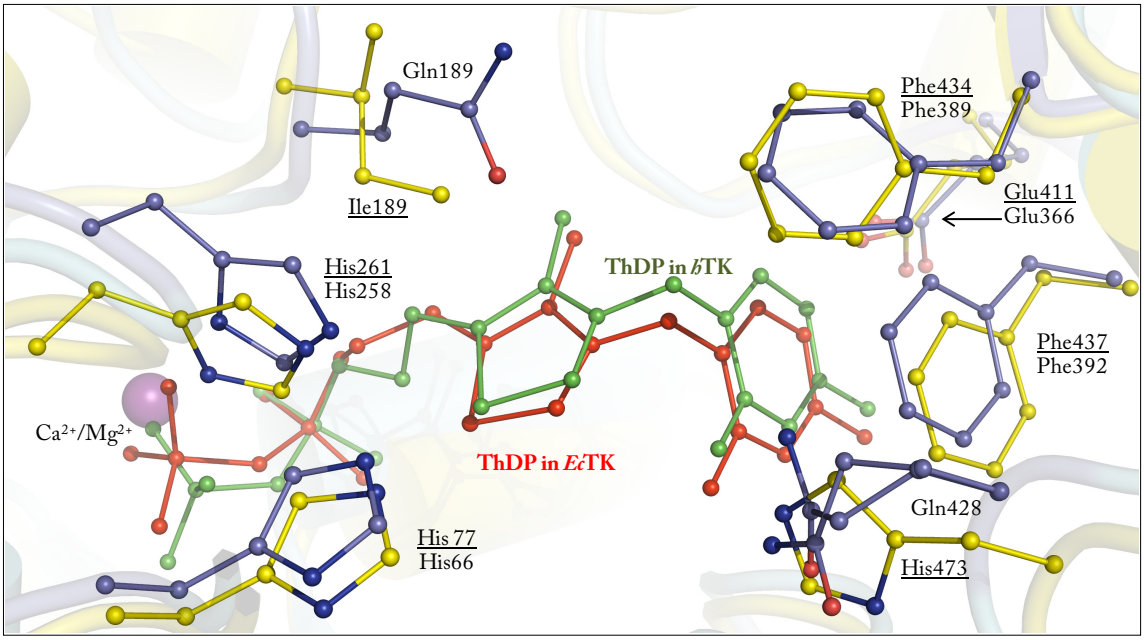

Fig. 14: Superposition of the active sites of *h*TK and *Ec*TK. Detailed view of the substrate binding pocket (cartoon presentation) onto the bound cofactor. For reasons of clarity just selected active site residues are shown and labeled (ball and stick representation, *Ec*TK (yellow), *h*TK (purple)). Labels belonging to *Ec*TK are underlined. ThDP bound to *Ec*TK (red) and *h*TK (green) as well as the bivalent cation are labeled.

A yet undescribed structural difference between both TKs is the conformation of the bound coenzyme which is difficult to observe by over-all superposition of both structures but well visible by individual alignment of both ThDP molecules as shown in Fig.15. While both cofactors adopt the canonical V-like conformation and are well superimposable for the aminopyrimidine (AP) and thiazolium (TH) ring, a positional difference is observable for the diphosphate moiety which functions to bind the cofactor to the enzyme. Additionally, ThDP bound to *Ec*TK adopts a more compact V-like conformation which is reflected by the small structural difference at the top of the AP ring.

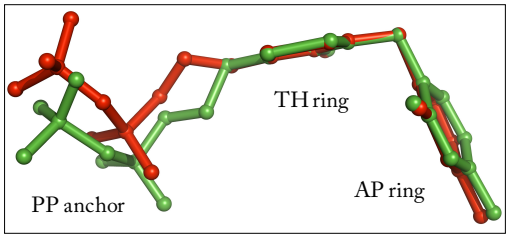

Fig.15: Superpositions of active-site bound ThDP in *Ec*TK (red) and *h*TK (green). Cofactors` aminopyrimidine- (AP ring) and thiazolium ring (TH ring) as well as the pyrophosphate moiety (PP anchor) are labeled.

For conversion of native substrates X5P and R5P *Ec*TK has a k_{cat} value of 40-50 s^{-1} (Asztalos, 2007 b; Sprenger et al., 1995) whereas k_{cat} values reported for *h*TK are approx. 3-4fold lower (Mitschke et al., 2010; Schenk et al., 1998). Furthermore, Schenk and colleagues reported a norrower substrate specificity of *h*TK relative to *Ec*TK (Schenk et al., 1998). Both kinetic differences are not yet understood.

Previous work (Mitschke, 2008) and initial kinetic and biophysical experiments revealed that human transketolase is prone to aggregation. Especially rapid mixing techniques, as well as working at moderate temperature (25 °C–37 °C) caused visible aggregation of the protein. Since protein aggregation is concentration dependent methods that require high protein concentrations are severely affected by this undesired site effect. To test if the presence of additives or/and cofactors have a positive effect on *h*TK stability/solubility a fluorescence based assay was performed. Here, we observe very similar apparent unfolding temperature in absence and presence (up to 700 mM) of different additives like NaCl, KCl, $MgCl_2$, imidazol and ThDP (data not shown). Moreover, the thermodynamic stability of *h*TK represented by a moderate, apparent unfolding temperature of 70.5 °C (Fig. 16) can be excluded as source of precipitation. Remarkably, apo (56.4 °C) and holo (58.2 °C) *Ec*TK have identical apparent unfolding temperatures, while apo *h*TK (55 °C) is thermodynamically unstable relative to holo *h*TK demonstrating a higher importance of cofactor binding for enzyme stability in *h*TK. These findings are in line with previous studies demonstrating that ThDP is irreversibly bound by *h*TK whereas *Ec*TK binds the coenzyme reversibly (Schenk et al., 1998; Wang et al., 1997). The molecular origin of this difference is currently under investigation in our group. Since we have yet solely determined the structure of apo *h*TK (data not shown) a structural comparison of both apo TKs is not feasible.

While protein crystallization worked well for *h*TK, other techniques (fast kinetics, ITC) could not be performed with the human enzyme as aggregation falsifies a quantitative analysis or makes it even impossible. For this reason we performed these methods solely with *Ec*TK. This TK offers additional advantages as it can be produced easily in very high amounts and stored for month without losing a considerably fraction of activity (Schenk et al., 1998).

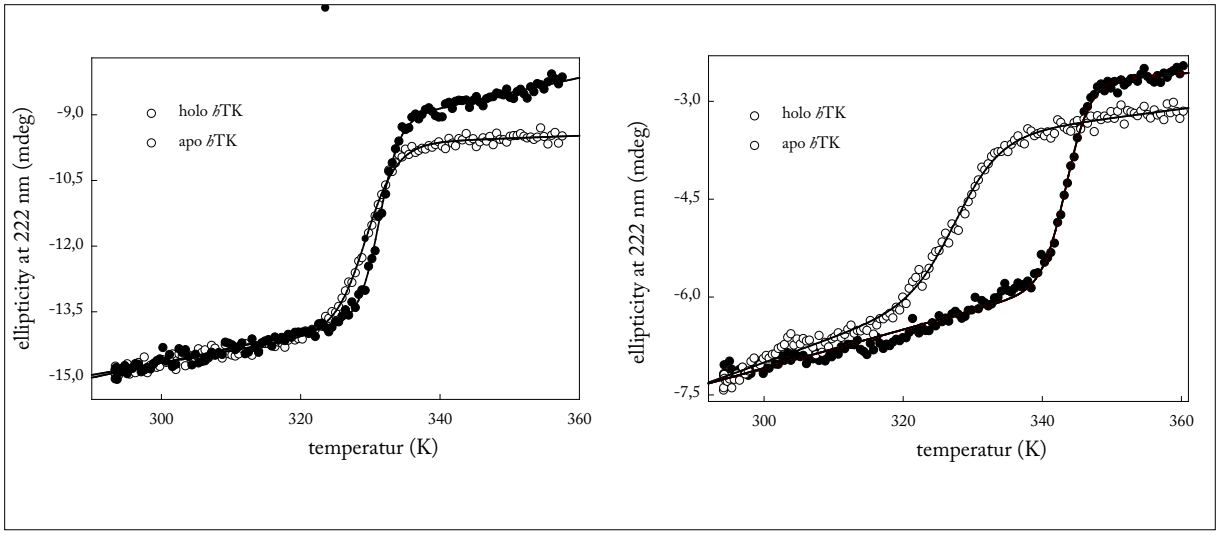

Fig. 16: Thermodynamic stability of *b*TK and *Ec*TK. Temperature-induced unfolding of of 100 µg/ml *b*TK or *Ec*TK in 50 mM Na phosphate (pH 7.5), 2.5 mM $MgCl_2$, in absence (apo) or presence (holo) of 300 µM ThDP. Data points were fitted (black lines) according to eq. 2 (Pace et al., 1998).

3.2. Kinetic Analysis of Elementary Catalytic Reaction Steps of *Ec*TK

Although macroscopic kinetic constants are available for a set of TKs (Asztalos, 2007 b; Mitschke et al., 2010; Schenk et al., 1998; Sprenger et al., 1995) microscopic constants for isolated reaction steps are rare (Asztalos, 2007 b; Fiedler et al., 2001; Golbik et al., 2005). For reasons of substrate availability and purity microscopic rate constant were determined for the reaction of F6P with R5P to form S7P and E4P (*Ec*TK, k_{cat} = 60-70 s^{-1})(Sprenger et al., 1995)

3.2.1. Kinetic Analysis of Donor-ThDP Intermediate Formation

To analyze the formation of covalent F6P-ThDP intermediates kinetically we performed stopped-flow absorbance spectroscopy experiments in absence of acceptor and assigned spectral signatures originating from covalent donor-coenzyme intermediates by ^{1}H NMR-spectroscopy.

It was previously shown that addition of donor substrate F6P to *Ec*TK causes an absorbance difference in the near UV range with a maximum between 295-305 nm and a minimum between 320-335 nm (Lüdtke, 2008) (Fig. 81) and that those two signals appeared with similar rate constants suggesting identical chemical origins. These spectral signatures probably reflect the protonation state of cofactors´ six-membered ring (295-305 nm IP form, 320-335 nm AP form).

To verify if these signals originate from the formation of covalent F6P-ThDP intermediate we quenched the reaction of *Ec*TK wt with 2.5 mM F6P after 8, 14 and 28 ms by addition of acid in a quench-flow device and analyzed the covalent reaction intermediates by NMR (MM). After 8 ms 28.6 % covalent F6P-ThDP intermediate is accumulated and this fraction just slightly increases after

14 ms (35.5 %) and 28 ms (35.8 %) (Fig.17). Noteworthy, no other covalent intermediates are formed under the chosen conditions. By plotting the fraction of F6P-ThDP intermediate against time-points of quenching a reaction transient was created and could be compared with a reaction kinetic monitored by stopped-flow absorbance spectroscopy (detection at 295 nm) under very similar conditions (Fig.17 b.), c.)). Aside from the fact that data points for the quenched-flow-transient between 0 and 8 ms are missing (instrument dead time) both transients are very similar and most likely monitor formation of F6P-ThDP. F6P-ThDP intermediate formation occurs very fast under the chosen conditions with an apparent rate constant of 960 ± 124 s^{-1}. Because the stopped-flow instrument has a dead time of 1-1.5 ms such fast kinetics are at the detection limit and exhibit smaller accuracy. Analogous kinetic experiments couldn´t yet been performed for the two other natural donor substrates X5P and S7P due to a limited availability of both compounds.

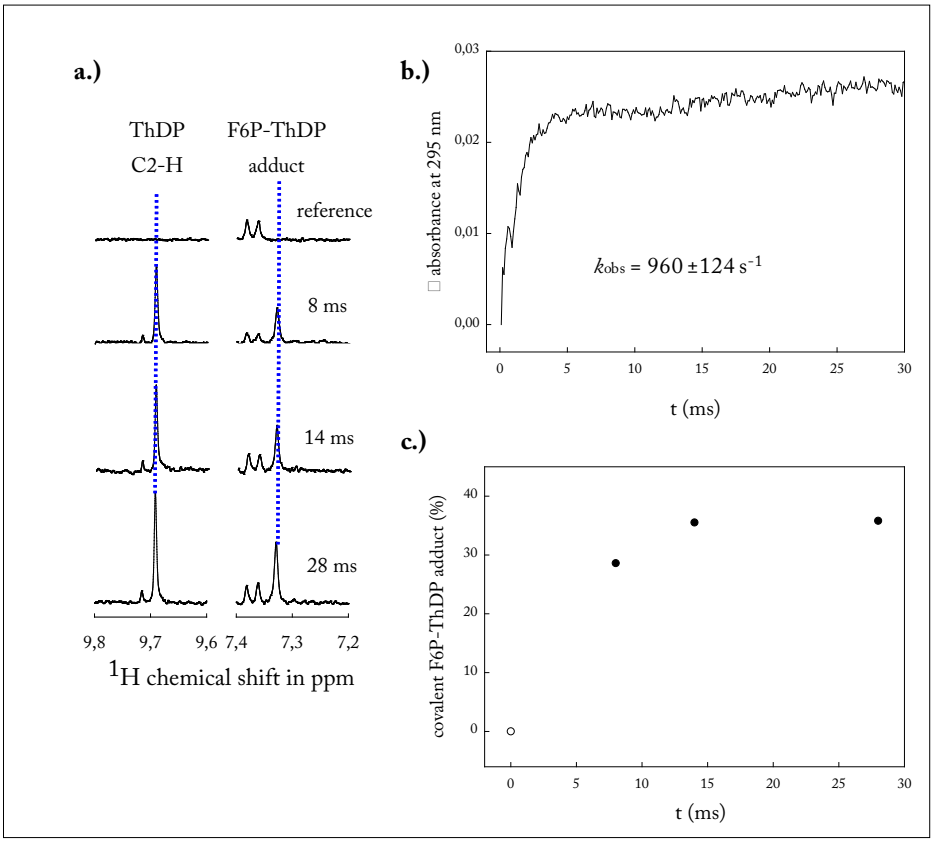

Fig.17: Kinetic analysis of F6P-ThDP intermediate formation by combination of ^{1}H-NMR- and UV-Vis-spectroscopy. a.) Acidic quenched-flow ^{1}H-NMR spectroscopic analysis for the reaction of 7.5 mg/ml *Ec*TK (104 µM active sites), 104 µM ThDP, 2.5 mM $CaCl_2$, 50 mM glycylglycine (pH 7.6) with 2.5 mM F6P at 25 °C (reference = F6P no TK). Reactions were initiated and stopped at defined time points by addition of acid in a quench-flow apparatus (performed by Prof. Dr. Kai Tittmann). Covalent intermediates were identified and quantified by ^{1}H NMR spectroscopy. The fraction of covalent F6P-ThDP adduct was plotted against time (**c.)**). **b.)** Stopped-flow absorbance transient (10 mm pathlength, detection at 295 nm) for the reaction of 2 mg/ml (27.8 µM active sites) *Ec*TK wt, 300 µM ThDP, 2.5 mM $CaCl_2$, 50 mM glycylglycine (pH 7.6) with 2.5 mM F6P at 25 °C. Fitting of the transient according to a double exponential equation gave the shown rate constant k_{obs} (k_{obs} = rate constant for first fast phase).

The very high rate constant for F6P-ThDP formation contradicts NMR-based H/D-exchange experiments monitoring the activation process of enzyme bound ThDP of approx. 350 s^{-1} (Asztalos, 2007 b). Since cofactor activation is a prerequisite for formation of covalent intermediates their formation can´t be faster than 350 s^{-1}. However, this is not the first experimental observation indicating a disagreement between the rates for H/D exchange and formation of substrate–cofactor intermediates (Weidner, 2010). Limitations of the H/D exchange method are discussed in detail elsewhere (Tittmann, 2000).

In order to determine more microscopic kinetic constants for this process we performed stopped-flow measurement with different concentrations of F6P. All reaction transients reveal a biphasic behavior indicating that two molecular processes are monitored at the chosen wavelength. By plotting the observed rate constants for the first and second phase against the utilized F6P concentrations a hyperbolic dependency for both phases is observable (Fig.18). The low quality of the data is reflected by the high errors determined by hyperbolic fitting making quantitative statements difficult. Both phases monitor fast kinetic events but show different apparent equilibrium constants (Ks_{app}). The first phase saturates earlier ($Ks_{app} \approx 0.26 \pm 0.33$ mM) and has an approximately two fold higher maximum rate constant ($k_{max} \approx 860 \pm 230\ s^{-1}$)

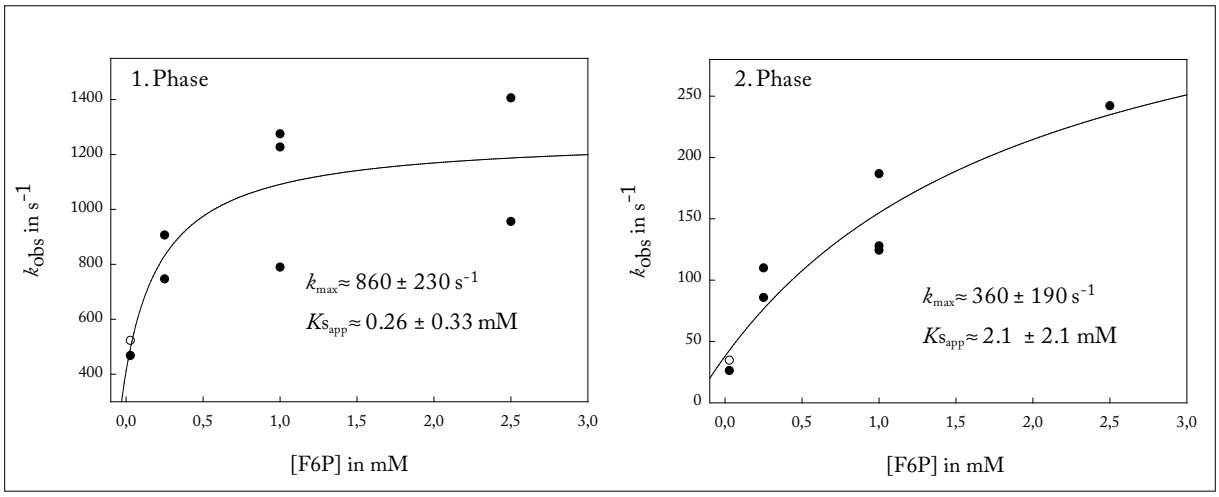

Fig.18: Kinetic analysis of F6P-ThDP intermediate formation by stopped-flow absorbance spectroscopy. Stopped-flow absorbance transients (10 mm pathlength, detection at 295 nm) for the reaction of 2 mg/ml (27.8 µM active sites) *Ec*TK, 300 µM ThDP, 2.5 mM $CaCl_2$, 50 mM glycylglycine (pH 7.6) with different concentrations of F6P at 25 °C. Fitting of the transient according to a double exponential equation gave two apparent rate constants (1. and 2. Phase) which were plotted against the utilized F6P concentration. Data points were fitted according to a hyperbolic equation.

The exact origin of both phases is so far not completely understood and has to be analyzed in more detail; for example at lower temperature and a higher number of data points.

3.2.2. Reaction of Transketolase-Bound DHEThDP Intermediate with Acceptor Substrate Ribose 5-phosphate

The reaction of enzyme-bound DHEThDP intermediate with increasing concentrations of acceptor substrate R5P was monitored using UV-Vis absorbance spectroscopy and double-jump stopped-flow mixing technique and analyzed quantitatively.

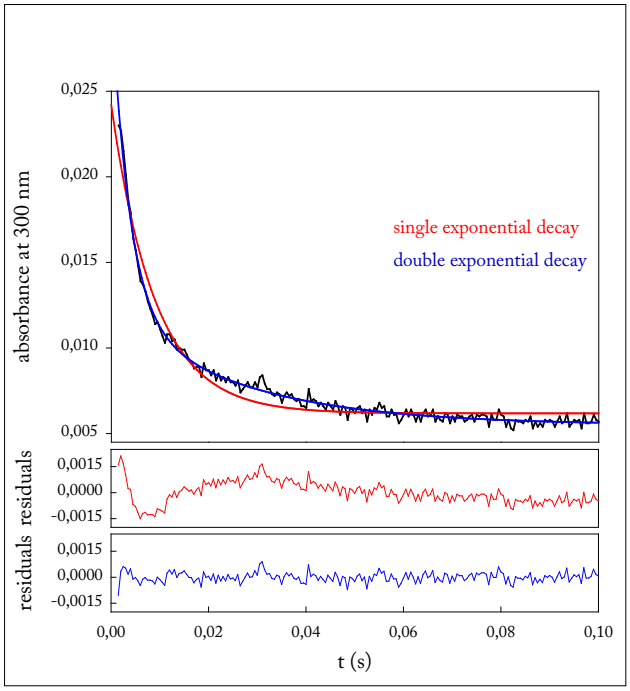

Fig.19: Transient for the reaction of enzyme bound DHEThDP intermediate in *Ec*TK with acceptor substrate R5P. Sequential stopped-flow kinetics for reaction of 1 mg/ml *Ec*TK (13.88 µM active sites) that were initially mixed with equimolar concentration of HPA to form enzyme-bound DHEThDP intermediate with 2.5 mM R5P in 0.3 mM ThDP, 2.5 mM $CaCl_2$, 50 mM glycylglycine (pH 7.6) at 25 °C. Measurements were performed with a stopped-flow spectrophotometer at a pathlength of 10 mm. The transient was fitted according to a single exponential equation first order (red, A = A1 * e^{-k1*t} + offset) and a double exponential equation first order (blue, A = A1 * e^{-k1*t}+ A2 * e^{-k2*t}+ offset). The residuals for both fits are shown color-coded below the transient.

After initial equimolar mixing of donor analogue β-hydroxypyruvate (HPA) with *Ec*TK the DHEThDP intermediate was generated on the enzyme. In a second mixing step the so accumulated DHEThDP was rapidly mixed with acceptor substrate R5P and the reaction was monitored by UV-Vis absorbance spectroscopy. A typical stopped-flow transient for the reaction of DHEThDP intermediate with acceptor R5P is shown in Fig.19. The distribution of data points is way better represented by a double exponential than by a single exponential equation suggesting that two processes contribute to signal depletion at 300 nm:

a.) The very fast, first phase could monitor R5P binding whereas the second phase might represent the reaction of R5P with DHEThDP. Since binding of such a small molecule can be assumed to occur almost diffusion-controlled it is questionable if the first process monitors R5P binding.

b.) Another interpretation of biphasic behavior would be the existence of two active sites with different catalytic competence. This could be generated by negative cooperativity within the TK dimer, a controversially discussed phenomenon for ThDP-dependent enzymes (Frank et al., 2007).

c.) It is also reasonable to assume that the first phase monitors the reaction of DHEThDP with R5P and the second phase monitors the liberation of S7P (product of the reaction). This proposal is supported by kinetic measurements of *Ec*TK with the donor F6P indicating that donor-ThDP formation is associated with an absorbance signal between 290-300 nm.

Transients were collected for a set of R5P concentrations. The rate constants for the first and second phase were plotted against the utilized R5P concentrations (Fig. 20) and fitted according to a hyperbolic equation to derive the kinetic parameters k_{max} and K_{Sapp}. The depletion of the DHEThDP intermediate in presence of acceptor substrates is a very fast process for *Ec*TK wt with a k_{max} = 531 ± 37 s^{-1}. The second phase, which presumably monitors release of S7P, has a smaller signal amplitude relative to the first phase and a k_{max} value of 42.5 ± 2.2 s^{-1}.

In order to assign both phases unambiguously a ^{1}H-NMR based intermediate analysis in combination with rapid quenched-flow technique has to be performed for *Ec*TK. Given that the DHEThDP intermediate in *Ec*TK wt depletes relatively fast (k_{depl} = 0.0057 s^{-1}, Fig. 50) and that quenched-flow experiments can´t be carried out in the required sequential mixing mode such experiments are technically demanding. *Ec*TK active site variants with prolonged life-times of the DHEThDP intermediate, which became available recently, are promising candidates for such experiments.

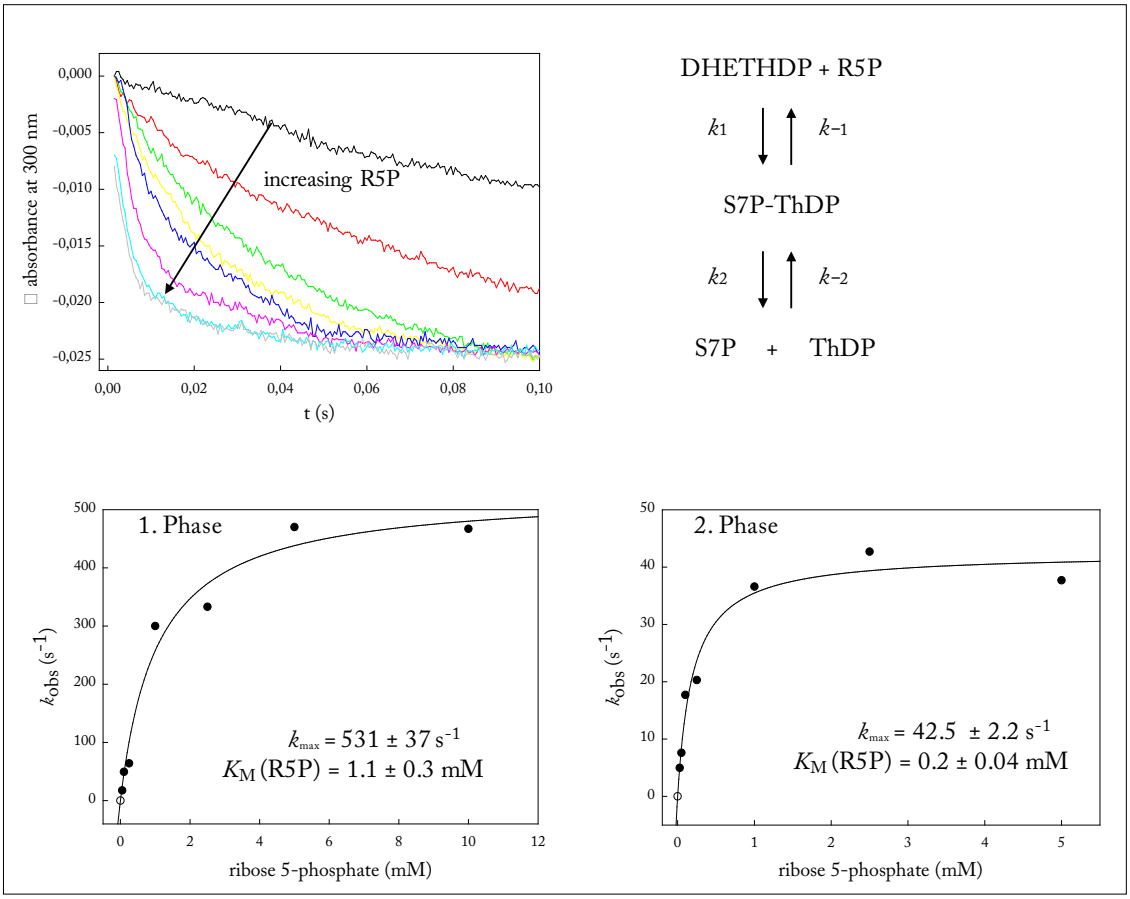

Fig. 20: Kinetic analysis for the reaction of enzyme bound DHEThDP intermediate in *Ec*TK with acceptor substrate R5P. Reaction of 1 mg/ml *Ec*TK wt (13.88 µM active sites) that were initially mixed with equimolar concentration of HPA to form enzyme-bound DHEThDP intermediate in 0.3 mM ThDP, 2.5 mM $CaCl_2$, 50 mM glycylglycine (pH 7.6) at 25 °C with increasing concentrations of acceptor R5P. Kinetics were initiated by 1/1 mixing and monitored in a stopped-flow absorbance spectrometer (pathlength 10 mm at 300 nm).**Top left:** Selected reaction transients.**Top right:** Simplified kinetic scheme for the experiment. **Bottom:** Rate constants (k_{obs}) were determined according to a double exponential equation (A = A1 * e^{-k1*t} + A2 * e^{-k2*t} + offset) and then plotted against the utilized R5P concentration. Kinetic parameters (k_{max} and K_M (R5P)) were determined according to a hyperbolic equation.

All reaction transients presented in this chapter revealed a biphasic behavior which coud be explained with the existence of two active sites with different catalytic competence. Such non-equivalence of active sites within a functional oligomer was reported for numerous ThDP-dependent enzymes (Frank et al., 2007) and Seifert *et al.* could demonstrate for human pyruvate dehydrogenase that elementary catalytic steps like cofactor activation, binding and conversion of substrate proceed 2-3 orders of magnitude faster in one active site relative to the second, so called, "dormant" site (Seifert et al., 2006). Additional crystallographic and functional evidence for the catalytic non-equivalence in pyruvate dehydrogenase was presented recently (Nemeria et al., 2010). These experiments are consistent with a previously suggested model of active site synchronization or "cross-talk" via a proton wire (Frank et al., 2007; Frank et al., 2004). Such fascinating regulation of enzyme activity that fixes two active sites in

an alternating activation state was thereafter also in discussion for transketolases. However, to our knowledge no direct kinetic or structural evidence was yet presented that such a mode of regulation does exist in any transketolase. Moreover, our recent and also previous x-ray crystallographyic experiments (Asztalos et al., 2007; Fiedler et al., 2002) as well as results from NMR-based intermediate analysis revealed the formation of covalent intermediates in both active sites of the functional dimer (Asztalos et al., 2007; Mitschke et al., 2010).

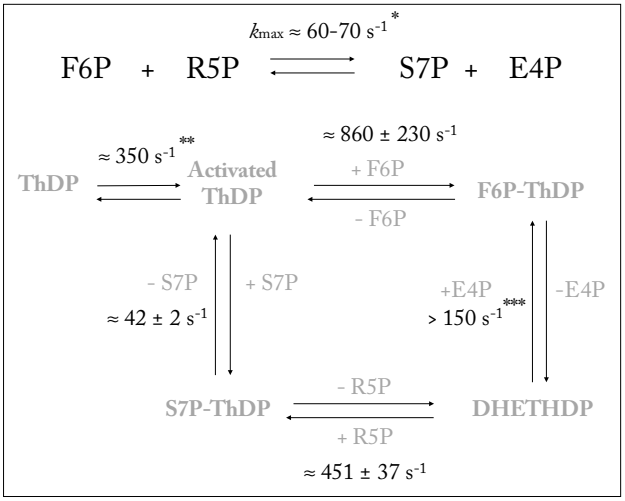

Fig. 21: Summary for the microscopic kinetic analysis of the *Ec*TK-catalyzed conversion of F6P and R5P to form S7P and E4P. Product (S7P, 42 ± 2 s^{-1}) release or donor cleavage are the rate limiting step of the over-all reaction (*(Sprenger et al., 1995), **(Asztalos, 2007 b), ***(Lüdtke, 2008)).

The kinetic analysis of microscopic reaction steps of *Ec*TK indicates that the rate-limiting step of the TK over-all reaction (Fig. 21) is the liberation of donor substrates which requires the cleavage of the C-C single bond connecting cofactor and substrate. The same conclusion based on equilibrium distribution of covalent intermediates in *Ec*TK was made recently (Asztalos et al., 2007). However, since donor cleavage could not yet been analyzed quantitatively it´s not excluded that this reaction step, which requires C-C bond cleavage as well, is rate-limiting. Unfortunately, analogous experiments with *h*TK failed due to precipitation of the enzyme.

3.3. Structure of Transketolase in Non-Catalytic States

Although the structural resolution of *h*TK (1.75 Å, pdb-code: 3MOS) and *Ec*TK (1.9 Å, pdb-code: 1QGD) enabled the describtion of TKs´ active site architecture, subtle atomic details, which might be of importance for catalysis like low populated side chain conformations, protein backbone flexibility and the protonation state of the cofactor as well as of active site residues can´t be analyzed at this resolution. One aim of this study was to determine the x-ray structure of both TKs at very high resolution to visualize these atomic details and to analyze their possible influence on catalysis. Furthermore, we were interested to derive information about the activation process of TK-bound coenzyme. A correlation of our structural findings with spectroscopic results in solution was applied whenever possible.

3.3.1. Structure of *h*TK in Ground-State

Two high-resolution x-ray structures of *h*TK in space group $P2_1$ form A (1.16 Å, R_{work} = 13.89, R_{free} = 16.41) and C2 (1.09 Å, R_{work} = 12.01, R_{free} = 14.26) could be determined. As a result of the improved resolution numerous structural details are observable compared to the already published structure of *h*TK at 1.75 Å (Mitschke et al., 2010). Details of mechanistical importance shall be discussed, relying on the better resolved structure, below.

Protein Structure of hTK

Each *h*TK monomer comprises in total 623 residues plus 14 additional residues of the C-terminal His-tag, of which residues 2-621 are well defined by their electron density maps. Each monomer harbors two peptide bonds partially present in the energetic unfavorable cis configuration. The electron density map for those two peptide bonds connecting Thr122 and Gly123 (60 % cis, 40 % trans) as well as Pro441 and Thr442 (57 % cis, 43 % trans) is well defined and enabled the refinement of the occupancies of each configuration (see Fig. 77). While Pro441 and Thr442 are located in the protein periphery and have contact with solvent the peptide bond betweenThr122 and Gly123 is located in close proximity to the cofactor ThDP. Moreover, the backbone oxygen of Gly123 is involved in a highly conserved (Jordan, 2003) hydrogen bonding interaction with cofactors N4´amino function. The cis/trans bond causes a positional change of the Gly123 backbone carbonyl (Fig. 22) and influences the strength of the hydrogen bonding interaction with N4´ suggesting a catalytic role of this cis/trans arrangement. N4´, as an important component of the coenzyme, is involved in intramolecular proton transfer reactions (Nemeria et al., 2009). Thus, dynamics influencing the cis/trans conformation could also have an impact on elementary catalytic steps performed by cofactors´ N4´. Noteworthy, the interaction of Gly123 in both conformations with N4´ has almost linear proton transfer geometry (optimal value 120°) and just slightly deviates for the proton transfer distances. Thus the energetic difference of both interactions is presumably relative small.

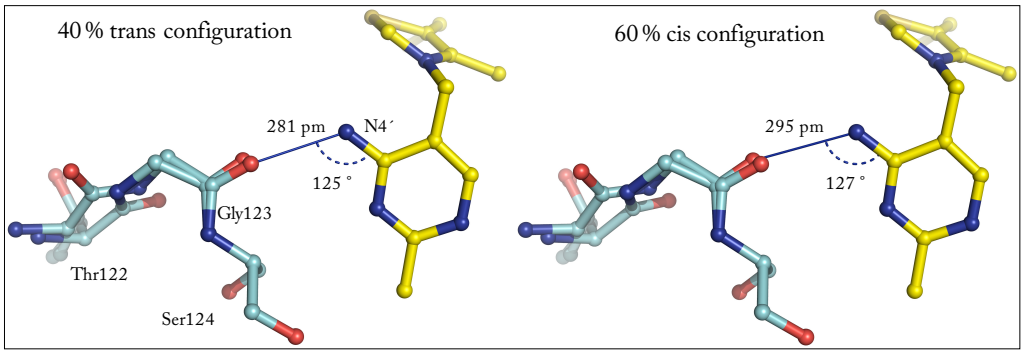

Fig. 22: Detailed view on the interaction between Gly123 and cofactors N4´. Hydrogen bonding interaction between cofactors´ (yellow) N4´ functionality and the backbone carbonyl of Gly123 (cyan) in trans (left) and cis (right) configuration. Hydrogen bonding distances and –geometry are indicated.

Mitschke and colleagues reported (Mitschke et al., 2010) that each monomer of *h*TK contains a sodium ion which is octahedrally coordinated by five oxygens and one sulfur ligand. The identity of this structural sodium ion could be confirmed using the high-resolution data and finally verified by a difference anomalous electron density map (Fig. 78).

Structure of hTK-bound ThDP

A comparison of atomic B-factors for the cofactor relative to its surrounding residues revealed that it is bound with full occupancy. Very surprising and unexpected structural features of the cofactor are significant deviations from planarity for both aromatic ring systems (Fig. 23 b.)). While atoms C4´ and N4´ in the six-membered ring are just slightly out-of-plane, a stronger deviation from planarity is detectable for the entire five-membered thiazolium ring and especially for C2. An analysis of bond length for the thiazolium ring revealed very long bonds for S1-C2 (176 pm) and for S1-C5 (176 pm) suggesting a significant loss of aromaticity. Furthermore, cofactors´ C2 has an unexpected, much weaker electron density agglomeration relative to all other carbon atoms of ThDP which was verified by different residue omitted electron density maps (Fig. 23 a.)). An explanation for this finding could be radiation-induced damage of the thiazolium ring caused by the high-energy synchrotron radiation used for data collection. However, data collection statistics as well as the fact that no other radiation damage is observable in the structure contradict this hypothesis. Also, a partially, radiation-induced ring opening of the thiazolium ring is not supported by any electron density map. Another explanation for the observable out-off-plane distortion of C2 could be that the C2 atom has high flexibility and swings through the thiazolium ring plane with a higher probability of presence for the position that is detectable. Such high flexibility of C2 is not supported by the well defined electron density at this position and further by the characteristics of a planar, aromatic thiazolium ring. However, C2

(10.82 Å²) possesses the highest atomic B-factor which is apparently 50 % increased relative to neighboring atoms N3 (7.11 Å²) and S1 (7.45 Å²) a remarkable finding for an endocyclic atom (Fig. 23 c.)).

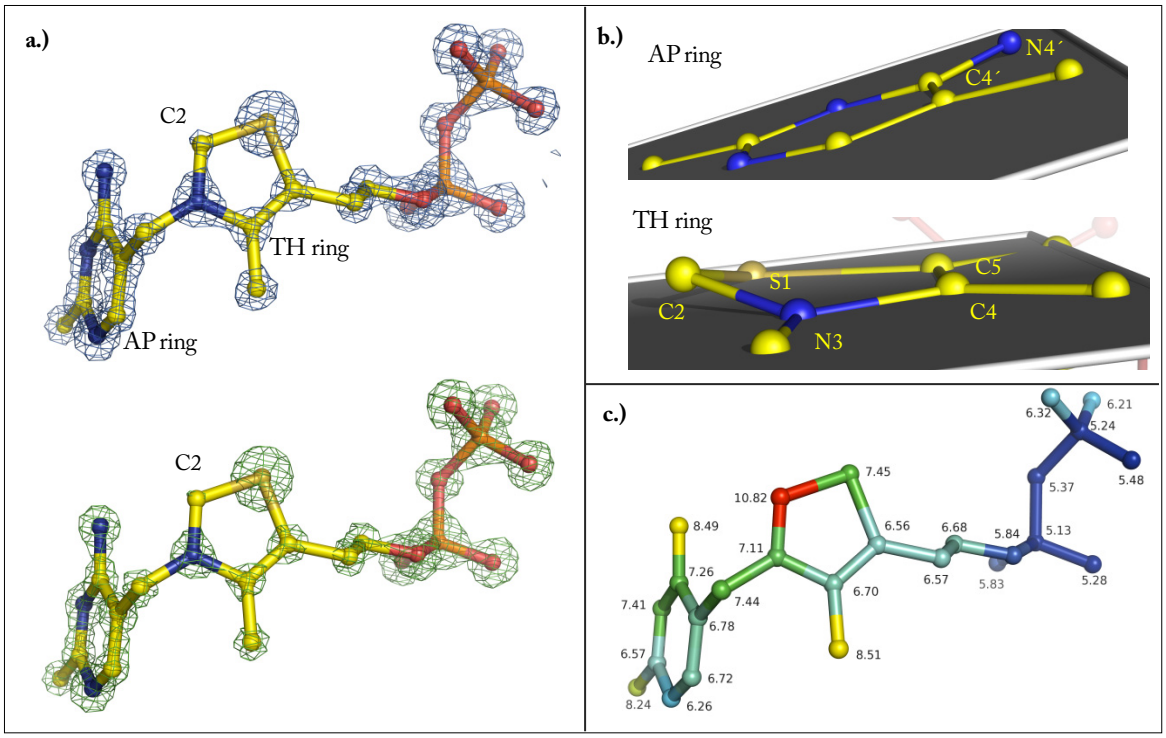

Fig. 23: Detailed view on un-substituted ThDP in the x-ray structure of *b*TK. Enzyme-bound ThDP is shown in ball and stick representation. Selected atoms are labeled. **a.)** ThDP surrounded by a residue omitted 2mFo-DFc electron density contoured at 5σ (top, blue) or surrounded by a residue omitted mFo-DFc difference electron density contoured at 14σ (bottom, green). **b.)** Detailed view on the aminopyrimidine (AP) and thiazolium (TH) ring of the cofactor. Auxilary planes (grey) illustrate deviation from planarity of both aromatic systems. **c.)** Atoms of ThDP are color-coded according to their individual B-factors (in Å²) showing less mobile atoms in blue (5.2-6.6 Å²) and the most mobile one in red (10.8 Å²).

The relatively weak electron density peak at C2 could also be explained with the presence of a C2-carbene which possesses a bivalent carbon atom with an electron sextet. This proposal is further supported by the bonding geometry of N3 that is not planar, expected for protonated or carbanion form of ThDP, but trigonal pyramidal-like in a carbene state. Arduengo (Arduengo et al., 1997) succeded to characterize a thiazol-2-ylidene (C2 carbene, 3-(2,6-diisopropyl-phenyl)thiazol-2-ylide, Fig. 24 b.)) structurally and spectroscopically which represents a suitable reference structure for a ThDP carbene. The authors found that mayor structural differences between C2 protonated and deprotonated form exist for the S1-C2-N2 angle which is approx. 8° smaller in a carbene state as well as for both C-S bonds. Those two bonds are significantly stretched in a carbene structure relative to

the protonated from. As mentioned, the structural analysis of *h*TK-bound ThDP revealed that both C-S bonds are enlarged thus suggesting a carbene-like structure (Fig. 24 a.)). In contrast, the S1-C2-N3 angle of 111.6° is suggestive of a C2 protonated cofactor form. Hence, the exact chemical state can´t be assigned unambiguously solely relying on this x-ray structure. Notably, similar deviations from planarity of the thiazolium ring system and weak density for C2 are observable for all high-resolution structures of unsubstituted ThDP bound to *h*TK (<1.2 Å, in total 6 structures). Furthermore, since structure refinement was performed with a model which is protonated at C2 the increased apparent, atomic B-factor of C2 relative to S1 and N3 could also originate from a smaller number of electrons in the "truly" existing state further supporting the presence of a ThDP carbene.

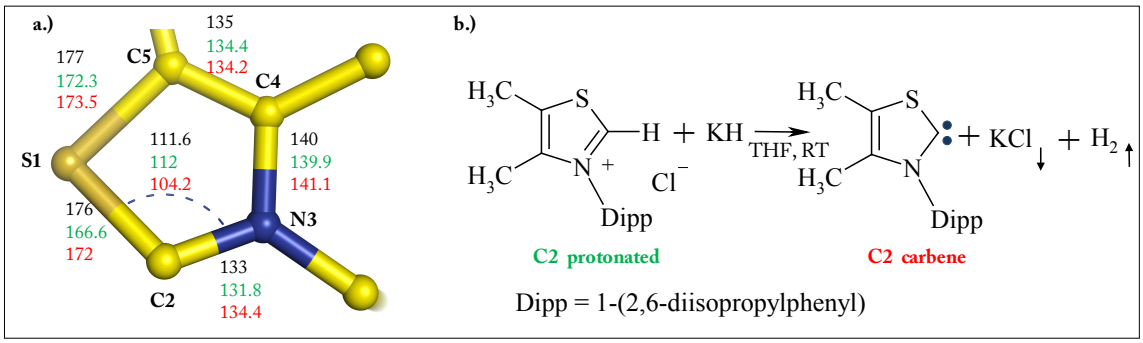

Fig. 24: Analysis of bond lengths and -angles of cofactors` thiazol ring. a.) Selected atoms are labeled (bold). Determined bond length (black) for the structure of *h*TK in complex with unsubstituted ThDP (1.09 Å) and for C2 protonated (green) as well as C2 carbene (red) small molecule structures are indicated. **b.)** Scheme: Reaction of 3-(2,6-diisopropylphenyl)-4,5 dimethylthiazolium chloride (green) with potassium hydride in tetrahydrofuran (THF) at room temperature (RT) to form the stable carbene 3-(2,6-diisopropylphenyl)thiazol-2-ylidene (red). The crystal structures of both compounds, which were solved by Arduengo et al., were used as references in a.). The figure was adapted according to Arduengo (Arduengo et al., 1997).

The involvement of a C2 carbene rather than a polarized C2 carbanion as authentic ThDP catalyst is subject of debate in the field (Berkessel et al., 2011; Enders and Balensiefer, 2004; Jordan, 2003) but could yet not been proven or excluded experimentally. While n-heterocyclic carbenes are common ligands in organic chemistry which could be characterized structurally and spectroscopically in great detail (Arduengo et al., 1994 a; Arduengo et al., 1994 b; Arduengo et al., 1992; Arduengo et al., 1994 c; Arduengo et al., 1997; Enders and Balensiefer, 2004) there is to our knowledge no direct observation reported for a bioorganic carbene. The presence of a thiazol carbene would automatically require that the majority of ThDP bound to *h*TK is deprotonated which contradicts the current mechanism for cofactor activation (Hübner et al., 1998; Kern et al., 1997).

The high resolution of the x-ray structure enabled an assignment of the majority of hydrogen positions in a difference electron density map contoured at a level of 3σ (Fig.25). However, even at very low

contour levels (<2σ) no hydrogen at C2 is traceable again indicating a predominantly deprotonated C2 for *h*TK in ground state. For the six-membered ring hydrogen atoms at C6, C6´, N1´ and at N4´ can be clearly located relying on a positive difference electron density map contoured at 2.7-3σ. While the bonding geometry for hydrogen atoms at C2´ and C6 falls into expected range hydrogens bound to N1´and N4´ reveal larger deviations. The hydrogen at N1´ is coplanar with the ring but has no perfect linear bonding geometry relative to N1´ (N4´-N1´-H=150°). Moreover, the N1´-H bond length (106 pm) deviates 4.5 % from the expected value (101 pm). In contrast the hydrogen bound to N4´ is not coplanar with the six-membered ring and also the bond length of 137 pm strongly deviates (36 % deviation) from expected values.

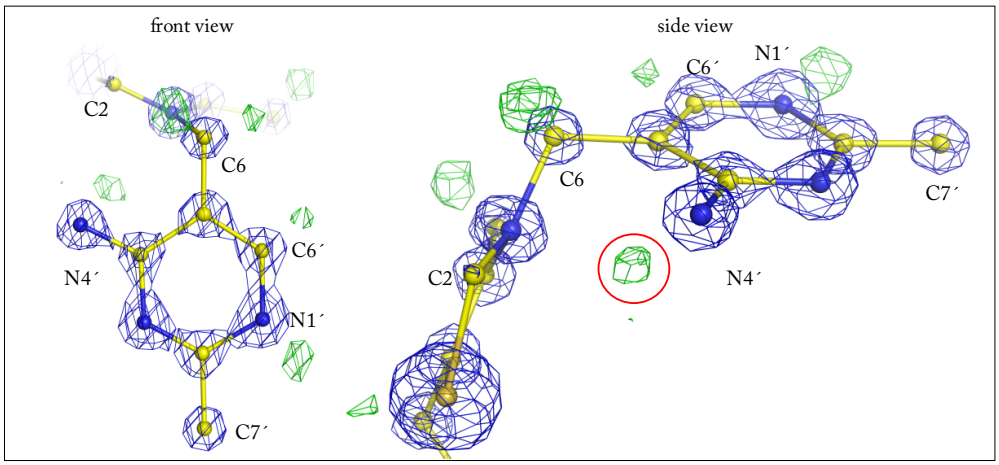

Fig.25: Protonation state of cofactors aminopyrimidine ring in *h*TK ground-state. X-ray structure of *h*TK in ground-state (1.09 Å). The un-substituted cofactor is shown in ball and stick representation surrounded by a 2mFo-DFc electron density map at 4σ and a mFo-DFc difference electron density map at 3σ. Selected atoms that are discussed in the text are labeled. The difference electron density peak between C2 and N4´ is highlighted (red circle).

CD-spectra of *h*TK in solution reveal a TK-typical, negative CD-signal with a minimum at 320-330 nm (Mitschke, 2008) which is generally assigned as spectral signature for the AP form. In case IP or APH^+ form would predominantly accumulate at this stage the N4´-bonded hydrogen atom should be co-planar with the imino group according to the chemical drawings in Fig. 4. The side view in Fig.25 clearly reveals that this is not the case. The density peak (red circle) is directed towards C2 of the thiazolium ring. One might speculate that the observed density peak is the abstracted proton from C2 on the "fly" to N4´. This question can´t be answered here as protons are "invisible" in x-ray crystallography since they don´t possess electrons.

While an unambiguous assignment of the protonation state of un-substituted cofactor in *h*TK is not feasible the well defined density for the hydrogen atom at N1´ suggests the presence of either IP- or

APH^+-form and excludes the presence of the AP form. Importantly, this assignment further supports a predominant deprotonated thiazolium ring

In order to confirm our experimental results higher resolved x-ray structures of *h*TK in ground state have to be collected and combined with other biophysical methods like neutron crystallography. Noteworthy, Arduengo and colleagues reported a ^{13}C NMR signal of 254.3 ppm for the thiazol-2-ylidene compound (Arduengo et al., 1997) depicted in Fig. 24 that shouldn´t interfere with protein-derived signals offering the possibility to confirm the presence of a TK-bound carbene by ^{13}C solid state NMR spectroscopy.

3.3.2. Structure of *Ec*TK in Ground-State

Protein Structure of EcTK

The structure of *Ec*TK in ground-state (1.048 Å, R_{work} = 9.17 %, R_{free} = 12.11 %, Fo > 4σ) could be determined to high resolution. Each *Ec*TK monomer comprises in total 663 residues and 6 additional residues of the C-terminal His-tag, of which residues 2-667 are well defined by their electron density maps. Furthermore, we could identify one structural sodium ion per monomer that was previously modeled as a water molecule (Fig. 79). The position of this sodium ion (AP-domain) is not identical to that one located in *h*TK (PYR-domain). Another structural difference relative to *h*TK is that none of the peptide bonds in *Ec*TK adopts cis-configuration.

Moreover, 107 amino acid residues per *Ec*TK monomer revealed alternate side chain conformations whereas this was just reported for 9 amino acids in the currently deposited *Ec*TK structure. While two arginine residues which were already shown to function in positioning the phosphate moieties of substrates (Arg520 and Arg358) reveal an elevated flexibility, all remaining active site residues are rigid. Solely Gly114 adopts two alternate back-bone conformations.

Structure of EcTK-bound ThDP

The electron density maps for the cofactor in both active sites after refinement against data higher than 1.2 Å resolution revealed additional positive electron density peaks in close proximity to the thiazolium ring sulphur (S1) and to some atoms of cofactors diphosphate group (Fig. 26 a.)). Moreover, the difference electron density map for S1 contoured at higher sigma level (mFo-DFc map, 12σ) deviates from an expected spherical shape and is ellipsoid. Furthermore, both methylen groups bridging the thiazolium and the diphosphate anchor are poorly defined implying a higher flexibility of this part of the molecule or indicating the existence of hidden alternate conformations. After modeling and refinement of the cofactor in its ground-state position with full occupancy the difference electron

density maps indeed strongly suggested the presence of an alternate cofactor conformation (Fig. 26 b.)). This second conformer was modeled relying on different omit maps and refined. Superposition of the deposited *Ec*TK structure (pdb code:1QDG) and the here presented high resolution x-ray structures of *Ec*TK revealed significant differences for both ground-state conformations of the cofactor seemingly indicating that the previous ThDP ground-state conformation was modeled into a mixed electron density map originating from multiple ThDP states. The apparent high cofactor flexibility in *Ec*TK is further supported by significant higher atomic B-factors of those parts of the molecues (Fig. 26 c.)).

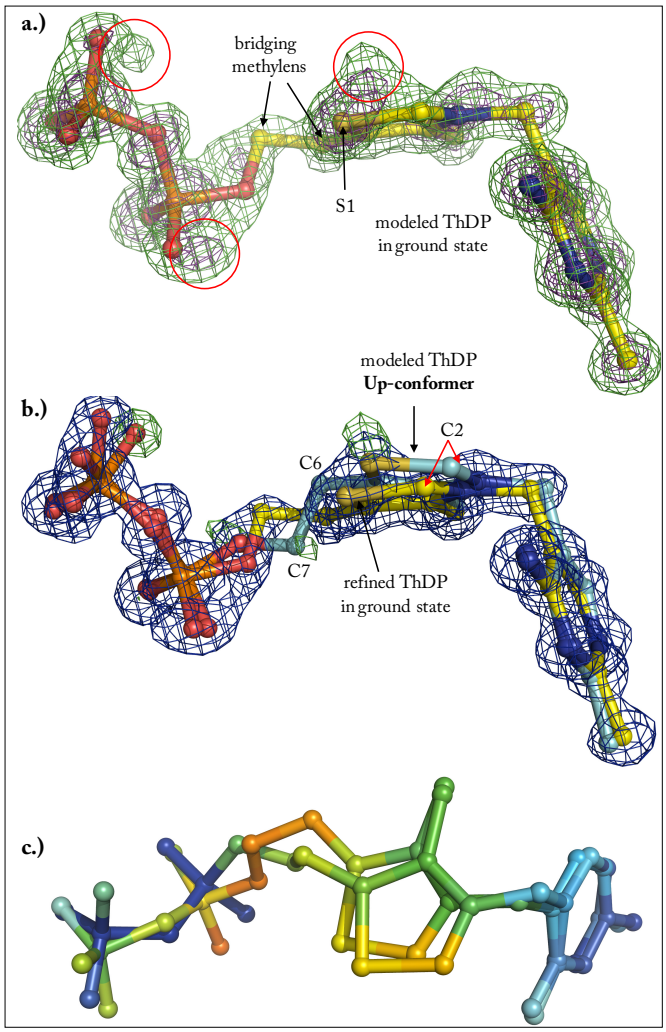

Fig. 26: Cofactor flexibility in *Ec*TK. X-ray structure of *Ec*TK at 1.048 Å. **a.)** ThDP (yellow) modeled in ground state conformation is shown surrounded by a mFo-DFc omit map contoured 5σσ (green) and 12σσ (purple). The thiazolium sulphur (S1) and both bridging methylen groups are labeled. Electron density peaks that are not described by the ground state model of ThDP are highlighted (red circles). **b.)** ThDP in ground state conformation (yellow, identical to **a.)**) that was refined is shown with the corresponding 2mFo-DFc map (1.5σσ, blue and mFo-DFc map (4σ, green). A second ThDP conformer (up-conformer, cyan) that was modeled and selected atoms (C2, C6 and C7) are labeled. **c.)** Atoms of both ThDP conformers are color-coded according to their individual B-factors (after anisotropic refinement) showing less mobile atoms in blue (5.2-9.5 Å^2) and most mobile ones in orange (≈ 22 Å^2).

According to occupancy refinement 67 % of enzyme bound cofactors adopt the ground state and 33 % the previously hidden conformation. In this newly found conformation the thiazolium ring is rotated slightly relative to the resting state resulting in a approx. 1 Å displacement of cofactors C2 atom but keeping the thiazolium methyl group at almost the same position (not shown). Given that the reactive center the C2 atom is now above its resting state position we named this minor populated

conformation up-conformation. The small occupancy of the up-conformer is compensated by the displaced S1 atom and its higher number of electrons (16 electrons) relative to C2 carbon (6 electrons in the protonated form) which is hard to trace. The second bridging methylene (C7) group is displaced significantly and the diphosphate anchor also adopts a different conformation relative to ground state. In order to prove whether the enzyme induces cofactor flexibility in *Ec*TK we performed a detailed structural analysis of all active site residues which are involved in cofactor binding. The only significant structural fluctuation is that of a backbone carbonyl (Gly114) which is involved in a strictly conserved (Jordan, 2003) hydrogen bonding interaction with the 4´ group of cofactors amino-pyrimidine ring. In its predominantly (81 %) occupied position Gly114 is involved in a strong (270 pm) hydrogen bonding interaction with almost linear hydrogen bonding geometry to cofactor N4´ (Fig. 27). In contrast to that, the lower populated (19 %) carbonyl conformer shows an increased distance to N4´ (307 pm) and a more unfavorable hydrogen bonding geometry. Both aspects will decrease the strength of this interaction. Because both pairs of alternate conformers are present in similar ratios one might speculate that cofactor flexibility originates from this small structural fluctuation of the protein. This model would represent a simple and elegant mechanism how enzymes could "communicate" with their cofactors.

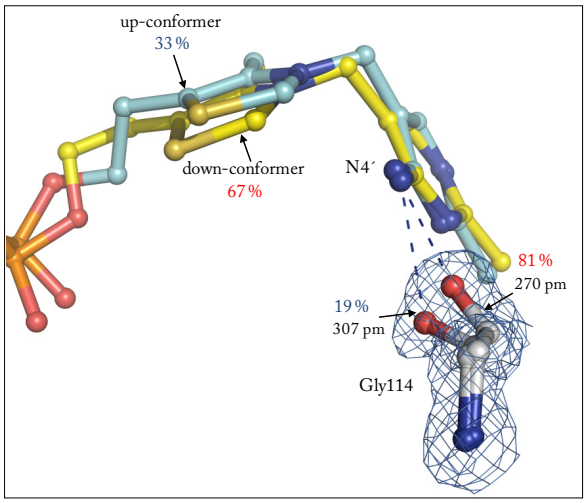

Fig. 27: Correlation of protein backbone fluctuation with cofactor flexibilty in *Ec*TK. ThDP in two conformations (up- and down-conformer) is shown in close proximity to active site residue Gly114 that is surrounded by a 2mFo-DFc map (1.5σ) in the x-ray structure of *Ec*TK (1.048 Å). Hydrogen bonding interactions (blue dashed lines) and the occupancy of individual cofactor- and backbone conformers are indicated.

Another conceivable origin of the observed cofactor flexibility could be encoded in the high-energy V-conformation of enzyme-bound ThDP. Analogous to a "molecular spring" a small fraction of this energy could be used to induce dynamics in some parts of the coenzyme. In order to prove that

cofactor flexibility is not just observable in one single x-ray structure we reinvestigated all determined high-resolution structures of *Ec*TK with unsubstituted ThDP which are mostly not presented in this thesis. All structures of *Ec*TK or active site variant thereof in ground state (4 structures with a resolution range of 1.08-1.18 Å) and all structures of *Ec*TK in non-covalent complex with substrates or analogues thereof revealed approx. 70 % "down"- and 30 % "up"-conformer of ThDP (4 structures with a resolution range of 0.96–1.02 Å). Given that the ratio between up- and down form is identical to the ground-state structures indicates, that cofactor flexibility in *Ec*TK is not affected by substrate binding.

Unfortunately and despite of the high resolution of the *Ec*TK structures an unambiguous assignment of hydrogen positions for the cofactor could not been perfomed which most probably originates from the highly dynamic cofactor itself.

3.3.3. Spectroscopic Evidence for a Thermodynamically Stabilized Carbanion/Carbene Species in the Active Site of *Ec*TK

In order to address the question whether *Ec*TK stabilizes an observable fraction of C2-unprotonated cofactor we performed NMR-based pH/solvent jump experiments relying on a protocol previously established in our group (Koers, 2010). For that purpose apo *Ec*TK was transferred by several rounds of ultrafiltration into 50 mM glycylglycine buffer (in D_2O, at pD 7.6), 5 mM $CaCl_2$ (in D_2O) and equimolar amounts of ThDP (in D_2O) were added to form the holo enzyme. After 30 min of recombination a 1 to 100 volume jump into 20 % formic acid (H_2O, pH ≈ 1) was performed (Fig. 28 a.)), which provokes liberation of the cofactor from holo enzyme. Cofactor molecules which are unprotonated (carbanion/carbene) will immediately incorporate a proton at position C2 forced by the acidic environment. After lyophyllisation of the sample and resolvation in an acidic buffer (pH ≈ 0.75) the apo protein (precipitate) was removed by filtration and the cofactor, that was either deuterated or protonated at C2, was analyzed by ^{1}H NMR spectroscopy.

Two experiments with different concentrations of *Ec*TK (1 and 2 mM active sites = 72 and 144 mg/ml) and the coresponding reference (pH/solvent jump of free ThDP from D_2O into H_2O) were performed under identical conditions. Both experiments revealed that the majority of cofactor C2 is deuterated. However, a significant fraction of 5-8 % protonated coenzyme was detectable (Fig. 28 b.)). Noteworthy, we also observed a small signal of protonated ThDP in the control experiment. The presence of this residual protonated fraction might be explained with manual performance of the solvent jump experiment or a slow H/D exchange of C2 during sample preparation.

After signal correction the Handerson-Hasselbalch equation was applied to calculate the pK_A of enzyme bound ThDP. For the observed fraction 5 to 8 % unprotonated C2 a pK_A in the range of 8.7

to 8.9 was calculated. Notably, a similar pK_A of 8.3 for ThDP bound to pyruvate dehydrogenase was calculated by Nemeria and co-workers (Nemeria et al., 2009) relying on own measurements and data from Seifert (Seifert et al., 2006). In contrast to free ThDP (pK_A 17-18) (Washabaugh and Jencks, 1988) TK-bound cofactor seems to populate a considerable fraction of highly reactive, unprotonated form. Contrary to our experimental results Kern et al. observed by liquid state ^{13}C NMR spectroscopy for yeast pyruvate decarboxylase reconstituted with ^{13}C2-ThDP an identical C2 signal relative to free ThDP (Kern et al., 1997). Remarkably, the signal of enzyme-bound ^{13}C2-ThDP had a very small line width typical for small molecules suggesting that the observed signal indeed originated from free and not enzyme-bound cofactor. In addition, even if the ^{13}C NMR signal (at approx. 155 ppm) corresponds to enzyme-bound cofactor its small signal to noise ratio doesn´t allow the visualization of small fractions of unsubstituted cofactor. Moreover, in a very recent publication the ^{13}C-NMR results of Kern et al. couldn´t been confirmed (Paramasivam et al., 2011). The same authors found a modest but observable increase of C2-acidity.

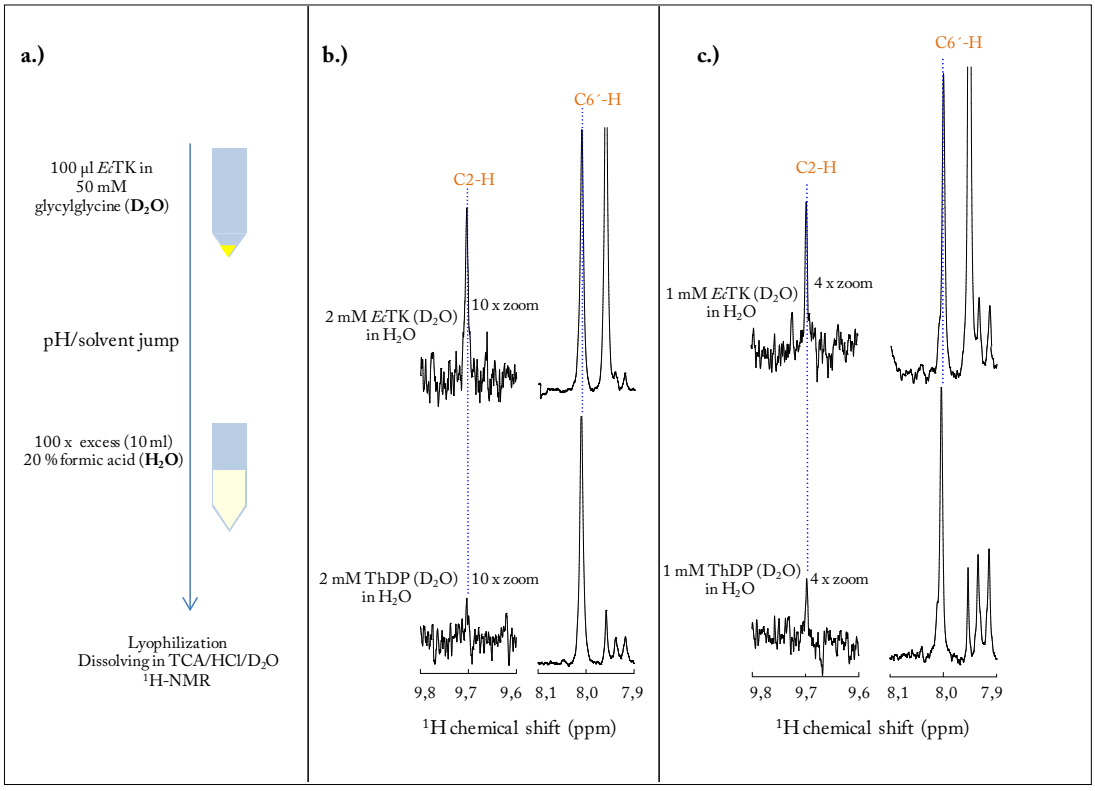

Fig. 28: pH/solvent jump ^{1}H NMR experiments for the detection of enzyme derived unprotonated ThDP. a.) Workflow of the performed technique, with minor modification adopted from Elisabeth Koers, (Koers, 2010): After transfer of apo *Ec*TK by ultrafiltration into deuterated buffer $CaCl_2$ (in D_2O) was added in excess (5 mM) and ThDP (in D_2O) in equimolar concentration to form the holo enzyme. Reconstituted holo enzyme was then used to perform a pH/solvent jump into 100 fold excess of 20 % formic acid. The samples were subsequently lyophyllized, resolved in an acidic buffer and after removal of protein precipitate analyzed by ^{1}H NMR spectroscopy. **b.)** D/H solvent jump of 2 mM active sites (144 mg/ml) holo *Ec*TK (top) and the control, 2 mM ThDP (bottom) as well as of **c.)** 1 mM active sites (72 mg/ml) holo *Ec*TK (top) and the control 1 mM ThDP (bottom). ThDP signals of the acidic C2-proton as well as the non-exchanging C6´-proton are labeled (dashed blue lined).

Our experimental results in solution indicate that transketolase as a representative member of ThDP-dependent enzymes populates a considerable fraction of unprotonated species in the active site. The thereby formed cabanion/carbene is most probably not transient (Kern et al., 1997) but stabilized on the enzyme.

This pH/solvent jump method is currently applied and optimized for other ThDP-dependent enzymes but couldn´t yet been performed for *h*TK. According to our structural findings for *h*TK, which implicated accumulation of a C2 carbene, a higher amount of C2-deprotonated cofactor should be detectable.

3.4. The Catalytic Cycle of TK Trapped by X-rax Crystallographic Snapshots of Reaction Intermediates

The main goal in enzymology is the understanding of enzyme catalyzed reactions on a molecular level. This requires the characterization of all transient, often metastable reaction intermediates by means of structure and reactivity. Various methods like nuclear magnetic resonance (NMR) spectroscopy, electron paramagnetic resonance (EPR) spectroscopy or various vibrational spectroscopical methods are routinely used to analyze inorganic or organic catalytic systems. However, large and complex enzymatic systems often exclude the possibility to be studied by those methods. Due to methodological advances (Moffat, 2001; Petsko and Ringe, 2000) like rapid data collection, micro-spectrophotometry (Pearson et al., 2004), cryo-crystallography, development of photolabile caged compounds or time-resolved crystallography (Laue crystallography) x-ray crystallography became the method of choice for structure determination of short-lived or unstable intermediates in enzyme catalysis over the last two decades.

In order to performs such studies conditions have to be found which facilitate the accumulation of certain states at high occupancy within the entire volume of a crystal. Different approaches like the usage of substrate- or cofactor analogues, creation of enzymes variants, working far from optimal catalytic conditions, establishment of pseudo-steady-state conditions, usage of reaction products etc. are routinely used to accumulate a desired intermediate. The by far most commonly used technique for trapping intermediate states is "freeze-trapping". For this purpose the reaction intermediate is generated and accumulated within the crystal at moderate temperatures and subsequently trapped by flash-cooling due to transfer of the crystal into liquid nitrogen. Below a temperature of 200 K collective motions of protein crystals are "frozen out" (Demmel et al., 1997; Rasmussen et al., 1992) and those cooled crystals adopt a "glass-like" state.

Different approaches to accumulate a certain intermediate were used in this study and the individual strategy is mentioned in each subchapter. All approaches have in common that the enzyme-intermediate complexes were trapped by rapid cooling. Since modern data collection usually occurs at cryogenic temperatures this method doesn´t cause any drawbacks.

3.4.1. The Michaelis Complex of TK and Donor Substrates

Since TK utilizes donor substrates of different length (C5-C7) that all have to be recognized and prealigned for reaction with the coenzyme we aimed to analyze this catalytic step by x-ray crystallography. Noteworthy, this particular reaction step could yet not been trapped for any TK.

Sugars and their phosphate derivates are present in aqueous solution in a dynamic equilibrium of different cyclic and acyclic states (see Fig. 34, Fig. 61). In contrast to X5P both other native donors adopt multiple of these states. For the C6-donor F6P just 2.2 % are present as the acyclic keto form

(Pierce et al., 1985) whereas the majority adopts furanose states (81.8 % β-anomer, 16.1 α-anomer). C7-donor S7P is reported to be present in aqueous solution as α-pyranose (16 %), α-furanose (17 %) and β-furanose (67 %) (Franke et al., 1985) revealing no acyclic keto form. Importantly, solely the acyclic keto form harbors carbonyl reactivity which is required for the ligation to the cofactor. To understand how TK accumulates and aligns this state, probably by active furanose or pyranose ring opening, was an important motivation for the presented experiments.

For visualization of donor binding the native cofactor ThDP had to be removed from the holo enzyme and apo TK was recombined with the catalytically inactive cofactor analogue N3´-pyridyl ThDP (N3ThDP). The N1´-nitrogen found in ThDP is replaced by carbon in this analogue (Fig. 29). It is therefore not possible that the conserved glutamate protonates the pyridine ring, a necessary prerequisite for cofactor activation. Catalytically inactive ThDP analogues were already shown to be suitable compounds for visualizing substrate binding for a manageable number of ThDP dependent enzymes (Pei et al. 2008, ; Versees et al., 2007). Previous studies were conducted with 3deaza thiamin diphosphate or 1,2,3 triazol thiamin diphosphate. The usage of N3ThDP instead of 3deazaThDP might offer the advantage to posses a positive charge at the N3 nitrogen of the thiazol moiety which might influence substrate binding.

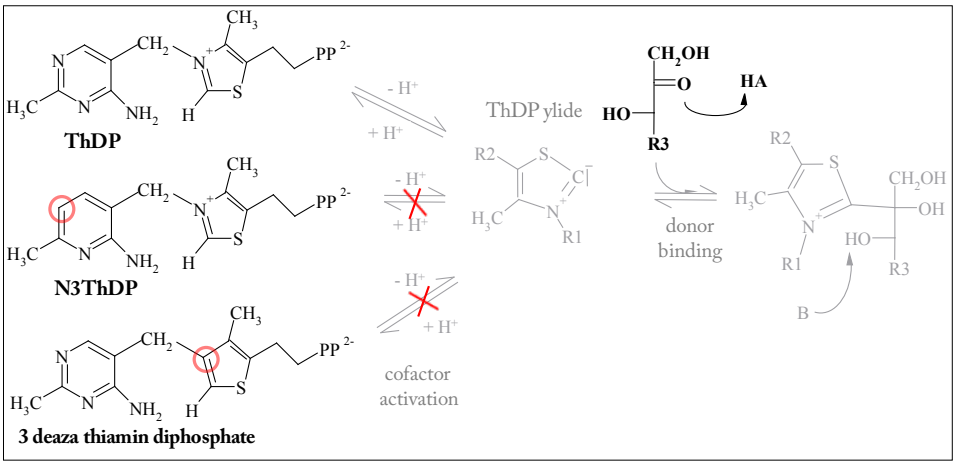

Fig. 29: Visualization of donor substrate binding by usage of cofactor analogues. In contrast to native cofactor (ThDP) the activation deficient analogues N3ThDP and 3deaza thiamin diphosphate cannot form the reactive ylide form of the cofactor which is a prerequisite for formation of covalent substrate-cofactor adducts. Atomic substitutions which are the molecular origin of cofactor analogue inactivity are highlighted with red circles.

In order to prove whether the cofactor analogue adopts an identical conformation relative to native ThDP we determined the structures of the *b*TK-N3ThDP (1.3 Å, R_{work} = 13.17, R_{free} = 15.74) and *Ec*TK-N3ThDP (0.97 Å, R_{work} = 9.63, R_{free} = 12.24, Fo > 4σ) complex. The cofactor analogue adopts, as the native cofactor, the canonical V-conformation enabling a close proximity of 4´-amino function

of the aminopyrimidine ring and the reactive center the C2 atom of the thiazolium ring. While the active site residues of both TKs are well superimposable, just minor structural displacements relative to native cofactor are observable for the thiazolium moiety and the methylene groups in *h*TK (Fig. 30). Furthermore Glu366 (*h*TK) and Glu411 (*Ec*TK) are slightly displaced in both structures reconstituted with the cofactor analogue presumably due to the missing hydrogen bonding interaction with N1´. This missing hydrogen bonding interaction seemingly causes an elevated flexibility of N3ThDP in *h*TK demonstrated by elevated atomic B-factors for the aminopyridine ring and both methylen bridges connecting thiazolium ring and diphosphate moiety (not shown). Such differences are not observable for the *Ec*TK-N3ThDP complex. In the *Ec*TK-N3ThDP complex the analogue is, like native coenzyme, present in two alternate conformations ("up" and "down" conformer). Furthermore, the ratio of those conformers (68 % "down" and 32 % "up") is almost identical relative to native ThDP (67 % "down" and 33 % "up"). Importantly, since N3ThDP is deficient in C2 deprotonation the "up"-conformer can´t represent an already activated state, that is a C2 deprotonated carbanion or carbene.

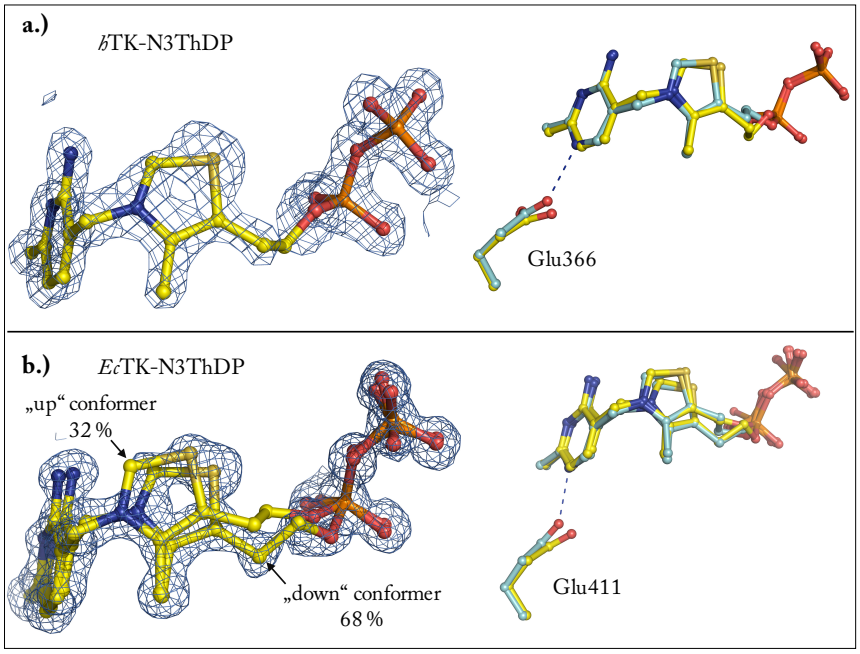

Fig. 30: Atomic details in the high resolution structure of *h*TK and *Ec*TK in complex with the cofactor analogue N3ThDP. Left side: Ball and stick representation of N3ThDP bound to the active site of *h*TK (**a.)**) or *Ec*TK (**b.)**). The 2mFo-DFc-maps are shown with a contour level of 1σ. For reasons of clarity active site residues are omitted. **Right side:** Superposition of the TK-ThDP (cyan) and TK-N3ThDP (yellow) complexes. Active site residue Glu366 or Glu411 and its hydrogen bonding interaction with the N1´-atom of native ThDP are indicated by a dashed blue line.

Because N3ThDP is bound to both TKs in an almost identical mode as native ThDP, this analogue can be fairly adopted to visualize donor substrate binding to *h*TK and *Ec*TK.

3.4.1.1. Michaelis Complex of *h*TK with Donor X5P

The structure of the *h*TK-N3ThDP-X5P complex could be determined to high resolution (1.15 Å, R_{work} = 11.65, R_{free} = 14.00). The strong additional electron density peaks found in close proximity to the cofactor analogue enabled an unambiguous modeling of X5P present in its acyclic keto-form (Fig. 31 a.)). The electron density for the ligand molecule is well defined and revealed no traces of the hydrate form of the substrate. An analysis of atomic B-factors revealed smaller values for X5P relative to the surrounding active site residues suggesting full occupancy and low flexibility of bound X5P. The donor substrate forms multiple polar interactions including hydrogen bonds (Ser345, Asp424, Gln428, His37, 258 and 461) and electrostatic interactions (Arg318 and 474) with the protein and is pre-oriented for the subsequent carboligation reaction with the cofactor (Fig. 31 b.)). The inter-atomic distance between the two reactive centers of carboligation the C2 carbon atom of X5P and the C2 of the thiazol moiety of the cofactor (analogue) is 392 pm. A prerequisite for an effective nucleophilic attack is an inter-atomic distance between both reactants of 1.5 to 3 Å (Burgi et al., 1974; Burgi et al., 1973). Additionally, the relative orientation of the two reactants of approx. 34° is very unfavorable and strongly deviates from the optimal value of 107° (Dunitz-Bürgi trajectory, Fig. 31 c.)). Both facts suggest a rearrangement of either the cofactor or/and the donor substrate in the subsequent reaction steps on the way to the covalent donor-cofactor adduct.

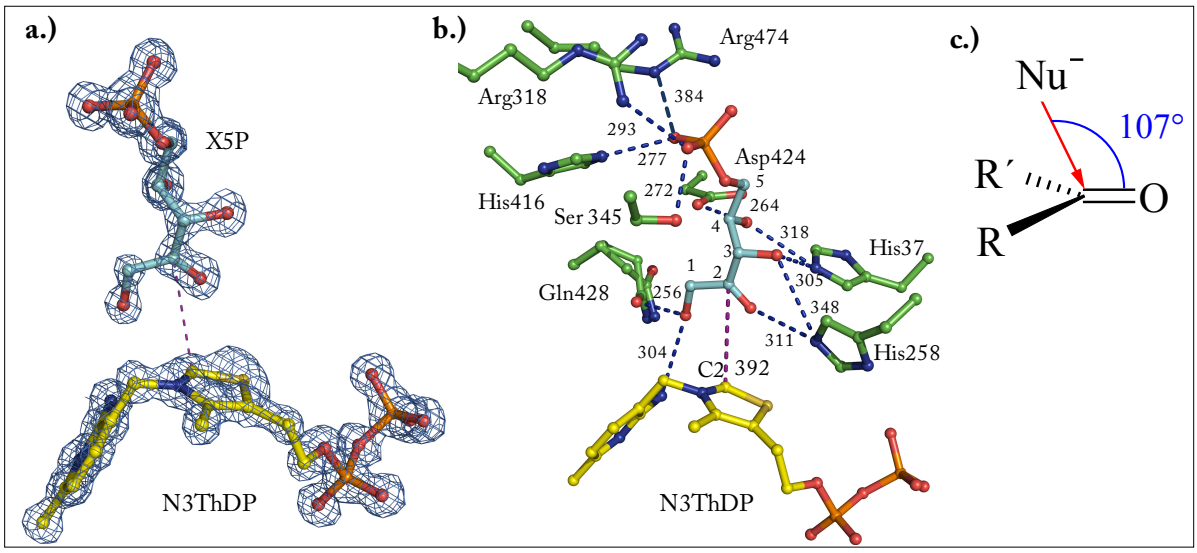

Fig. 31: Michaelis complex of *h*TK-N3ThDP with donor substrate X5P. a.) X5P bound in close proximity to N3´-pyridyl-ThDP. The 2mFo-DFc electron density map surrounding ligand and cofactor analogue is contoured at 2σ. **b.)** Polar interactions of donor X5P with active site residues of *h*TK or the cofactor are indicated by blue dashed lines, distances are labeld (in pm). Additionally, the inter-atomic distance of 392 pm between the C2 of the thiazolium ring and the C2α of the X5P is indicated by a purple dashed line. Selected active site residues and X5Ps´ carbon atoms are labeled. **c.)** Geometrical requirements for nucleophile reactions according to Bürgi and Dunitz (see text).

3.4.1.2. Michaelis Complexes of *h*TK with Donors F6P and S7P

Motivated by our successful attempt to trap the non-covalent complex of *h*TK and X5P we performed analogous experiments with the C6 and C7 donors F6P and S7P. Several high resolution datasets were collected to determine the structures of *h*TK in non-covalent complexes with those donors but the additional electron density peaks found in the active sites of those structures were difficult to interpret. Two strong positive difference electron density peaks were found at the entrance of the active site. According to their shape and coordination sphere (Arg318 and Arg474, not shown) it is plausible to assume that these density peaks originate from phosphate moieties bound at low occupancy. Hence, the density map is suggestive of two phosphate binding sites (Fig. 32).

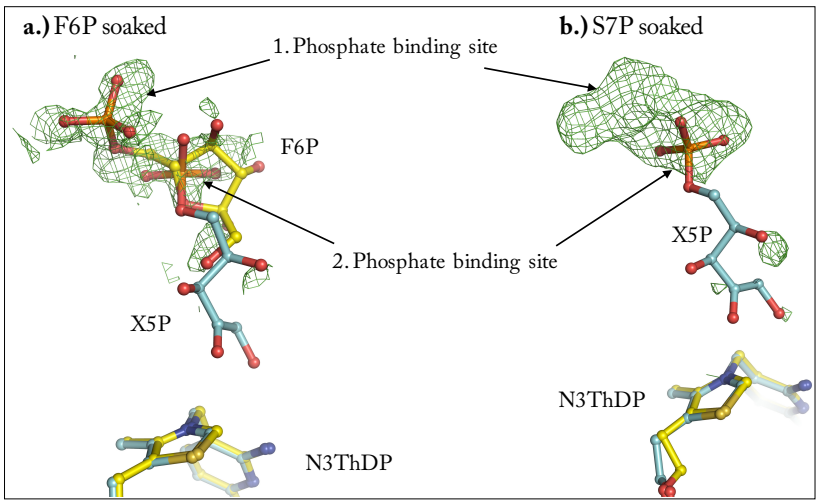

Fig. 32: Michaelis complex of *h*TK-N3ThDP with F6P (1.2 Å) and S7P (1.37 Å). For both figures a residue omitted mFo-DFc density map contoured at 3σ is shown. **a.)** Superposition of the x-ray structures of *h*TK (co-crystallized with N3´-pyridyl ThDP) in complex with X5P (cyan) or F6P (yellow). F6P present in α anomeric form was modeled into the positive difference density but wasn´t refined. The observed difference electron density peak found after soaking with the C6-donor can´t be explained with the presence of either a cyclic or acyclic form of F6P alone. **b.)** Superposition of the x-ray structures of *h*TK (co-crystallized with N3´-pyridyl ThDP) in complex with X5P (cyan) or S7P (yellow). In this case none of the five possible forms (acyclic, furanose and pyranose) of S7P were modeled into the difference electron density peak found after soaking with the C7-donor.

In contrast to that, positive difference density peaks found in close proximity to the cofactor analogue are diffuse suggesting that the non-phosphate part of those donors is highly flexible. Thus, it was impossible to reasonably model and refine complete models of F6P or S7P. For F6P it was at least possible to fit the phosphate moiety of an α furanose form into the positive difference electron density map. However, the conformation of the remaining part of F6P shown in Fig. 32 is not well represented by the difference electron density map. Hence, proposals for an active participation of active site residues in ring opening of either F6P or S7P are not feasible. Superposition with the *h*TK-

N3ThDP-X5P complex revealed that the phosphate moiety of X5P fits nicely into the second phosphate binding site supporting the idea of two binding sites for phosphate in TK.

The determined recognition complexes with donor substrates F6P and S7P suggest that after initial binding in the first binding site donors slide deeper into the active site and will be positioned in a second binding site (Michaelis complex) in closer proximity to the cofactor. This approximation is probably necessary to enable suitable conditions for carboligation to cofactors´ C2.

3.4.1.3. The Michaelis Complexes of *Ec*TK with Donor Substrates

We performed similar crystallographic experiments with *Ec*TK in order to compare donor binding in both TKs. As for *h*TK we could solely visualize binding of donor substrate X5P whereas experiments (crystal soaking and co-crystallization) with F6P and S7P generated uninterpretable, additional electron density peaks in the active site of *Ec*TK (data not shown).

The x-ray structure of *Ec*TK-N3ThDP in complex with X5P was determined to 1.4 Å (R_{work} = 12.34, R_{free} = 16.68). The additional positive electron density map found in proximity to the cofactor analogue is well defined and was modeled as acyclic keto form of X5P (Fig. 33 a.)). The coordination sphere of X5P as well as its orientation relative to the cofactor is almost identical in both studied transketolases (Fig. 33 b.)). Minor differences for X5P binding present in *Ec*TK are:

a.) Ser385 (Ser345 in *h*TK), which is involved in binding of the phosphate moiety of X5P, adopts two alternate conformations in contrast to just one traceable conformation in *h*TK.

b.) His473 (Gln428 in *h*TK) is involved in a strong (257 pm) hydrogen bonding interaction with O1α of X5P.

As found for *h*TK, the distance between cofactor C2 and X5P C2 of 376 pm as well as the angular conditions (Dunitz-Bürgi trajectory) are unfavorable for a spontaneous carboligation reaction indicating structural rearrangements of X5P and/or the cofactor itself in the course of reaction to realize suitable conditions for carboligation.

Noteworthy, *Ec*TK-bound ThDP as well as the analogue N3ThDP were found to possess high cofactor flexibility in the substrate-free and substrate-bound state. It is reasonable to assume that this cofactor flexibility is also present for this complex even if the structural resolution precluded modeling of both conformers. Mechanistically interesting, in the lower populated, so called “up” conformation the distance between the reactants would be decreased to 281 pm (Fig. 33 c.)), a suitable distance for carboligation. However, since the angular conditions would be still unfavorable X5P has to adopt a different position relative to the trapped Michaelis complex position. While *Ec*TK obviously exhibits an encoded cofactor flexibility that can be correlated to function in donor ligation *h*TK-bound cofactor

doesn´t possess such characteristics. Thus approximation of the reactants for carboligation can solely be realized by X5P.

Remarkably, our crystallographic results on *Ec*TK strongly indicate that this enzyme samples different cofactor conformations already in the substrate-free state that are necessary during catalysis. In contrast the side chains of the active site residues are rather rigid. This is an extraordinary observation since bio-catalytic cofactors are assumed to be tightly incorporated into the protein component. It is widely believed that the dynamic part of catalysis is realized by the protein (Eisenmesser et al., 2005; Henzler-Wildman and Kern, 2007) whereas the cofactor "just" offers chemical reactivity that can´t be supplied by amino acids. Noteworthy, experimental and computational evidence for dynamic characteristics of ThDP (Asztalos et al., 2007; Cavazza et al., 2006; Chabriere et al., 2001) and other bioorganic cofactors could already been presented (Jensen and Ryde, 2005). Especially flavins are known to link the cofactor conformation with their redox status and the lifetime of intermediate states (Kao et al., 2008). However, to our knowledge an analogous conformational sampling of a cofactor was so far not reported.

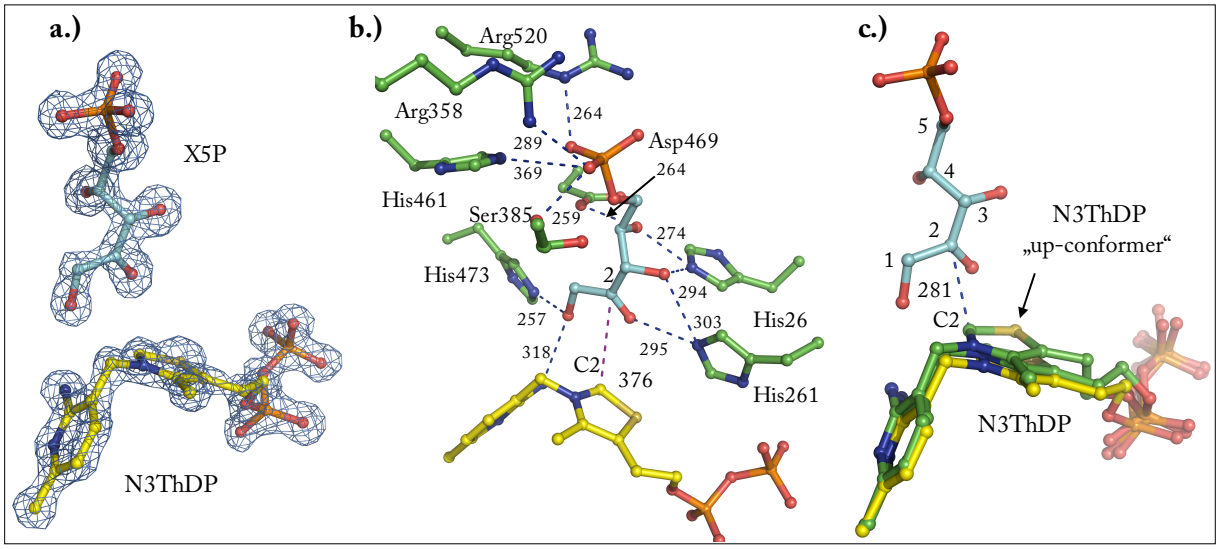

Fig. 33: Michaelis complex of *Ec*TK-N3ThDP with X5P. **a.)** Donor X5P (cyan) bound in the active site of *h*TK complexed with the analogue N3ThDP (yellow). The 2mFo-DFc density map is contoured at 1.5σ. **b.)** Polar interactions of donor X5P (yellow) with active site residues (green) are indicated by blue dashed lines (distances in pm). The interatomic distance of 376 pm between the C2 of the thiazolium ring and the C2α of the X5P is indicated by a purple dashed line. **c.)** Superposition of *Ec*TK-N3ThDP- (green) and *Ec*TK-N3ThDP-X5P complex. The interatomic distance between X5P C2 and C2 of the "up"-conformer (labeled) of N3ThDP is indicated (281 pm).

The interaction between *Ec*TK-N3ThDP and X5P could be analyzed quantitatively using ITC (Fig. 46) revealing a high K_D = 135 ± 38 µM. Moreover, X5P binding is favoured enthalpically (polar

interactions) and entropically (repulsion of water). ITC experiments using *h*TK or *Ec*TK with other donor substrates failed.

3.4.1.4. Which Conformer of Fructose 6-phosphate Will be Bound by TK ? - Implication for the Ring-Opening Reaction of Cyclic Donor Substrates

Our structural results presented in the previous chapters indicate that both TKs don´t bind selectively one certain conformer of F6P and S7P. Thus, structural heterogeneity of both donors is probably an important origin of the uninterpretable electron density peaks found in the active sites after substrate soaking. Additionally, it has to be considered that even if one certain cyclic state will be bound, the enzyme has to populate and align the acyclic keto form to enable forward commitment of the reaction. In this case one would also expect to observe different conformers in the active site which again would result in a diffuse electron density map.

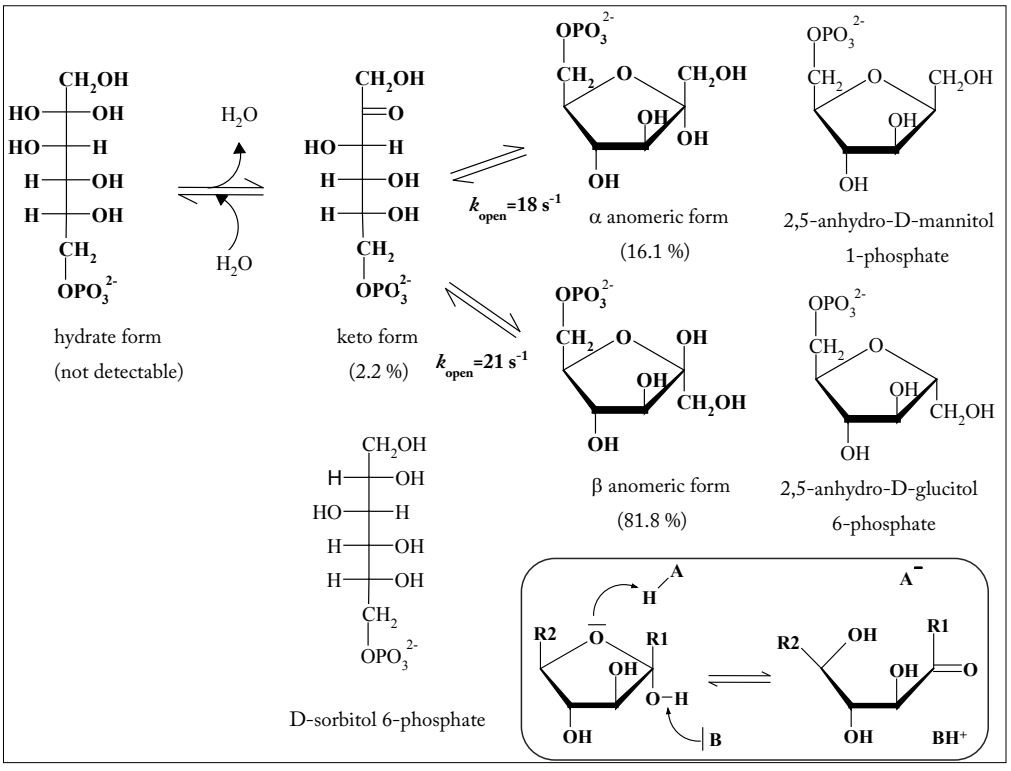

Fig. 34: Conformational equilibrium of F6P in aqueous solution. The chemical structure of four possible conformations of F6P is depicted in bold as well as the relative distribution at 6 °C and pH 4.5. Please note that F6P is predominantly present as cyclic furanose (97.8 %) showing just traces of the reaction competent keto form. Substrate analogues mimicking individual conformations of F6P are shown in Fischer or Haworth projection. Rate constants for the conversion of α and β anomer into the acyclic keto form at 40 °C and pH 7.5 (Pierce et al., 1985) are shown bold. **Boxed:** Simplified reaction scheme for the ring opening of an α-furanose into its acyclic carbonyl form.

In order to solely visualize binding of one discrete F6P conformer to *h*TK we used substrate analogues mimicking acyclic- (sorbitol 6-phosphate), α anomeric furanose- (2,5 anhydro-D-mannitol 1-phosphate) or β anomeric furanose form (2,5 anhydro-D-glucitol 6-phosphate) of F6P (Fig. 34). Unfortunately, such analogues are not commercially available for the C7-donor S7P. The rate constant for ring-opening of F6P in aqueous solution at 40 °C and pH 7.5 is 20 s^{-1} (Pierce et al., 1985) strongly indicating that this step is rate-limiting for the TK overall reaction (*Ec*TK $k_{cat} \approx 50\ s^{-1}$) and in particular for formation of covalent donor-ThDP adducts (*Ec*TK and F6P, $860 \pm 230\ s^{-1}$). It is therefore reasonable to assume that transketolases accelerate the ring opening by direct catalysis. Conversion of cyclic semiacetal form into the acyclic keto form requires protonation of the ring oxygen and proton abstraction from the anomeric hydroxyl group (Fig. 34, boxed). Since there are numerous polar residues (His, Ser, Asp) and water molecules in the active site that could either participate as a base or acid a proposal for a ring opening mechanism requires structural trapping of a cyclic donor substrate.

First the inhibitory ability of those analogues on the over-all TK reaction was tested by steady-state kinetic methods (Fig.35). A detailed quantitative analysis of inhibition couldn´t been carried out due to limited availability of those analogues. For this reason the native substrates R5P and X5P were used in a sub-K_M concentration of 0.2 mM for donor- and acceptor-substrate and the activity was determined in presence of different concentrations of each analogue.

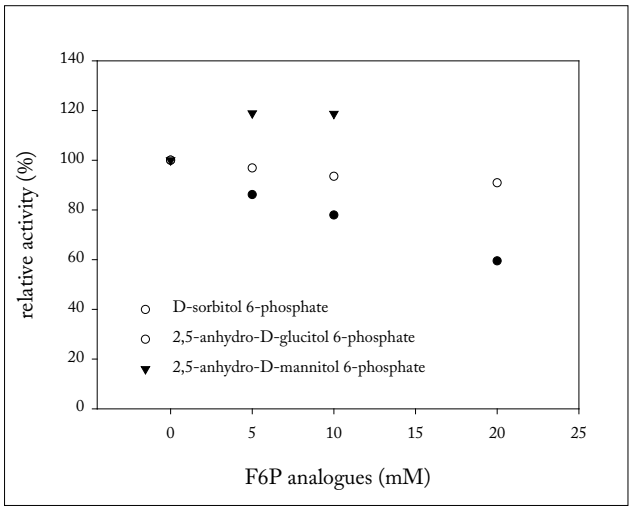

Fig.35: Inhibitory effect of different F6P analogues on *h*TK activity. Kinetics were carried out with 100 µg/ml (1.45 µM active sites) *h*TK, 5 mM $CaCl_2$, 100 µM ThDP, 0.2 mM R5P, 0.2 mM X5P, 3.6 U/ml G3PDH/TIM in 50 mM glycylglycine (pH 7.6) at 30 °C in absence and presence of either D-sorbitol 6-phosphate (black circles), 2,5-D-anhydro-glucitol 6-phosphate (white circles) or 2,5-D-anhydro-mannitol 1-phosphate (black triangle) at different concentrations.

Interestingly, even when a 400 fold molecular excess of both cyclic substrate analogues relative to the natural substrate was used *h*TK activity was only slightly (2,5-anhydro-D-glucitol 6-phosphate) or not

at all inhibited (2,5-anhydro-D-mannitol 1-phosphate). A very weak inhibition to approx. 60 % residual activity was observed in case 400fold molecular excess S6P was added to the reaction kinetics suggesting that TK preferentially binds acyclic F6P. To receive a more comprehensive insight on donor substrate recognition, we determined the x-ray structure of *h*TK in complex with each analogue (*h*TK + S6P, 1.45 Å R_{work}=15.83, R_{free}=20.05; *h*TK + 2,5-anhydro-D-glucitol 6-phosphate 1.09 Å R_{work}=12.01, R_{free}=14.26, *h*TK + 2,5-anhydro-D-mannitol 1-phosphate 1.14 Å, R_{work}=19.16, R_{free}=22.75)

As already suggested by the kinetic measurements, binding of the two cyclic substrate analogues to *h*TK seems to be very weak and the resultant electron positive electron density maps after substrate soaking with 100 mM of the individual sugar phosphate revealed only weak additional positive difference electron density peaks at the active site entrance of *h*TK. However, a density peak could be interpreted in both cases according to its shape and coordination sphere as a phosphate moiety bound with low occupancy. For both cyclic F6P-analogues solely this phosphate moiety could be modeled indicating that all ring atoms are most likely disordered. Remarkably, the analogue 2,5-anhydro-D-glucitol 6-phosphate did not bind to the active site but at low occupancy in a solvent exposed pocket (Fig. 76). For S6P, the analogue of the acyclic state of F6P, we found additional, interpretable positive difference density in the active site (Fig. 36). While the majority of the analogue atoms and especially the phosphate moiety are well defined, density for the first and second hydroxyl group is missing suggesting a higher flexibility of this part relative to the rest of the molecule.

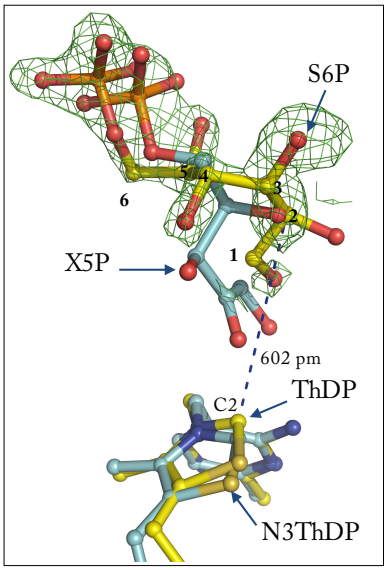

Fig. 36: Binding of acyclic S6P to *h*TK. Superposition of the x-ray structures of *h*TK in non-covalent complex with S6P (yellow) and X5P (cyan) in stick and ball representation. The residue omitted mFo-DFc map found after soaking with the analogue (green, contoured at 3σ) is well defined for the phosphate moiety of S6P whereas some parts of the molecule are poor defined like the C1 and C2 hydroxyl groups. Selected atoms are labeled.

Further structural analysis revealed that S6P is bound with low occupancy (<60 %) and adopts a different position within the active site relative to native substrate X5P. This deviation has consequences for the next catalytic step. The nucleophilic attack of cofactor C2 to the C2 carbonyl of the donor substrate becomes more unfavorable due to an increased distance (602 p) of both reactants. It is therefore questionable if this structure represents the Michaelis complex between *h*TK and native acyclic F6P.

3.4.2. The Covalent Donor-ThDP Intermediates in *b*TK

Nucleophilic attack of C2-deprotonated cofactor to the keto carbon of a donor molecule generates the first covalent intermediate in TK catalysis (Fig.37). Asztalos and colleagues succeeded recently in solving the high-resolution x-ray structures of covalent X5P- and F6P-ThDP intermediates in *Ec*TK (pdb-codes: 2R8O, 2R8P) (Asztalos et al., 2007). The authors made the extraordinary observation that the newly formed C-C single bond is not planar with the thiazolium ring system but harbors a strong angular distortion (25°-30°) generating intermediates which are rich in energy.

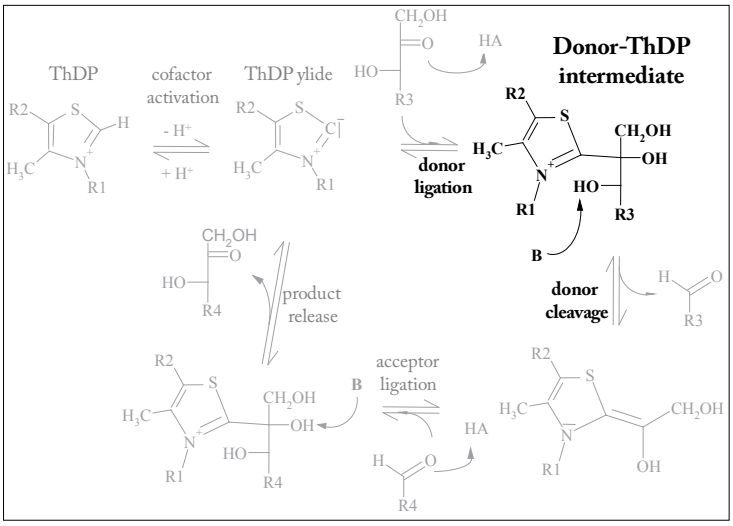

Fig.37: Formation and depletion of covalent donor-ThDP adduts. Simplified reaction scheme for TK catalyzed overall reaction in presence of donor and acceptor substrates. In absence of acceptor substrates this scheme is simplified to the donor ligation and –cleavage (bold) step and the corresponding reverse reaction.

The goal of our experiments was to determine all native covalent donor-ThDP intermediates in *b*TK to high resolution by x-ray crystallography. Those structural insights should answer mechanistic questions like:

- What is the exact chemical state of donor-ThDP intermediates?
- How does TK realize selective cleavage of strong covalent C-C-bond?
- Why does TK stabilize high-energetic donor-ThDP intermediates?
- What are the energetic contributors for the generation of bond distortion between sugar and coenzyme?

3.4.2.1. Intermediate Distribution for the Reaction of Donor Sugars with TK

In order to analyze which covalent intermediates accumulate after addition of donor substrates in solution we carried out a NMR-based intermediate analysis (Kluger and Tittmann, 2008; Tittmann et al., 2003). This approach in solution provides assistance to assign intermediates in the crystalline state as well. Under steady-state conditions, substrate saturation of each donor and in absence of any acceptor we find clear differences in equilibrium for the three different donor sugars (Fig. 38)(Asztalos et al., 2007; Mitschke et al., 2010). For X5P we find approx. 25 % unsubstituted cofactor as a reporter for the Michaelis complex and 75 % covalent X5P-ThDP adduct. However, there is no cleavage product (DHEThDP) observable in the sample. After reaction with F6P 12 % DHEThDP, 72 % F6P-ThDP adduct and 16 % Michaelis-complex are observable. For the reaction of *b*TK with the seven carbon donor S7P we found a higher fraction of DHEThDP (40 %) and just 10 % unreacted ThDP. The signal at 7.35 ppm that appeared after the reaction with S7P was assigned as the S7P-ThDP adduct. Despite the fact that no standard for this compound exists its similar chemical shift compared with those of the X5P- and F6P-ThDP adducts strongly suggests that the singlet originates from the S7P-ThDP adduct. Several mechanistic conclusions can be made from these experiments. The fraction of the cleavage intermediate DHEThDP accumulates with increasing chain length of the donor. Whereas we observe no or just traces of DHEThDP for the reaction with X5P and F6P almost half of all active sites are occupied with this intermediate in case S7P was used. S7P was synthesized chemo-enzymatically using HPA and R5P as educts. An impurity of the S7P sample with HPA, which would be an alternative explanation for the increased signal at 7.32 ppm, could be excluded by mass spectrometry (data not shown). By inspection of the reaction scheme depicted in Fig. 38 b.) two possible explanations are feasible to address the changed distribution of covalent donor adducts and cleavage products. It could either be that the relative reactant state energy of the donor adducts relative to the cleavage product are changing with longer donor chain length or that there is a different affinity of DHEThDP in *b*TK for the three acceptor sugars (Mitschke et al., 2010). Whereas the first explanation is difficult to analyze experimentally the second one can be excluded as it is already known that for example R5P is a better substrate relative to GAP (Sprenger et al., 1995). Therefore, we conclude that reactant state energy is increasing with increasing chain length of the donor. To verify these conclusions and to calculate the absolute energies of C5-, C6- and C7-adduct quantum mechanical modeling methods like density functional theory (DFT) have to be performed. A similar intermediate distribution can be found for *Ec*TK, suggesting similar energetics of donor-cofactor adducts in both TKs. However, the reaction of *Ec*TK and S7P revealed accumulation of DHEThDP (40 %) and just traces of the S7P-ThDP adduct while the majority of the active sites remained un-substituted.

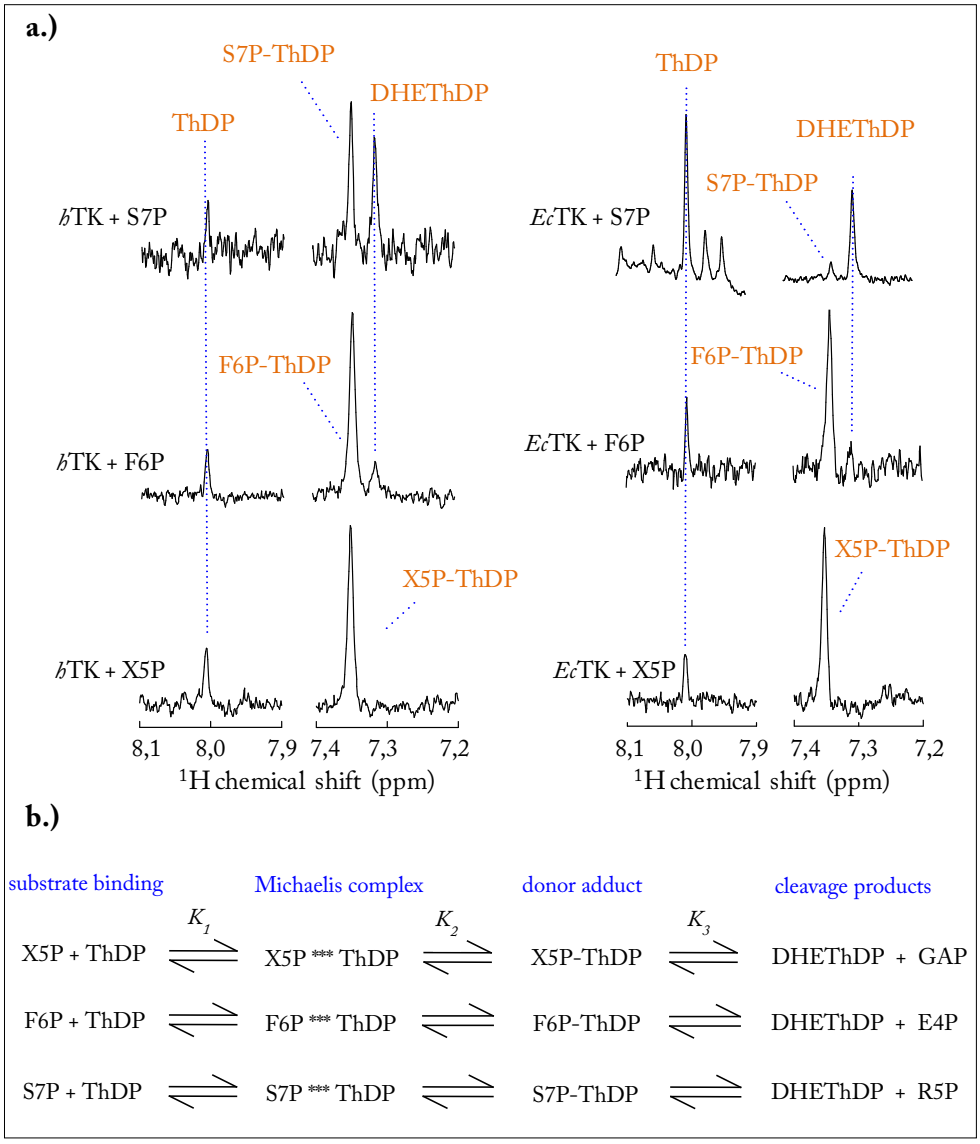

Fig. 38: Distribution of covalent intermediates for the reaction of *b*TK and *Ec*TK with native substrates X5P, F6P and S7P. a.) ^{1}H-NMR-based intermediate analysis for the reaction of 7.5 mg/ml *b*TK (109 µM active sites) or *Ec*TK (104 µM active sites) with either 25 mM X5P, F6P or S7P in 5 mM $CaCl_2$, 50 mM glycylglycine (pH 7.6) at 8 °C and 1 min reaction time. Signals of DHEThDP, X5P-ThDP and F6P-ThDP were identified according to synthesized standards. (Sample preparation of *b*TK with X5P and F6P was carried out by Lars Mitschke. The samples of *Ec*TK with X5P and F6P were prepared by Dr. Peter Asztalos) **b.)** Underlying equilibria for the reaction of transketolase with donors X5P, F6P and S7P (donor-half reaction) in absence of acceptors. After substrate binding the Michaelis complex is formed in which substrates are oriented for the subsequent carboligation yielding covalent adducts. Donor cleavage finally results in formation of the DHEThDP intermediate and liberation of an aldose phosphate.

Based on these results from NMR experiments in solution we carried out substrate soaking experiments at the same temperature and 4fold higher donor concentration with single crystals of *b*TK co-crystallized with native cofactor ThDP (Tab. 3).

3.4.2.2. Covalent Donor-ThDP Intermediates Trapped to Ultra-High Resolution in *h*TK

By combination of substrate soaking and cryo-crystallography we succeded in determination of x-ray structures of C5-donor X5P (0.97 Å, R_{work} = 8.24, R_{free} = 9.51, Fo > 4σ), C6-donor F6P (0.98 Å, R_{work} = 8.37, R_{free} = 10.03, Fo > 4σ) and of C7-donor S7P (1.03 Å, R_{work} = 11.90, R_{free} = 13.99) covalently attached to *h*TK-bound cofactor at ultra-high resolution. Because all trapped reactant states revealed very similar structural features just the best resolved *h*TK-X5P complex will be described in detail below. Furthermore, general structural features of all donor-ThDP intermediates shall be compared and linked to chemical reactivity. Figures and brief descriptions of F6P- and S7P-ThDP intermediates can be found in the appendix (Fig. 82).

In very good agreement with the NMR intermediate studies in solution we found after refinement of occupancy that 71 % of the active sites are occupied with X5P-ThDP while 29 % ThDP remained unsubstituted and correspond to X5P positioned in the docking site (Fig. 39). For F6P and S7P approx. 70 % of the active sites accumulated either the F6P-ThDP or S7P-ThDP intermediate whereas the resulting 30 % represent unreacted ThDP. This finding deviates from our solution ^{1}H-NMR experiments performed under substrate saturation of both donor molecules (Fig. 38) which revealed just traces of unsubstituted ThDP. Moreover and in contrast to X5P, no F6P or S7P bound in the docking site of *h*TK is detectable. Hence, there seems to be a difference between X5P and both other native donors as X5P has a visualizable, internal equilibrium between its Michaelis complex and the covalent adducts whereas for F6P and S7P the Michaelis complex is probably very transient and doesn´t accumulate. This is in line with our unsuccessful attempts to trap the Michaelis complex of those two donors using the catalytically inactive cofactor analogue N3ThDP. Noteworthy, according to the NMR experiments 12-40 % post-cleavage intermediate (DHEThDP) were accumulated in solution. A detailed inspection of the electron density map revealed that solely the covalent donor-ThDP addcuts have accumulated in the crystal structures.

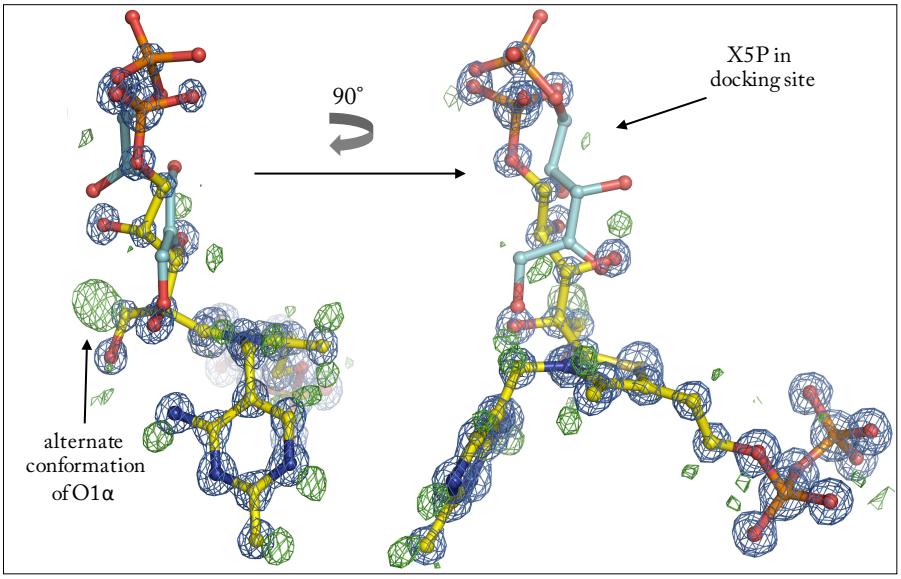

Fig. 39: X-ray structure of *b*TK X5P-ThDP adduct determined at 0.97 Å resolution. Covalently bound X5P (yellow) and the minor populated un-reacted X5P (cyan), located in the docking-site, are shown in ball and stick representation. For reasons of clarity all active site residues as well as solvent molecules were omitted. A minor populated alternate conformation of a sugar derived hydroxyl group (O1α) is indicated. The final 2mFo-DFc (blue) and mFo-DFc (green) maps for covalent X5P-ThDP adduct are shown in a contour level of 3σ, respectively. Cofactor derived hydrogen atoms are visible as green spheres (hydrogen-omitted mFo-DFc map).

3.4.2.3. Interactions of the X5P-ThDP Intermediate with the Active Site of *b*TK

The intermediate molecule forms multiple polar interactions with active site residues and interestingly, the cofactor itself is involved in intra-molecular hydrogen bonding interactions (N4´ to O1α and O2α) (Fig. 1 a.)). The O1α group is flexible and samples between two alternate conformations suggesting that the sugar derived part of the intermediate is not tightly fixed in the active site. In its predominantly adopted conformation O1α can perform hydrogen bonding interactions with His110, Gln428, 4´-imino group of ThDP and an active site water molecule (W1 in Fig. 40 b.)) whereas in its lower populated conformation (occupancy approx. 10-20 %) just a productive interaction with His110 and the X5P derived O4α is feasible. All other polar interactions of the intermediate with the active site are very similar to that observed for the analogous intermediate structure in *Ec*TK (Asztalos et al., 2007). Differences are observable for Gln428 (His473 in *Ec*TK) that is present in two alternate conformations. In one of these conformations Gln428 (235 pm) could indeed be involved in a very strong hydrogen bonding interaction (Cleland et al., 1998) with the sugar derived atom O2α. However, the very small occupancy of this orientation of 31 % indicates that Gln428 avoids this orientation upon intermediate formation (71 % covalent X5P-ThDP intermediate). Additionally, an unambiguously assignment of the side chain conformation in the lower occupied state of Gln428 is

not reliable which is visualized in Fig. 40 as this functional group is shown 180 ° rotated in a.) relative to b.).

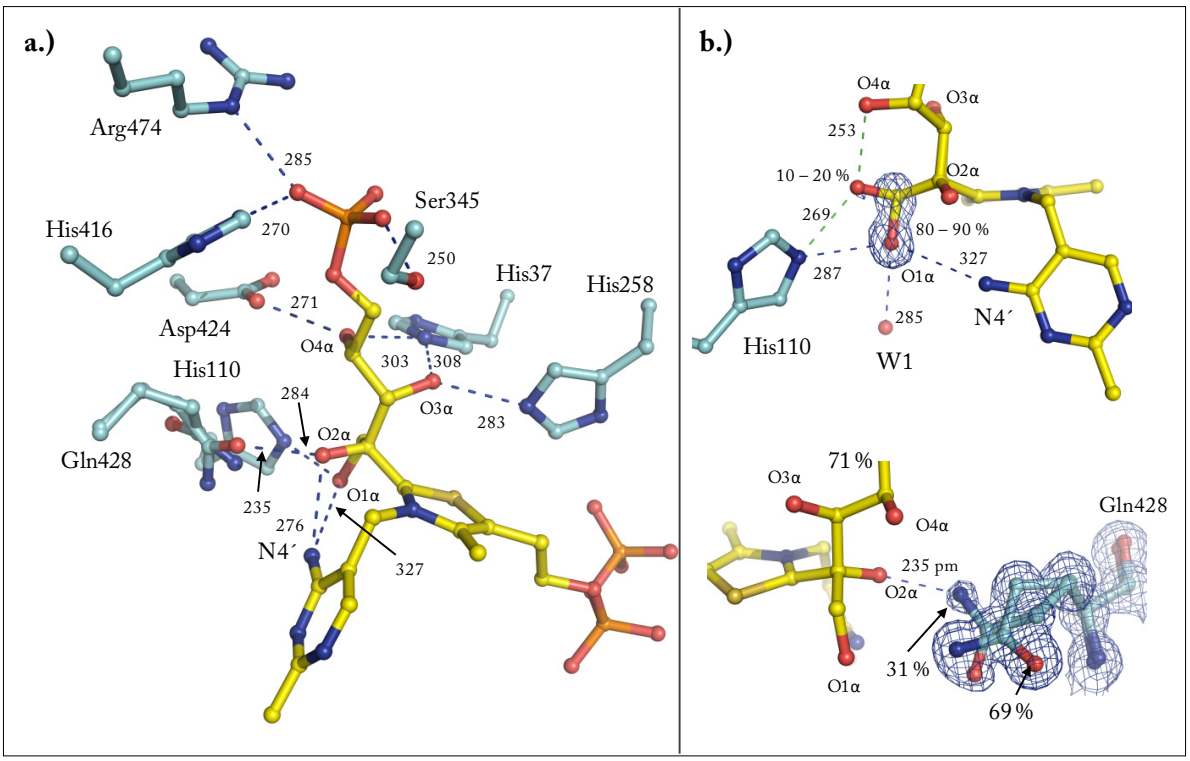

Fig. 40: Active-site interactions with the X5P-ThDP adduct. a.) Amino acid site chains that are involved in binding and positioning of the covalently bound X5P-ThDP adduct (0.97 Å) are shown in cyan whereas the intermediate is shown in yellow. Major polar interactions are highlighted as dashed blue lines, distances are indicated (in pm). The sugar derived hydroxyl groups and cofactor N4´are labeled. **b.) Top:** Detailed view on the inteactions of intermediates O1α which adopts two alternate conformations (occupancies indicated). Electron density map is solely shown for O1α and C1α. Interactions of both alternate conformation of His110 are indicated by dashed lines (green and blue). **Bottom:** Interaction of Gln428 with X5P-ThDP. The occupancy of the X5P-ThDP intermediate (71 %) as well as for both Gln428 orientations are indicated. 2mFo-DFc maps are contoured at 1σ. Selected atoms are labeled.

3.4.2.4. Donor Intermediates Predominantly Exist as 1´, 4´ Iminotautomeric State

The electron density maps for all three donor-intermediates are well defined and enabled tracing of all cofactor-derived hydrogen atoms at a standard level of 2.8-3σ in a mFo-DFc difference electron density map. Protonation of N1´ and N4´ for the six-membered ring of donor-ThDP intermediates strongly indicates a predominant accumulation of the 1´, 4´-iminotautomeric (IP) form (Fig. 41). The bond lengths for N4´-H (97-109 pm) and N1´-H (97-110 pm) don't deviate more than 10 % from expected values (101 pm) further supporting the correct assignment of the protonation state. Remarkably, while the N4´-H bonds have expected coplanar bonding geometry (deviation 3-12°) the geometry for the hydrogen linked to N1´ constantly deviates 20-30° from linearity (N4´-N1´-H ≈

150-160°). A correlation of this deviation with catalytic competence such as cofactor activation must yet remain open.

By decreasing the contour level of the map to 2.4-2.5σ a weak, positive difference electron density peak is observable at N4´ (not shown) suggesting that a small fraction APH^+ is formed at this catalytic step as well. However, the three native donor intermediate structures (X5P-, F6P- and S7P-ThDP) revealed 30 % unreacted coenzyme which also contribute to electron density maps and could generate a second positive difference electron density peak at N4´.

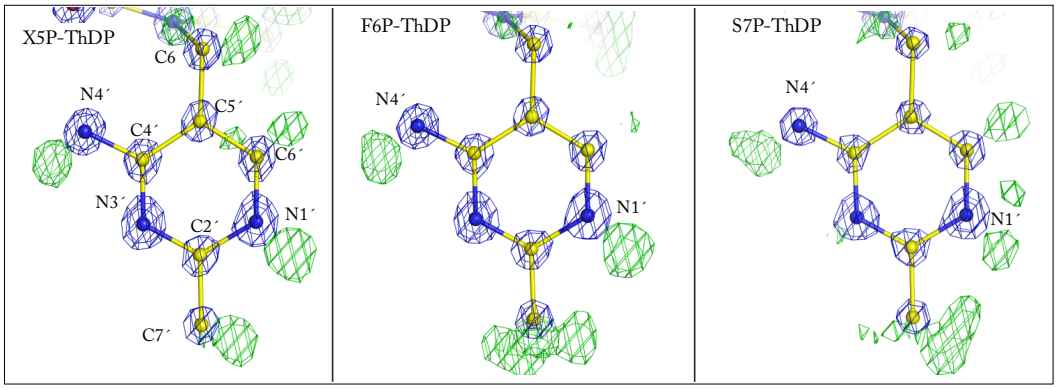

Fig. 41: Protonotion state of the donor-ThDP intermediates revealed by x-ray crystallography. X-ray structures of covalent X5P-ThDP- (0.97 Å), F6P-ThDP- (0.98 Å), S7P-ThDP- (1.03 Å) intermediate shown in stick and ball representation surrounded by a 2mFo-DFc electron density map at 5σ (blue) and a mFo-DFc positive difference electron density map at 3σ (green). Selected atoms are labeled. The positive electron density peaks at N4´ and N1´ strongly suggest accumulation of the IP form.

Although numerous spectroscopic studies already suggested that covalent, sp^3-hybridized substrate intermediates exist in the IP form (Nemeria et al., 2004; Nemeria et al., 2009) this is the first structural assignment of the IP form for this particular enzymatic reaction intermediate in any ThDP-dependent enzyme so far. Noteworthy, covalent donor-ThDP adducts in *Ec*TK possess a hypsochrom-shifted IP signature with a maximum at approx. 295 nm which was assigned using UV/Vis absorbance spectroscopy in combination with an NMR-based intermediate analysis (Fig.17, Fig. 81).

3.4.2.5. Bond Lengths Analysis of the Donor-ThDP Intermediates

TKs cleave two strong C-C bonds either to enable donor release (C2-C2α bond) or donor cleavage (C2α-C3α bond). In order to facilitate C-C bond cleavage proton abstraction from either O2α (donor release) or O3α (donor cleavage) forming presumably transient alkoxids is required (Fig. 42). The product of those cleavage reactions is a C2α cabanion in resonance with its enamine component or the

cofactor C2 carbanion in resonance with a C2 carbene. This electronic stabilization can be considered as a thermodynamic driving force for C-C bond cleavage in both cases. Furthermore, ionization of other sugar-derived OH-groups like O4α can potentially occur. The products of those C-C-bond cleavage reactions are isolated carbanions like the C3α carbanion depicted in the middle scheme of Fig. 42. Isolated carbanions lacking any potential stabilization are unstable and the equilibrium of the reaction lies consequently on the side of the uncleaved state.

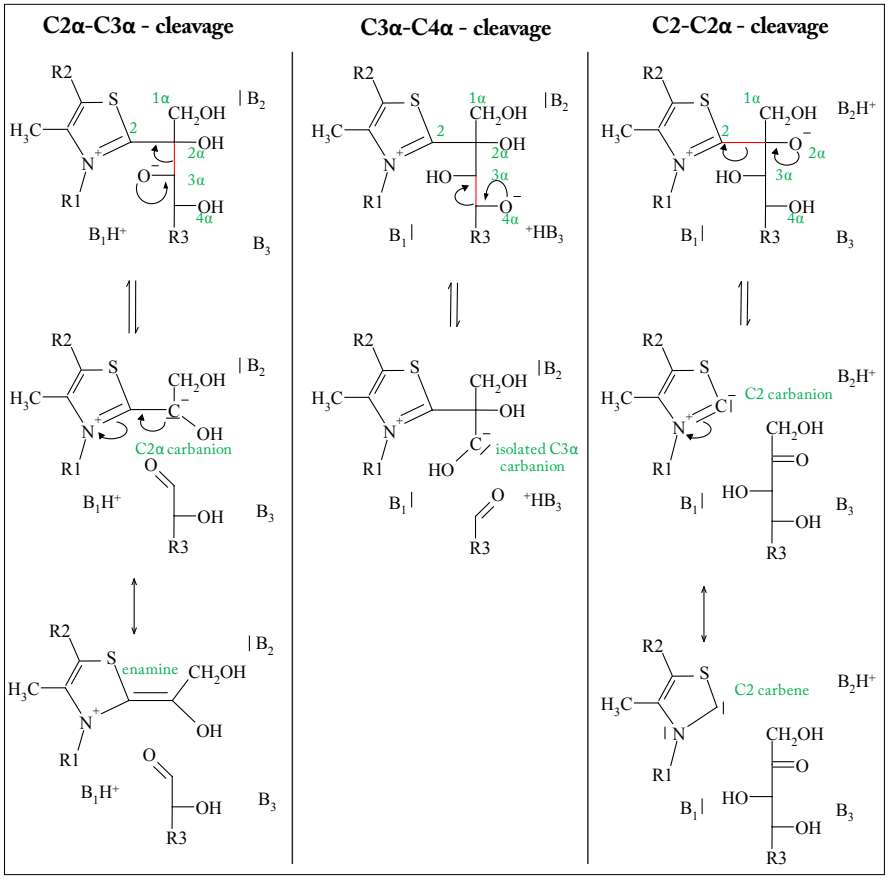

Fig. 42: Reversible C-C bond cleavage of donor-ThDP intermediates. Chemical structure of donor-ThDP adduct including possible C-C bond cleavage mechanism via the formation of carbanions. Scissile C-C bonds are highlighted in red. Brønsted bases (B1, B2 and B3) are labeled. For explaination see text.

Analysis of all three native donor substrate-intermediates revealed very similar tendencies. The scissile C2α-C3α and C2-C2α bonds are significantly elongated (Tab. 5, Tab. 13) indicating that they are already relaxed by physical stress or electronic effects potentially facilitating the subsequent cleavage reactions. The presence of these long bonds was verified for the X5P- and F6P-ThDP intermediate by estimation of standard deviation using a pre-release version of *SHELXL-11* (Sheldrick, 2008) which was kindly provided by Prof. George Sheldrick. Here, it is important to consider that the C2-C2α

bond, which connects an aromatic ring carbon with an exocylcic carbon, should be slightly shorter than a standard C-C bond of 154 pm (Allen et al., 1987).

Tab. 5: Selected C-C-bond lengths of *h*TK in complex with X5P-ThDP, F6P-ThDP (refined with *SHELXL-11*) and S7P-ThDP (refined with *PHENIX*). For X5P- and F6P-ThDP and estimation of standard deviation was calculated. (* C2α-C3α and C2-C2α bonds were not included for calculation)

	C2α-C3α bond (pm)	C2α-C2α bond (pm)	avarage of all sugar derived C-C bonds * (pm)	range of all sugar derived C-C bonds * (pm)
X5P-ThDP	162.5 ± 1.5	152.3 ± 1.2	151.8	148.0-155.1
F6P-ThDP	155.2 ± 1.7	160.4 ± 1.5	153.1	149.2-156.2
S7P-ThDP	162	161	152.2	151-153

In cases of the C2α-C3α bond physical stress could be generated by two attractive "poles", the active site residues positioning the substrate derived phosphate moiety and the strained C2-C2α bond which itself is pulled into a planar arrangement. However, the hydrogen bonding network around the phosphate moiety is not rigid and should allow smaller positional changes arguing against a tight "anchor" function for this group. Another origin for the enlarged C2α-C3α bond could be the presence of a small fraction DHEThDP intermediate and an aldose (cleavage products). This possibility has to be excluded because acceptor sugars adopt sp^2 hybridization at C1 which is not supported by the electron density map. It is further conceivable that the cofactor pulles binding electrons into the thiazolium ring (electron sink) thereby causing the observed prolongated and C-C bonds. A bond prolongation of 8 pm (e.g. 154 to 162 pm) would dramatically decrease the bond dissociation energy by more than 30 kcal/mol, from 90 kcal/mol to less than 60 kcal/mol (Zavitsas, 2003). Importantly, all stated, speculative mechanisms have to be validated by computational or independent biophysical methods.

While elongated C-C bonds could be observed for sterically compressed, small-molecule structures (Kaupp and Boy, 1997; Maslak et al., 1995; Schreiner et al., 2011; Toda, 2000) there is to our knowledge no structural information available for an enzymatic reaction intermediate possessing such characteristics. Notably, Chabriére and co-workers (Chabriere et al., 2001) succeded to trap a covalent reaction intermediate (pdb-code:1kek) for the ThDP-dependent enzyme pyruvate:ferridoxin oxidoreductase with exceptionally long C-C bonds (C2-C2α bond 175-195 pm) connecting cofactor and substrate-derived part. However, the authors could prove a fractional radical character of those long bonds ("one-electron" bond) which is compatible with knowledge from small-molecule cation radicals (Bellvile et al., 1985). Since neither cofactor- nor substrate-centered radical species could so far be detected at any reaction step of TK this source for the elongated C2α-C3α bond can probably be excuded. The involvement of radicals is further unlikely due to the lack of any redox-active cofactor like flavins or iron-sulfur clusters in TK which is a prerequisite for ThDP-mediated radical

biochemistry (Tittmann, 2009). However, X-band electron paramagmnetic resonance spectroscopic measurements of enzyme bound donor-ThDP intermediates are currently in preparation to prove the presence or absence of radical species.

Furthermore the C2α-O2α and C3α-O3α bonds are slightly but significantly shorter than all other C-O single bonds of the intermediate suggesting that a small fraction of O2α and O3α might be deprotonated and present as alkoxids. However, for the S7P-ThDP intermediate the C3α-O3α is not shortened.

Tab. 6: Selected C-O-bond lengths of *h*TK in complex with X5P-ThDP, F6P-ThDP (refined with *SHELXL-11*) and S7P-ThDP (refined with Phenix). For X5P- and F6P-ThDP and estimation of standard deviation was calculated. (* C2α-C3α and C2-C2α bonds were not included for calculation)

	C2α-O2α bond (pm)	C3α-O3α bond (pm)	avarage of all sugar derived C-O bonds (pm)	range of all sugar derived C-O bonds (pm)
X5P-ThDP	135.6 ± 1.1	141.1± 1.3	145.4	143.7-147.1
F6P-ThDP	141.6 ± 1.4	139 ± 1.6	144.2	144-144.5
S7P-ThDP	138	145	143	142-145

After nucleophilic attack of the C2 carbanion to the keto carbon of the donor O2α is indeed first present as an alkoxide. Since no potential general acid is located in a suitable orientation the functional group acting as proton donor is very likely the 4´-amino group of the cofactor itself (APH^+ form) which thereby changes its protonation state from APH^+ to IP form (Nemeria et al., 2009).

While the determined bond lengths between C4 and C5 of 137-139 pm suggest a predominant double bond character, both bonds that C2 is involved in are significantly enlarged (C2-N3 136–140 pm instead of 132 pm, C2-S1 172–173 pm instead of 167 pm, Tab. 13).

The bond lengths in the six-membered IP moiety have similar values relative to those observed for small molecule structures of ThDP present as AP form (Pletcher et al., 1979). Solely the C5´-C6´ and C6´-N1´ bonds are slightly elongated. A correlation of this enlarged bond with catalytic competence must yet remain open.

3.4.2.6. Structural Evidence for the Presence of Angular Strain in Both Aromatic Ring Systems of Donor-ThDP Intermediates

As already described (Asztalos et al., 2007; Mitschke, 2008; Tittmann and Wille, 2009) covalent donor-ThDP adducts in transketolase exhibit a severe distortion of the newly formed C2-C2α single bond connecting the cofactor- and the sugar moiety of the covalent donor-ThDP intermediate. Importantly, a strong angular distortion (22° for X5P-ThDP, 24.5° for F6P-ThDP and 21° for S7P-ThDP) is an extraordinary observation for a sp^2 hybridized carbon atom. In order to prove whether

C2 is protonated we carefully inspected hydrogen omitted difference electron density maps of the intermediates. Since no density peak is observable in close proximity (1-1.5 Å) to atom C2 even at a very low contour level of 2σ sp^3 hybridization of C2 can indeed be excluded.

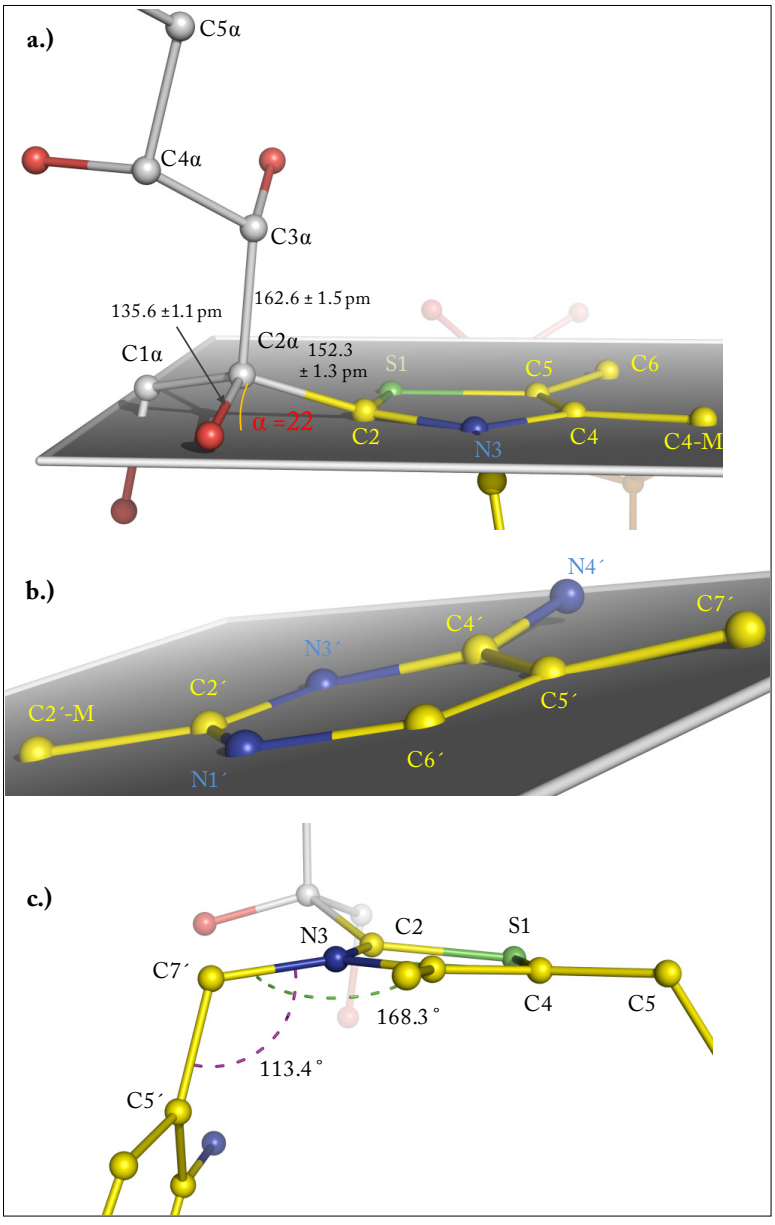

Fig. 43: Angular distortion in both aromatic ring systems of the X5P-ThDP intermediate. a.) Thiazolium ring of X5P-ThDP. A plane was generated (fixed points S1, N3 and C5) to visualize a deviation from planarity in the covalent X5P-ThDP adduct. The C-C single bond connecting cofactor and donor (C2-C2α bond) has a strong angular distortion of 22° (red). Selected atoms and bond length are labeled. X5P derived carbons are grey. **b.)** Aminopyrimidine ring of X5P-ThDP. A plane was generated (fixed points N1´, N3´ and C5´) to visualize a deviation from planarity in the 1´, 4´ iminopyrimidine ring of the covalent X5P-ThDP adduct. Please note that C4´ and as result thereof N4´ are significantly out-of-plane. Slight positional deviations are observed for C6 and C7´ giving the entire moiety a bent shape. **c.)** Detailed view on the bonding geometry of atom N3. Tortion angle (blue) and N3-C7´-C5´ bonding angle (purple, 113.4°) are indicated.

The angular distortion of the C2-C2α bond seems to induce strain in the entire thiazolium ring system of ThDP. While four atoms of the ring are almost perfectly arranged in-plane, C2 is slightly out-of-plane (Fig. 43, Fig. 82). Additionally, strain seems to be conducted into other parts of the molecule. The carbon atoms C4-M (methyl group) and C6 (methylen group) are also slightly above the imaginary plane formed by S1, N3 and C5. Those distortions finally provoke that the entire ring system is bent.

Also the second aromatic ring system is significantly distorted (Fig. 43 b.)). Moreover, the methylen group bridging both rings is prone to angular distortion reflected by an enlarged bonding angle for N3-C7´-C5´ of 113.4° (expected value 109°). In addition to some enlarged bonds (C2-S1, C2-N3) those ring distortion indicate a significant loss of aromaticity for the entire intermediate. In contrast all small molecule x-ray structures of ThDP show almost perfectly planar thiazolium and aminopyrimidine ring systems. However, a slight distortion of the aminopyrimidine ring was reported for a small molecule x-ray structure of a chemically synthesized ThDP-intermediate (Turano et al., 1982) which might allude that the electronic state of intermediates promote this ring distortion. Notably, a slight distortion of the six-membered ring is also observable for unsubstituted cofactor in *h*TK.

Thiazol N3 atom, which should adopt trigonal planar bonding geometry at this state of catalysis, reveals a significant deviation from planarity of approx. 12°. While the remaining 30 % unreacted cofactor, probably in their carbene state, could be adopted to explain this deviation the true atomicity of N3 and all other non-hydrogen atoms of the intermediate is suggestive for the accumulation of one discrete state. Thus, the exact electronic distribution within the thiazol ring remains to be further investigated. The observation of a drastically reduced aromaticity of enzyme bound ThDP, a process generally considered to be energetically unfavorable, is supported by other x-ray crystallographic snapshots of geometrically distorted reaction intermediates (Chabriere et al., 2001; Meyer, 2012).

Notably, relying on the distribution of covalent intermediates after the reaction of *h*TK with all three native donors we suggested that reactant state energy increase with the length of the donor molecule. However, our crystallographic results revealed that the strongest angular distortion is observable for F6P-(24.5°) followed by X5P-(22°) and S7P-ThDP (21°). If we put the angular distortion on a level with reactant state energy there is no correlation between chain length and the energy of an intermediate.

3.4.2.7. Structural Comparison of Donor-Intermediate Stabilization in *h*TK

The interactions of all native donor (C5-C7 sugars) substrate-ThDP intermediates with the active site of *h*TK are very similar and even the hydrogen bonding distances and geometry is almost identical for the hydroxyl groups that all three donors have in common (O1α to O4α). Significant differences originate from the fact that F6P and S7P are extended by 1 or 2 carbon atoms relative to X5P.

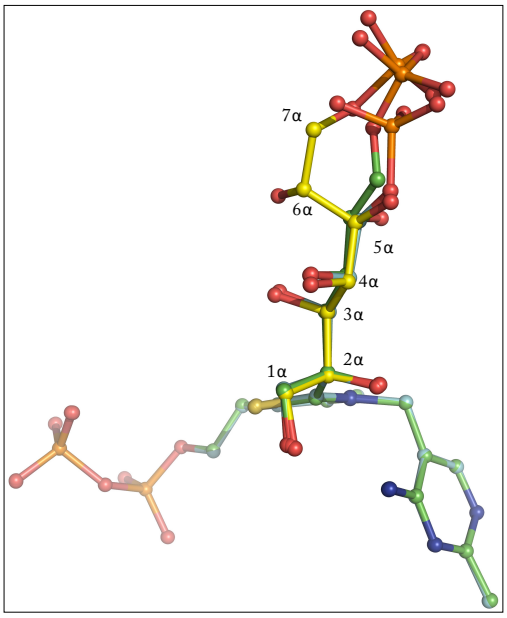

Fig. 44: Superposition of all three native donor-ThDP intermediates in *h*TK. The models for the X5P- (cyan), F6P- (green) and S7P (yellow)-cofactor adducts bound to the active site of *h*TK are shown in ball and stick representation. The sugar derived carbon atoms of S7P-ThDP are labeled. For clarity active site residues are omitted.

In consequence the phosphate moieties of F6P and S7P accommodate closer to the active site entrance. Those two phosphates are additionally complexed by Arg318 (not for X5P-ThDP). Remarkably, the positions for both sugar derived phosphates of F6P- and S7P-ThDP are almost identical which originates from a different conformation of S7P starting with a rotation of the C4α-C5α single bond (≈90°) and a completely different position for C6α, O6α and C7α (Fig. 44). Noteworthy, the O6α function of S7P is the only hydroxyl group which is not involved in polar interactions with the active site of *h*TK. There are no structural differences for the active site residues involved in intermediate binding observable suggesting that TKs active site is already pre-orientated to stabilize all native donor substrates without any structural rearrangements.

3.4.2.8. Structural Analysis of Donor-ThDP Intermediate Cleavage

The scissile C2α-C3α single bond of the donor intermediate adopts a perpendicular orientation relative to the aromatic ring system (Fig. 43 a.)). After bond cleavage the generated free electron pair at C2α can easily be distributed in an enlarged conjugated system due to an optimal orientation relative to the thiazolium ring (electron sink). Turano and colleagues (Turano et al., 1982) postulated such a maximum overlap mechanism that was later on verified by theoretical considerations (Friedemann and Breitkopf, 1996) and has already been shown to exist in ThDP-dependent enzymes catalyzing decarboxylation reactions (Arjunan et al., 2006; Brandt et al., 2009; Bruning et al., 2009; Meyer et al., 2010; Wille et al., 2006). However, even if this process of generating a larger conjugated

system is reasonable on the first view it has several energetic and catalytic drawbacks that will be discussed in more detail in chapter 3.4.3.5 and 3.4.4. Bond cleavage is initiated by proton abstraction from O3α by a histidine (Schneider and Lindqvist, 1998; Wikner et al., 1997). Two strictly conserved histidine residues (His37 and His258 in *h*TK) are well orientated to act as base and it has been suggested that both residues act in a concerted mode at this step of catalysis in TK (Wikner et al., 1997). His37 is found in dual hydrogen bonding interaction with O3α (N3-O3α = 308 pm) and O4α (N3-O4α = 303 pm), and thus serves a clamping function to ensure a proper positioning of the intermediate (Fig. 45). His258 is involved in hydrogen bonding interactions with Lys244 (N1-εN = 281 pm) and the O3α hydroxyl group (N3-O3α = 283 pm). This entire arrangement is very similar to that found in the catalytic triad of serine proteases whereas Lys is exchanged by Asp in those enzymes. An enlarged network of hydrogen bonding interactions that lightens dispersion of charges would presumably decrease the pK_A of the hydroxyl group (pK_A 15 to 7 jump in serine proteases)(Voet, 2008) and facilitate donor cleavage. However, Lys244 is replaced by isoleucine in non-mammalian TKs (Schenk et al., 1997). It remains to be elucidated whether an exchange of lysine to isoleucine has a kinetic effect on donor cleavage.

For proton abstraction from O3α by a histidine ring nitrogen (N1 or N3) this particular nitrogen atom should possess a free electron pair. In consequence of the excellent quality of the mFo-DFc electron density map all carbon bound hydrogen atoms are locatable at a standard contour level of 3σ for both histidine residues. Unfortunately, the protonation state of nitrogen atoms N1 and N3 of His258 and His37 can´t be assigned unambiguously. Starting from a contour level of 2.5σ a positive density peak is observable at N3 but not at N1 for His258 potentially indicating that N3 is predominantly protonated. N1 and N3 atoms of His37 don´t reveal any positive difference electron density peaks even at a contour level of 1.5-2σ.

Initial kinetic and thermodynamic experiments with $His^{37}Gln$ and $His^{258}Gln$ single variants as well as the double variant ($His^{37}Gln/His^{258}Gln$) variant show a dramatically decreased formation of donor-ThDP intermediates which complicates mechanistic conclusions for the subsequent reaction step, that is the cleavage of donors (data not shown). In line with these results Asztalos and co-workers (Asztalos et al., 2007) could show for the analogous *Ec*TK double alanine variant (*Ec*TK $His^{26}Ala/His^{261}Ala$) that formation of donor adducts is strongly decreased. In order to get further information about the individual functions of both histidine residues a computational analysis of pK_A-values (Bas et al., 2008) for *h*TK in ground state as well as in complex with the X5P-ThDP intermediate was performed using *PROPKA* (Bas et al., 2008). However, the calculated pK_A for both histidine residues are very small or even negative and thus probably not reliable. Other computational methods for pK_A calculations should be applied in future. Structural and functional data neither support nor exclude a concerted mechanism for ionization of O3α that was early suggested (Schneider and Lindqvist, 1998; Wikner et al., 1997).

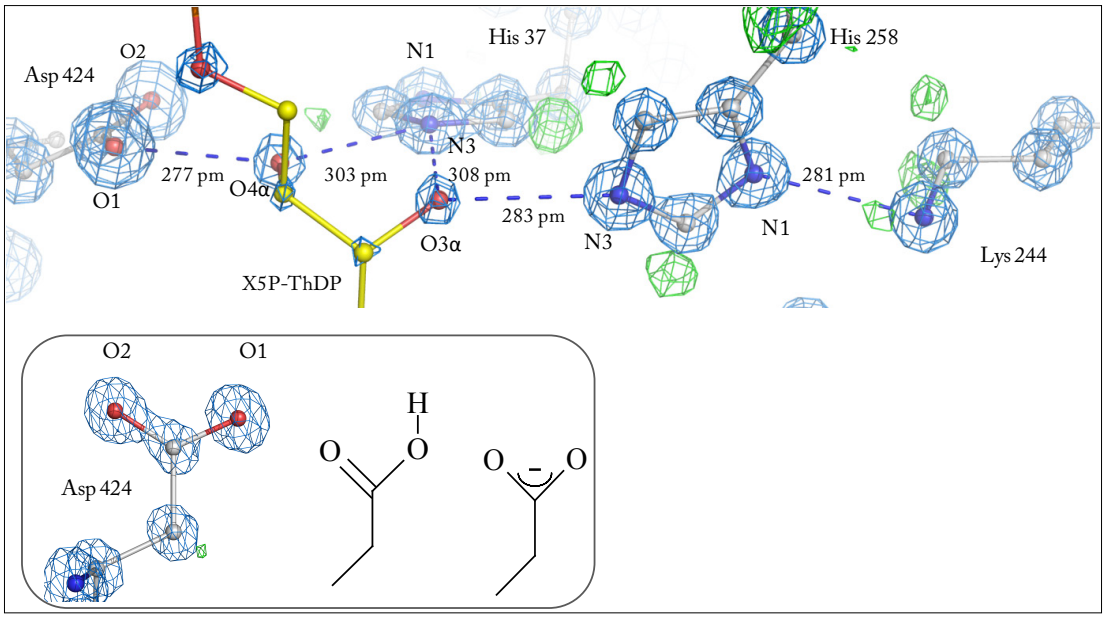

Fig. 45: Donor-ThDP intermediate cleavage in *b*TK. The complex between X5P-ThDP intermediate and *b*TK (0.97 Å) was used to generate the figure. Selected proton transfer distances are labeled. A 2mFo-DFc map (4σ, blue) and a mFo-DFc map (3σ, green) are shown. Deprotonation of O3α is required for donor cleavage and is performed by His37 and/or His258. Please note that His258 could be part of a catalytic dyade with Lys244 to deprotonate O3α. Deprotonation of O4α by His37 or Aps424 is an undesired side reaction. **Boxed:** Detailed view on Asp424 and chemical structure of protonated and deprotonated Asp side chain. The electron density map for Asp424 is better explained with a predominantly protonated state.

Interestingly, the O4α hydroxyl function, which all native donors have in common, is well coordinated in a dual hydrogen bonding arrangement with Asp424 and His37. In particular Asp424, which is supposed to determine the enantioselectivity of TK (Nilsson et al., 1998), is positioned precisely to abstract a proton from O4α (277 pm). Deprotonation of this hydroxyl group and cleavage of the C3α-C4α bond is an undesired side reaction which is intrinsically unfavorable because an unstable C3α carbanion would be formed (see Fig. 42). Inspection of the electron density map for Asp424 suggests a predominantly protonated state of the carboxyl functionality. Although the hydrogen bonded to the acidic side chain can´t be traced in a mFo-DFc map at 2.5-3σ the electron density distribution for the 2mFo-DFc map strongly supports a more protonated state. Thus, TK seemingly adjusts the pK_A of Asp424 to prevent deprotonation of O4α.

3.4.2.9. Energetic Contributions for Strain in the Donor-Coenzyme Intermediates in Transketolase

The strong angular distortions of the carbon single bond connecting substrate and coenzyme as well as angular strain in both aromatic ring systems of the coenzyme are energetically unfavorable states. Such dramatic distortions of bonds and aromatic rings must be compensated energetically. Density functional theory (DFT) studies on X5P-thiamin models (Asztalos et al., 2007) that were derived from the x-ray structure of the X5P-ThDP intermediate in *Ec*TK were the first approach to analyze the origin of the angular distortion energetically. While the resolution (1.47 Å) of the intermediate trapped in the active site of *Ec*TK was sufficient to observe strain in the C-C single bond (25-30°) connecting substrate and coenzyme the distortions of both aromatic rings could not been detected. Nevertheless, single-point calculations and full-optimizations were performed to address the question, how much energy is required to strain this intermediate. The authors found that a partial optimized X5P-thiamin model which was forced into a planar arrangement (torsion angle C5-S1-C2-C2α = 180°) was 75 kJ/mol higher in energy than the experimentally observed intermediate structure. The molecular origin for this unexpected calculation was found in an intra-molecular, repulsive interaction between atoms N4´ and O1α (Fig.47 a.)) which was just present in the in-plane conformation. Thereafter, a fully optimized intermediate structure was calculated that is 517 kJ/mol lower in energy relative to the experimentally observed intermediate but doesn´t show the enzyme-enforced, typical V-conformation of the cofactor. The huge energetic benefit of 517 kJ/mol calculated for the model in the non-V-conformation indicates that forcing the cofactor into the V-conformation can potentially account for considerably thermodynamic stabilization of reactant states. Because partial and fully optimized intermediate models still showed a deviation from planarity of 9°-10° (C2-C2α single bond) the authors denoted that strain might be additionally promoted by the intrinsic electronic and chemical characteristics of the coenzyme. Additionally, several energetic contributors like substrate binding energy, reaction energy of carboligation and intra-molecular repulsions were discussed for the generation of the observed, strained intermediates. The following chapter presents experiments to quantify and validate individual energetic contributions for intermediate stabilization in TK.

a.) Binding energy of the donor could be channeled to stabilize the strained intermediate

The X5P molecules bound in the docking site of TK is positioned by numerous (9-11, Fig. 33) polar interactions. But as already mentioned, further structural rearrangements are necessary for successful carboligation of donor to cofactor (see chapter 3.4.1.3). These rearrangements will probably consume a fraction of the binding energy that is finally missing for intermediate stabilization. While we couldn´t determine binding parameters for the interaction of donor substrates with *h*TK several ITC experiments with *Ec*TK (reconstituted with inactive cofactor analogue N3ThDP) and the donor X5P

were performed (Fig. 46 a.)). The binding enthalpy (-11.3 kJ/mol) as well as the overall free binding enthalpy (-21.7 kJ/mol) are relatively small (as expected for enzyme-substrate interactions) implying that substrate binding can solely contribute a minor fraction for intermediate stabilization. Interestingly, binding is strongly favored by the entropic term (34.7 J*mol)/K) that is presumably just caused by the replacement and liberation of water molecules (Leavitt and Freire, 2001) or the desolvation of X5P. Other entropic contributors like order-disorder-transitions of loops or isolated residues are not compatible with our structural results. For F6P and S7P we couldn´t determine binding constants by ITC which most probably originates from their very weak thermodynamic affinity or a very small binding enthalphy. This assumption is supported by high K_M values for S7P (4 mM) and F6P (1.1 mM) (Sprenger et al., 1995).

b.) Reaction energy of the carbonyl addition

Reaction enthalpy of the carbonyl addition could be stored in the strained intermediate. This enthalpy could either be released upon donor cleavage or donor liberation (back reaction). In order to prove this proposal we performed ITC experiments with *Ec*TK to quantify the reaction enthalpy produced or consumed upon carboligation (Fig. 46 b.)). If we assume that a certain part of the reaction enthalpy is indeed utilized to strain the intermediate then the detectable amount of enthalpy is just the fraction that was not used for this process. Therefore, these titration experiments can´t provide information about the exact amount of enthalpy that is used to strain the intermediate but can give an estimate how much enthalpy is potentially producible upon C-C bond formation in this enzymatic system.

Two to three times more (Q1 in Fig. 46 b.)) enthalpy is released upon titration of X5P into catalytically active (reconstituted with ThDP, C-C bond formation) than into inactive (reconstituted with N3ThDP, no C-C bond formation) enzyme implying the presence of a stronger exothermic process presumably the carboligation reaction. It is important to note that multiple events (carboligation, substrate cleavage, unproductive site reaction, etc.) contribute to the system enthalpy detected by this method. Therefore an ultimate statement of the amount of available enthalpy derived from the carbonyl addition can`t be made. The thermogram depicted in Fig. 46 b.) shows two timely distinguishable events. According to the time regime the first event represents most likely substrate binding and donor ligation (860 ± 230 s^{-1} for *Ec*TK and donor F6P, see chapter 3.2) whereas the second one (Q2) is the summation of all other side reactions. Unfortunately, an unambiguous assignment of both phases is not feasible. Due to the complexity and reversibility of its reaction cycle TK is probably not the best system to answer such mechanistic questions. More suitable enzymatic systems to characterize the thermodynamics of carbonyl addition to enzyme bound cofactor are pyruvate-converting, ThDP dependent enzymes like pyruvate oxidases or pyruvate decarboxylases. Notably, severely strained intermediates bound to these enzymes could been tapped recently using cryo-crystallography (Arjunan et al., 2006; Wille et al., 2006) (Fig. 87). Here, pyruvate analogues exist

(e.g. methylacetyl phosphonate) that covalently attach to cofactors C2 but won´t be cleaved due to a very stable C-P bond. ITC experiments could be performed in analogous manner like described above (Meyer, 2009) but with such substrate surrogates which posses the advantage that undesired side reactions like dephosphorylation or reactions of the cleavage product don´t occur. The group of Jordan already performed thermodynamic measurements with pyruvate analogues to address such mechanistic questions (Kale and Jordan, 2009). However, thermodynamic parameters like binding enthalphies and -entropies were determined by circular dichroism titrations at different temperature. Titration data analysis was finally performed according to van´t Hofft plots. Those experiments were often shown to be affected by enthalphy-entropy compensation (Naghibi et al., 1995). A direct and very accurate method for such studies is ITC that enables the direct determination of binding enthalpy and entropy in a single experiment. But again, the exact amount of enthalphy that is used to strain the intermediate can´t be determined experimentally. Hence, just computational methods will probably give reliable energies.

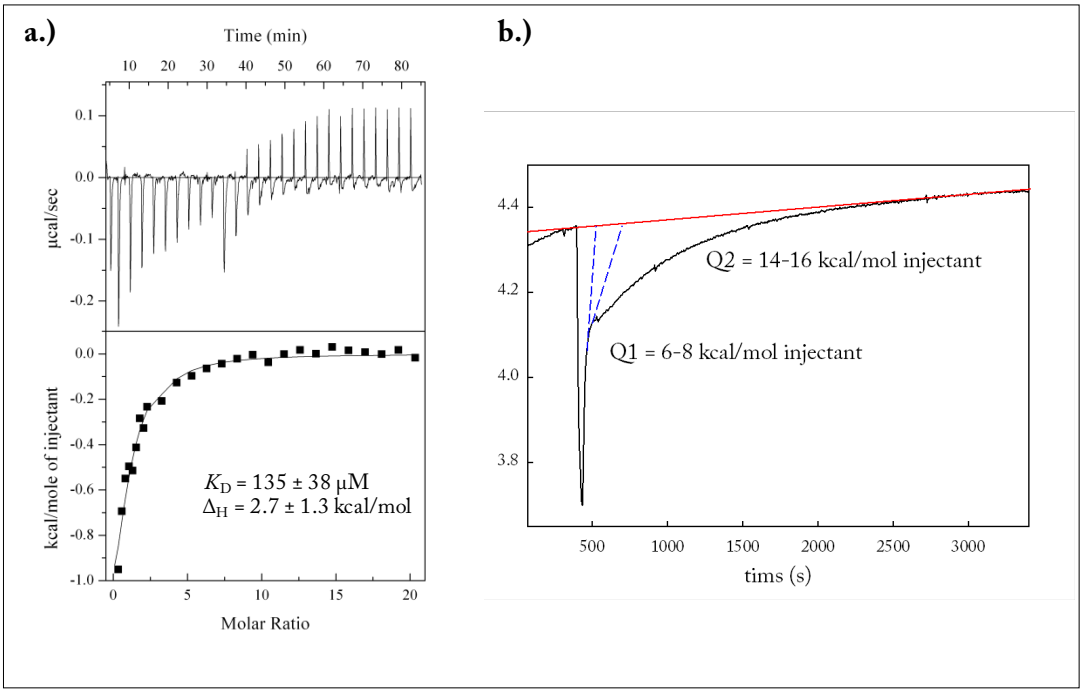

Fig. 46: Micro-Calorimetric analysis of covalent and non-covalent interaction between *Ec*TK and donor substrate X5P. a.) Isothermal titration calorimetry (ITC) experiment for quantification of the non-covalent interaction of *Ec*TK and the donor substrate X5P. Multiple titration experiment: Titration of 10 mM X5P (0.3 mM N3ThDP, 5 mM $CaCl_2$, 50 mM glycylglycine, pH 7.6) into 100 µM active sites *Ec*TK (0.3 mM N3ThDP, 5 mM $CaCl_2$, 50 mM glycylglycine, pH 7.6) at 8 °C. The binding curve was fitted according to a single binding-site model with a restrained stochiometry of 1 (Lit.). **b.)** Single titration ITC-experiment: Titration of X5P into *Ec*TK (final concentrations: 25 µM *Ec*TK, 33µM X5P, 1 mM ThDP, 5 mM $CaCl_2$, 50 mM glycylglycine, pH 7.6). The thermogram shows two timely distinguishable phases which were integrated separately. For the first phase two alternative courses were manually chosen (blue dashed lines) and integrated (Q1, Q2 = Q_{total} – Q1). For explanation see text.

c.) Channeling of cofactor strain into the intermediate

The energetically unfavorable V-conformation of the cofactor could be the source of energy to generate the strain. As already described enzyme bound ThDP adopts an enzyme-enforced, energetically unfavorable V-conformation upon binding to the protein component. This process is pivotal to all ThDP dependent enzymes and is widely believed to solely serve a pre-orientation function bringing C2 and N4´ in close proximity. In our opinion an alternative function could be that a considerable fraction of cofactor strain is channeled into high-energetic intermediates. To verify this hypothesis computational methods are required.

d.) Repulsive interaction within the intermediate

Intra-molecular repulsion between sugar derived O1α and O2α with cofactor derived N4´ in an in-plane conformation, derived from *DFT* calculations, were mainly addressed for generation of strain in the donor-ThDP intermediates in *Ec*TK (Fig.47 a.) (Asztalos et al., 2007). Short distances of 2.2 Å (O1α-N4´) and 2.6 Å (O2α-N4´) in a calculated planar state were suggested as source of repulsion.

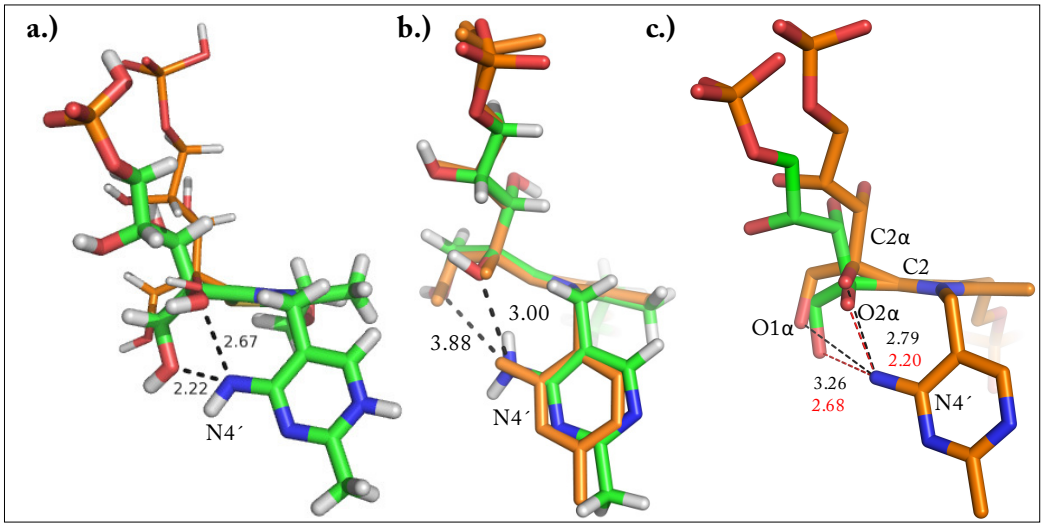

Fig.47: Modeling and regularization approaches for X5P-thiamin and –thiamin diphosphate models. Superimposed X5P-thiamin- or X5P-thiamin diphosphate models are shown in stick representation. While experimentally observed models are depicted in orange those generated by modeling or regularization approaches are depicted in green. Selected atoms and distances are labeled. **a.)** Planar X5P-thiamin-intermediate (IP form) model calculated using *DFT* (starting model, X5P-ThDP adduct in *Ec*TK, pdb-code: 2R8O). The figure is derived from Asztalos et al. (2007). **b.)** Model of the X5P-ThDP intermediate derived from energy minimization (800 cycles) with *CHIMERA*. **c.)** Planar X5P-ThDP model generated by manual regularization in *PYMOL*. The starting model for approaches shown in b.) and c.) is the X5P-ThDP intermediate (0.97 Å, AP-form).

We performed similar modeling approaches with the analogous intermediate trapped in *h*TK using the grapics program *CHIMERA* to force the C2α atom into the plane of the thiazolium moiety.

However, energy minimizations (500-8000 cycles) of the experimentally observed X5P-ThDP adduct didn´t generate a planar but still remarkably distorted (angle C2-C2α = 21.5°, Fig.47 b.)) molecule suggesting that the intrinsic electronic state of the intermediate promotes formation of strained intermediate molecules.

While the sugar-derived moiety of the optimized X5P-ThDP-model is well superimposable relative to the starting model structural difference are solely detectable for the aminopyrimidine ring. Hence, the interactions with the active site are very similar for this model (not shown). In contrast, a reinspection of the DFT-model revealed that the sugar derived part and especially its phosphate moiety would clash with active site residues suggesting that such an intermediate conformation can´t exist on the enzyme.

In order to create a planar *h*TK-X5P-intermediate model manual regularization of bond-length and -angles was carried out using the graphics program *PYMOL*. Importantly, no energy minimization was performed for this intermediate model. Here, the inter-atomic distance between O2α and N4´ atom decreases from 279 pm for the strained state to 220 pm in the so modeled planar state (Fig.47 c.)), which would indeed generate repulsion of both groups. In addition, neither after modeling nor regularization a repulsive interaction between N4´and O1α is detectable (326 or 268 pm).

In order to test the importance of repulsion between N4´and O1α experimentally we used donor substrate analogues D-1-desoxy-xylulose 5-phosphate (1desX5P) and D-arabinose 5-phosphate (A5P) which are substituted at C1-O1 by a methyl group or a hydrogen atom relative to the native donor molecules (Fig. 48). Given that O2α is derived from the carbonyl group of the donor a substitution at this position of the donor is not feasible.

The x-ray structures of covalently bound A5P (0.99 Å, R_{work} = 12.95, R_{free} = 14.68) and 1desX5P (1.07 Å, R_{work} = 12.40, R_{free} = 14.47) were determined and refined to high resolution. Both artificial donor-ThDP adducts harbor angular strain in both aromatic systems and in the C2-C2α bond (23.5° for 1desX5P and 29° for A5P-ThDP) connecting substrate and cofactor (Fig. 83). Given that the aforementioned repulsion between substrates derived oxygen atom O1α and cofactor N4´ atom is not present in those intermediates this repulsive interaction can´t be a major factor for the generation of strained donor intermediates. Importantly, an energetic contribution of the repulsion between N4´ and O2α can´t be excluded. For further structural analysis the usage of cofactor-substrate conjugates are desirable which either lack atom O2α or N4´ (2α-desoxy-sugar-ThDP- or sugar-4-desamino-ThDP-derivatives). In order to improve stability and lifetime of such compounds it is in addition probably necessary to exchange the thiazolium ring nitrogen by carbon (2α-desoxy-sugar-3deaza-ThDP or sugar-4-desamino-2deaza-ThDP). Hence, the sugar-derived moiety of such analogues can´t be eliminated after incorporation into apo TK. Structural proposals for such analogues which base on the F6P-ThDP adduct are shown in Fig. 80.

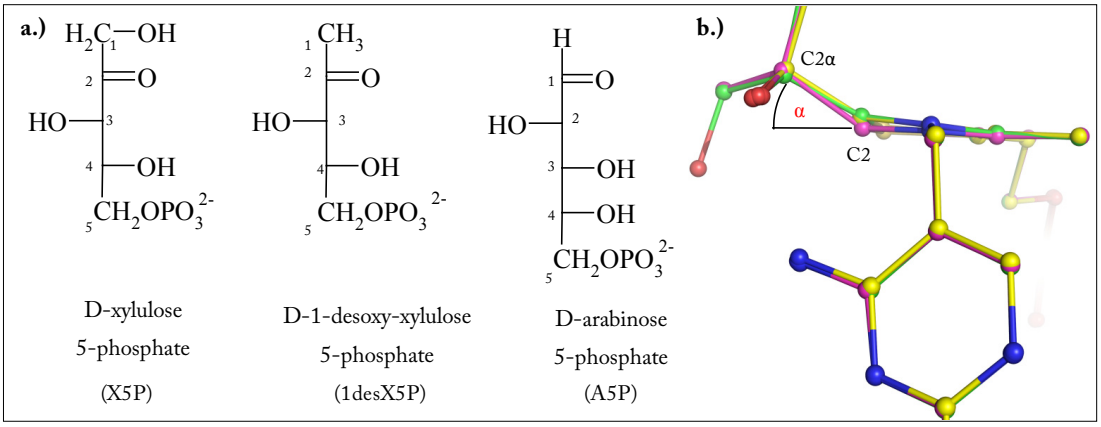

Fig. 48: X-ray structures of *h*TK-donor analogue complexes. a.) Chemical structure of native donor X5P and donor analogues 1desX5P and A5P. Carbon atoms are labeled. **b.)** Superposition of *h*TK in covalent complex with X5P- (green carbon), 1desX5P- (magenta carbon) and A5P-ThDP intermediate (yellow carbon). All covalent donor analogue-cofactor adducts reveal a strong angular distortion α (red) of the C2-C2α single bond.

e.) Active site hydrogen bonding network

Based on the regularization approach in *PYMOL*, which is described in **d.)** and illustrated in Fig.47 c.), we compared the hydrogen bonding networks of the intermediate in the strained (out-of-plane) and in-plane conformation. Although the in-plane intermediate could be stabilized by numerous polar interactions the strength and number of interactions is decreased relative to the strained conformation. Remarkably, in the in-plane conformation the intermediate and Asp424 would sterically clash (152 pm) demonstrating that this orientation of the intermediate can´t exist in the active site of *h*TK (Fig. 49). However, the practical importance of this steric clash must remain open since rotation of the C4-C5 single bond (X5P-derived part of the intermediate) could circumvent repulsion between Asp424 and the phosphate moiety.

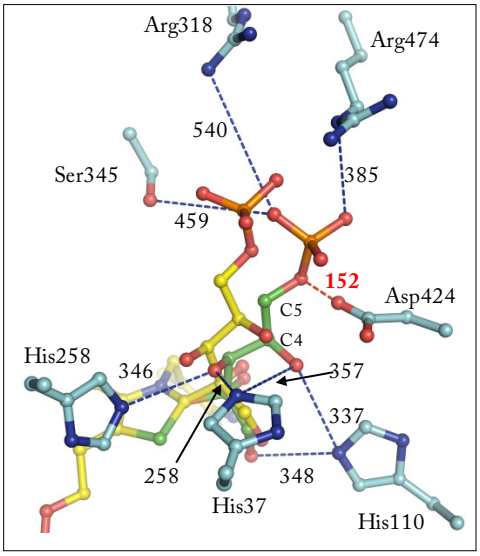

Fig. 49: Interactions of a planar X5P-ThDP intermediate with the active site of *h*TK. Planar X5P-ThDP model generated by manual regularization in *PYMOL* (green). Polar interactions (blue dashed lines, in pm) of active site residues (cyan) with the in-plane intermediate are indicated. The repulsive interaction between Asp424 and the X5P-derived phosphate moiety is highlighted (red). The strained X5P-ThDP intermediate (yellow) is shown for comparison. Selected atoms are labeled (C4 and C5).

Preorientation of *h*TKs´ active site seems to favor binding of the strained intermediate. This is presumably achieved by offering productive interactions and precluding a fully planar intermediate by repulsion. It is therefore reasonable to postulate that the active site acts as a major stabilizer of the strained conformation or in another sence as a destabilizer of an in-plane conformation

To summarize, the strained conformation of X5P-ThDP adducts is presumably enforced by multiple factors like binding energy of substrate (**a.)**) and cofactor (**c.)**) as well as by reaction enthalphy (carbonyl addition, **b.)**) and a built-in structural non-complementarity (repulsion, **d.) e.)**) for a small part of the intermediate. Analogous computational calculations like those described in the beginning of the chapter are required for native, covalent donor-intermediate in *h*TK. Those intermediates, which have a very high accuracy due to their out-standing resolution, possess unprecendent, atomic details (ring distortions, bond elongations etc.) and represent better starting models for DFT-calculations. One should also consider performing such calculation in presence of the most important active site residues. Furthermore, it would be imaginable to solely involve a "minimal" active site in which active site residues are exchanged by small organic compounds (serine → methanol, histidine→ imidazole, glutamate→ acetate etc.) to facilitate calculations.

3.4.3. The Post-Cleavage Intermediate Dihydroxyethyl Thiamin Diphosphate - Crystallographic Evidence for the Stabilization of an Enzyme-Bound Strained Enolate

After cleavage of donor substrates TKs form a C2α-carbanion (dihydroxyethyl thiamin diphosphate intermediate short DHEThDP) that is potentially stabilized with the corresponding enamine (or enaminol) through electronic delocalization (Fig. 50). This central intermediate is often referred as the second carbanion in the reaction mechanism of ThDP-enzymes. While the chemical nature of the first carbanion, which is the deprotonated coenzyme itself (ThDP ylide in Fig. 50), is subject of debate (see chapter 3.3.1) it is reasonable to assume that the C2α carbanion lies on pathway for many ThDP dependent enzymes (Kluger and Tittmann, 2008). The reactivity of the DHEThDP intermediates is considered to determine the fate of the second part of the reaction cycles and is doubtless modulated by the physical and chemical properties of each individual enzyme.

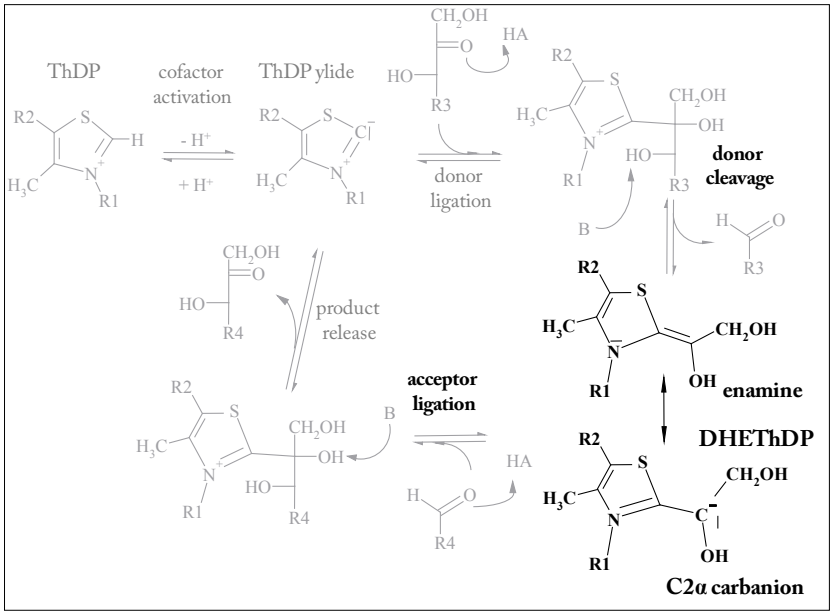

Fig. 50: Formation and depletion of the covalent DHEThDP intermediate. Simplified reaction scheme for TK-catalyzed over-all reaction in presence of donor and acceptor substrates (R1 = aminopyrimidine moiety, R2 = ethyldiphosphate moiety). The central intermediate DHEThDP (bold) is formed after cleavage of a donor ketose and depleted upon carboligation to an acceptor aldose.

Fiedler and colleagues (Fiedler et al., 2002) determined the x-ray structure of this intermediate bound to the active site of *Sc*TK and claimed a planar, enamine-like state for DHEThDP in TK. This is in line with other structural reports about analogous intermediates (Wille et al., 2006) that denoted a

more planar, resonance stabilized state for post-cleavage intermediates. As opposed to this observation the DHEThDP intermediate in phosphoketolase was reported to be stabilized as a sp^3 hybridized, presumably protonated form (C2α atom) (Suzuki et al., 2010). Since it is crucial for understanding of reactivity we aimed to determine high-resolution structures of this intermediate in TK to clearly assign its chemical state.

3.4.3.1. Accumulation of the DHEThDP Intermediate in TK – Spectroscopic and Kinetic Efforts

In order to trap this particular reaction intermediate on the enzyme the artificial substrate analogue β-hydroxypuruvate (HPA) was used. HPA is bound by transketolases and converted, passing a short-lived hydroxylactyl-ThDP intermediate (Asztalos, 2007 b), to form DHEThDP. Unfortunately, the highly reactive DHEThDP intermediate can be depleted by several off-pathway reactions (Fig. 51 a.)) like:

- protonation of C2α and formation of a sp^3 hybridized DHEThDP intermediate; glycolaldehyde will finally be eliminated
- protonation of O1α coupled to dehydration and formation of acetyl-ThDP; this reaction lies probably on-pathway for phosphoketolases (Frey, 1989; Yevenes and Frey, 2008)
- carboligation to another molecule HPA (Asztalos, 2007 b) and formation of hydroxyacetohydroxylactyl-ThDP
- carboligation to glycolaldehyde that was previously eliminated and formation of erythrulose-ThDP

In order to analyze under which conditions the covalent DHEThDP adduct accumulates predominantly in solution a NMR-based intermediate analysis was carried out (Tittmann et al., 2003) (Fig. 51 b.)). For the reaction of *h*TK with 25 mM HPA we could quantify 25 % DHEThDP intermediate and 75 % un-substituted cofactor. Importantly, under these conditions no other covalent intermediates are detectable. For the reaction of *Ec*TK with HPA we found, in line with previous results (Asztalos, 2007 b), that at equimolar reaction condition solely DHEThDP is formed with an occupancy of approx. 80 % (data not shown) but in excess of HPA numerous other covalent adducts accumulate to high amount. At this point it is important to state that the NMR-based intermediate analysis occurs after acidic quench (pH 0.75) of the reaction. All compounds are therefore present as conjugated acid irrespective of their enzyme bound protonation state. Thus, discrimination between carbanion, enamine or protonated form of DHEThDP is not feasible with this method.

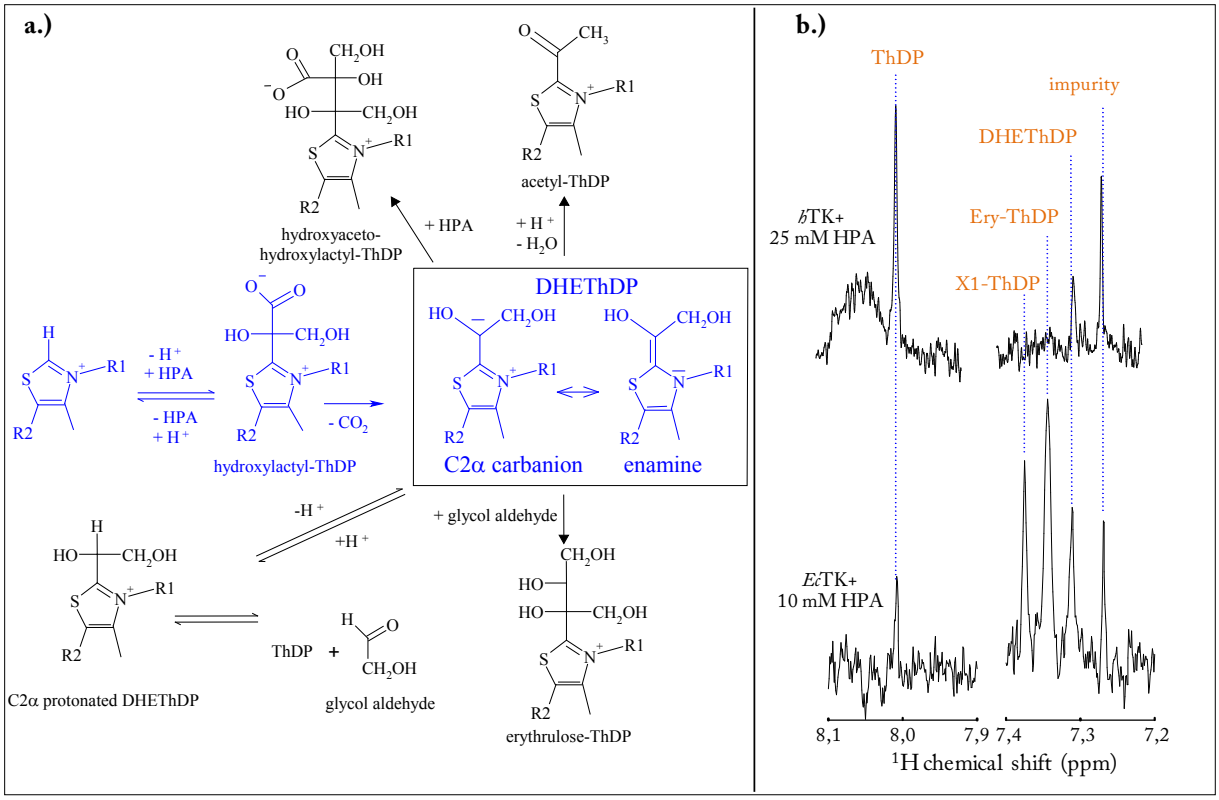

Fig. 51: Trapping the DHEThDP intermediate in transketolase by reaction with HPA. a.) Simplified reaction scheme for the conversion of HPA by TK. After HPA binding and initial formation of hydroxylactyl-ThDP the DHEThDP intermediate will be formed by irreversible decarboxylation (blue). Side reactions that are responsible for depletion of DHEThDP like protonation (formation of protonated DHEThDP), protonation coupled to dehydration (formation of acetyl-ThDP), carboligation with HPA (formation of hydroxyacetolactyl-ThDP) or carboligation to glycolaldehyde (formation of erythrulose-ThDP) are presented in black (R1 = aminopyrimidine moiety, R2 = ethyldiphosphate moiety). **b.)** Distribution of covalent intermediates after reaction of either *b*TK or *Ec*TK with the artificial donor HPA. In both samples we found an impurity at 7.25 ppm that was also present in the control (just HPA). For the reaction of *Ec*TK with 10 mM HPA we found beside already identified signals (Ery-ThDP = erythrulose thiamin diphosphate, DHEThDP = dihydroxyethyl thiamin diphosphate) a so far unidentified covalent intermediate (X1-ThDP) which might represent the hydroxyaceto-hydroxylactyl-thiamin diphosphate adduct.

We were further interested to study the stability of the intermediate on the enzyme. Thus, single-turn-over experiments with the artificial donor HPA were performed using stopped-flow technique (Fig. 52). Given that formation of the DHEThDP intermediate gives rise to absorption at 300 nm this spectral signature can be exploited for a kinetic analysis. The signal at 300 nm was recently assigned unambiguously using ^{1}H-NMR-spectroscopy (Asztalos et al., 2007). *Ec*TK forms the DHEThDP intermediate rapidly (k_{for} = 0.93 s^{-1}, full amplitude after 5 s) after equimolar mixing with HPA. The so formed intermediate has a half life of approx. 120 s precluding co-crystallization with HPA as method of choice to trap this particular reactant state.

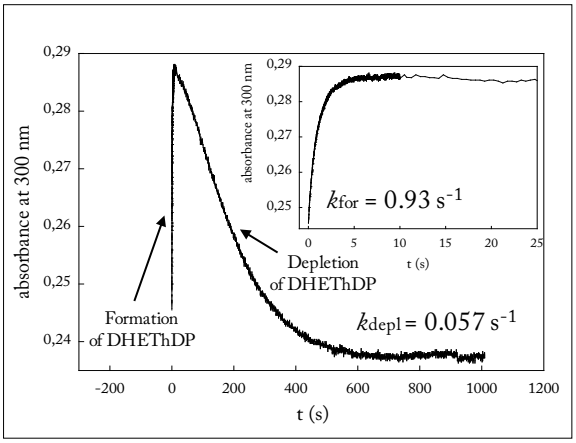

Fig. 52: Single-turn over kinetics for the reaction of *Ec*TK with β-hydroxypyruvate (HPA). Reaction of 2 mg/ml *Ec*TK wt (27.75 µM active sites) with an equimolar concentration of HPA in 0.3 mM ThDP, 2.5 mM $CaCl_2$, 50 mM glycylglycine (pH 7.6) at 25 °C. Kinetics were initiated by 1/1 mixing and monitored in a stopped-flow absorbance spectrometer (pathlength 10 mm). Rate constants for formation (k_{for}) and depletion (k_{depl}) were determined according to single exponential equations. **Inserts:** Initial formation of DHEThDP-intermediate.

3.4.3.2. Structure Determination of the DHEThDP Intermediate in *Ec*TK and *h*TK

After numerous trials we succeeded in determination of x-ray structures with an acceptably high occupancy of DHEThDP intermediate for *h*TK and *Ec*TK (Fig. 53, Fig. 84). Notably, the condition in solution couldn´t been easily transferred to the crystalline state. For *h*TK we found that approx. 40-50 % DHEThDP intermediate had accumulated upon soaking with 20 mM for 3 min, whereas the remaining active sites contain just unsubstituted ThDP. Unfortunatly, the resolution of *h*TK crystals soaked with HPA didn´t exceed 1.45-1.6 Å resolution in numerous further trials. For *Ec*TK we succeded in determination of two real atomic x-ray structures to 0.95 Å (5 min soak) and 0.97 Å (20 min soak) resolution after soaking in 20 mM HPA. Since the occupancy of the intermediate in the x-ray structure determined to 0.97 Å of 75 % (R_{work} = 9.02, R_{free} = 11.31, Fo > 4σ) was slightly better than for the second structure (0.95 Å, R_{work} = 10.21, R_{free} = 11.24, ≈ 50 % DHEThDP, data not shown) the discussion is focused on the slightly lower resolved complex. Importantly, even at very low contour levels in 2mFo-DFc (0.3-1σ) and mFo-DFc (1-3σ) electron density maps no traces of carboligation adducts are visible for all determined structures. Furthermore, because acetyl-ThDP (Fig. 51 b.)) couldn´t been detected under any chosen condition using NMR the trapped intermediate can be assigned as DHEThDP or the C2α-protonated form thereof. Unfortunately, a partial accumulation of the later form can neither be excluded by our x-ray crystallography results nor by the NMR-based intermediate method.

A fully unrestrained refinement was carried out for the model of the *Ec*TK-DHEThDP complex using *SHELXL-11* (Sheldrick, 2008). The outstanding resolution of the structure further enabled estimation of standard deviations for bond lengths. Because of the low occupancy in combination with

the significantly lower resolution of 1.45 Å a refinement with weaker restrains for the *b*TK-DHEThDP intermediate molecule using *PHENIX* was not successful and caused disruption of the intermediate model. Thus, tighter refinement restrains had to be used in order to obtain a reliable model. The refined bond parameters for this structure are in consequence biased by the input restrains.

A detailed analysis of bond lengths for DHEThDP bound to *Ec*TK (Tab. 13, Fig. 53) revealed that the C2-C2α bond (140 ± 2.7 pm) is much shorter than a standard C-C single bond (154 pm) consequently implying strong double character (typical C-C double bond 134 pm). In addition the C2α-O2α bond (123 ± 2.2 pm) has double bond character (143 pm for C-O single bond and 124 pm for C-O double bond). An analogous tendency for bond length is also observable for the intermediate in *b*TK (Fig. 84) and the second *Ec*TK-DHEThDP complex (0.95 Å, data not shown).

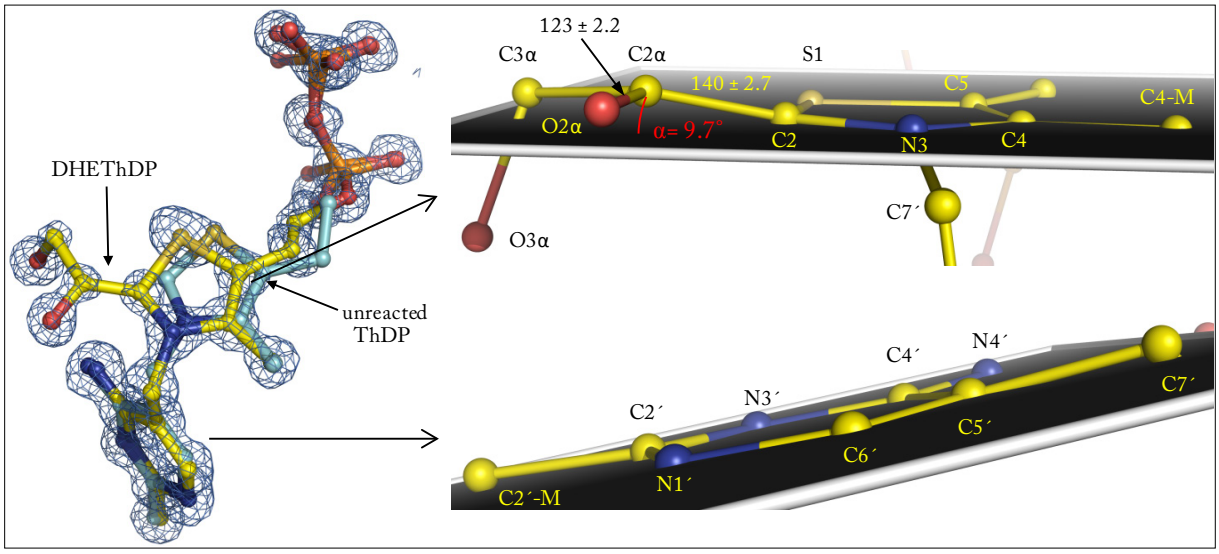

Fig. 53: Detailed view on DHEThDP intermediate in *Ec*TK (0.97 Å). On the left side the DHEThDP intermediate is shown surrounded by a 2mFo-DFc map contoured at 2σ (blue). DHEThDP and unreacted coenzyme are labeled. Thiazolium moiety (top right) and aminopyrimidine moiety (bottom right) are shown with auxillary planes to illustrate deviations from planarity. The angular distortion (α) of the carbon bond connecting sugar and cofactor moiety of each intermediate is indicated (red). Selected atoms and distances (in pm) are labeled.

A very surprising and unexpected feature of the thiazolium ring is the significant out-of-plane distortion of C2 as well as of the C2-C2α bond. Contrary to the generally accepted, planar enamine state of DHEThDP in TK (Fiedler et al. 2002) we observe a considerable deviation from planarity of 14° (*b*TK) and 9.7° (*Ec*TK) for the C2-C2α bond connecting cofactor and dihydroxyethyl moiety. Although most of the bond lengths of the thiazol ring are suggestive for a predominantly aromatic character the C2-S1 bond (184.7 ± 2.2 pm) is drastically elongated, typical for a C-S single bond (Allen et al., 1987), which should result in reduction of aromaticity.

Furthermore, the six-membered ring of the intermediate exhibits deviations from planarity for C2´, C7´and C2´-M but not for C4´and N4´. For the donor-ThDP intermediates a strong deviation from planarity for this entire ring and especially for C4´and N4´ was detectable suggesting that strain in this ring is partially released upon donor cleavage. However, a correlation of this structural change with catalytic competence must yet remain open.

A closer inspection of the intermediate revealed that C2α is neither trigonal planar, as it would be assumed for a sp^2 hybridized state, nor perfectly tetragonal (sp^3 hybridized) in a protonated or carbanion state. Additionally, the thiazol ring nitrogen (N3) can serve as a monitor for the electron distribution of the intermediate. In the carbanion state N3 is planar whereas in an enamine or enolate state N3 adopts trigonal pyramidal geometry. The DHEThDP intermediate bound to *Ec*TK possess a deviation of 16.5° from planarity at N3 but no perfect, trigonal pyramidal angles further suggesting that the electronic state of the intermediate can be explained with a more enamine-like structure.

By superposition of the post-cleavage intermediate in both transketolases structural differences for the thiazolium ring as well as for the diphosphate anchor are observable Fig.54. Additionally, we detect for *Ec*TK a more pronounced deviation from planarity at C2α suggesting a higher fraction of C2α carbanion or C2α-protonated form for this TK.

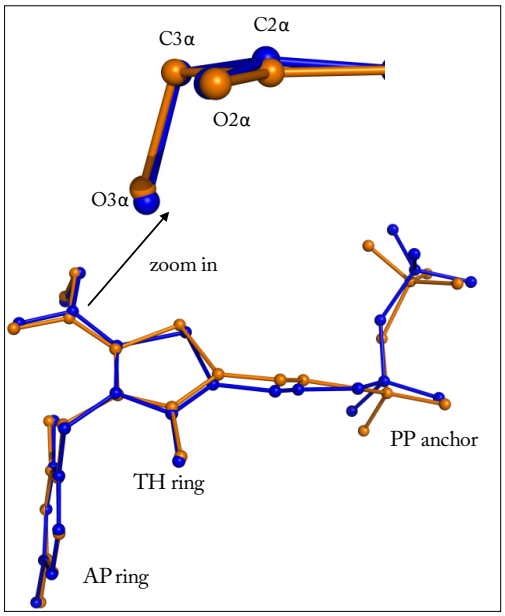

Fig.54: Superposition of DHEThDP intermediates trapped in *b*TK and *Ec*TK. In order to visualize structural changes between the DHEThDP intermediates trapped in the active sites of *b*TK (orange, 1.45 Å) and *Ec*TK (blue, 0.97 Å) both structure are superimposed. Aminopyrimidine (AP ring) and thiazol ring (TH ring) as well as the diphosphate moiety (PP anchor) are labeled. Please note that TH ring and PP anchor adopt slightly different orientations whereas the AP ring is perfectly superimposable between both molecules. The substrate derived dihydroxyethyl moieties reveal small positional changes (top, zoom in).

Furthermore, both TK-DHEThDP complexes reveal the presence of a considerable fraction of un-reacted coenzyme. While for *b*TK this un-reacted fraction is perfectly superimposable with the coenzyme-derived part of the intermediate larger structural differences are observable for reacted and unreacted cofactor in *Ec*TK. Similar structural differences were reported for the donor-ThDP intermediates in *Ec*TK (Asztalos et al., 2007) relative to the ground state. These positional changes are locatable to the thiazolium ring, the diphosphate moiety and both methylene groups connecting the aforementioned moieties of the cofactor.

3.4.3.3. Formation of an Enolate Form of DHEThDP

According to bond lengths of the dihydroxyethyl moiety of DHETHDP we conclude that the predominant state of the intermediate is an enolate. The negative charge of the DHEThDP enolate could potentially be dispersed between O2α, C2α and C2 circumventing an accumulation of highly reactive C2α carbanion which can easily be depleted by protonation (Asztalos, 2007 b). Therefore, the enolate state presumably represents a storage form for the C2α-carbanion. Other chemical states like a C2α keton would be compatible with the length of the C2α-O2α bond (123 ± 2.2 pm) but not supported by the predominat double bond character of the C2-C2α bond (140 ± 2.7 pm).

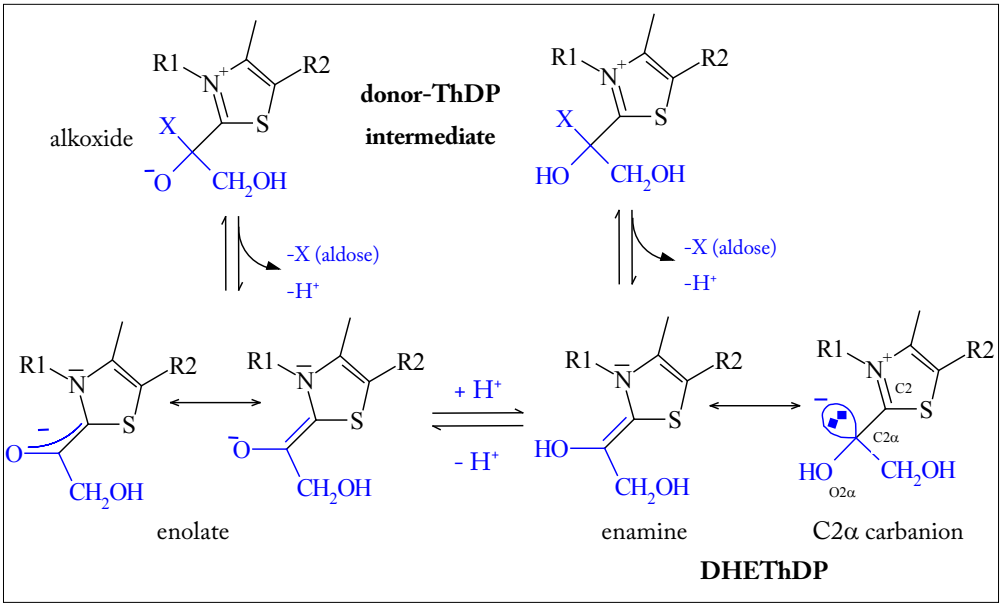

Fig. 55: Models for the formation of enolate form of DHETHDP. A direct enolate generation (left side) could be realized be cleavage of a deprotonated donor-ThDP intermediate (alkoxide). Alternatively, deprotonation of an enamine/carbanion intermediate after donor intermediate cleavage (right site) could form an enolate. Selected atoms and chemical structures are labeled (R1 = aminopyrimidine moiety, R2 = ethyldiphosphate moiety).

A DHEThDP enolate could be formed by different mechanism (Fig. 55):

a.) Donor-intermediate cleavage and subsequent deprotonation of O2α by a base (right side in Fig. 55). While for *Ec*TK His473 is well positioned to serve this function the analogous residue in *h*TK Gln428 can´t act as acid/base catalyst. However, exchange of *Ec*TK His473 by Ala indeed decreases the rate for the reaction of enzyme-bound DHEThDP with acceptor R5P 80fold suggesting a pivotal role of His473 for this catalytic step in *Ec*TK (Fig. 86). Moreover, an intramolecular proton transfer form O2α to cofactors´ N4´ could be taken into consideration. This interaction is conserved in both TKs and should be feasible accoding to distances (Fig. 56: 306 pm for *h*TK and 311 pm for *Ec*TK) and proton transfer geometry (not shown). The six-membered ring would thereby change its protonation state from IP- to APH$^+$-form.

b.) An alternative and direct route would be the cleavage of an already deprotonated donor-intermediate (Fig. 55 left side). Remarkably, all high resolution structures of donor-ThDP intermediates in *h*TK (chapter 3.4.2.5) suggested that the O2α is partially deprotonated (alkoxide). The cleavage of donor-adducts generate a transient C2α carbanion (negative charge at C2α) in the transition state of the reaction. In case the alkoxide (negative charge at O2α) would be the educt for cleavage reaction a neighboring negative charge would dramatically increase the activation barrier for the reaction steps. It is therefore questionable if an O2α alkoxide is on-pathway for cleavage of donor-ThDP intermediates.

3.4.3.4. Interactions of the DHEThDP Intermediate with the TKs Active Site

The substrate-derived part of DHEThDP ((*E*)-configuration) is positioned in the active site of *h*TK and *Ec*TK by analogous, polar interactions (6 for *Ec*TK and 4-5 for *h*TK) which are partially mediated by water molecules (Fig. 56). One of these interactions is that of N4´ with O2α which might serve a mechanistic function for stabilization of charges or acid/base catalysis. For *h*TK two alternate side chain conformations of Gln428 are observable. In the lower populated conformation (30 %) Gln428 could potentially form a hydrogen bonding interaction with O1α (distance 253 pm). However, the small occupancy of this conformation doesn´t allow an unambiguous modeling of the carbonylamide. An analogous observation was made for this particular residue after formation of the covalent donor-ThDP intermediates. Contrary, the analogous residue in *Ec*TK (His473) is involved in a strong hydrogen bonding interaction with O1α (263 pm) and a weaker one with O2α (320 pm).

Although polar interactions can be addressed for positioning of the intermediate or Brønsted acid/base catalysis the interaction pattern doesn´t reveal any repulsive or strongly attractive interactions which cause the observed out-of-plane distortion of the C2-C2α bond. Thus, strain in DHEThDP

intermediates is presumably a remainder of binding- and carboligation energy or promoted by the intrinsic electronic properties of the coenzyme.

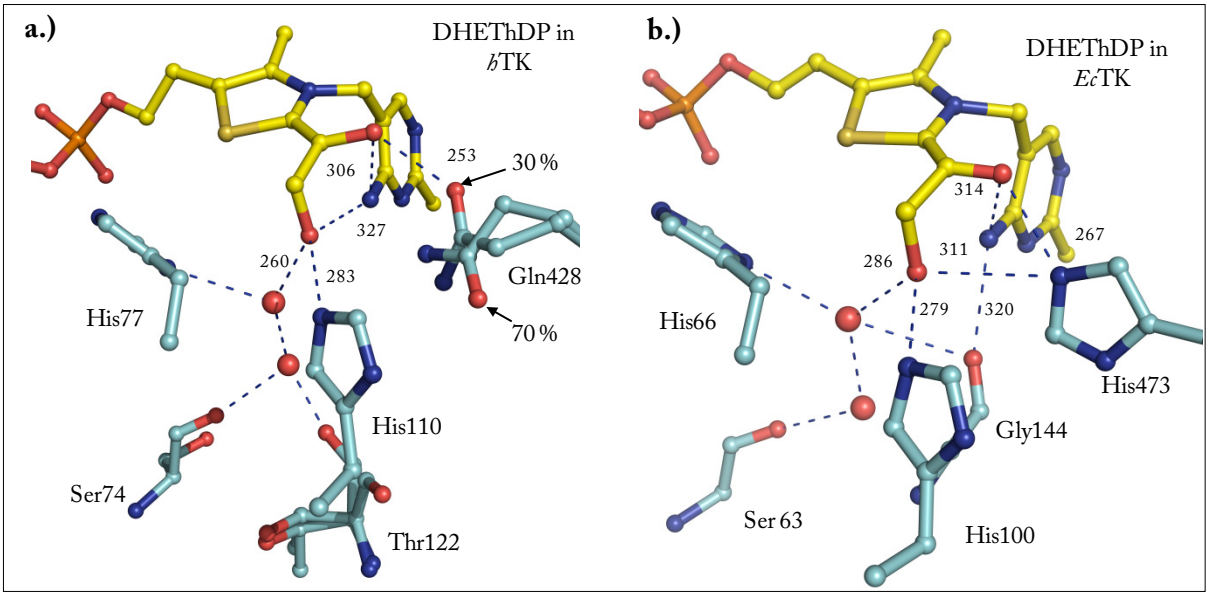

Fig. 56: Hydrogen bonding interactions of the DHEThDP intermediate with the active site of *b*TK and *Ec*TK. Active site residues (cyan) that are involved (direct or mediated by water molecules) in hydrogen bonding interactions (blue dashed lines, in pm) with the dihydroxyethyl moiety of the intermediate are shown in stick and ball representation. Water molecules are shown as red spheres. The occupancy of the two alternate conformations of Gln428 are indicated.

However, in comparison to the donor-ThDP intermediates a considerable fraction of angular strain (approx. 10°) is indeed released upon donor cleavage and formation of DHEThDP. Thus strain release might be a driving force for donor cleavage (Tittmann and Wille, 2009) and separation of reactants. Nonetheless, the post-cleavage intermediate is not stabilized as a low-energy planar enamine. Such an over-stabilized state must probably be avoided on the enzyme because it represents a thermodynamic pit-fall for the catalytic system (see Fig. 9) that increases the activation barrier for the subsequent reaction step. A very similar conclusion was made for authentic Schiff-base intermediates in transaldolase (Lehwess-Litzmann et al., 2011) trapped by x-ray crystallography. In consideration of the partial double bond character for this bond this species is presumably a high energy intermediate.

Importantly, an alternative chemical explanation for distorted enamines as described for conformationally restricted, pyramidalized alkenes (Vazquez and Camps, 2005) is not compatible with the geometrical and structural characteristics of the DHEThDP intermediate.

3.4.3.5. Is the Enamine Intermediate On-Pathway in Thiamin Catalysis?

The existence of low-energy, resonance-stabilized enamines is a paradigm in the field of ThDP-research. In line with our results, which represent a modification of the generally accepted model, are three recent studies:

a.) Amara and colleagues suggested, relying on theoretical approaches, that for certain ThDP-dependent enzymes the enamine/carbanion state doesn´t lie on-pathway (Amara et al., 2007).

b.) Berkessel and co-workers characterized the analogous post-cleavage intermediate for the non-enzymatic system of benzoin condensation which can be catalyzed by cyanide ions or thiazolium salts. Using NMR-spectroscopy the conversion of propionaldehyde by a 1,3,4-triphenyl-4,5-dihydro-1*H*-1,2,4-triazol-5-ylidene catalyst was monitored and key intermediates were assigned. The authors solely identified the C2α-keto form of the post cleavage intermediate (Berkessel et al., 2011).

c.) Meyer and co-workers determined the high resolution x-ray structure of the analogous hydroxyethyl-ThDP (HEThDP) intermediate in *Lp*POX (Meyer, 2012). *Lp*POX catalyzes the oxidative decarboxylation of pyruvate and transfers the transiently formed acetyl-fragment to phosphate finally yielding the high-energy compound acetyl-phosphate (Fig. 87). The HEThDP intermediate in this particular enzyme was interpreted as a mixture of a thiazolium centered carbanion and a thiazoline bearing keton functionality. The authors made the important conclusion that the reactivity of the post-cleavage intermediate is inverted (Umpolung) by internal proton transfer. While a C2α carbanion is a potent nucleophil both chemical structures postulated in this report exhibit an electrophilic C2α and could explain the ability of HEThDP in *Lp*POX to react with the nucleophilic oxygen of phosphate. Remarkably, our crystallographic observations for TK also support intra-molecular proton transfer and formation of a yet not considered chemical state for the post-cleavage intermediate (Fig. 58). However, as TK requires nucleophilicity of C2α to enable carboligation with aldoses this state presumably represents a storage form of the C2α carbanion.

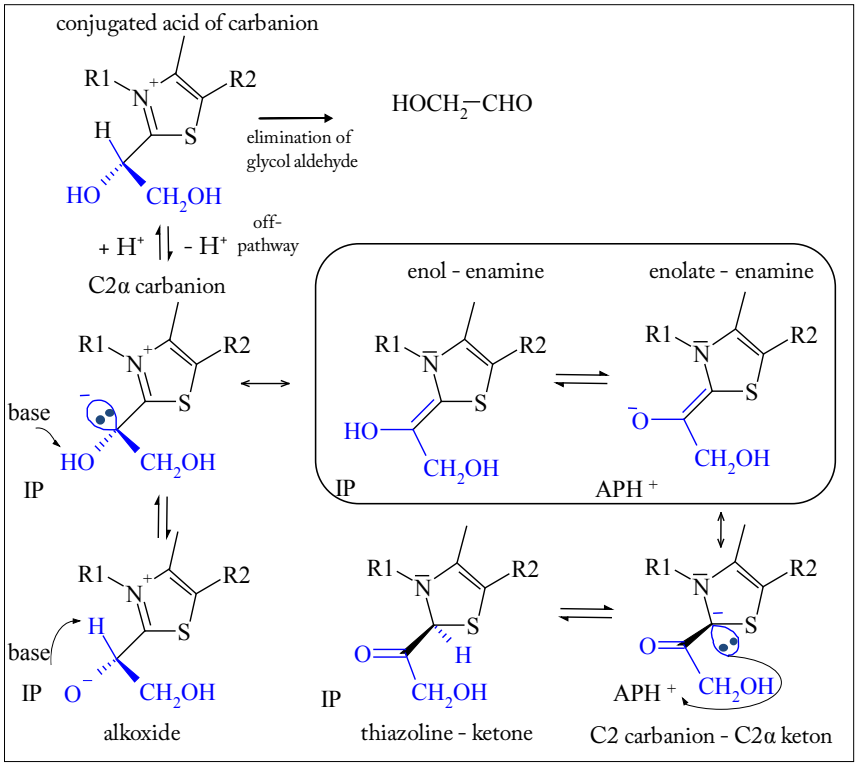

Fig. 57: Chemical structure of DHEThDP including possible tautomeric and ionization states. The expected tautomeric state of the cofactor six-memebered ring (IP, APH⁺) is indicated. Substrate derived atoms are shown in blue. Species suggested to predominantly accumulate in TK are boxed. Please note that the base (IP or active site residue) which is responsible for the enolate formation is yet not certainly identified. The figure is adapted from Meyer et al. (2012).

3.4.3.6. The Protonation State of DHEThDP Intermediate in *Ec*TK– Indications for the Presence of Cofactors´ 1´-4´-Imino Tautomeric State

The *Ec*TK-DHEThDP intermediate structure determined to 0.97 Å revealed at a standard contour level of 2.8σ in a mFo-DFc map all expected hydrogens (C6-methylen, C6´and C7´methyl, Fig. 58). Furthermore, one hydrogen can be traced at N1´ (IP) and at N4´ (no AP or APH⁺), respectively. When the contour level is finally decreased to low values of less than 2.4σ a weak second density peak is observable for N4´ which is suggestive for the presence of a small fraction of AP or APH⁺. At this contour level the map is noisy but reveals no hydrogen bonded to N3´ which can serves as an internal quality control for the electron density map since this nitrogen should never be protonated.

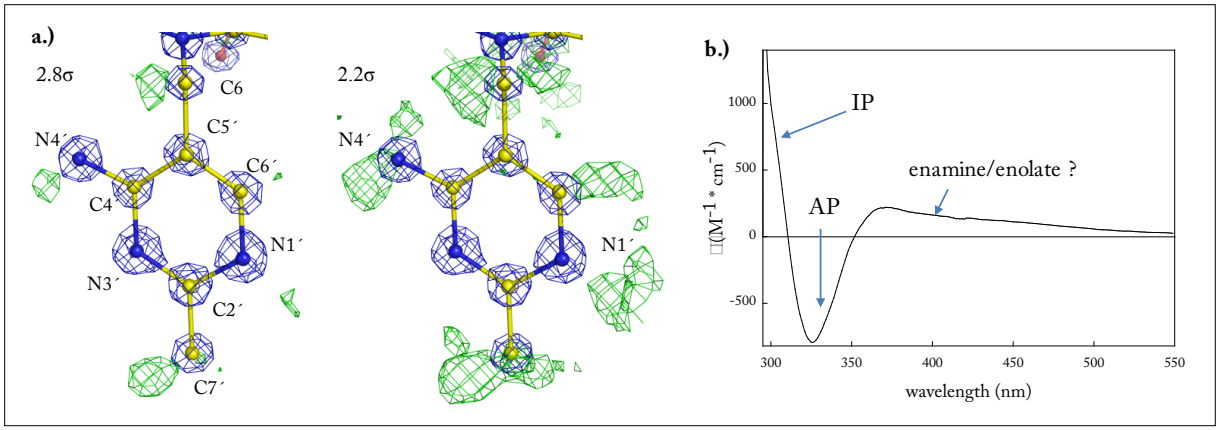

Fig. 58: Protonotion state assignment of the DHEThDP intermediates using x-ray crystallography and absorbance spectroscopy. X-ray structure of covalent DHEThDP-intermediates (0.97 Å) shown in stick and ball representation surrounded by a 2mFo-DFc electron density map contoured at 5σ (blue) and a mFo-DFc difference electron density map in green at contour levels of 3σ (left panel), 2.2σ (middle panel). Selected atoms are labeled. b.).

The assignment of a predominat IP protonation state is further supported by spectral signatures derived from a UV/Vis difference spectrum for a single-turn-over reaction of *Ec*TK with HPA in solution (Fig. 58, b.)). While the AP form (minimum at 320-330 nm) disappears two signals at 300 nm (IP) and 380-500 nm are generated. The later signal can´t be clearly assigned but could originate from a charge transfer between the enamine or enolate and the six-membered cofactor ring. Similar spectroscopic bands were recently reported and assigned as enamine-induced for human pyruvate dehydrogenase (Seifert, 2010), pyruvate decarboxylase (Meyer, 2009) and for benzoylformate decarboxylase (Nemeria et al., 2009). A kinetic analysis of the spectral signatures using absorbance spectroscopy and photodiode array detection (Fig. 85 b.)) further revealed that the signals at 300 nm and 380-500 nm are formed with very similar rate constants indicating identical molecular origins for both signals. Notably, the presence of a considerable fraction APH^+ form can´t be ruled out with our spectroscopic approach since this protonation state is supposed to lack any absorbance signal (Nemeria et al., 2009).

Our assignment of the protonation state contradicts previous spectroscopic reports which suggested that post-cleavage intermediates in thiamin catalysis exist predominantly as APH^+ form (Chakraborty et al., 2008; Chakraborty et al., 2009; Jordan et al., 2003). Those assignments rely on CD-spectroscopic measurements for different ThDP-dependent enzymes (no TKs) lacking any signal between 300-310 nm.

3.4.3.7. X-ray Structure of the DHEThDP Analouge 1,2 dihydroxyethy-3-deaza-Thiamin Diphosphate bound to *h*TK

Since our first trials to trap authentic DHEThDP intermediate in TK failed, we alternatively co-crystallized apo *h*TK with a catalytically inactive, isosteric analogue which lacks the ability to eliminate the dihydroxyethyl moiety. For this purpose we used chemically synthesized dihydroxyethyl-3-deaza-thiamin diphosphate (3deazaThDP) that was kindly provided by Prof. Finian Leeper (University of Cambridge). Exchange of nitrogen (thiazol nitrogen of ThDP) by carbon makes the five-membered ring (thiophen ring system) catalytically inactive. The structure of the co-crystallized *h*TK-3deazaThDP complex was determined by x-ray crystallography to 1.259 Å and refined to reasonable R-facors (R_{work} = 14.48, R_{free} =17.77).

While the superposition of the x-ray structures of *h*TK in complex with 3deazaThDP or native DHEThDP intermediate revealed almost no positional changes for aminopyrimidine ring and diphosphate anchor, significant changes are observable for the dihydroxyethyl moiety and the five-membered rings (Fig. 59 b.)). Relative to native DHEThDP the C2-C2α bond of 3deazaThDP is rotated by 127° resulting in completely different positions for O1α, C3α and O3α. In consequence the interactions of the dihydroxyethyl moiety with active site residues are also changed presumably causing that O3α adopts two alternate conformations (Fig. 59 a.)). Because C3α and O3α loom into the acceptor binding site, they probably hinder proper binding and pre-orientation of acceptor substrates (see chapter 3.4.6). Aside from the circumstance that 3deazaThDP doesn´t represent a suitable mimic for authentic DHEThDP intermediate we can receive valuable, mechanistic and energetic conclusions from this structure:

1. The experimentally observed conformation of native DHEThDP can just be adopted because the C2-C2α bond has significant double bond character. A more relaxed conformation of the dihydroxyethyl moiety is observed for 3deazaThDP which has a C2-C2α single bond suggesting that the "native" conformation (*Ec*TK-DHEThDP complex) is higher in energy.
2. The five-membered ring of the analogue is still strained (angle C2-C2α = 8.6°, Fig. 59 c.)) indicating that angular strain is a phenomenon which is partially encoded in the cofactor conformation. We can exclude any binding- or reaction enthalphy as well as intra-molecular, repulsive interaction that might contribute to a destabilization of the analogue. Furthermore, this structural observation proves that ring distortions are not restricted to thiazolium systems as the analogue possesses a thiophen ring.

Another interesting structural finding is that the six-membered ring is protonated at N1´ suggesting either IP or APH^+ form for the analogue (not shown). Since we yet solely observed IP or APH^+ form of enzyme-bound ThDP, it remains to be further investigated if cofactors´ AP form accumulate at any catalytic step of TK. Notably, after refinement of both analogue conformers additional positive

difference electron density peaks indicated another low populated (approx. 10-15 % occupancy), alternate cofactor conformer. This conformer couldn´t been modeled with the analogue in R- but S-configuration (not shown). Importantly, this residual S-configumer which is an inpurity of chemical synthesis (personal communication of Prof. Finian Leeper) doesn´t interfere our mechanistical analysis.

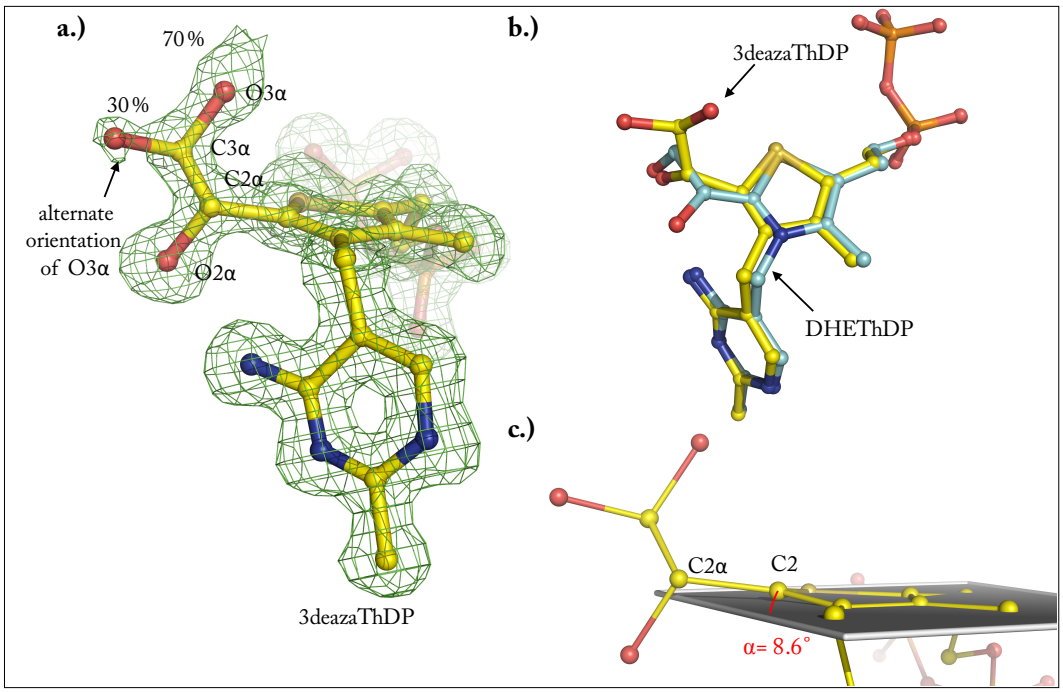

Fig. 59: X-ray structure of 1,2 dihydroxyethyl-3-deaza-thiamin diphosphate (3deazaThDP) bound to *b*TK. Models are shown in ball and stick representation. Selected atoms are labeled. **a.)** Model of 3deazaThDP shown with positive difference electron density map (residue omitted mFo-DFc map contoured at 3σ). Please note that O3α adopts two alternate conformations (occupancy is indicated). **b.)** Superposition of the x-ray structures of 3deazaThDP (1.259 Å resolution, yellow) with the native intermediate DHEThDP (1.45 Å resolution, cyan). **c.)** Closer view on the thiophen ring system of 3deazaThDP. The angular distortion α of C2α relative to the thiophen ring is indicated (red).

3.4.4. Strain in Enzymatic Catalysis – Covalent Reaction Intermediates in TK

Although geometrical and electronic strain are widely discussed principles for the destabilization of an enzymatic ground state its significance for catalysis is subject of debate (Fersht, 1999; Warshel et al., 2006). Usually, strain refers to raising the free energy of bound substrate in the active site before any chemical transformation has occurred (Petsko, 2004; Voet, 2008). Fersht noted that substrates aren´t distorted physically but binding enthalpy is exclusively used to stabilize the transition state of a reaction (Fersht, 1999). Those conclusions mainly originate from energetic calculations which demonstrated that substrate binding alone can´t be addressed to distort strong covalent bonds.

Moreover, according to computational calculations steric strain alone is not believed to provide a considerable catalytic effect by ground state destabilization (Warshel et al., 2006).

In contrast, recent experimental and computational results provide evidence that molecular strain plays an important role for typical biochemical reactions like cleavage of covalent bonds (Asztalos et al., 2007; Jensen and Ryde, 2005; Milic et al., 2011; Tittmann and Wille, 2009) or hydride transfer causing geometrical distortion of coenzymes or cosubstrates (Berkholz et al., 2008). These results further suggest that molecular strain functions not exclusively in ground-state destabilization but also for reactant-state destabilization (Lehwess-Litzmann et al., 2011; Milic et al., 2011) of covalent intermediates. From an energetic point of view reaction enthalpy generated upon formation of covalent bonds might be the driving force to promote even distortion of covalent bonds (Asztalos et al., 2007).

In addition, it could be speculated that reports of strained reaction intermediates might be under-estimated because subtle structural deviation of bond length and -angles remain undetected at medium or even high resolution. A protein data bank search (http://www.rcsb.org/pdb/home/home.do) revealed that the number of enzymatic reaction intermediate structures determined to true atomic resolution (≤ 1 Å) is relatively small (54) in comparision to the total number of 460 structures (updated 03.01.2012). Moreover, in almost all cases those structures represent non-covalent complexes between enzyme and substrate, product, anologues or inhibitors. None of the deposited structures in this resolution range represent a native, covalent reaction intermediate.

All true-atomic x-ray structures of authentic reaction intermediates in TK described in the previous chapters revealed strong angular distortions demonstrating that strain is a common mechanistic tool and a major contributor for reactant state destabilization at least for TK. Since all ThDP-dependent enzymes are confronted with analogous mechanistical barriers (Kluger and Tittmann, 2008) those conclusions are transferable to the entire coenzyme super-family (Kluger and Tittmann, 2008)(Fig. 87).

3.4.5. Limitations for Locating Hydrogen Positions by X-ray Crystallography – Outlook for Further Studies on Transketolases

Previous chapters contained assignments of protonation states for intermediates or protein residues which were deduced from high-resolution x-ray structures. A brief discussion of limitations and alternatives of this method is given below.

Because hydrogen atoms harbor solely a single electron their interaction with incoming x-rays is very weak. Thus, even at ultra-high resolution protons are hard to localize in protein crystal structures. This scenario is even more problematic for hydrogens bound to groups with a small rotational barrier or

hydrogens involved in strong hydrogen bonding interactions. Steiner and Saenger demostrated for very strong hydrogen bonds, so called low barrier hydrogen bonds (Cleland et al., 1998; Steiner and Saenger, 1994), that the hydrogen is diffusely located between donor and acceptor with an average position in the center (Cleland et al., 1998). Such hydrogen positions can´t be observed by x-ray crystallography and were traced by reevaluation of low-temperature neutron crystallographic structures (Steiner and Saenger, 1994). Additionally, in Brønstedt acid/base catalysis, a fundamental mechanism found in countless enzymatic reactions, the hydrogen atom can principally be located in certain fractions at two or more (e.g. three-centered interaction) participating, electronegative atoms. Hydrogens bound at such positions are extremely hard to locate and quantifiable by x-ray crystallography.

Other biophysical methods such as NMR spectroscopy or neutron crystallography enable the unambiguous assignment of protonation states even for large macromolecules. The main disadvantages of these methods are in case of NMR spectroscopy the size of the macromolecule, at least for the liquid state, and in case of neutron crystallography the required size of protein crystals. While early neutron diffraction experiments with proteins required large crystal volumes of several mm^3, state of the art beamlines can appropriate protein crystals with a volume of less the 0.15 mm^3 (Adams and Langan, 2010 b; Blakeley et al., 2008).

To receive a comprehensive and detailed insight of the TK reaction cycle and to verify current results it has to be considered to combine our x-ray crystallographic studies with one of the methods mentioned above (Kovalevsky et al., 2010). Notably, the applicability of solid state NMR spectroscopy to assign protonation states of ThDP-dependent enzymes trapped at certain steps of catalysis was recently presented (Paramasivam et al., 2011). However, the proteins used for this approach are very large (200-250 kDa) and the obtained spectra couldn´t visualize minor populated species. TK would be an interesting model enzyme for such experiments since certain catalytic steps can easily be accumulated in solution and the smaller size of the transketolase dimer (144 kDa) might simplify NMR data collection and analysis. Neutron crystallography was yet not applied for any ThDP-dependent enzyme. Transketolases are interesting research objects for this method as *Ec*TK crystals already reach in some cases sizes of approx. 0.1 mm^3 (1.0 mm x 0.3 mm x 0.3 mm) by crystallization in hanging drops.

3.4.6. Acceptor Substrate Binding in *h*TK and *Ec*TK

*H*TK, *Ec*TK and the majority of functionally characterized TKs convert three native acceptors of different chain length: glyceraldehyde 3-phosphate (GAP, C3), erythrose 4-phosphate (E4P, C4) and ribose 5-phosphate (R5P, C5). Moreover, glucose 6-phosphate (Willige et al., 2009) and numerous un-phosphorylated aldoses were described as substrates for individual TKs (Schenk et al., 1998; Sprenger et al., 1995).

Structural and mechanistic studies on acceptor substrate binding in TK could yet just be presented for two acceptors in *Ec*TK (Asztalos et al., 2007) and *Sc*TK (Nilsson et al., 1997). Thus important details about the selection of acceptors and the pre-orientation of functional groups during carboligation with the covalent DHEThDP intermediate are limited. However, x-ray structural analysis of acceptor substrate E4P bound to *Sc*TK allowed to delinate interactions of the acceptor with the protein in the immediate vicinity of the active site (Nilsson et al., 1997)(pdb-code: 1NGS) and contributed to explain the stereospecificity of TK (Nilsson et al., 1998; Schneider and Lindqvist, 1998).

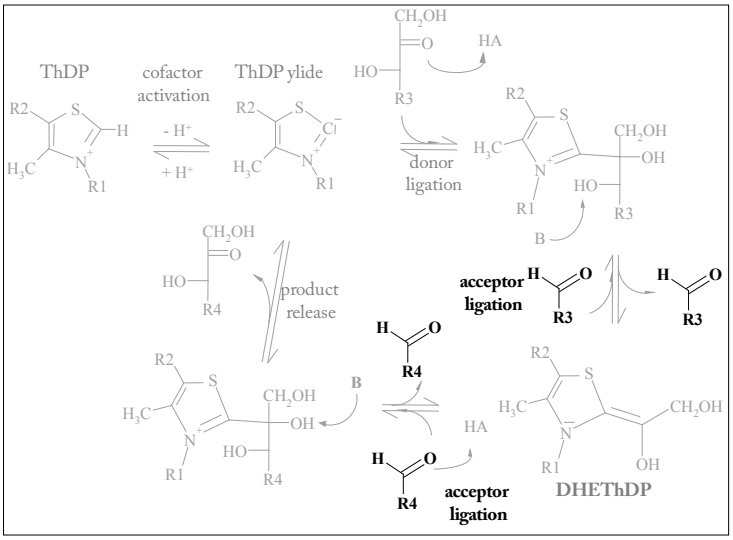

Fig. 60: Acceptor substrate binding to TK. Simplified reaction scheme for TK catalyzed over-all reaction (R1 = aminopyrimidine moiety, R2 = ethyldiphosphate). The central intermediates DHEThDP, shown as enamine structure, can react in a competitive equilibrium with different acceptor substrates. The direction of the reactions is dependent on the affinity for each acceptor and its concentration and thus linked to cellular conditions.

Furthermore, our group recently succeeded in determination of *Ec*TK in non-covalent complex with acceptor ribose 5-phosphate (Asztalos et al., 2007)(pdb-code: 2R5N). Mechanistically interesting, the electron density map for ligand R5P differed in both active sites suggesting a structural non-equivalence for acceptor binding. While one active site was occupied with R5P predominantly present as β-D-furanose form the electron density map in the second active site was interpreted as a mixture of

two different R5P conformers. Beside β-D-furanose form a considerable fraction of approx. 50 % of the substrate was interpreted as acyclic aldehyde (Fig. 61 a.)). Given that R5P is present in aqueous solution almost exclusively as cyclic furanose (99.9 %)(Pierce et al., 1985). In consequence *Ec*TK had preferentially bound the acyclic form (0.05-0.1 %) or catalyzed the furanose ring opening (Fig. 61 a.)). Two processes were addressed for the stabilization of the reaction competent acyclic aldehyde form relative to the unreactive cyclic form. First, the β-furanose ring (C2 exo conformation) was reported to be significantly distorted presumably caused by binding to TKs active site. Ring opening was discussed to release this distortion. This proposal is interesting since it would represent a reasonable example for ground-state destabilization on an enzyme. Second, the acyclic form was reported to be stabilized by a hydrogen bonding interaction with an active site histidine (*Ec*TK His473). The authors interpreted this reaction-competent conformation as a near attack conformer (Hur and Bruice, 2003; Hur et al., 2004) which can, per definition, easily convert into the transition state. Since His473 is replaced by Glu428 in *h*TK we were particularly interested how recognition and stabilization of acyclic R5P is realized in *h*TK. Furthermore, the energetics of acceptor substrate recognition should be studied by ITC.

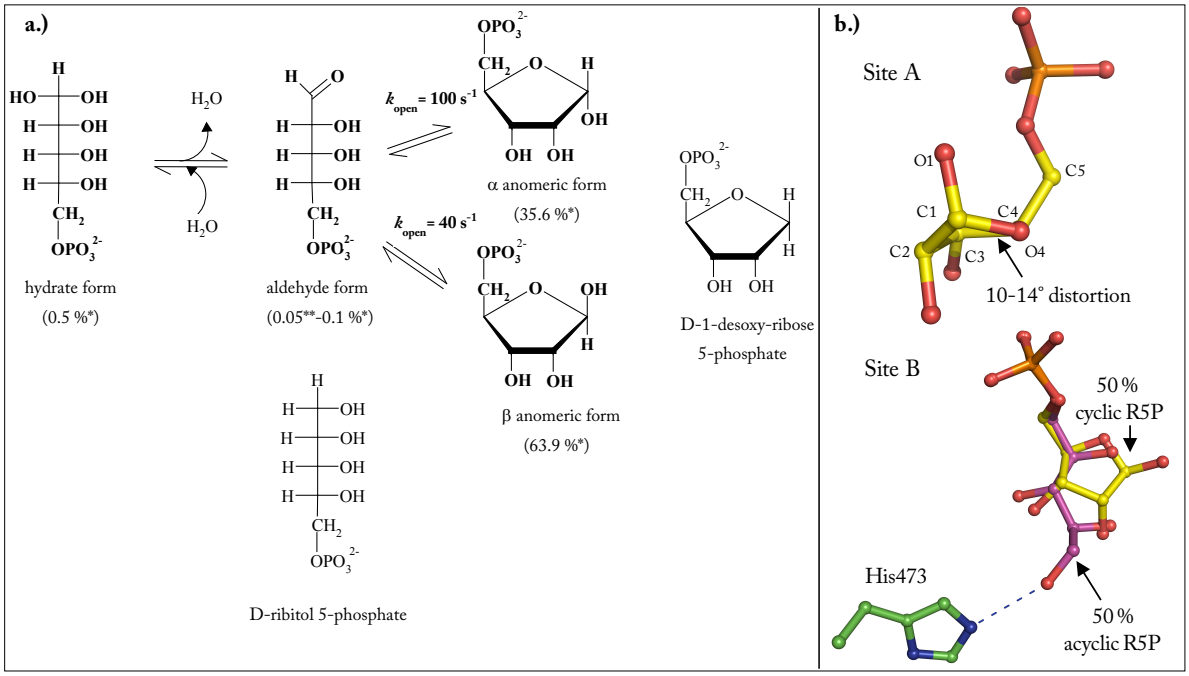

Fig. 61: Ribose 5-phosphate binding in TK. a.) Structural heterogeneity of acceptor substrate R5P in aqueous solution. Chemical structures of four possible forms of R5P are shown in bold as well as the relative distribution at 6 °C and pH 4.5 (* values from Pierce et al. 1985, ** value from Hayward & Angyal, 1977). R5P is predominantly present as cyclic furanose (99.9 %). Substrate analogues mimicking individual states of R5P are shown in Fischer or Haworth projection. Rate constants for the conversion of α and β anomer into the acyclic aldo form at 40 °C and pH 7.5 (Pierce et al., 1985) are shown bold. **b.)** Detailed view on both active site of the *Ec*TK-R5P complex (Asztalos et al., 2007)(1.73 Å, pdb-code: 2R5N). Selected atoms and residues are labeled. The distortion from coplanarity in the furanose ring in site A as well as the relative ratio of cyclic and acyclic form of R5P in site B is indicated. For explanation see text.

To visualize binding of an acceptor sugar to enzyme bound DHEThDP the usage of "native" and therefore reactive DHEThDP is not feasible. The lifetime of such a complex under substrate saturation is a few milliseconds (Fig. 20). We therefore exchanged native DHEThDP with an isosteric analogue that is catalytically inactive and completely inert for carboligation (1,2-dihydroxyethyl-3deaza-thiamin diphosphate short 3deazaThDP). This complex was then co-crystallized and single crystals were used for soaking experiments with different acceptors. Unfortunately, all attempts to visualize acceptor binding with this analogue were unsuccessful presumably originating from a different conformation of the dihydroxyethyl moiety of 3deazaThDP (Fig. 59) relative to authentic DHEThDP that hinders acceptor binding (see chapter 3.4.3.7). Acceptor binding was consequently only studied in *h*TK co-crystallized with ThDP. For substrate soaking experiments two native acceptor substrates (E4P, R5P) as well as two substrate analogues that mimick cyclic (1-desoxy-ribose 5-phosphate short 1desR5P) or acyclic (ribitol 5-phosphate short Rib5P) conformation of R5P were used. Analogues 1desR5P and Rib5P were synthesized and kindly provided by Anatol Spork and Prof. Dr. Christian Ducho (Bioorganic and Medical Chemistry, University of Göttingen).

3.4.6.1. Binding of E4P to *h*TK

The structure of E4P non-covalently bound to the active site of *h*TK was determined to 1.17 Å and refined to reasonable R-factors (R_{work} = 13.08, R_{free} = 15.79). The acceptor molecule (81 % occupancy) is positioned by polar interactions (Arg474, Arg318, His416, 37, 258, Asp424 and Ser345) mainly accomplished by its phosphate moiety. The hydroxyl functions of E4P are weaker coordinated (Fig. 62) and the O2α hydroxyl group has no stabilizing interaction. Relative to the tightly integrated cofactor the 4-carbon acceptor reveals a 2-3fold increased flexibility represented by its atomic B-factors (Fig. 62c.). Moreover, atomic B-factors for the non-phosphate part of E4P are approx. 50 % increased relative to the phosphate moiety, suggesting a lower flexibility for the phosphate. The carbonyl oxygen of E4P is positioned by hydrogen bonding interactions with His258 and His37. Noteworthy, three positive difference electron peaks in close proximity of E4P could be identified as water molecules bound at low occupancy.

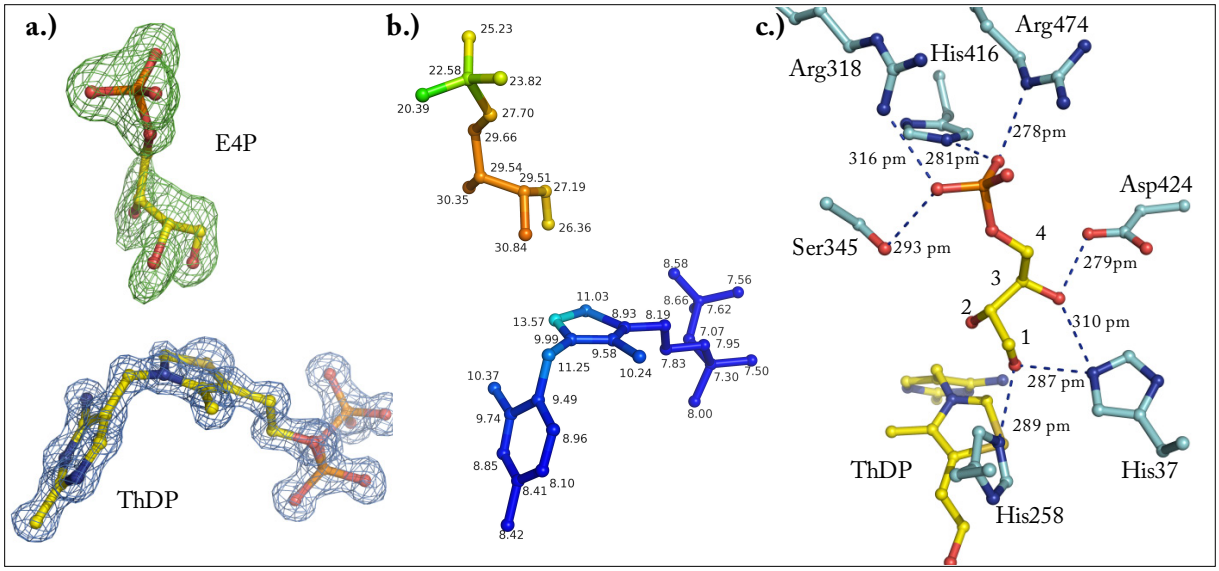

Fig. 62: Binding of acceptor E4P to *b*TK. X-ray structure of *b*TK in non-covalent complex with E4P determined to a resolution of 1.17 Å. **a.)** E4P shown with a residue-omitted mFo-DFc map (contour level 3σ) bound in close proximity to the cofactor ThDP which is surrounded by a 2mFo-DFc map (contour level 2σ). **b.)** Atoms of E4P and ThDP are color-coded according to their individual B-factors showing less mobile atoms in blue (7-10 Å^2) and most mobile ones in orange (≈ 30 Å^2). **c.)** Interactions of the acceptor substrate with active site residues are illustrated as blue dashed lines in addition to inter-atomic distances.

As a tetrose phosphate E4P can´t cyclize and is in aqueous solution (pD = 1.4, 20 °C) up to 93 % hydrated (Duke et al., 1981). It was additionally found for concentrated solutions (pD = 1.4, 20 °C) of E4P that it predominantly adopts numerous dimeric states which slowly convert into monomers. While it is very unlikely that an E4P dimer can be bound by TK even binding of the hydrate form would be catalytically unfavorable as hydrates lack carbonyl reactivity which is required for carboligation to the DHEThDP intermediate. Since no hydrate form is observed in the x-ray structure the question arise whether *b*TK preferentially binds the non-hydrated carbonyl form of E4P or whether it actively catalyzes dehydration. Potential candidates for this reaction are His258 and His37 which are both well positioned to protonate the C1-hydrate thereby accelerating the elimination of water. Small rate constants for uncatalyzed dehydration of E4P hydrate forming the aldehyde determined for pD 1.4 and 6.4 at 27 °C of 6 s^{-1} and 1 s^{-1} (Duke et al., 1981) strongly suggest an active participation of TK in dehydration of E4P. This idea is further supported by a microscopic rate constant of > 150 s^{-1} determined for the reaction of DHEThDP intermediate with E4P in *Ec*TK (Lüdtke, 2008).

To illustrate the carboligation reaction between DHEThDP intermediate and E4P yielding the F6P-ThDP intermediate structurally we superimposed those experimentally determined x-ray structures (Fig. 63). The inter-atomic distance between C2α (DHEThDP intermediate) and C1 of E4P of

387 pm as well as the relative orientation of the reactants is unfavorable for a spontaneous carbonyl reaction (Burgi et al., 1974; Burgi et al., 1973) indicating that all atoms of the non-phosphate part of E4P have to change their position to enable ligation to C2α. Whether this dynamic event proceeds spontaneously or might be mediated by active site residues is not readable from static x-ray structures and remains to be studied in more detail. However, the elevated atomic B-factors of E4Ps´ non-phosphate moiety which suggest a higher flexibility could also indicate that carboligation proceeds mainly self-driven.

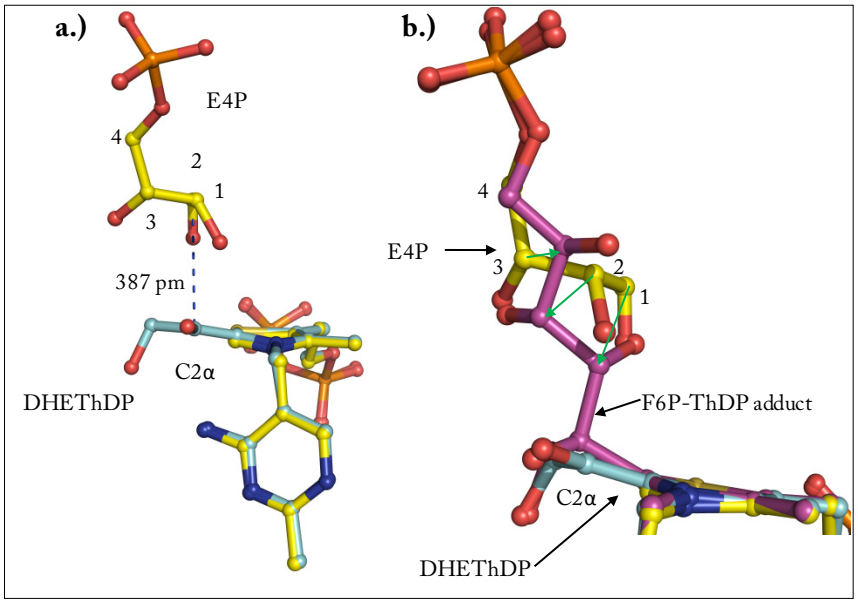

Fig. 63: Model for carboligation of the DHEThDP intermediate with E4P. a.) Superposition of the *b*TK-E4P complex (yellow) with the *b*TK-DHEThDP intermediate complex (cyan). The inter-atomic distance between R5P C1 and DHEThDP C2α of 387 pm is indicated by a blue dashed line. **b.)** Superposition of covalent F6P-ThDP intermediate (purple) with superposition shown in a.) Reversible carboligation of DHEThDP and E4P is responsible for formation of the covalent F6P-ThDP adduct. Positional changes of E4P upon formation of F6P-ThDP are indicated (green arrows). Selected atoms are labeled.

3.4.6.2. Binding of E4P to *Ec*TK

Given that the non-covalent *Ec*TK-E4P complex could yet just be solved to a resolution of 1.45 Å (R_{work} = 12.28, R_{free} = 14.59) but delivers complementary information we resigned to describe this complex here in detail. Notably, the relative position of E4P and its interactions with the active sites of *b*TK and *Ec*TK differ slightly.

3.4.6.3. Binding of R5P to *h*TK

The x-ray structure of *h*TK in non-covalent complex with R5P was determined to 1.2 Å resolution, refined to reasonable R values (R_{work} = 12.28, R_{free} = 14.59) and finally also the occupancy of R5P could be calculated (76 %). The additional positive difference electron density map found in the active site was interpreted and modeled as α-furanose form of R5P in C2-endo conformation (Fig. 64). In this conformation four atoms (ring oxygen, C1, C3 and C4) forming a plane and C2 is out of plane at the same side as C5 (tortion angle O4-C1-C3-C4 ≈ 168°). The phosphate moiety of R5P is coordinated by Arg474, Arg318, His416 and Ser345 (Fig. 65). The anomeric hydroxyl group (O1) is positioned by strong hydrogen bonding interactions with His37 and His358 and O3 is involved in a hydrogen bonding interaction with Asp424. Notably, the interaction between O2 and Gln189 is questionable in terms of hydrogen bonding geometry (not illustrated). While the phosphate moiety of R5P has a similar atomic B-factor relative to the surrounding active site residues increased B-factors are detectable for the atoms of the furanose ring which is suggestive for a higher flexibility of this part. In line with the elevated dynamics of the furanose ring is the observation that the electron density map for C5, which connects phosphate moiety and furanose ring, is diffuse. A similar observation can be made for E4P in the previous chapter suggesting similar principles for acceptor substrates binding in TK.

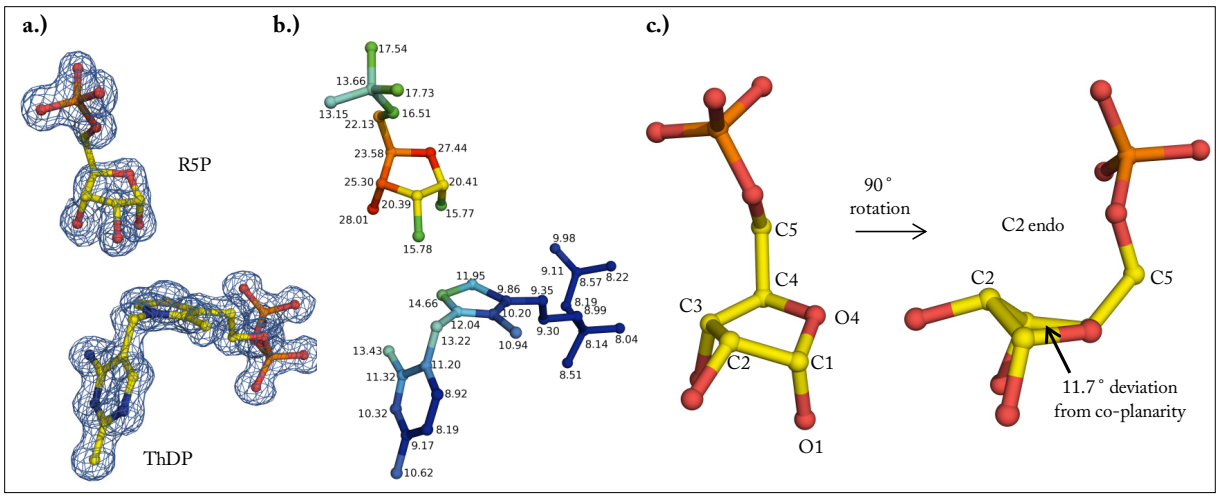

Fig. 64: Binding of acceptor R5P to *h*TK-1. X-ray structure of R5P in non-covalent complex with *h*TK determined to a resolution of 1.2 Å. **a.)** R5P bound in close proximity to the cofactor ThDP both surrounded by electron density (2mFo-DFc map, contoured at 1σ). **b.)** Atoms of R5P and ThDP are color-coded according to their individual B-factors with less mobile atoms in blue (8–11 Å²) and most mobile ones in red (25-28 Å²). **c.)** Detailed view on bound R5P. The substrate is bound as α anomer in C2 endo conformation (C2 and C5 on the same side). The side view (right) of the ligand illustrates the deviation (11.7°) of the coplanar arrangement of C1, O4, C3 and C4.

Even at very low contour levels (0.5-1 σ) in a 2mFo-DFc map no fraction of β-form which contributes 63.9 % of R5P in solution (Pierce et al., 1985) is detectable. However, additional positive difference electron density peaks (mFo-DFc and 2mFo-DFc map) are observable which could be interpreted as acyclic aldehyde form of R5P. Notably, the fraction of the modeled acyclic R5P is obviously smaller than the 50 % found for the analogous *Ec*TK-R5P complex suggesting differences for R5P binding between both TKs (Asztalos et al., 2007). Because the additional positive density peaks are diffuse modeling of the acyclic form was performed by real space refinement in *COOT* (Emsley et al., 2010) using a mFo-DFc residue omitted map. In this modeled but not refined position we determine a very short distance between R5Ps´ aldehyde carbon and cofactor C2 of 207 pm implicating strong repulsion in case both atoms are not covalently linked. This exceptionally long C–C bond can´t be easily explained and we have yet no clear assignment of this trapped state.

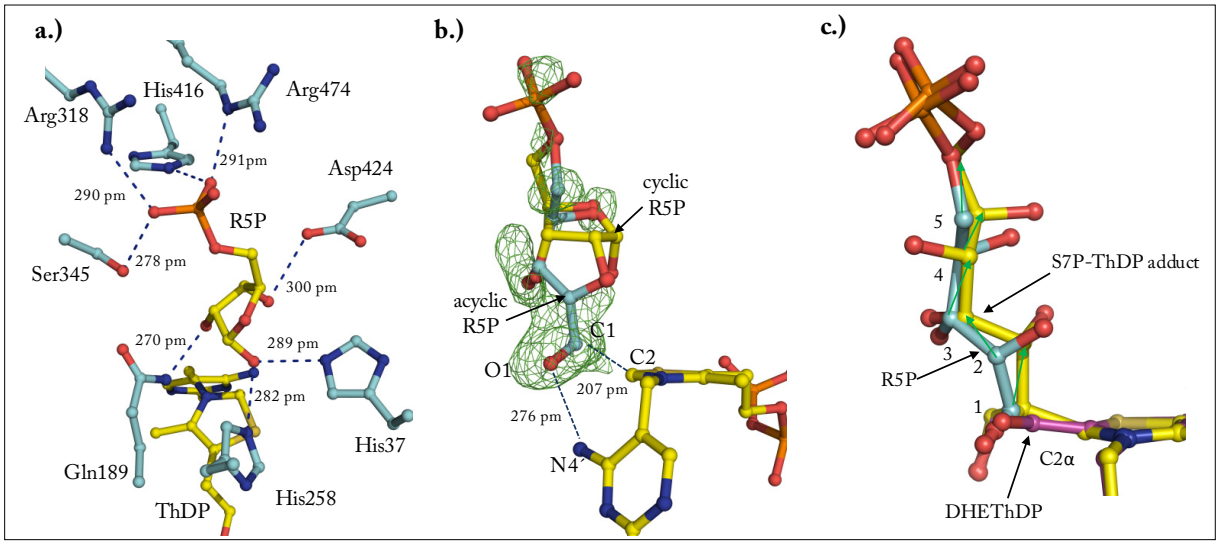

Fig. 65: Binding of acceptor R5P to *b*TK-2. a.) R5P is shown bound in close proximity to the cofactor ThDP (both yellow). Interactions of the acceptor substrate with active site residues are shown as blue dashed lines in addition to inter-atomic distances (in pm). **b.)** Acyclic R5P (cyan) that was modeled into difference electron density (mFo-DFc map contoured at 3σ) is shown as well as ThDP and cyclic R5P. Inter-atomic distances that are discussed in the text are highlighted by dashed blue lines. **c.)** Superposition of acyclic R5P (cyan) with the DHEThDP intermediate (purple) and the S7P-ThDP intermediate. Positional changes of R5P upon formation of S7P-ThDP are indicated (green arrows). Selected atoms are labeled.

Thus, the modeled orientation of acyclic R5P should be considered as an initial proposal. A higher resolved structure of the *b*TK-R5P complex is needed to clearly identify the atomic position of the minor populated acyclic aldehyde form and to verify our model. In addition a ^{1}H NMR based intermediate method is planed to prove if the so interpreted acyclic R5P is indeed covalently linked to the coenzyme. Interestingly, the only hydrogen bonding partner for the aldehyde oxygen is the cofactor N4´-amino group. A hydrogen bonding interaction with Gln428 has to be excluded as the

interatomic distance of less than 2 Å clearly predicts repulsion. This is again a difference to the *Ec*TK-R5P complex for which a stabilizing interaction with His473 was reported (Asztalos et al., 2007)(Fig. 61). In analogy to the mechanistic analysis performed for E4P we superimposed the *b*TK-R5P complex with the DHEThDP intermediate (Fig. c.)) to visualize the carboligation reaction in this case to form the S7P-ThDP intermediate. The alignment reveals that the reacting atoms, R5P C1 and DHEThDP C2α, accomondate closely (< 0.5 Å) but in an unfavorable orientation. Larger positional rearrangements of the entire R5P molecule would be necessary to engage the corresponding positions in the S7P-ThDP intermediate. It seems to be more reasonable that the carboligation reaction proceeds immediately after furansoe ring opening of cyclic R5P. In consequence, our structural data indicate that for both native acceptor substrates the reactant state with the DHEThDP intermediate is probably transient.

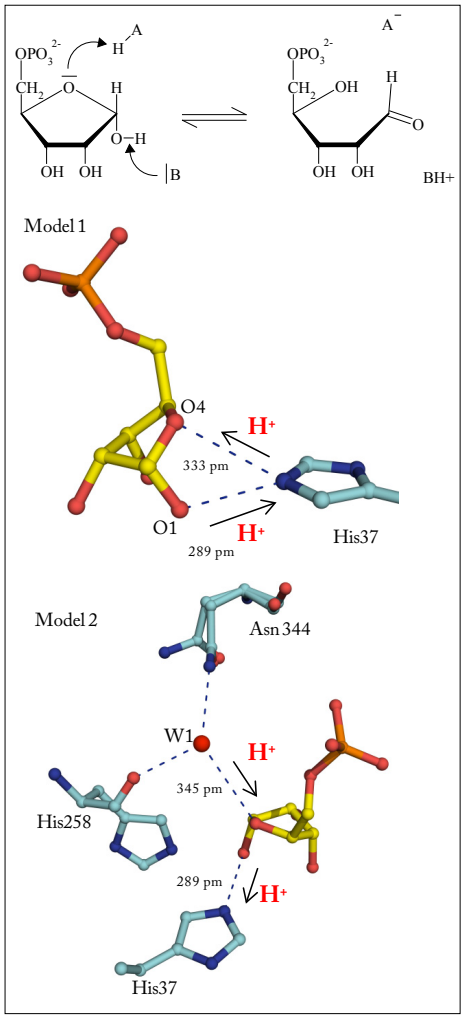

Fig. 66: Proposed Models for ring opening of the acceptor substrate R5P in *b*TK. A general, schematic mechanism for acid-base catalized ring opening of R5P (α furanose) is depicted on top. Ring opening requires protonation of the ring oxygen (O4) and deprotonation of the anomeric hydroxyl group (O1). In **Model 1** His37 would act as base and acid to perform a cyclic proton transfer. For the alternative **Model 2** an active site water molecule (W1) would protonate the ring oxygen and His37 would deprotonated the anomeric hydroxyl group. The direction of the proposed proton transfer models is highlighted by arrows. Putative hydrogen bonding interaction (dashed blue lines) and selected distances for each model are shown.

The conversion of cyclic α furanose form of R5P into the acyclic aldehyde form (100 s^{-1} at 40 °C) is not rate-limiting for the overall reaction (*Ec*TK k_{cat} = 40-50 s^{-1}) (Asztalos, 2007 b; Sprenger et al., 1995)(*b*TK k_{cat} = 6-19 s^{-1})(Mitschke et al., 2010; Schenk et al., 1998) but for the carboligation with the DHEThDP intermediate (approx. 530 s^{-1} for *Ec*TK). Two models (Fig. 66) are feasible how *b*TK could accelerates the ring opening reaction of cyclic R5P. In Model 1, which is very reasonable in terms of bond length and proton transfer geometry, His37 would act simultaneous as Brønstedt base and acid to enable a cyclic proton relay. Alternatively, in Model 2 a water molecule could act as proton donor while His37 could deprotonate the anomeric hydroxyl group. As already mentioned a deviation from coplanarity of 11.7° was observed for R5P bound to the active site of *b*TK that fits quite well to the 10-14° distortion reported for R5P bound to *Ec*TK (Asztalos et al., 2007). Furanose rings are conformationally inhomogeneous in

solution and exist in multiples envelope- and twist conformers. Given that the energy barrier between those conformers is relatively small a rapid interconversion of conformers is typical in solution (Levitt and Warshel, 1978). Hence, it is reasonable to assume that such deviations from coplanarity result from ordinary flexibility of the furanose ring. In contrast the small molecule x-ray structure of R5P present in C2 endo conformation (Koziol and Lis, 1991) shows a perfectly coplanar arrangement (0.2° deviation). Since no absolute energies for a coplanar and the observed distorted envelope conformation of enzyme bound R5P are yet available the small distortion can´t be addressed as a driving force for ring opening.

3.4.6.4. Usage of R5P Analogues Rib5P and 1desR5P

As shown in Fig. 61 R5P analogues Rib5P and 1desR5P can be classified as acyclic and cyclic mimics of R5P. These analogues were used to solely trap and visualize first R5P binding (1desR5P) and second the orientation of reactive R5P aldehyde form (Rib5P) necessary for carboligation to the DHEThDP intermediate. In the previous chapter we observed a small fraction of so interpreted acyclic from of R5P. The usage of Rib5P was supposed to accumulate this state and thereby validate our results and conclusions. Steady-state kinetic measurements revealed that both substrate surrogates are weak inhibitors for *Ec*TK and *h*TK (Fig.67). For *Ec*TK inhibition was slightly stronger and both substrates showed a different strength of inhibition. The difference between both TKs is surprising in consideration of their structural similarities. Due to a limited availability of both R5P analogues and their weak inhibitory effect a determination of an inhibitory constant (K_i) couldn´t be performed.

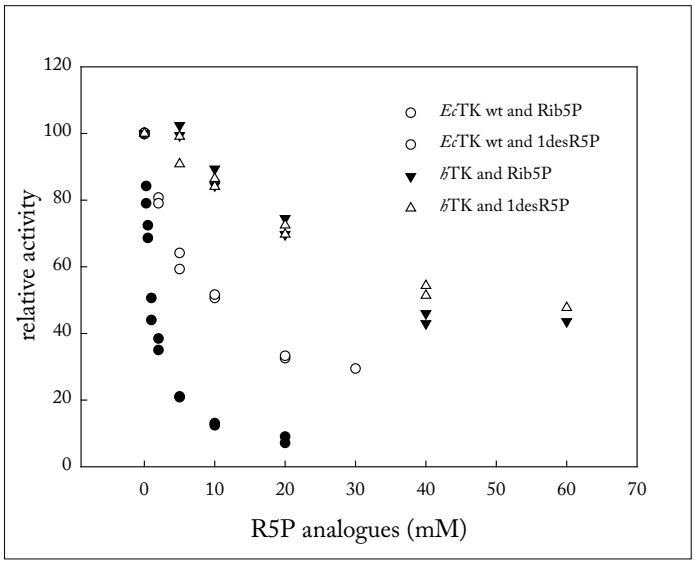

Fig.67: Inhibition of TK activity by R5P analogues. Kinetics were carried out with 100 µg/ml (1.45 µM active sites) *h*TK or 20 µg/ml (0.29 µM active sites) *Ec*TK, 5 mM $CaCl_2$, 100 µM ThDP, 0.2 mM R5P, 0.2 mM X5P, 3.6 U/ml G3PDH/TIM in 50 mM glycylglycine (pH 7.6) at 30 °C in absence and presence of either Rib5P or 1desR5P at different concentrations. Kinetics were measured in duplicates.

3.4.6.5. Binding of Rib5P to *h*TK

Binding of R5P analogue Rib5P to *h*TK was determined to a resolution of 1.18 Å (R_{work}= 12.42, R_{free} = 14.58). According to the postitive difference electron density peaks found in the active site of *h*TK two alternate conformations (54 % and 26 % occupancy) of the ligand molecule were modeled (Fig. 68). Notably, even after inclusion of both conformations for refinement numerous positive difference electron density peaks remained in close proximity to the cofactor which is indicative for the presence of additional unmodeled Rib5P conformers. The apparent, high flexibility of Rib5P is further supported by higher atomic B-factors relative to ThDP (Fig. 68b.)) and the surrounding active site residues (not shown). Superposition of acyclic R5P found in the *h*TK-R5P complex with both Rib5P conformers reveals that neither the phosphate moiety nor the remaining hydroxyl functionalities are congruent. It is an unexpected observation that the binding mode relative to native, acyclic R5P has so strongly changed which is solely caused by the exchange of the C1-aldehyde functionality. Due to these structural differences mechanistic statements on the carboligation process with the DHEThDP intermediate were not performed.

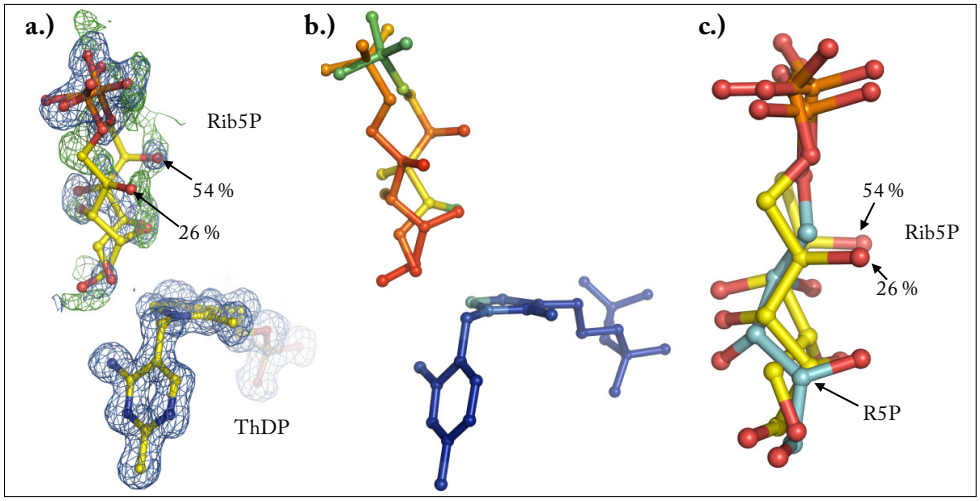

Fig. 68: X-ray structure of *h*TK in non-covalent complex with Rib5P. X-ray structure Rib5P in non-covalent complex with *h*TK determined to a resolution of 1.18 Å. **a.)** Substrate analogue Rib5P bound close to ThDP. Both molecules are surrounded by a mFo-Fc map (countoured at 3σ, green) and a 2mFo-DFc map (contoured at 1σ, blue). **b.)** Atoms of Rib5P and ThDP are color-coded according to their individual B-factors showing less mobile atoms in blue (6–12 Å^2) and most mobile ones in red (24-27 Å^2). Values for individual B-factors were not shown for reasons of clarity. **c.)** Superposition of *h*TK in complex with Rib5P (yellow,) and acyclic R5P (cyan).

3.4.6.6. Binding of 1desR5P to *b*TK

The x-ray structure of *b*TK in complex with 1desR5P was determined to 1.14 Å (R_{work} = 12.25, R_{free} = 14.47). The cyclic R5P analogue adopts one traceable conformation (Fig. 69 a.)) and is bound with an occupancy of approx. 85 %. The 1desR5P ligand reveals elevated flexibility relative to its surrounding active site residues and a slight B-factor difference within the molecule. As found for the native substrates the phosphate moiety is more rigid than the remaining part of 1desR5P (Fig. 69 b.)).

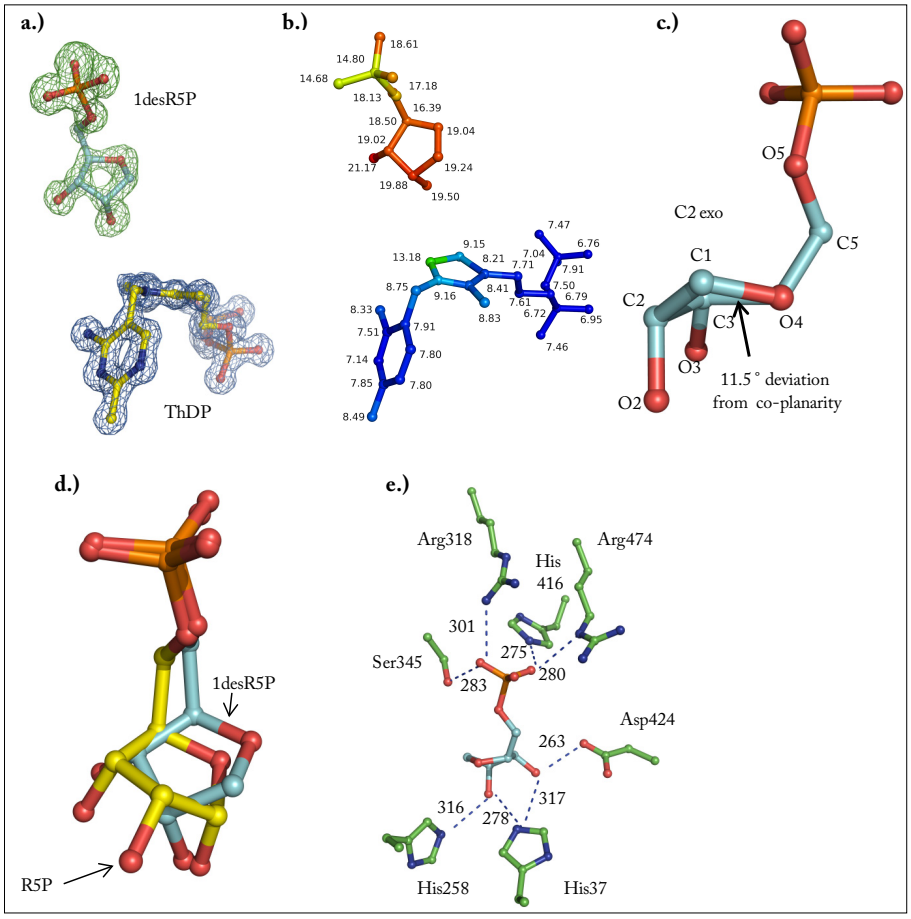

Fig. 69: X-ray structure of *b*TK in non-covalent complex with 1desR5P. X-ray structure of 1desR5P in non-covalent complex with *b*TK determined to a resolution of 1.14 Å. **a.)** Substrate analogue 1desR5P (cyan) surrounded by a mFo-Fc map (contour level 3σ, green) and bound in close proximity to ThDP (yellow) which is surrounded by a 2mFo-Fc map (contour level 2σ, blue). **b.)** Atoms of 1desR5P and ThDP are color-coded according to their individual B-factors showing less mobile atoms in blue (6.8–10 Å²) and most mobile ones in red (18-21 Å²). **c.)** Closer view on 1desR5P. Deviations from co-planarity in the furanose ring are indicated. **d.)** Superposition of *b*TK-bound 1desR5P (cyan) and R5P (yellow). **e.)** Polar interactions of 1desR5P with the active site of *b*TK. Active site residues and inter-atomic distances (in pm) are labeled.

The furanose ring of 1desR5P which adopts C2 exo conformation exhibits a deviation from coplanarity of 11.5° (11.7° for R5P in *b*TK). Hence, one could speculate that the acceptor analogue is,

like discussed for the native substrate R5P, prone to ground state destabilization. However, superposition with the structure of the *h*TK-R5P complex revealed that apart from the phosphate moieties of both compounds the remaining substrate atoms are not congruent. Thus, also the interaction pattern (Fig. 69 d.)) are not identical. It is therefore questionable why an analogue bound in a "non-native" mode should be distorted by the enzyme. Hence, it could be reasonable to postulate that the deviation from coplanarity is a coincidal event.

3.4.6.7. Furanose Ring-Opening of R5P bound to *Ec*TK – Proposal for an Acid/Base Mechanism

Although Asztalos and colleaques suggested reasonable models for stabilization of the reaction-competent acyclic relative to the cyclic form of R5P bound to *Ec*TK no proposal for an acid/base mechanism was so far presented. A reinspection of this complex revealed that in contrast to the analogous complex in *h*TK no active site residue is positioned to protonate R5Ps´ ring oxygen (O4) to enable ring opening. This function is presumably fulfilled by one of two suitably positioned active site water molecules (W1 and W2 in Fig. 70). Moreover, proton abstraction from the anomeric hydroxyl group (O1) is not performed by an active site histidine (His37 in *h*TK, Fig. 66) but by Ser385 or by W2.

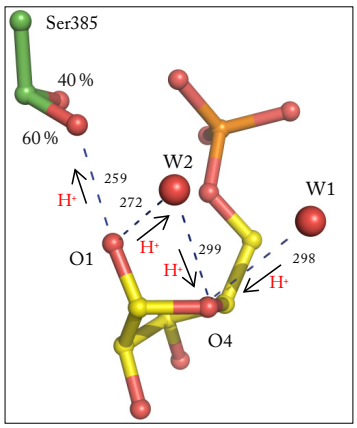

Fig. 70: Model for ring opening of the acceptor substrate R5P in *Ec*TK. Directions of proposed proton transfer are highlighted by black arrows. Putative hydrogen bonding interaction (dashed blue lines) and selected distances (in pm) are indicated. Selected atoms and active site water molecules W1 and W2 are labeled. Occupancies of both alternate conformations of Ser385 are indicated. Figure was prepared according to the structure of the *Ec*TKwt-R5P complex (Asztalos et al., 2007).

Notably, W1 and W2 exhibit 3 to 4fold higher atomic B-factors relative to their surrounding residues indicating an elevated flexibility and suggesting that protonation of the ring oxygen could be performed in a dynamic process. Thereby, the distances between W1 and W2 relative to O4 could be decreased. To test the role of Ser385 for R5P ring opening a Ser^{385}Ala variant could be analyzed kinetically using absorbance spectroscopy with double-jump stopped-flow technique.

3.4.6.8. X-ray Structure of *Ec*TK His^{473}Ala in Non-Covalent Complex with R5P

A crucial interaction between His473 and the aldehyde oxygen of acyclic R5P is considered to stabilize this reactive near-attack-conformer (Hur and Bruice, 2003; Hur et al., 2004) relative to the cyclic furanose form. In order to test this hypothesis and to qualify the importance of this interaction we determined the structure of the *Ec*TK His^{473}Ala-R5P complex (1.8 Å, R_{work} = 14.2, R_{free} = 18.1). Remarkably, the positive difference electron density map for R5P differs for both active sites suggesting a structural non-equivalence for R5P binding (Fig. 71). A similar observation was also reported for *Ec*TK wt (Asztalos et al., 2007). However, in both active sites the additional density map is poorly defined for the anomeric hydroxyl functionality which is indicative of the presence of both R5P anomers or a dynamic process like the furanose ring opening. Those conclusions are further supported by refinements with solely β-anomeric form of R5P that generated a strong negative difference electron density peak for the anomeric hydroxyl group. Inspection of the density map showed that a considerable fraction of acyclic R5P has to be taken into consideration to explain the observed electron density distribution. Thus, His473 can just have a minor role in stabilization of acyclic R5P. Modeling of an acyclic R5P conformer into the density map revealed a similar position of this acyclic state compared to the *Ec*TK wt-R5P complex (not shown). Interestingly, upon exchange of bulky His473 against Ala three additional water molecules are locatable within the active site. One of these water molecules (W2) has a suitable position to resume the stabilizing function of His473. Noteworthy, also thermodynamic (Lüdtke, 2008) and kinetic measurements (Fig. 86) support an inferior role of His473 for acceptor binding and alignment.

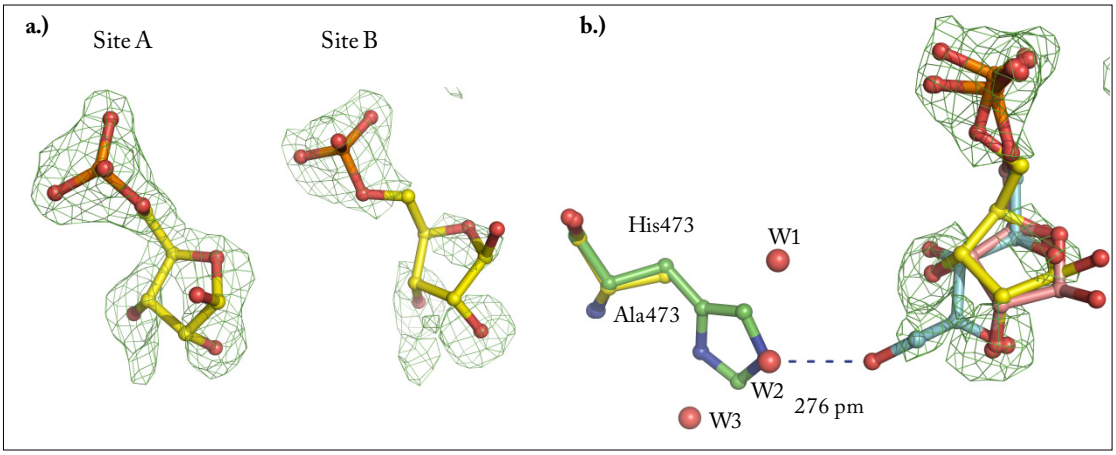

Fig. 71: Structural insights into the *Ec*TK His^{473}Ala-R5P complex. a.) Detailed view on R5P bound to each active site of the protein dimer. **b.)** Superposition of active site B of the *Ec*TK wt-R5P and *Ec*TK His^{473}Ala-R5P complex, Ala473 and cyclic R5P shown in yellow. Cyclic R5P (pink), His473 and water molecules (*Ec*TK His^{473}Ala) are shown. Please note that acyclic R5P bound to *Ec*TK His473Ala is not shown for reasons of clarity. A residue omitted mFo-DFc difference electron density map (contour level 3σ, green) is shown R5P bound to EcTK His^{473}Ala in a.) and b.).

3.4.6.9. Binding of Rib5P and 1desR5P to *Ec*TK- A Structural and Thermodynamical Analysis

The non-covalent complex between acceptor analogue *Ec*TK and Rib5P (0.974 Å, R_{work} = 9.56, R_{free} = 11.14) was determined to solely accumulate the reactive, acyclic form of R5P. Thereby, we aimed to receive a comprehensive understanding how *Ec*TK preferates this state relative to the cyclic furanose form. The additional positive density peaks for this analogue are diffuse and could just been explained with 2 alternate conformations of the ligand (Fig. 72). Both Rib5P conformers exhibit slightly increased flexibility relative to ThDP as well as a B-factor difference witin the molecule with a rigid phosphate group and more flexible remaining part. The electron density map for the substrate analogue is almost identical in both active sites. Superposition with the *Ec*TK-R5P complex (Asztalos et al., 2007) revealed that Rib5P adopts a less extended conformation relative to native acyclic R5P and is shifted approx. 0.5 Å towards the active site entrance. Both facts cause that Rib5Ps´ O1-hydroxyl group can´t be stabilized by His473 (> 4.2 Å,), a crucial interaction reported for native R5P. Unfortunatly, none of the analogue conformers is congruent with acyclic form of R5P and thus statements on the carboligation reaction are difficult. All those structural characteristics for *Ec*TK-bound Rib5P are very similar to the *h*TK-Rib5P complex described earlier.

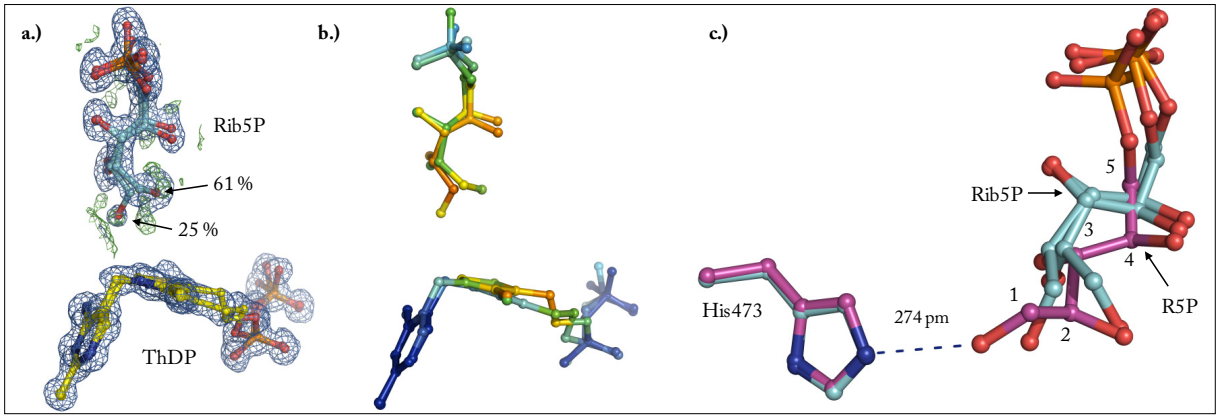

Fig. 72: X-ray structures of *Ec*TK in non-covalent complex with Rib5P. X-ray structure of RibP in non-covalent complex with *Ec*TK determined to a resolution of 0.974 Å. **a.)** Rib5P bound in two alternate conformations (ration are indicated) to the active site of *Ec*TK. **b.)** Atoms of Rib5P and ThDP , shown in two alternate conformations respectively, are color-coded according to their individual B-factors showing less mobile atoms in blue (6–10 Å^2) and most mobile ones in orange (22-28 Å^2). Values for individual B-factors were not shown for reasons of clarity. **c.)** Superposition of *Ec*TK in complex with acyclic R5P (purple, Asztalos et al., 2007 a) and Rib5P (cyan). The hydrogen bonding interaction between His473 and acyclic R5P is indicated (blue dashed line); carbon atoms of R5P are labeled.

Notably, crystals of *Ec*TK soaked with this analogue had out-standing diffraction properties and enabled the collection of three true atomic datasets (0.96 Å, 0.97 Å, 0.974 Å, not all data shown) which might implicate a positive role of this compound in cryo-protection.

In the *Ec*TK-1desR5P complex (1.028 Å, R_{work} = 11.79, R_{free} = 13.95) the analogue is bound with approx. 78 % occupancy in one traceable conformation (Fig. 73). Several positive density peaks in close proximity of 1desR5P could be identified as water molecules acting as placeholder (W1-3). The 1desR5P furanose ring adopts C2 exo conformation and reveals a deviation of 6° from perfect coplanarity (tortion angle O4-C1-C3-C4 ≈ 174°). Thus, the analogue molecule is less strained than native R5P (10-14°). Superposition with the *Ec*TK-R5P complex illustrates that R5P and the analogue 1desR5P are well superimposable and also their interactions with the active site are almost identical in terms of interaction partners and –distances (Fig. 73 d.)). However, Ser385 which adopts two alternate conformations is involved in a hydrogen bonding interaction with the O1 functionality of R5P which is obviously not possible for the analogue. Loss of this interaction for the analogue could be responsible for the decreased deviation from coplanarity within the furanose ring. This finding suggests an active involvement of *Ec*TKs´ active site in destabilization of R5P and makes Ser385 again to an interesting candidate for further structural and kinetic experiments on acceptor binding.

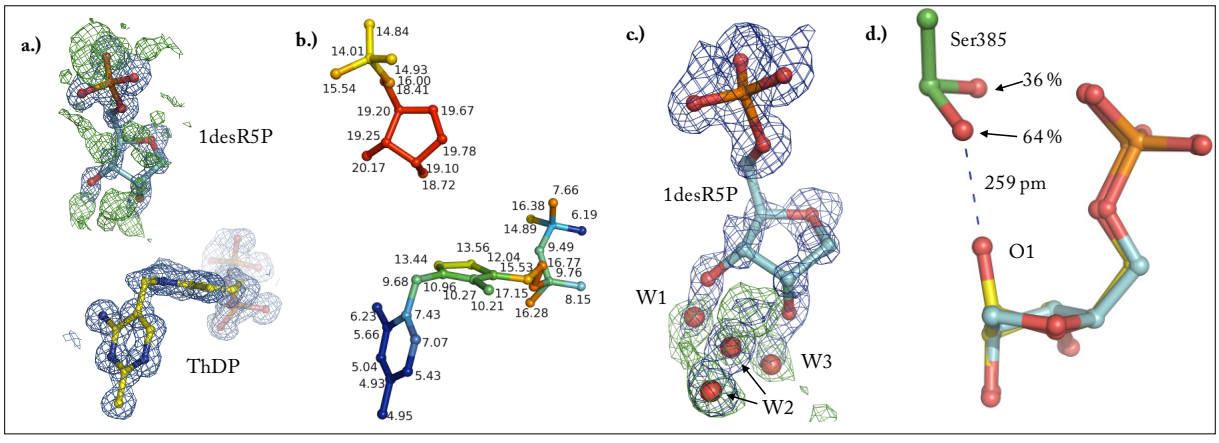

Fig. 73: X-ray structures of *Ec*TK in non-covalent complex with 1desR5P. X-ray structure Rib5P in non-covalent complex with *Ec*TK determined to a resolution of 1.028 Å. **a.)** Acceptor analogue 1desR5P bound in the active site of *Ec*TK. **b.)** Atoms of 1desR5P and ThDP are color-coded according to their individual B-factors showing less mobile atoms in blue (5–8 Å²) and most mobile ones in red (18-20 Å²). **c.)** Detailed view on 1desR5P. Water molecules (W1-3) that will be displaced upon 1desR5P binding are shown as red spheres. **d.)** Superposition of *Ec*TK in complex with cyclic R5P (yellow, Asztalos) and 1desR5P (cyan). Ser 385 which adopts two alternate conformations (occupancies are indicated) is shown in green. Hydrogen bonding interaction between Ser385 and O1 of R5P is indicated (blue dashed line). Models in a.) and c.) are shown surrounded by a 2mFo-DFc (blue, contour level 1σ) and a mFo-DFc map (green, contour level 3σ). Selected atoms are labeled.

In order to correlate our kinetic and structural results on R5P analogue binding with thermodynamic parameters ITC measurements were performed for R5P and each analogue. These calorimetric experiments (Fig. 74) revealed very high but similar K_D values ($K_{D\ (1desR5P)} \approx 1.5–2$ mM, $K_{D\ (Rib5P)} \approx 2.5–3$ mM) for both analogues that are approx. 3-6fold higher in comparison to R5P ($K_{D\ (R5P)} \approx 0.5$-0.7 mM). In consideration that the interactions of R5P and 1desR5P with the active site of *Ec*TK are almost identical the 3-4fold drop in affinity is remarkable and presumably solely attributed to the interaction between Ser385 and O1. Moreover, Rib5P is positioned by 9 and R5P by 8 polar interactions but the affinity is significantly decreased by a factor of 5-6 for the substrate analogue. Both findings demonstrate the challenges of affinity estimation based on structural results. Importantly, weak binding events (> 100 µM) are intrinsically problematic to characterize by biophysical methods. Given that the thermograms show a hyperbolic shape and a deviation from "S"-like curvature an analysis of thermodynamic parameters has a high intrinsic error (Turnbull, 2003). Analogous experiments with *h*TK revealed uninterpretable data caused by strong precipitation of the enzyme.

Ground state destabilization of R5P, that is the postulated distortion the furanose ring, can solely be compensated by binding enthalphy. Using ITC a weak interaction and thus a small free binding enthalphy (7.9–8.4 kJ/mol) for the interaction of R5P with *Ec*TK could be determined. Therefore it remains to be further studied by computational methods how much energy is needed to transfer substrate molecule R5P from a perfect coplanar into this distorted furanose conformation and if this this process has a considerable impact on ring opening.

Asztalos speculated about a near-attack-conformation for acyclic R5P which should adopt a "transition-state-like" conformation (Asztalos et al., 2007). Given that the affinity for the transition state is generally considered to be very high one would also expect to observe tight binding for acyclic R5P. The affinity for Rib5P is very low demonstrating that this compound is a poor analogue for acyclic R5P or that acyclic R5P is not bound as near-attack-conformer. The first proposal is supported by our structural result revealing that the highly flexible Rib5P is not congruent with acyclic R5P in both TKs.

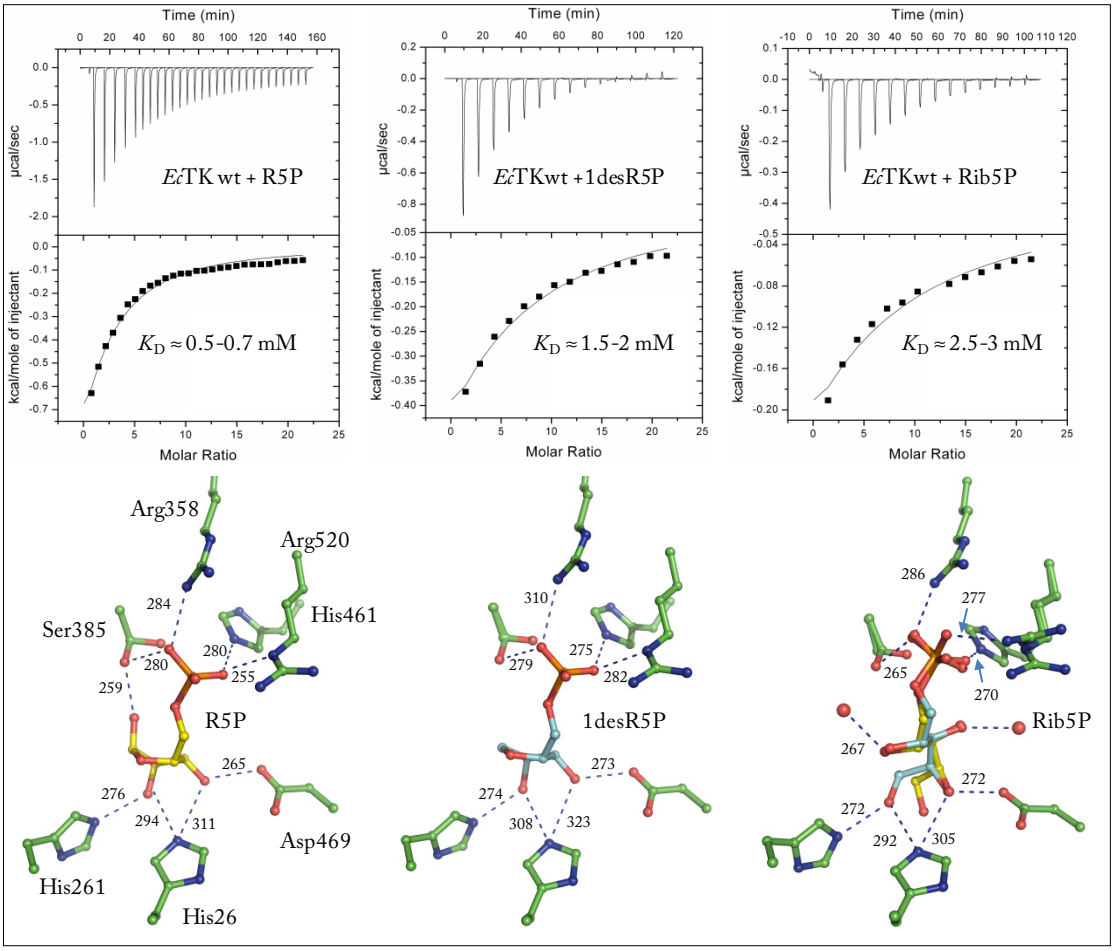

Fig. 74: Isothermal Titration Calorimetry (ITC) experiments for the interaction of *Ec*TK wt with R5P, 1desR5P and Rib5P. Top: ITC-experiments: Titration of 15 mM R5P (left), 1desR5P (middle) or Rib5P (right) into 7.2 mg/ml *Ec*TK wt (100 µM active sites) in 1 mM ThDP, 5 mM $CaCl_2$, 50 mM glycylglycine (pH 7.6) at 8 °C. Binding curves were fitted according to one-site model with a restrained binding stoichiometry of 1 (Freyer and Lewis, 2008). **Bottom:** Polar interaction network between *Ec*TK and R5P (left, 1.74 Å), 1desR5P (middle, 1.02 Å) and Rib5P (right, 0.974 Å). Distances are indicated (in pm). Selected active site residues are labeled for the *Ec*TK-R5P-complex.

3.4.6.10. General Principles of Acceptor Binding in TK

The structure determination of non-covalent complexes between *h*TK and *Ec*TK with two native substrates and two substrate surrogates reveal common principles of acceptor substrate alignment. While the substrate phosphate moiety is generally well coordinated the remaining part of the molecule harbors more flexibility. This elevated flexibility is presumably a prerequisite to enable suitable orientations relative to the DHEThDP intermediate and facilitate carboligation in a transient complex. Contrary, a perfect prealignment of the reactants is not observed for any acceptor.

Structural results with R5P and 1desR5P in both TKs give no clear tendency for an active participation of TK in destabilization of furanose rings (Asztalos et al., 2007). This idea is further

supported by energetic consideration derived from ITC measurements of *Ec*TK with R5P and 1desR5P which revealed high K_D and thus small free binding enthalpies for both compounds.

Models for ring opening of R5P by acid/base catalyis could be proposed for both TKs. Remarkebly, the participating residues and water molecules for this process are not identical in both TKs. Furthermore, acceptor binding in *b*TK and *Ec*TK differed slightly or in significant details for all studied analogous complexes demonstrating that structural information for intermediates are not easily transferable from one to another enzyme-substrate complexe. This is an unexpected observation in consideration of the structural similarities of both TKs.

4. Summary & Conclusion

The ThDP-dependent enzyme transketolase (TK), which is almost ubiquitous found, excerts its activity in cellular carbon metabolism (e.g. pentose phosphate pathway, Calvin cycle). TK catalyze the reversible transfer reaction of a dihydroxyethyl-fragment from a donor ketose to an acceptor aldose and thereby stabilizes numerous non-covalent and covalent substrate-cofactor intermediates. Recent structural findings of trapped reaction intermediates in TK revealed that molecular strain within substrate-cofactor adducts and bound acceptor substrates plays a crucial role for the forward commitment of TK-catalyzed reaction, an enzymatic tool presumably generalizable to all enzymes requiring this coenzyme. This doctoral thesis presents a comprehensive structural analysis of central intermediates that are transiently formed along the reaction coordinate of *h*TK and *Ec*TK and correlates structural properties of intermediates with chemical reactivity. By combining high-resolution x-ray crystallography with kinetic and biophysical methods a detailed picture of the entire TK reaction cycle is illustrated.

C-terminal, hexa-histidine tagged *Ec*TK and *h*TK were expressed by high-density cell fermentation, purified to homogeneity and crystallized relying on established protocols. The kinetic analysis of microscopic reaction steps for *Ec*TK revealed that the ligation of donor substrates to the cofactor (for F6P, k_{obs} = 860 ± 230 s^{-1}) as well as the ligation of acceptors substrates to the DHEThDP intermediate (for R5P, k_{obs} = 531 ± 37 s^{-1}), both C-C bond forming steps, are very fast chemical reactions. The rate-limiting step of the TK over-all reaction is the liberation of product (for S7P, 42 s^{-1}) or the cleavage of the donor-ThDP intermediate, which both require cleavage of C-C bonds.

The structure of *h*TK could be solved from three new polymorphic crystal forms in monoclinic space group $P2_1$, which were all shown to be applicable for structural studies on TK mechanism.

Structures of *h*TK and *Ec*TK were determined to very high-resolution. This enabled the visualization of subtle, structural fluctuations of a conserved active-site glycine residue which potentially influence cofactor catalysis. In case of *Ec*TK we observed for all high-resolution structures that the cofactor samples conformations which are obviously needed at certain catalytic steps (ligation and cleavage of donors). This built-in cofactor dynamic is not dependent on the presence of substates or the activation state of the cofactor. Numerous high-resolution structures of *h*TK in ground state revealed geometrical distortions for the thiazolium moiety of ThDP and a weak electron density agglomeration of atom C2 which is suggestive for the accumulation of a considerable fraction C2 carbene. This proposal is further supported by the assignment of either IP or APH^+ form for the second cofactor ring system. Moreover, results from NMR-based H/D-solvent jump experiments with *Ec*TK provide evidence that

enzyme-bound ThDP, contrary to the currently accepted models (Hübner et al., 1998; Kern et al., 1997), is at least partially deprotonated at C2.

For the first time binding of donor substrate X5P to the docking site of both TK could be visualized by x-ray crystallography using a catalytically inactive cofactor analogue (N3ThDP) instead of native ThDP. Multiple non-covalent interactions with active site residues coordinate the donor and serve an orientation function to enable the subsequent ligation to the coenzyme. Analogous experiments with six- and seven-carbon donors or analogues thereof failed for both TKs, which most probably originate from a structural and conformational heterogeneity of those ligands and high dissociation constants. Structural evidence is mounted that TKs possess two phosphate binding sites to enable first substrate recognition and second substrate alignment for catalysis.

All native donor (X5P, F6P, S7P)-cofactor intermediates in complex with *b*TK could be determined to true atomic resolution. In line with previous spectroscopic studies (Nemeria et al., 2009) the protonation state of these intermediates could be unambiguously assigned as IP form. Moreover, all determined donor –or donor analogue-cofactor adducts possess a significant angular distortion (21–29°) of the C-C single bond connecting substrate and coenzyme confirming earlier findings for analogous structures (Asztalos et al., 2007). Angular distortions are also observable for both aromatic ring systems as well as for the bridging methylene group indicating that the entire intermediate is strained and high in energy. Thermodynamic experiments (ITC) and modeling approaches suggest that the carboligation reaction, a structural non-complementarity between an in-plane intermediate and the active site as well as intrinsic, electronic and physical properties of ThDP are presumably major contributors for the generation of the strained intermediates. Substrate binding and intra-molecular repulsion, at least between N4´ and O1α, can probably just be addressed to a minor extent for this process. TK selectively promotes C-C bond cleavage by pK_A adjustment of active site residues and elongation of the scissile covalent bonds. These specific bond stretchings could drastically accelerate bond cleavage by reducing the bond dissociation energy an unprecedent observation for an enzymatic reaction intermediate.

The adaption of TKs active site to bind the three donor substrates differing in chain length (C5-C7) is accomplished by a conserved pattern of polar interaction for the substrate derived hydroxyl groups and the phosphate moieties. All three structures are well superimposable for the protein part indicating that the active site is poised for catalysis.

The central branching point in enzymatical ThDP-catalysis is the post-cleavage intermediate. For the *Ec*TK-DHEThDP complex the formation, stability and ability to react with acceptor substrates were monitored and quantified by stopped-flow absorbance spectroscopy using an artificial donor. The DHEThDP intermediate is rapidly formed but just transiently stabilized on the enzyme (half life = 120 s) and reacts with acceptor R5P again rapidly (k_{obs} = 531 ± 37 s^{-1}). We further succeded to characterize this intermediate structurally in *b*TK to high resolution and for *Ec*TK to true-atomic

resolution (0.97 Å). The predominant form of this reactant state is a strained enolate (9.7 ° distortion of C2-C2α) which probably represents a storage form for the C2α carbanion. This finding demonstrates that, contrary to the general opinion, a planar, low-energy enamine doesn´t lie on pathway for TK. The post-cleavage intermediate in *Ec*TK mainly adopts the IP form but a minor fraction APH^+ form can´t be excluded.

Binding of acceptor substrates (E4P and R5P) and of substrate surrogates mimicking cyclic (1desR5P) and acyclic (Rib5P) conformation of R5P could be visualized in both studied TKs to high resolution. The structural data in combination with thermodynamic parameters derived from ITC measurements for *Ec*TK indicate that essential ring opening of acceptor R5P is mainly accomplished by enzyme-mediated Brønsted acid/base catalysis. Other promoting effects like furanose ring distortion or the specific accumulation of acyclic aldehyde form can´t be addressed unambiguously. For acceptor E4P an active participation in substrate dehydration is very likely in both TKs.

Notably, the *h*TK-X5P-ThDP (0.97 Å) and *h*TK-F6P-ThDP complex (0.98 Å) as well as *Ec*TK-DHEThDP complex (0.97 Å) are the yet best resolved structures of authentic covalent reaction intermediates found in the protein data bank.

Although ThDP is considered to be one of the best understood coenzymes results presented in this thesis and other recent reports (Frank et al., 2004; Kaplun et al., 2008; Meyer, 2012; Paramasivam et al., 2011) expand or even reverse our knowledge about this central bioorganic cofactor.

5. Appendix

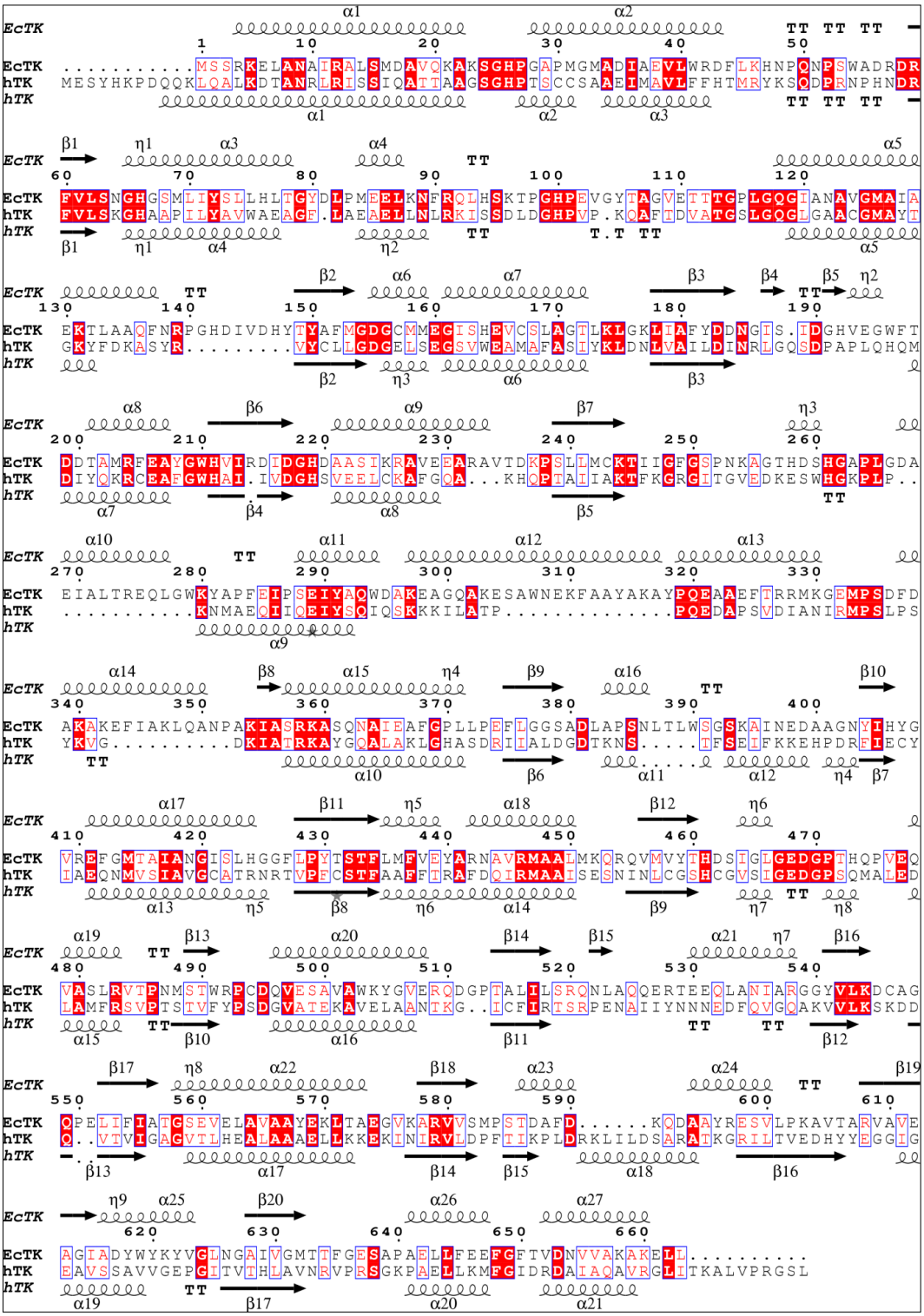

Fig.75: Amino acid sequence and secondary structure alignment of *h*TK versus *Ec*TK using programs ClustalW2 and ESPript 2.2. Numbering corresponds to the sequence of *Ec*TK. Identical residues are indicated by a red background, and conserved residues are indicated by red characters. The secondary structure elements of *Ec*TK are shown on top of the sequences, these of *h*TK at the bottom.

Tab. 7: X-ray statistics for the structures of human transketolase in ground state with native cofactor ThDP (*h*TK ground-state) and in ground state collected with high redundancy (*h*TK anomalous). X-ray statistics for the structures of *E.coli* transketolase in ground state with native cofactor ThDP (*Ec*TK ground state) and in complex with the cofactor analogue N3´-Pyridyl ThDP (*Ec*TK N3ThDP). X-ray statistics for the structure of the Michaelis complex between *E.coli* transketolase (reconstituted with N3´-Pyridyl ThDP) and X5P.

	***h*TK ground state**	***h*TK anomalous**	***Ec*TK ground state**	***Ec*TK N3ThDP**	***Ec*TK N3ThDP + X5P**
Data collection	SLS	home-source	SLS	SLS	Bessy 14.1
Wavelength (Å)	0.8	1.5418	0.8	0.8	0.91841s
Space group	$P2_1$	C2	$P2_12_12_1$	$P2_12_12_1$	$P2_12_12_1$
Cell dimensions					
a (Å)	73.26	114.15	90.08	90.29	87.96
b (Å)	86.3	86.04	101.93	101.92	99.85
c (Å)	92.8	73.17	133.13	133.43	130.13
α (°)	90	90	90	90	90
β (°)	94.01	125.72	90	90	90
γ (°)	90	90	90	90	90
Resolution range	46.286 -1.16 (1.22-1.16)	46.336-1.717 (1.82-1.717)	42.083- 1.048 (1.11-1.048)	47.479-0.97 (1.03-0.97)	19.464-1.400 (1.5-1.4)
No. of reflections	1105396 (152306)	994700 (147140)	2418028 (253594)	4381928 (428777)	890901 (161343)
No. of unique reflections	387546 (56632)	113059 (16980)	542807 (80170)	667216 (98472)	221025 (40690)
Completeness (%)	97.7 (96.2)	93.2 (89.7)	95.5 (87.2)	92.8 (79.1)	98.4 (97.8)
I/sigma(I)	12.9 (2.0)	22.9 (4.0)	12.8 (2.3)	16.8 (2.9)	20.0 (6.6)
R_{merge} (%)	3.8 (51.3)	6.9 (55.7)	6.7 (50.4)	5.7 (48.2)	5.2 (22.1)
Redundancy	2.8 (2.6)	8.2 (7.8)	4.5 (3.2)	6.1 (3.4)	4.0 (3.88)
B-factor from Wilson Plot (A^2)	11.25	17.38	7.88	8.74	6.95

	***b*TK ground state**	***b*TK anomalous**	***Ec*TK ground state**	***Ec*TK N3ThDP**	***Ec*TK N3ThDP + X5P**
Refinement	*PHENIX*	*PHENIX*	*SHELXL-11*	*SHELXL-11*	*PHENIX*
Resolution range (Å)	46.286 -1.16	46.336-1.717	42.083 - 1.048	47.479-0.97	19.464-1.400
Reflections (working/test)	387362/11623	112976/5651	3999087/10185	532156/8116	220973/11044
R_{work}/R_{free} (%)	13.89/16.41	15.76/19.55	9.17/12.11	9.63/12.82	12.34/16.68
Number of atoms					
Protein	10175	5300	12094	12166	10912
Ligands	210	39	250	177	146
Water	1372	600	1902	1807	1725
B-factor Protein	15.1	20.8	9.4	10.92	8.45
B-factor Ligands	18.8	17.8	16.5	15.2	12
B-factor Water	28.1	31.3	25.5	24.2	23.6
Deviations from ideals (r.m.s.d.)					
Bond distances (Å)	0.012	0.01	n.d.	n.d.	0.011
Bond angles (°)	1.5	1.1	n.d.	n.d.	1.45
Dihedrals (°)	14.11	13.08	n.d.	n.d.	13.67
Ramachandran plot					
favoured regions (%)	98	98	98	98	98
allowed regions (%)	2	2	2	2	2
outlier regions (%)	0	0	0	0	0

Tab. 8: X-ray statistics for the structures of human transketolase reconstituted with the ThDP analogue N3`-Pyridyl ThDP (*h*TK N3ThDP) and in non-covalent complex with donor substrates xylulose 5-phosphate (X5P), fructose 6-phosphate (F6P) and sedoheptulose 7-phosphate (S7P).

	***h*TK N3ThDP + X5P**	***h*TK N3ThDP + F6P**	***h*TK N3ThDP + S7P**	***h*TK N3ThDP**
Data collection	BESSY 14.1	BESSY 14.1	SLS	SLS
Wavelength (Å)	0.91841	0.91841	0.8	0.8
Space group	$P2_1$	$P2_1$	$P2_1$	$P2_1$
Cell dimensions				
a (Å)	73.53	73.47	109.56	73.43
b (Å)	77.92	77.76	78.3	78.01
c (Å)	112.19	112.36	146.92	111.51
α (°)	90	90	90	90
β (°)	92.335	92.246	94	92.889
γ (°)	90	90	90	90
Resolution range (Å)	29.09-1.15 (1.25-1.15)	19.64-1.2 (1.3-1.2)	49.054-1.37 (1.46-1.37)	48.88-1.3 (1.374-1.3)
No. of reflections	2510077 (542703)	1132327 (236722)	1464608 (267510)	1021734 (159630)
No. of unique reflections	446027 (98370)	391244 (83031)	502367 (89916)	306204 (46905)
Completeness (%)	99.7 (99.8)	99.5 (99.3)	96.8 (96.4)	99.4 (99.9)
I/sigma(I)	14.3 (2.9)	11.6 (2.3)	14.9 (2.7)	15.5 (3)
R_{merge} (%)	6.9 (63.4)	6.2 (54.0)	2.7 (50)	3.8 (52.6)
Redundancy	5.6 (5.5)	2.9 (2.9)	2.8 (2.9)	3.3 (3.4)
B-factor from Wilson Plot (A^2)	9.55	8.47	23.2	14.03

	***b*TK N3ThDP + X5P**	***b*TK N3ThDP + F6P**	***b*TK N3ThDP + S7P**	***b*TK N3ThDP**
Refinement	*PHENIX*	*PHENIX*	*PHENIX*	*PHENIX*
Resolution range (Å)	29.09-1.15	19.64-1.2	49.054-1.37	48.88-1.30
Reflections (working/test)	445966/22298	371680/19563	502339/17584	306147/9184
R_{work}/R_{free} (%)	11.65/14.00	12.09/14.52	13.48/16.3	13.17/15.74
Number of atoms				
Protein	11717	11597	19545	10288
Ligands	240	263	292	226
Water	1518	1426	2213	1506
B-factor Protein	13.9	12.5	26.7	18.6
B-factor Ligands	18.8	21.6	32.4	26.6
B-factor Water	27.7	26.2	39.1	34.4
Deviations from ideals (r.m.s.d.)				
Bond distances (Å)	0.011	0.009	0.01	0.02
Bond angles (°)	1.52	1.48	1.53	1.58
Dihedrals (°)	13.97	13.7	13.49	13.34
Ramachandran plot				
favoured regions (%)	98	98	97	98
allowed regions (%)	2	2	3	2
outlier regions (%)	0	0	0	0

Tab. 9: X-ray statistics for the structures of human transketolase (ThDP) in complex with fructose 6-phosphate analogues sorbitol 6-phosphate, 2,5-anhydro glucitol 6-phosphate or 2,5-anhydro mannitol 1-phosphate. X-ray statistics for the structures of *E. coli* transketolase $His^{473}Ala$ in non-covalent complex with acceptor substrate ribose 5-phosphate (*Ec*TK $His^{473}Ala$ R5P).

	***h*TK + 2,5-anhydro glucitol 6-phosphate**	***h*TK + 2,5-anhydro mannitol 1-phosphate**	***h*TK + S6P**	***Ec*TK $His^{473}Ala$ R5P**
Data collection	Bessy 14.1	Bessy 14.1	Bessy 14.1	in-house
Wavelength (Å)	0.91841	0.91841	0.91841	1.5418
Space group	C2	$P2_1$	$P2_1$	$P2_12_12_1$
Cell dimensions				
a (Å)	113.85	73.01	73.14	89.54
b (Å)	86.17	86.09	85.62	101.60
c (Å)	73.02	92.79	92.55	132.48
α (°)	90	90	90	90
β (°)	125.29	94.11	93.92	90
γ (°)	90	90	90	90
Resolution range (Å)	34.658-1-1.09 (1.21-1.09)	40.388-1.142 (1.24-1.142)	19.42-1.45 (1.55-1.45)	29.71-1.80 (1.90-1.80)
Completeness (%)	98.4 (98.2)	92.1 (91.7)	95.3 (95.2)	98.4 (92)
I/sigma(I)	12.78 (2.41)	6.52 (1.86)	16.03 (3.58)	17.8 (4.5)
R_{merge} (%)	5.8 (54.3)	8.0 (54.8)	4.4 (48.2)	8.6 (34.6)
Redundancy	2.5 (2.4)	2.2 (2.3)	4.1 (4.1)	5.7
B-factor from Wilson Plot (A^2)	8.21	12.8	13.3	17.8

	***h*TK + 2,5-anhydro glucitol 6-phosphate**	***h*TK + 2,5-anhydro mannitol 1-phosphate**	***h*TK + S6P**	***Ec*TK His^{473}Ala R5P**
Refinement	*PHENIX*	*PHENIX*	*PHENIX*	*REFMAC 5*
Resolution range (Å)	34.658-1-1.09	40.388-1.142	19.63-1.25	29.71-1.80
Reflections (working/test)	239713/7194	380120/18996	191318/9567	104893/5521
R_{work}/R_{free} (%)	12.01/14.26	19.16/22.75	15.83/20.05	14.2/18.1
Number of atoms				
Protein	5965	9498	10122	10706
Ligands	149	71	140	304
Water	723	1665	1075	1297
B-factor Protein	12.07	12.5	19.66	9.8
B-factor Ligands	17.74	9.32	20.21	18.2
B-factor Water	26.16	24.78	33.49	21.8
Deviations from ideals (r.m.s.d.)				
Bond distances (Å)	0.009	0.005	0.01	0.012
Bond angles (°)	1.43	1.08	1.33	1.32
Dihedrals (°)	15.73	11.92	13.92	13.23
Ramachandran plot				
favoured regions (%)	98	98	98	90
allowed regions (%)	2	2	2	10
outlier regions (%)	0	0	0	0

Tab. 10: X-ray statistics for the structures of human transketolase in covalent complex with fructose 6-phosphate (F6P), xylulose 5-phosphate (X5P), sedoheptoluse 7-phosphate (S7P), arabinose 5-phsphate (A5P) and 1-desoxy xylulose 5-phosphate (1desX5P).

	***h*TK + F6P**	***h*TK + X5P**	***h*TK + S7P**	***h*TK + A5P**	***h*TK + 1desX5P**
Data collection	ESRF 14.3	ESRF 14.3	Bessy 14.1	Bessy 14.1	ESRF 14.3
Wavelength (Å)	0.9393	0.9393	0.8551	0.8551	0.9393
Space group	C2	C2	C2	C2	C2
Cell dimensions					
a (Å)	113.76	113.67	113.68	113.7	113.65
b (Å)	85.88	85.98	86.1	85.9	85.94
c (Å)	72.99	73	73.02	73.03	73.06
α (°)	90	90	90	90	90
β (°)	125.31	125.3	125.43	125.23	125.373
γ (°)	90	90	90	90	90
Resolution range (Å)	34.62-0.98 (1.05-0.98)	41.98 – 0.97 (0.98-0.95)	18.53-1.03 (1.08-1.03)	27.598-0.99 (1.04-0.99)	46.34-1.077 (1.177-1.077)
No. of reflections	1357139 (171680)	4849631 (232887)	839674 (99526)	1386139 (173740)	804464 (104234)
No. of unique reflections	300587 (47462)	678851 (87567)	279021 (36822)	307287 (47398)	238263 (50289)
Completeness (%)	91.8 (77.8)	98.2 (92.0)	98.9 (98.6)	96.5 (84.2)	96.5(87.3)
I/sigma(I)	16.1 (2.93)	12.50 (2.2)	15.48 (2.35)	16.53 (2.67)	12.4 (2.0)
R_{merge} (%)	5.1 (50.3)	8.6 (46.5)	5.3 (53.4)	7.8 (47.3)	6.2 (45.3)
Redundancy	4.5 (3.6)	7.1 (2.7)	3 (2.7)	4.5 (3.7)	3.4 (2.1)
B-factor from Wilson Plot (A^2)	6.67	6.75	6.97	5.96	7.63

	***b*TK + F6P**	***b*TK + X5P**	***b*TK + S7P**	***b*TK + A5P**	***b*TK + 1desX5P**
Refinement	*SHELXL-11*	*SHELXL-11*	*PHENIX*	*PHENIX*	*PHENIX*
Resolution range	34.62-0.98	41.98 – 0.95	18.531-1.03	27.598-0.990	46.34 - 1.077
Reflections (working/test)	244494/2471	258570/13625	278825/13945	305910 /15297	238076/11900
R_{work}/R_{free} (%)	8.34/10.47	8.24/10.14	11.90/13.99	12.95/14.68	12.40/14.47
Number of atoms					
Protein	5967	5921	5885	5888	5963
Ligands	104	104	114	114	138
Water	835	717	687	704	640
B-factor Protein	10.93	10.82	12.62	10.28	12.79
B-factor Ligands	12.2	12.96	13.08	12.28	14.71
B-factor Water	23.7	21.23	23.26	22.2	24.83
Deviations from ideals (r.m.s.d.)					
Bond distances (Å)	n.d.	n.d.	0.012	0.016	0.01
Bond angles (°)	n.d.	n.d.	1.517	1.92	1.64
Dihedrals (°)	n.d.	n.d.	13.32	14.75	13.94
Ramachandran plot					
favoured regions (%)	98	98	98	98	98
allowed regions (%)	2	2	2	2	2
outlier regions (%)	0	0	0	0	0

Tab. 11: X-ray statistics for the structures of human and *E. coli* transketolase in covalent complex with the 1,2-dihydroxyethyl-ThDP intermediate (DHEThDP), human transketolase reconstituted with ThDP analogue 1,2-dihydroxyethyl-3-deaza-ThDP (3deazaThDP). X-ray statistics for the structures of *E. coli* transketolase in non-covalent complex with ribitol 5-phosphate (*Ec*TK Rib5P) and 1desoxy ribose 5-phosphate (*Ec*TK 1desR5P).

	***Ec*TK DHEThDP**	***h*TK DHEThDP**	***h*TK 3deazaThDP**	***Ec*TK Rib5P**	***Ec*TK 1desR5P**
Data collection	ESRF 14.3	Bessy 14.1	Bessy 14.1	SLS	Bessy 14.1
Wavelength (Å)	0.9393	0.91841	0.91841	0.8	0.91841
Space group	$P2_12_12_1$	$P2_1$	$P2_1$	$P2_12_12_1$	$P2_12_12_1$
Cell dimensions					
a (Å)	90.04	73.18	73.15	90.08	90.06
b (Å)	101.9	85.59	86.05	101.86	101.74
c (Å)	133.1	92.63	92.73	133.18	133.01
α (°)	90	90	90	90	90
β (°)	90	94.075	94.116	90	90
γ (°)	90	90	90	90	90
Resolution range (Å)	41.98 – 0.97 (1.03-0.97)	19.415-1.45 (1.55-1.45)	46.571-1.259 (1.29- 1.259)	42.065 -0.974 (1.03-0.974)	44.293-1.028 (1.05-1.028)
No. of reflections	2546586 (322234)	829963 (150203)	966994 (69532)	2902735 (399231)	665046 (23309)
No. of unique reflections	693120 (113923)	197062 (35329)	307778 (22660)	673433 (103048)	427230 (20079)
Completeness (%)	97.5 (92.5)	97.9 (97.2)	99.6 (99.7)	95.3 (89.3)	71.2/45.6
I/sigma(I)	10.3 (2.2)	10.6 (3.1)	13.1 (2.0)	12.57/2.77	10.84/1.12
R_{merge} (%)	7 (49.8)	6.2 (51.8)	6.6 (69.2)	5.6/52.2	4.2/55.4
Redundancy	3.7 (2.8)	4.2 (4.2)	3.1 (3.1)	4.1/3.5	1.1/0.5
B-factor from Wilson Plot (A^2)	6.75	12.85	8.37	7.51	6.77

	***Ec*TK DHEThDP**	***b*TK DHEThDP**	***b*TK 3deaza**	***Ec*TK Rib5P**	***Ec*TK 1desR5P**
Refinement	*SHELXL-11*	*PHENIX*	*PHENIX*	*PHENIX*	*PHENIX*
Resolution range	41.98 – 0.97	19.415-1.45	46.571-1.26	42.065 - 0.974	44.293 - 1.028
Reflections (working/test)	547268 /11188	196865/9845	307520/15372	673401/10103	529482 /26472
R_{work}/R_{free} (%)	9.02/11.31	15.45/19.60	14.48/17.77	9.56/11.14	11.79/13.95
Number of atoms					
Protein	12021	9936	10107	12178	12067
Ligands	197	174	220	261	116
Water	1864	1033	1423	1883	1719
B-factor Protein	8.56	18.88	12.31	9.09	9
B-factor Ligands	13.9	21.82	14	14.4	14.3
B-factor Water	21.84	31.19	26.59	23.6	23.4
Deviations from ideals (r.m.s.d.)					
Bond distances (Å)	n.d.	0.01	0.013	0.014	0.011
Bond angles (°)	n.d.	1.38	1.55	1.73	1.53
Dihedrals (°)	n.d.	13.45	13.28	14.88	14.13
Ramachandran plot					
favoured regions (%)	99	98	98	98	98
allowed regions (%)	1	2	2	2	2
outlier regions (%)	0	0	0	0	0

Tab. 12: X-ray statistics for the structures of human transketolase (ThDP) and in non-covalent complex acceptor substrates erythrose 4-phosphate (E4P), ribose 5-phosphate (R5P), and acceptor analogues ribitol 5-phosphate (Rib5P) and 1–desoxy-ribose 5-phosphate (1desR5P).

	***h*TK + E4P**	***h*TK + R5P**	***h*TK + 1desR5P**	***h*TK + Rib5P**
Data collection	Bessy 14.1	Bessy 14.1	Bessy 14.1	Bessy 14.1
Wavelength (Å)	0.91841	0.91841	0.91841	0.91841
Space group	C2	C2	C2	C2
Cell dimensions				
a (Å)	114.03	113.7	113.82	113.91
b (Å)	85.49	85.53	85.75	85.83
c (Å)	73.06	72.93	73.13	73.11
α (°)	90	90	90	90
β (°)	125.71	125.72	125.29	125.34
γ (°)	90	90	90	90
Resolution range (Å)	34.64-1.170 (1.25-1.17)	29.086-1.2 (1.25-1.20)	46.453-1.15 (1.25-1.15)	34.648-1.18 (1.25-1.18)
No. of reflections	473922 (87810)	902756 (101329)	745005 (99312)	585711 (96930)
No. of unique reflections	185594 (34547)	168156 (18795)	194760 (39540)	180701 (29810)
Completeness (%)	96.9 (95.5)	95.1 (92.6)	95.9 (88.3)	96 (94.2)
I/sigma(I)	16.75 (2.1)	26.22 (3.37)	11.93 (2.04)	15.02 (2.6)
R_{merge} (%)	3.9 (49.4)	4.1 (54.6)	6.1 (51.5)	5.1 (51.4)
Redundancy	2.5 (2.4)	5.1 (5.0)	3.7 (2.2)	3.1 (3.1)
B-factor from Wilson Plot (A^2)	10.19	10.01	9.96	9.33

	***b*TK + E4P**	***b*TK + R5P**	***b*TK + 1desR5P**	***b*TK + Rib5P**
Refinement	*PHENIX*	*PHENIX*	*PHENIX*	*PHENIX*
Resolution range	34.64-1.170	29.086-1.2	46.453-1.15	34.648-1.18
Reflections (working/test)	185548/9277	168133/3364	194669/9736	180690/7229
R_{work}/R_{free} (%)	13.08/15.79	12.28/14.59	12.25/14.47	12.42/14.58
Number of atoms				
Protein	5956	5244	5876	5889
Ligands	104	59	93	105
Water	533	505	581	663
B-factor Protein	16.29	17.17	14.6	14.84
B-factor Ligands	18.47	17.61	18.2	18.26
B-factor Water	28	25.49	26.96	27.98
Deviations from ideals (r.m.s.d.)				
Bond distances (Å)	0.009	0.009	0.009	0.009
Bond angles (°)	1.398	1.502	1.427	1.382
Dihedrals (°)	13.98	13.41	13.67	13.47
Ramachandran plot				
favoured regions (%)	98	98	98	98
allowed regions (%)	2	2	2	2
outlier regions (%)	0	0	0	0

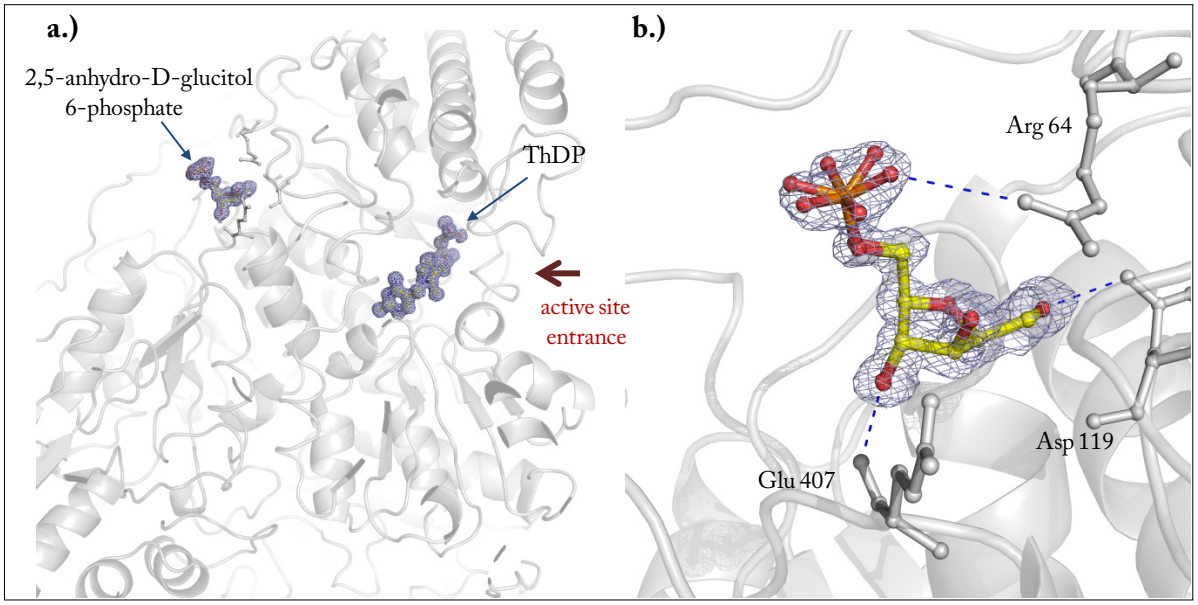

Fig. 76: Binding of 2,5-anhydro-D-glucitol 6-phosphate to a surface pocket of *b*TK. a.) Top-view on the transketolase dimer (cartoon representation, grey) with bound cofactor ThDP and the substrate analogue 2,5-anhydro-D-glucitol 6-phosphate (70 % occupancy). The analogue of donor substrate F6P is not specificly bound in or above the active site but in a solvent exposed pocket. **b.)** Closer view on the binding site of 2,5-anhydro-D-glucitol 6-phosphate. Polar interactions are indicated by blue dashed lines. The contour level of the 2mFo-DFc map is 1σ. Selected amino acid side chains are labeled. Although some ThDP-dependent enzymes are known to be allosterically regulated by their substrates (Kutter et al., 2009) binding of the substrate analogue 2,5-anhydro-D-glucitol 6-phosphate neither induces structural rearrangements of the protein nor influences the activity and seems to be an artificial event. Notably, a similar, unspecific substrate binding is reported for the ThDP-dependent enzyme *Lp*POX (Meyer, 2009; Wille et al., 2006).

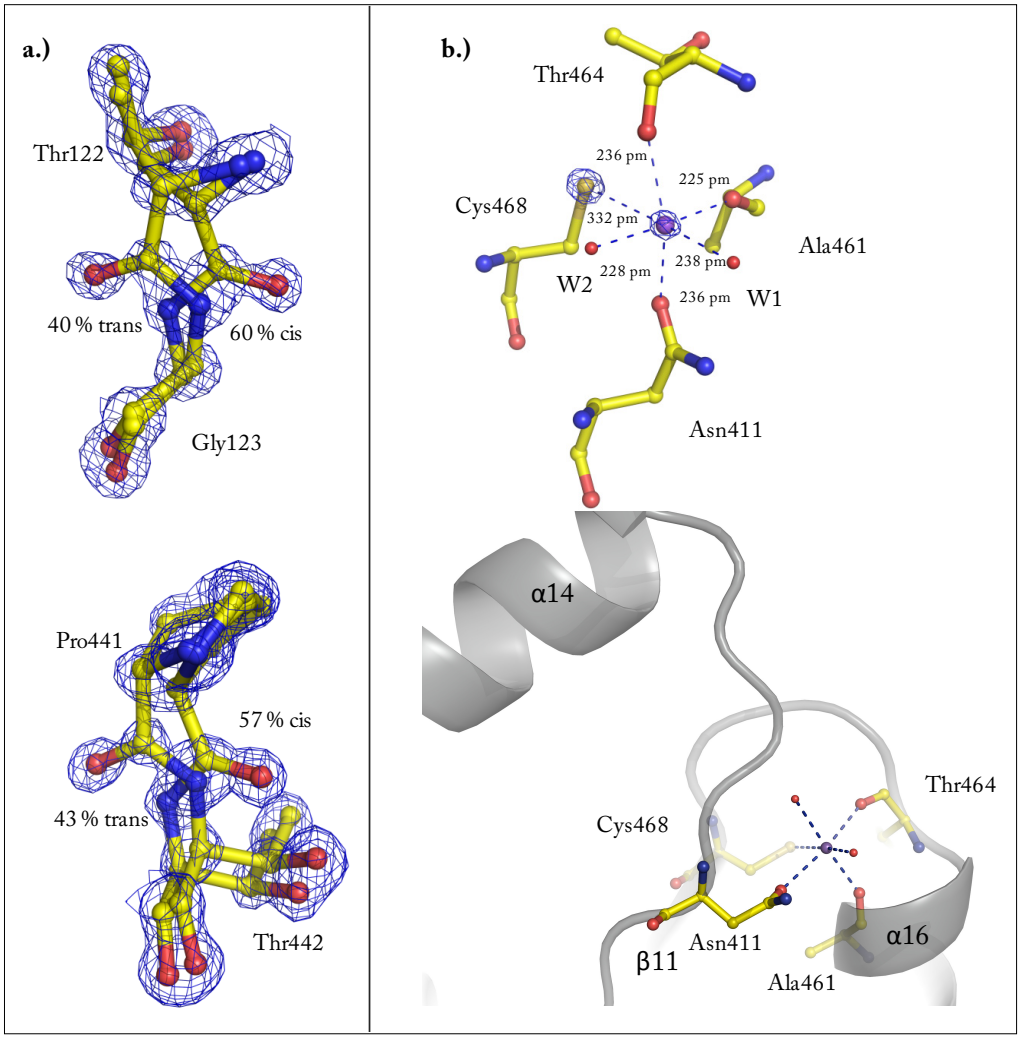

Fig. 77: Detailed view of Thr122–Gly123 and Pro441–Thr442 and bound sodium ion in *b*TK. The structure of *b*TK determined to a resolution of 1.09 Å was used for the preparation of the figures. Cis/trans peptide bonds connecting Thr122 and Gly123 in **a.)** as well as Pro441 and Thr442 in **b.)**. The fraction of cis- and trans configuration is indicated. Figures are shown in ball and stick representation surrounded by a 2mFo-DFc map contoured at a sigma level of 1.7. **c.) Top:** Structural sodium ion (purple sphere) is coordinated octahedrally (6 ligands) by four protein side chains and two water molecules W1 and W2 (red spheres). Interatomic distances between the ion and the coordinating atoms are indicated. An analysis of the coordination sphere (Hsin et al., 2008) revealed that cysteine is rarely found to be a coordinating residue of sodium ions and that all bonding interactions for sodium coordination sphere are within known boundaries. At a high contour level (11σ) of the 2mFo-DFc electron map the sulfur atom of Cys468, the modeled metal ion but no oxygen ligand is surrounded by the electron density map demonstrating that the metal ion has more electrons than oxygen. **Bottom:** The sodium ion probably aids to stabilize two adjacent loops in the PYR domain. Nomenclature of α-helixes and β-sheets according to Fig.75.

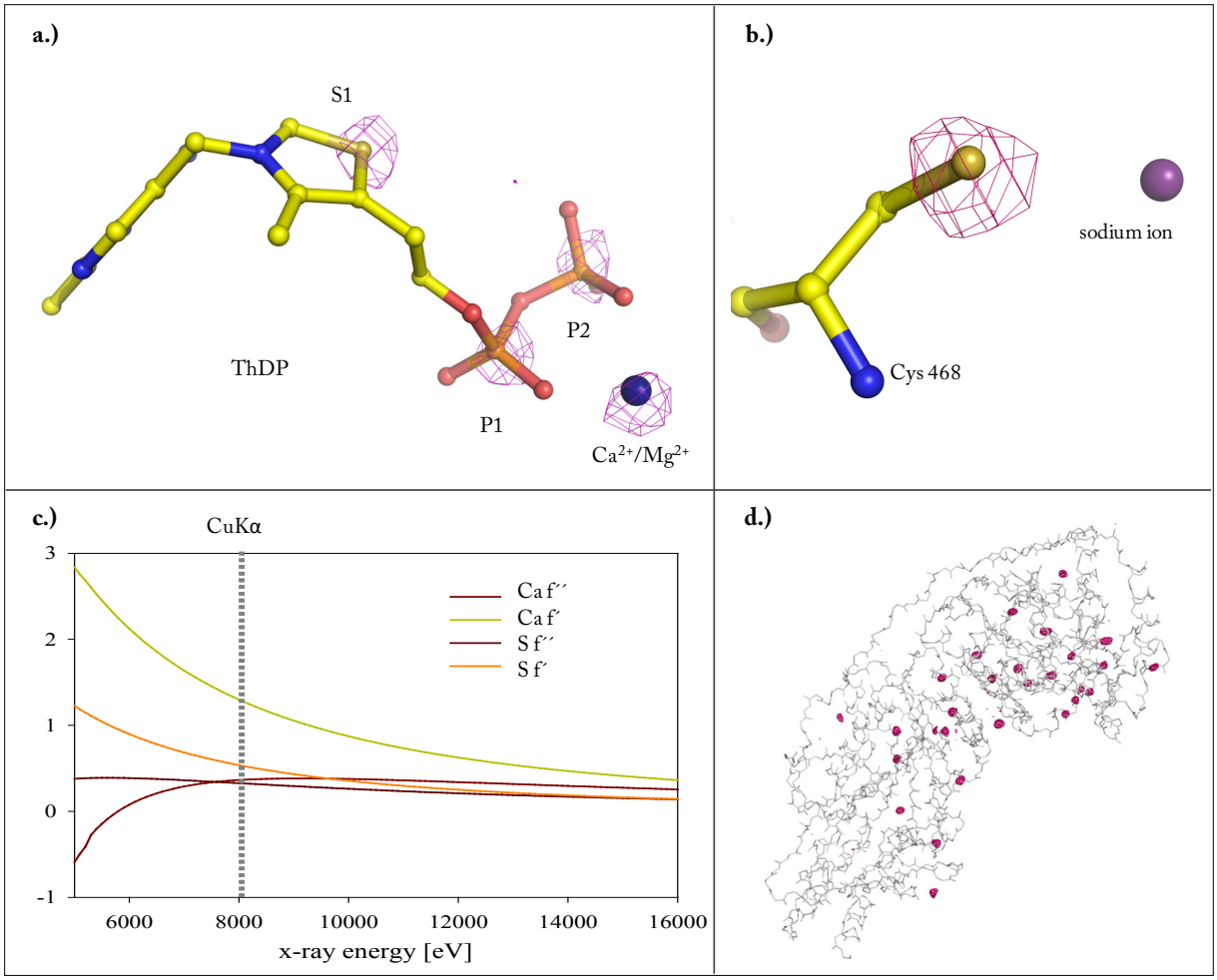

Fig. 78: Identification of bound ions in *h*TK by anomalous data. X-ray structure of *h*TK determined relying on data collected in-house with CuKα radiation and high redundancy and refined to a resolution of 1.717 Å (R_{work} = 15.76, R_{free} = 19.55). The anomalous differences have been phased with the final refined model and the calculated map (magenta) is contoured at 4σ. **a.)** Bound cofactor ThDP (ball and stick representation) with strong difference anomalous density for S1, P1 and P2 atoms and the bivalent cation (blue sphere) a mixture of Mg^{2+} and Ca^{2+}. **b.)** Sodium ion bound in close proximity to Cys 468. Please note that there is no anomalous density observable at the position of the modeled sodium ion excluding the presence of small amounts of potassium. **c.)** Calculated anomalous scattering coefficients for calcium and sulfur (http://skuld .bmsc.washington. edu/scatter/AS_form.html.). The x-ray energy for CuKα radiation is marked with a dashed line. At this wavelength calcium possesses stronger x-ray absorption than sulfur. f´ = dispersive term of the atomic scattering factor, f´´ = anomalous term of the atomic scattering factor **d.)** Monomer of *h*TK (line representation) and all anomalous scatterers (magenta spheres).

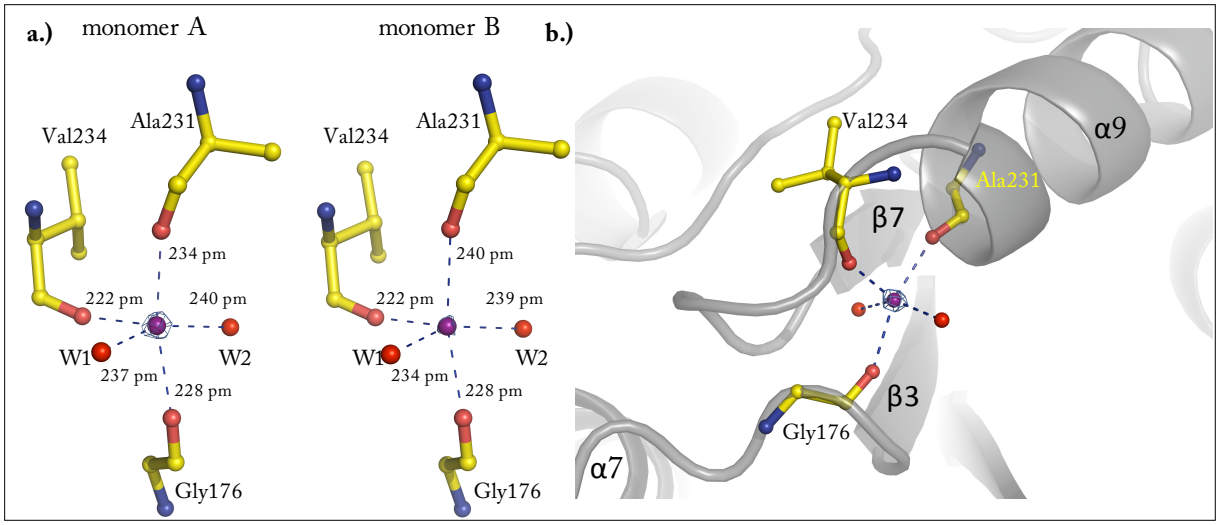

Fig. 79: Structural sodium ion in *Ec*TK. The structure of *Ec*TK determined to a resolution of 1.048 Å was used for the preparation of the figures. a.) Coordination sphere of the sodium ion. Na^+ (purple sphere) is coordinated trigonal bipyramidal (5 ligands) by three protein backbone oxygens and two water molecules W1 and W2 (red spheres). Interatomic distances between the ion and the coordinating atoms are indicated. At a high contour level (10σ) of the 2mFo-DFc electron map just the modeled metal ion but no oxygen ligand is surrounded by the electron density map demonstrating that the metal ion has more electrons than oxygen. Furthermore, the electron density map for the bound ion in monomer A is stronger than in monomer B indicating different occupancies of the structural ion in the dimer. b.) Structural function of the sodium ion. The complexed Na^+ ion presumably functions in stabilizing two adjacent loops in the AP domain. Nomenclature of α-helixes and β-sheets according to Fig.75.

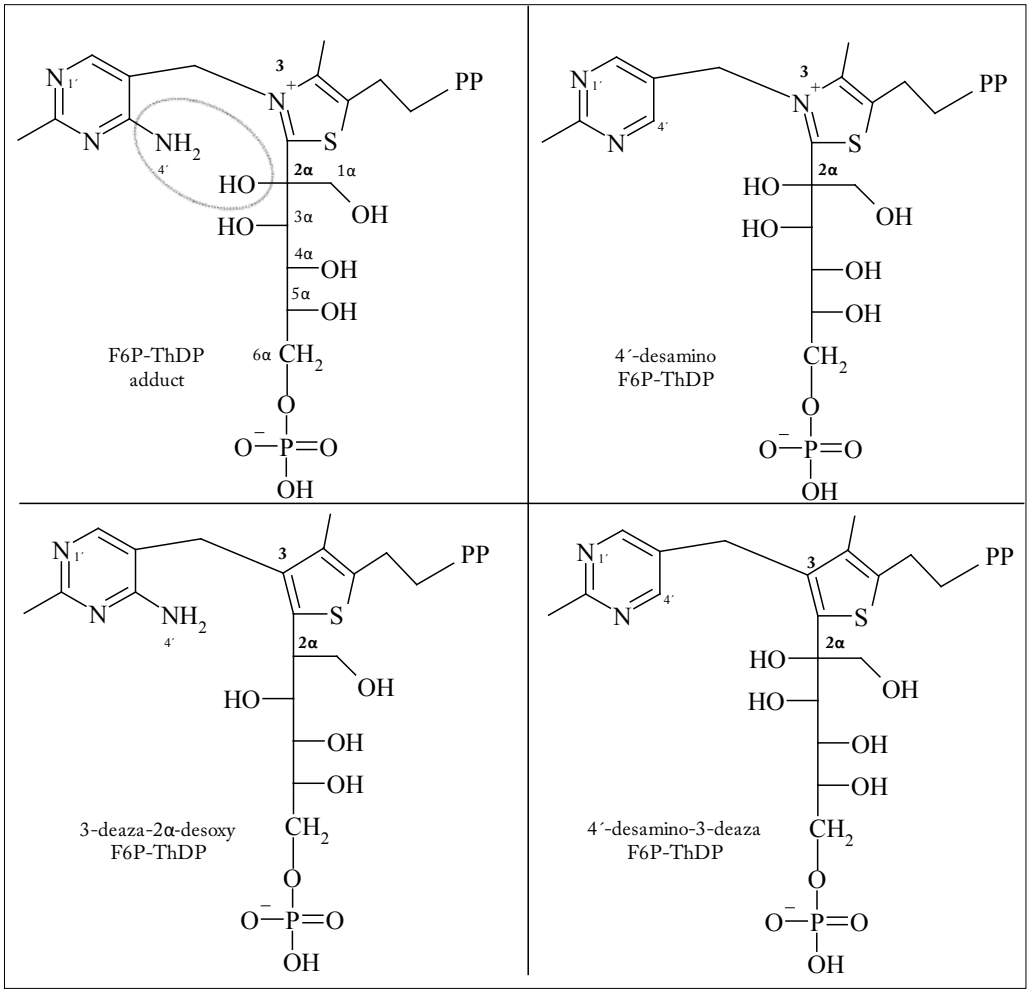

Fig. 80: Structural proposals for further TK-analogue complexes. Chemical structures of the F6P-ThDP adduct (top left) and proposed derivatives for further x-ray crystallographic studies addressing the importance of intra-molecular repulsion between N4´ and O2α (indicated by an ellipsoid) for angular strain in substrate-cofactor intermediates. Selected atoms are labeled. PP = diphosphate moiety.

Tab. 13: Selected bond length (Å) for the covalent donor-intermediate structures in *b*TK. Selected bond length for X5P-(0.97 Å) and F6P-(0.98 Å)-ThDP intermediates in *b*TK and DHEThDP intermediate (0.97 Å) in *Ec*TK. The nomenclature of the F6P- and DHEThDP intermediates is exemplarily illustrated below the table. Estimates of standard deviation (esd) for bond lengths were calculated with pre-release version of *SHELX-11* that was kindly provided by Prof. George Sheldrick.

Thiamine diphosphate * 4,5 H_2O (Pletcher *et al.*, ActaCryst, 1979)		X5P-ThDP intermediate (chapter)			F6P-ThDP intermediate (chapter)			DHEThDP intermediate (chapter)		
	bond length (pm)		bond length (pm)	esd (pm)		bond length (pm)	esd (pm)		bond length (pm)	esd (pm)
C2´-C2´M	148.5	C2´-C2´M	147.2	1.0	C2´-C2´M	147.7	1.2	C2´-C2´M	150.1	4.6
C2´-N3´	130.9	C2´-N3´	132.9	0.8	C2´-N3´	131.8	1.0	C2´-N3´	130.0	3.9
N3´-C4´	136.6	N3´-C4´	137.7	0.9	N3´-C4´	137.9	1.0	N3´-C4´	135.3	2.9
C4´-N4´	131.3	C4´-N4´	132.7	0.9	C4´-N4´	131.0	1.0	C4´-N4´	134.4	2.4
C4´-C5´	143.9	C4´-C5´	143.1	1.0	C4´-C5´	144.6	1.2	C4´-C5´	144.8	2.6
C5´-C6´	134.6	C5´-C6´	137.4	1.0	C5´-C6´	135.3	1.1	C5´-C6´	136.5	2.1
C6´-N1´	135.2	C6´-N1´	138.0	0.9	C6´-N1´	137.2	1.0	C6´-N1´	139.3	2.7
C2´-N1´	135.4	C2´-N1´	135.1	0.9	C2´-N1´	135.8	1.0	C2´-N1´	133.3	3.8
C5´-C7´	149.8	C5´-C7´	152.1	1.0	C5´-C7´	152.1	1.2	C5´-C7´	151.9	2.2
C7´-N3	149.5	C7´-N3	146.9	0.9	C7´-N3	147.6	1.2	C7´-N3	153.5	1.6
N3-C4	139.4	N3-C4	141.5	0.9	N3-C4	139.0	1.0	N3-C4	139.7	2.1
C4-C5	135.9	C4-C5	136.7	0.9	C4-C5	139.4	1.1	C4-C5	137.7	3.2
C5-S1	172.9	C5-S1	173.7	0.6	C5-S1	173.3	0.8	C5-S1	174.3	1.9
S1-C2	166.9	S1-C2	173.8	0.8	S1-C2	173.7	0.9	S1-C2	184.7	2.0
C2-N3	132.1	C2-N3	138.4	0.9	C2-N3	136.5	1.2	C2-N3	131.7	1.9
		C2-C2α	152.3	1.2	C2-C2α	160.4	1.5	C2-C2α	140.9	2.7
		C2α-O2α	135.6	1.1	C2α-O2α	141.6	1.4	C2α-O2α	122.9	2.2
		C2α-C1α	152.4	1.3	C2α-C1α	156.2	1.8	C2α-C1α	152.5	2.8
		C1α-O1α	143.7	1.2	C1α-O1α	144.5	1.4	C1α-O1α	148.3	2.4
		C2α-C3α	162.5	1.5	C2α-C3α	155.2	1.7			
		C3α-O3α	141.4	1.4	C3α-O3α	139.0	1.6			
		C3α-C4α	148.0	1.6	C3α-C4α	151.8	1.8			
		C4α-O4α	147.1	1.2	C4α-O4α	144.0	1.4			
		C4α-C5α	155.1	1.6	C4α-C5α	155.0	1.8			
					C5α-O5α	144.2	0.9			
					C5α-C6α	149.2	1.1			

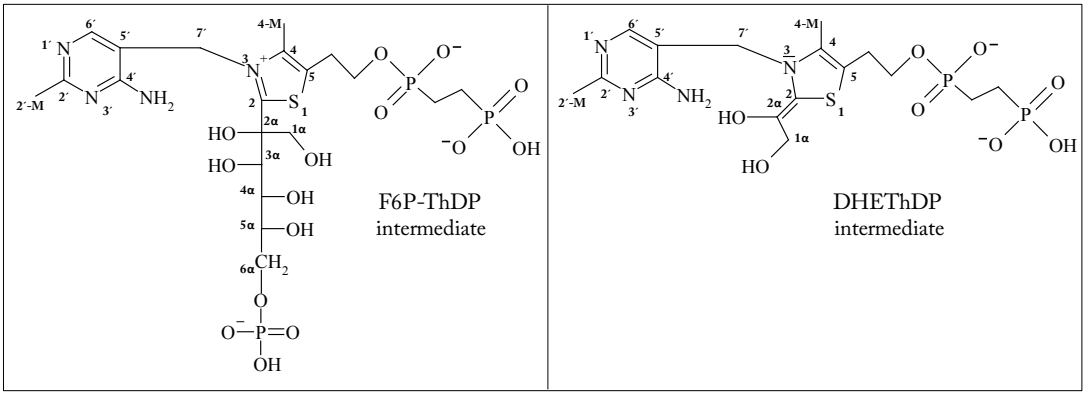

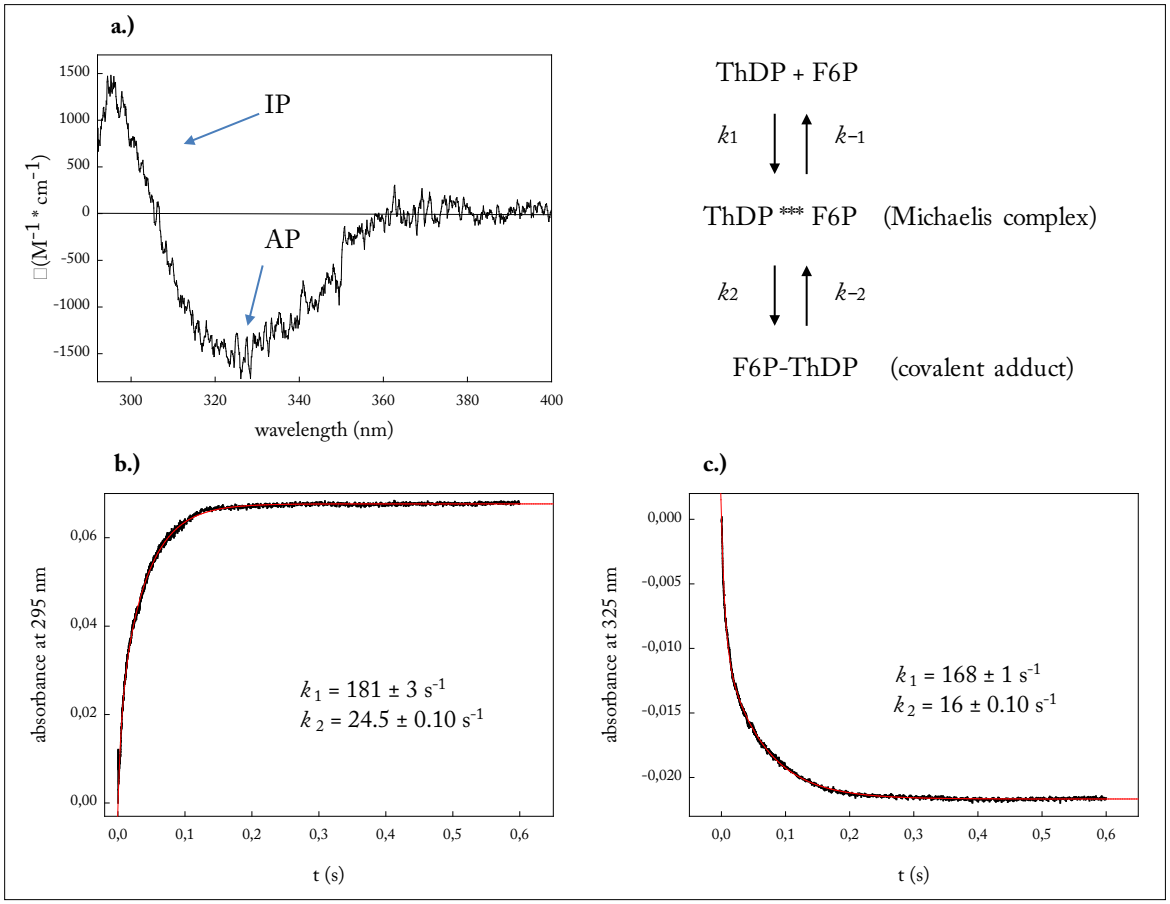

Fig. 81: Kinetic analysis of F6P-ThDP intermediate formation using UV-Vis-spectroscopy. a.) UV-Vis absorbance difference spectrum for the reaction of 2 mg/ml (27.8 µM active sites) *Ec*TK wt, 300 µM ThDP, 2.5 mM $CaCl_2$, 50 mM glycylglycine (pH 7.6) and 4.5 mM F6P to visualize spectral signature of intermediates. Spectrum was obtained after correction for buffer, substrate and *Ec*TK. Putative tautomerization states of cofactor six-membered ring (IP, AP) are indicated. Right side: Kinetic scheme for the experiment. **b.) and c.)** Stopped-flow absorbance transient (10 mm pathlength, detection at 295 nm **b.)** or 325 nm **c.)**) for the reaction of 2 mg/ml (27.8 µM active sites) *Ec*TK wt, 300 µM ThDP, 2.5 mM $CaCl_2$, 50 mM glycylglycine (pH 7.6) with 500µM F6P at 25 °C. Fitting of the transient according to a double exponential equation (red, $A = A1 * e^{-k1*t} + A2 * e^{-k2*t}$) gave the shown rate constants k_1 and k_2.

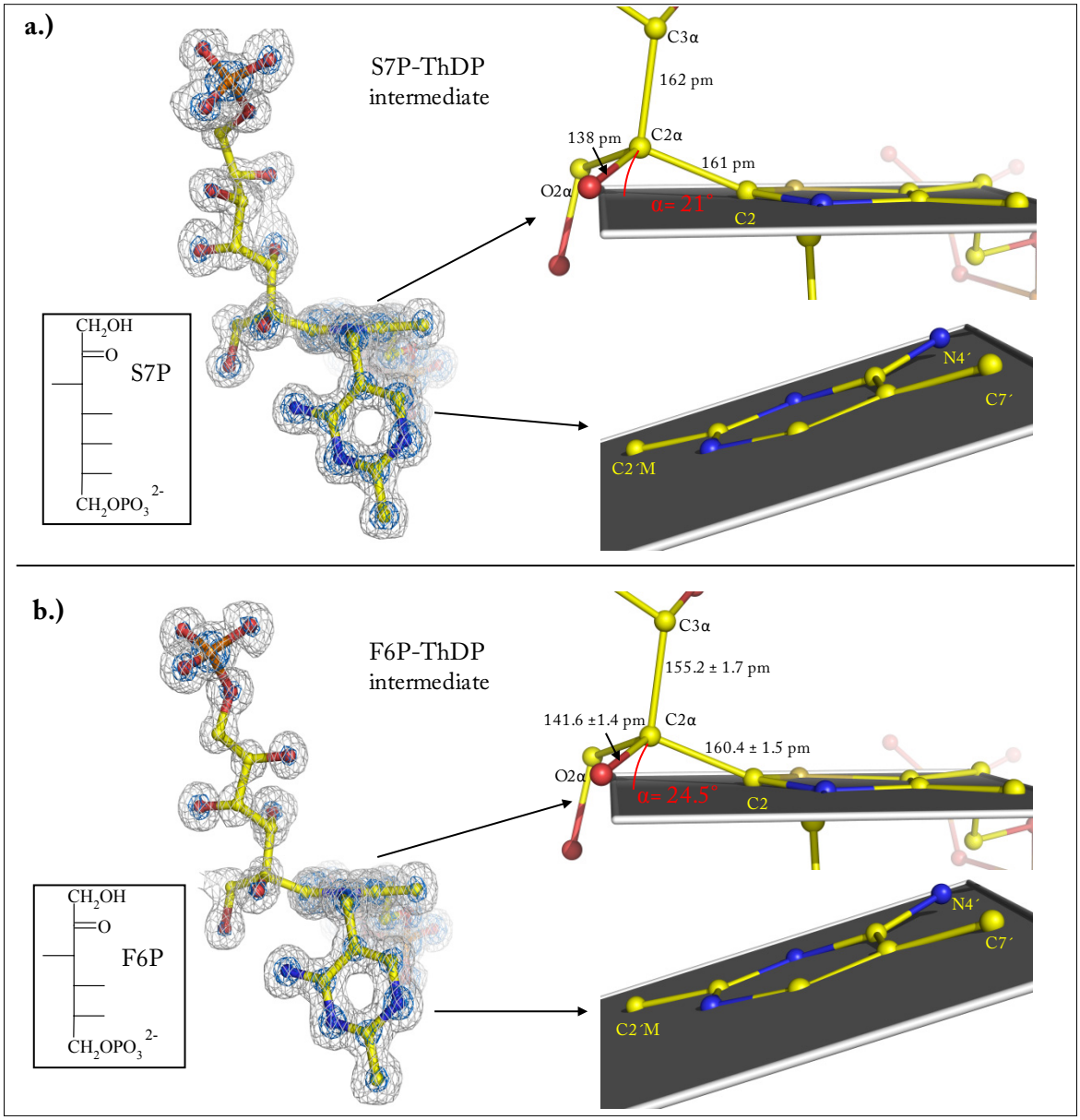

Fig. 82: X-ray structures of covalent S7P-ThDP (1.03 Å, a.)) and F6P-ThDP (0.98 Å, b.)) intermediates trapped in the active site of *b*TK. Intermediate models are shown in stick and ball representation. For reasons of clarity all active site chains are omitted. **Left side:** Donor-intermediates surrounded by a 2mFo-DFc map electron density map contoured at 1σ (gray) and 4σ (blue). **Boxed:** Chemical structure of donors S7P and F6P in Fischer projection. **Right side:** Detailed view on the thiazol (top right) and aminopyrimidine moieties (bottom right) of each intermediate. Planes were generated (fixed points: S1, N3 and C5, top; N1´, N3´ and C5´ bottom) to visualize deviations from planarity. The angular distortion α (C2-C2α bond, red) as well as selected atoms and bond length are indicated. For the F6P-ThDP intermediate estimations of standard deviations for bond length are indicated.

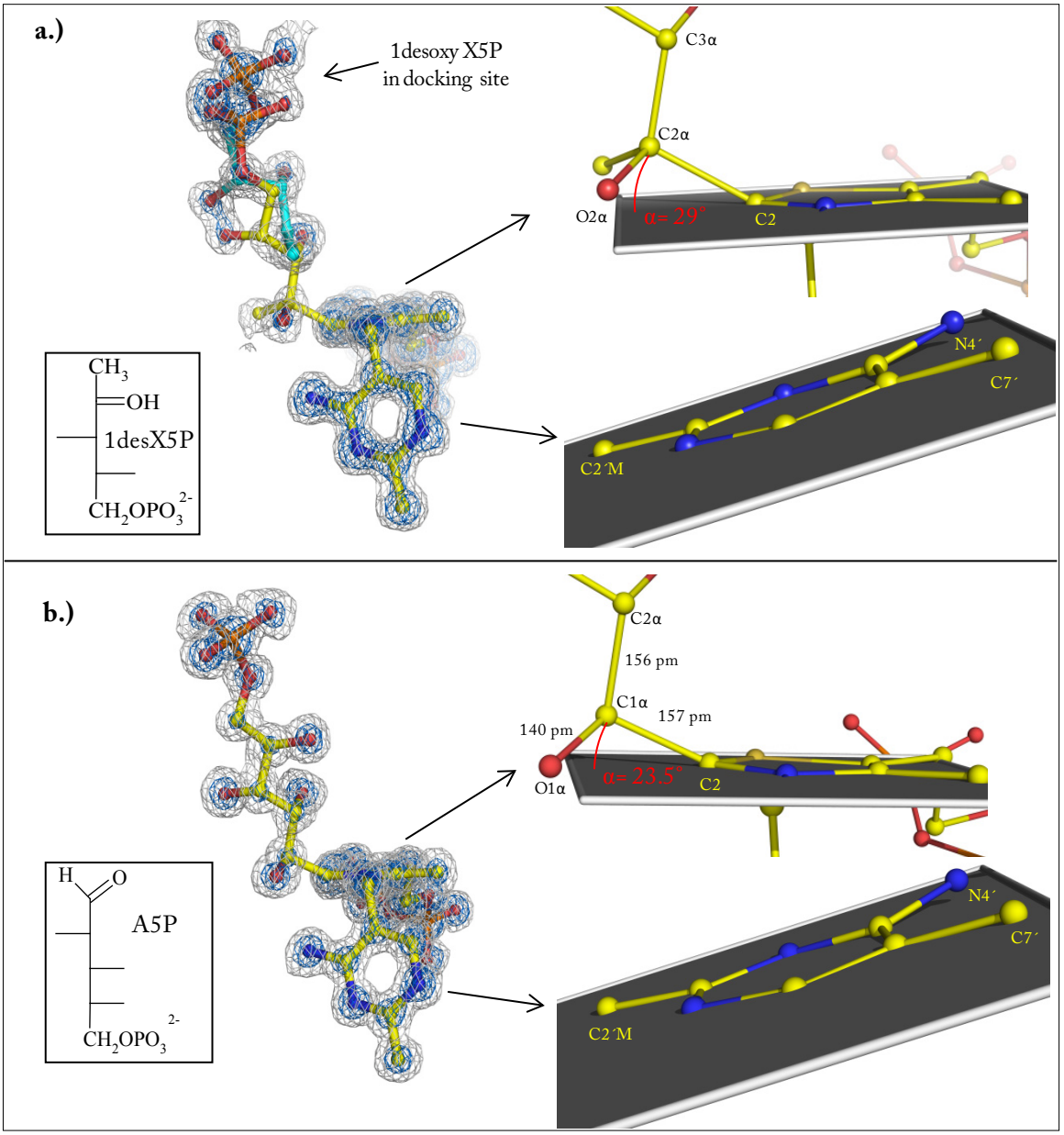

Fig. 83: X-ray structures of covalent 1desX5P-ThDP (1.07 Å, a.)) and A5P-ThDP (0.99 Å, b.)) intermediates trapped in the active site of *b*TK. Left side: Donor-analogue-intermediates surrounded by a 2mFo-DFc map electron density map contoured at 1σ (gray) and 3σ (blue). **Boxed:** Chemical structures of 1desX5P or A5P. **Right side:** Detailed view on the thiazol (top right) and aminopyrimidine moieties (bottom right) of each intermediate. Planes were generated (fixed points: S1, N3 and C5, top; N1´, N3´ and C5´ bottom) to visualize deviations from planarity.The angular distortion α (C2-C2α bond, red) as well as selected atoms and bond length are indicated. Intermediate models are shown in stick and ball representation. For reasons of clarity all active site chains are omitted. 1desX5P that is located in the docking site position is shown in cyan. The nomenclature of the A5P-derived part of the intermediate is different in comparison to the all other donor-THDP intermediates since A5P harbors an aldehyde- instead of a keto-functionality. A refinement of the occupancy revealed that the A5P-ThDP adduct (selected bond lengths in table) accumulated to almost full occupancy whereas the 1desX5P-ThDP adduct was just populated in approx. 50 % of the active sites. The remaining 50 % of bound 1desX5P were located in the docking site that is identical with the docking site of the native donor substrate X5P.

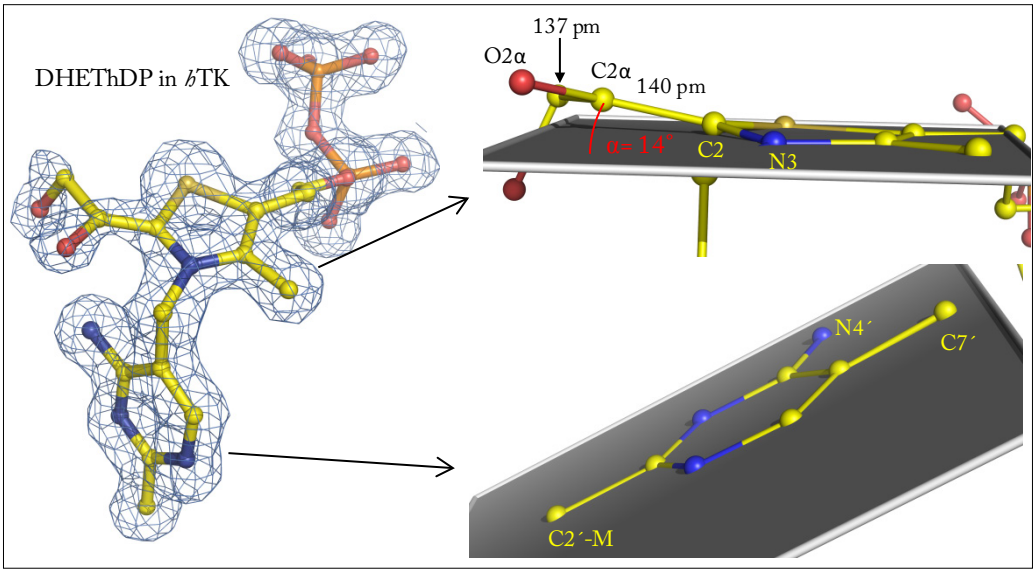

Fig. 84: Detailed view on DHEThDP intermediate in *b*TK. Ball and stick representation of the DHEThDP intermediate in *b*TK (1.45 Å, R_{work} = 15.45, R_{free} = 19.60). On the left side the DHEThDP intermediate is shown surrounded by a 2mFo-DFc map contoured at 1σ (blue). Thiazolium moiety (top right) and aminopyrimidine moiety (bottom right) are shown with auxillary planes (fixed points: S1, N3 and C5, top; N1´, N3´ and C5´ bottom) to illustrate deviations from planarity. The angular distortion (α) of the carbon bond connecting sugar and cofactor moiety is indicated in red. The C2-C2α bond has strong double bound character (140 pm). Selected atoms and distances (in pm) are labeled.

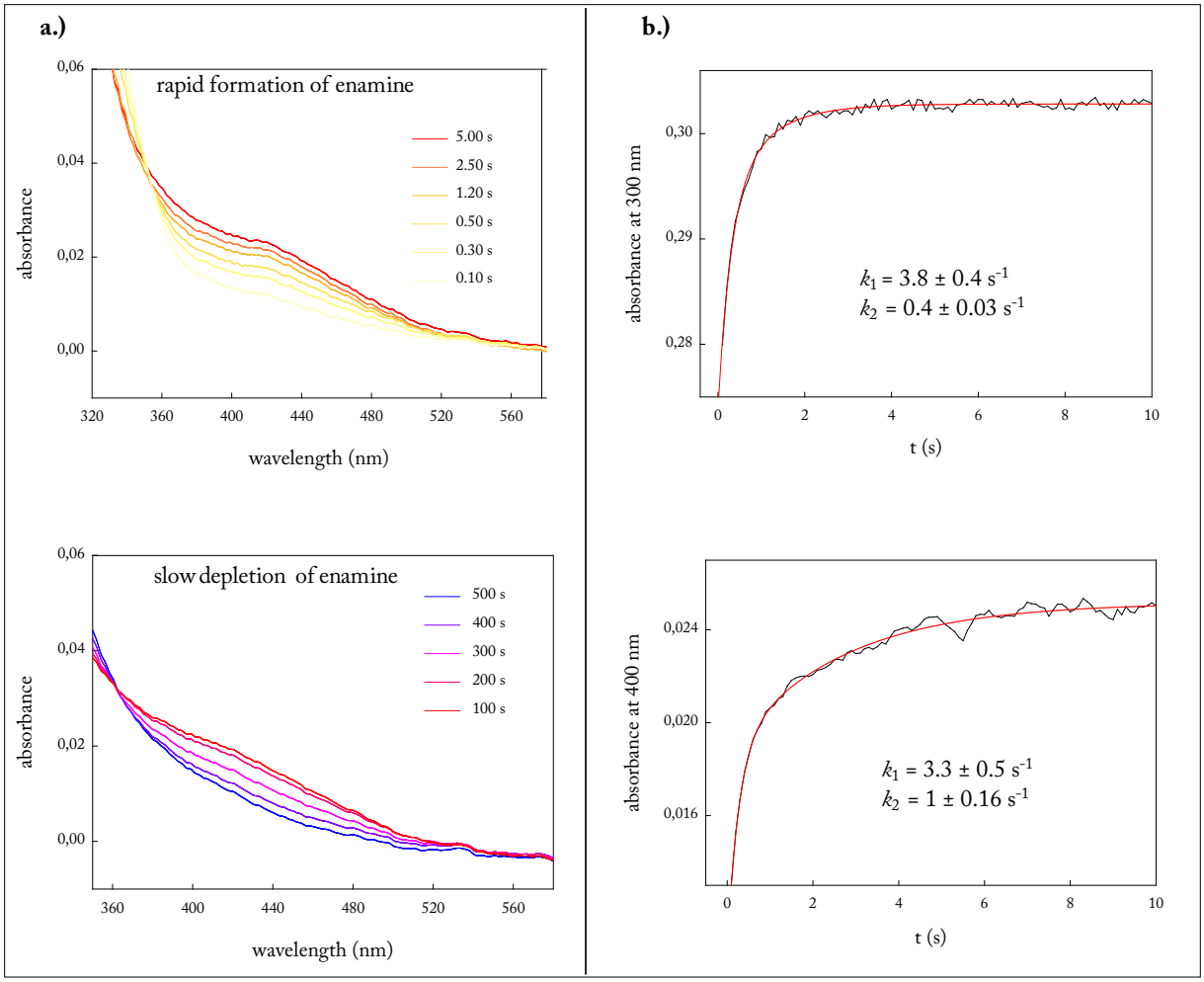

Fig. 85: Kinetic analysis of DHEThDP intermediate formation using UV-Vis-spectroscopy. a.) UV-Vis absorbance diode array spectra for the reaction of 5 mg/ml (69.44 µM active sites) *Ec*TK wt, 300 µM ThDP, 2.5 mM $CaCl_2$, 50 mM glycylglycine (pH 7.6) and 69.44 µM HPA at 25 °C to monitor the formation (top) and depletion of a broad band between 370 - 540 nm. This long-wave band probably originates from a larger conjugated system like an enamine or enolate form of the DHEThDP intermediate. **b.)** Stopped-flow absorbance transients (10 mm pathlength, detection at 300 nm (top) or 400 nm (bottom) for the reaction of 5 mg/ml (69.44 µM active sites) *Ec*TK wt, 300 µM ThDP, 2.5 mM $CaCl_2$, 50 mM glycylglycine (pH 7.6) with 69.44 µM HPA at 25 °C. Fitting of the transients according to a double exponential equation (red, $A = A1 * e^{-k1*t} + A2 * e^{-k2*t}$) gave the shown rate constants k_1 and k_2. The spectral signatures at 300 nm and 400 nm are formed with very similar rate constants suggesting an identical molecular origin of the signals.

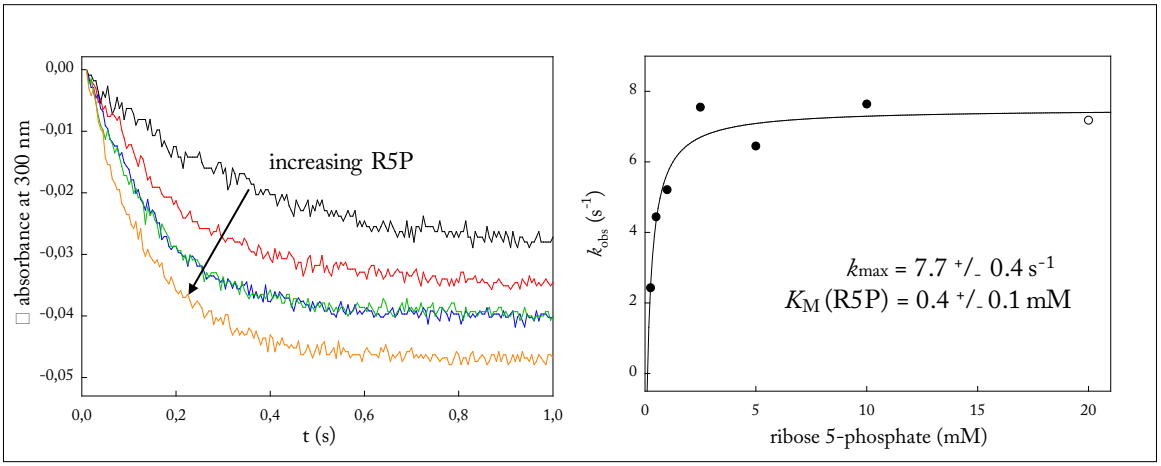

Fig. 86: Kinetic analysis for the reaction of enzyme bound DHEThDP intermediate in *Ec*TK His^{473}Ala with acceptor substrate R5P. Reaction of 7.5 mg/ml *Ec*TK wt (104 µM active sites) that were initially mixed with equimolar concentration of HPA to form enzyme-bound DHEThDP intermediate in 0.3 mM ThDP, 2.5 mM $CaCl_2$, 50 mM glycylglycine (pH 7.6) at 25 °C with increasing concentrations of acceptor R5P. Kinetics were initiated by 1/1 mixing and monitored in a stopped-flow absorbance spectrometer (pathlength 10 mm). **Left:** Selected transients are shown on the left side. **Top right:** Simplified kinetic scheme for the experiment. **Bottom:** Rate constants (k_{obs}) were determined according to a single exponential equation (A = A1 * e^{-k1*t} + offset) and then plotted against the utilized R5P concentration. Kinetic parameters ($k$max and K_M (R5P)) were determined according to a hyperbolic equation.

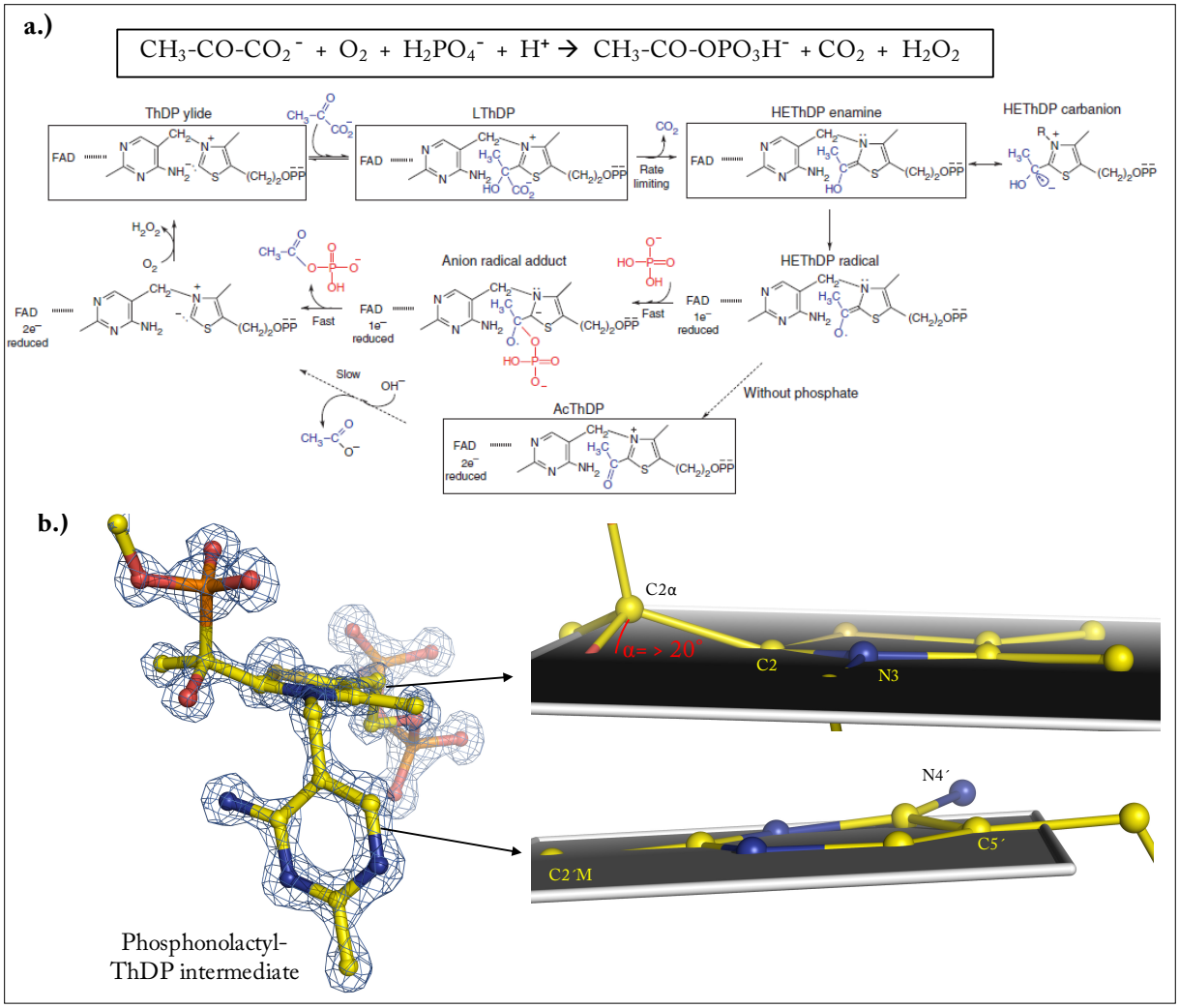

Fig. 87: High-resolution structure of the phosphonolactyl-ThDP intermediate trapped in the active site of *Lp*POX. The intermediate structure was trapped by soaking of *Lp*POX crystals with the pyruvate analogue methylacetyl phosphonate accoding to Wille et al. 2006. The thereby formed, stable phosphonolactyl-ThDP intermediate mimicks the substrate-ThDP intermediate lactyl-ThDP (L-ThDP in a.)) and can´t be further converted due to an stable C-P bond. Unpublished data presented with admission of Dr. Danilo Meyer and Dr. Piotr Neumann. **a.)** Simplified reaction mechanism of the ThDP- and FAD-dependent enzyme *Lp*POX that catalyzes the oxidative decarboxylation of pyruvate forming acetyl-phosphate and hydrogen peroxide (top, boxed). The enzyme forms numerous metastable and in part radical ThDP- and FAD-intermediates (Fig. depicted from Wille et al. 2006). **b.) Left side:** X-ray structure of the intermediate analogue phosphonolactyl-ThDP (1.19 Å, R_{work} = 9.38, R_{free} = 11.68, Fo > 4σ, data not shown) bound to the active site of *Lp*POX as stick and ball representation surrounded by a 2mFo-DFc map (contoured at 3σ). **Right side:** Detailed view on thiazolium (top) and aminopyrimidine moiety of the analogue (bottom). Planes were generated (fixed points: S1, N3 and C5, top; N1´, N3´ and C5´ bottom) to visualize deviations from planarity. The C-C single bond connecting cofactor and substrate (C2-C2α bond) has a strong angular distortion α (red) of more than 20°. Please note that such strong deviations from ring planarity or bond geometry could not been resolved in the previously reported structure of this intermediate and thus remained undetected (1.6 Å, pdb-code: 2EZ9, Wille et al. 2006). Selected atoms are labeled.

6. Bibliography

Adams, P., and Langan, P. (2010 b). Opportunities and challenges with the growth of neutron crystallography. Acta Crystallographica Section D-Biological Crystallography *66*, 1121-1123.

Adams, P.D., Afonine, P.V., Bunkoczi, G., Chen, V.B., Davis, I.W., Echols, N., Headd, J.J., Hung, L.W., Kapral, G.J., Grosse-Kunstleve, R.W., *et al.* (2010 a). PHENIX: a comprehensive Python-based system for macromolecular structure solution. Acta Crystallographica Section D-Biological Crystallography *66*, 213-221.

Albery, W.J., and Knowles, J.R. (1976). Free-Energy Profile for Reaction Catalyzed by Triosephosphate Isomerase. Biochemistry *15*, 5627-5631.

Allen, F.H., Kennard, O., Watson, D.G., Brammer, L., Orpen, A.G., and Taylor, R. (1987). Tables of Bond Lengths Determined by X-Ray and Neutron-Diffraction .1. Bond Lengths in Organic-Compounds. Journal of the Chemical Society-Perkin Transactions 2, S1-S19.

Amara, P., Galvan, I.F., Fontecilla-Camps, J.C., and Field, M.J. (2007). The enamine intermediate may not be universal to thiamine catalysis. Angewandte Chemie-International Edition *46*, 9019-9022.

Arduengo, A.J., Bock, H., Chen, H., Denk, M., Dixon, D.A., Green, J.C., Herrmann, W.A., Jones, N.L., Wagner, M., and West, R. (1994 a). Photoelectron-Spectroscopy of a Carbene/Silylene/Germylene Series. Journal of the American Chemical Society *116*, 6641-6649.

Arduengo, A.J., Dias, H.V.R., Dixon, D.A., Harlow, R.L., Klooster, W.T., and Koetzle, T.F. (1994 b). Electron-Distribution in a Stable Carbene. Journal of the American Chemical Society *116*, 6812-6822.

Arduengo, A.J., Dias, H.V.R., Harlow, R.L., and Kline, M. (1992). Electronic Stabilization of Nucleophilic Carbenes. Journal of the American Chemical Society *114*, 5530-5534.

Arduengo, A.J., Dixon, D.A., Kumashiro, K.K., Lee, C., Power, W.P., and Zilm, K.W. (1994 c). Chemical Shielding Tenser of a Carbene. Journal of the American Chemical Society *116*, 6361-6367.

Arduengo, A.J., Goerlich, J.R., and Marshall, W.J. (1997). A stable thiazol-2-ylidene and its dimer. Liebigs Annalen-Recueil, 365-374.

Arjunan, P., Sax, M., Brunskill, A., Chandrasekhar, K., Nemeria, N., Zhang, S., Jordan, F., and Furey, W. (2006). A thiamin-bound, pre-decarboxylation reaction intermediate analogue in the pyruvate dehydrogenase E1 subunit induces large scale disorder-to-order transformations in the enzyme and reveals novel structural features in the covalently bound adduct. Journal of Biological Chemistry *281*, 15296-15303.

Asztalos, P. (2007 b). Untersuchung zu molekularen, strukturellen und biokatalytischen Aspekten des Vitamin B1-abhängigen Enzyms Transketolase A aus *Escherichia coli*.

Asztalos, P., Parthier, C., Golbik, R., Kleinschmidt, M., Hubner, G., Weiss, M.S., Friedemann, R., Wille, G., and Tittmann, K. (2007 a). Strain and near attack conformers in enzymic thiamin catalysis: X-ray crystallographic snapshots of bacterial transketolase in covalent complex with donor Ketoses xylulose 5-phosphate and fructose 6-phosphate, and in noncovalent complex with acceptor aldose ribose 5-phosphate. Biochemistry *46*, 12037-12052.

Bailey, S. (1994). The Ccp4 Suite - Programs for Protein Crystallography. Acta Crystallographica Section D-Biological Crystallography *50*, 760-763.

Bas, D.C., Rogers, D.M., and Jensen, J.H. (2008). Very fast prediction and rationalization of pKa values for protein-ligand complexes. Proteins *73*, 765-783.

Bellvile, D.J., Pabon, R.A., and Bauld, N.L. (1985). Long Bonds in Cation Radicals of Vicinally Difunctional Molecules. Journal of the American Chemical Society *107*, 4978-4979.

Berkessel, A., Elfert, S., Etzenbach-Effers, K., and Teles, J.H. (2011). Aldehyde umpolung by N-heterocyclic carbenes: NMR characterization of the Breslow intermediate in its keto form, and a spiro-dioxolane as the resting state of the catalytic system. Angew Chem Int Ed Engl *49*, 7120-7124.

Berkholz, D.S., Faber, H.R., Savvides, S.N., and Karplus, P.A. (2008). Catalytic cycle of human glutathione reductase near 1 A resolution. Journal of molecular biology *382*, 371-384.

Berthold, C.L., Toyota, C.G., Moussatche, P., Wood, M.D., Leeper, F., Richards, N.G.J., and Lindqvist, Y. (2007). Crystallographic snapshots of oxalyl-CoA decarboxylase give insights into catalysis by nonoxidative ThDP-dependent decarboxylases. Structure *15*, 853-861.

Bettendorff, L. (1994 a). The compartmentation of phosphorylated thiamine derivatives in cultured neuroblastoma cells. Biochim Biophys Acta *1222*, 7-14.

Bettendorff, L., and Wins, P. (2009). Thiamin diphosphate in biological chemistry: new aspects of thiamin metabolism, especially triphosphate derivatives acting other than as cofactors. Febs Journal *276*, 2917-2925.

Bettendorff, L., Wins, P., and Lesourd, M. (1994 b). Subcellular localization and compartmentation of thiamine derivatives in rat brain. Biochim Biophys Acta *1222*, 1-6.

Bettendorff, L., Wirtzfeld, B., Makarchikov, A.F., Mazzucchelli, G., Frederich, M., Gigliobianco, T., Gangolf, M., De Pauw, E., Angenot, L., and Wins, P. (2007). Discovery of a natural thiamine adenine nucleotide. Nature chemical biology *3*, 211-212.

Blakeley, M.P., Langan, P., Niimura, N., and Podjarny, A. (2008). Neutron crystallography: opportunities, challenges, and limitations. Current Opinion in Structural Biology *18*, 593-600.

Boros, L.G., Puigjaner, J., Cascante, M., Lee, W.N.P., Brandes, J.L., Bassilian, S., Yusuf, F.I., Williams, R.D., Muscarella, P., Melvin, W.S., *et al.* (1997). Oxythiamine and dehydroepiandrosterone inhibit the nonoxidative synthesis of ribose and tumor cell proliferation. Cancer Research *57*, 4242-4248.

Bradford, M.M. (1976). Rapid and Sensitive Method for Quantitation of Microgram Quantities of Protein Utilizing Principle of Protein-Dye Binding. Analytical Biochemistry *72*, 248-254.

Brandt, G.S., Kneen, M.M., Chakraborty, S., Baykal, A.T., Nemeria, N., Yep, A., Ruby, D.I., Petsko, G.A., Kenyon, G.L., McLeish, M.J., *et al.* (2009). Snapshot of a reaction intermediate: analysis of benzoylformate decarboxylase in complex with a benzoylphosphonate inhibitor. Biochemistry *48*, 3247-3257.

Breslow, R. (1957). Rapid deuterium exchange in thiazolium salts. J Am Chem Soc *79*, 1762-1763.

Brunger, A.T. (1992). Free R value: a novel statistical quantity for assessing the accuracy of crystal structures. Nature *355*, 472-475.

Bruning, M., Berheide, M., Meyer, D., Golbik, R., Bartunik, H., Liese, A., and Tittmann, K. (2009). Structural and kinetic studies on native intermediates and an intermediate analogue in benzoylformate decarboxylase reveal a least motion mechanism with an unprecedented short-lived predecarboxylation intermediate. Biochemistry *48*, 3258-3268.

Burgi, H.B., Dunitz, J.D., Lehn, J.M., and Wipff, G. (1974). Stereochemistry of Reaction Paths at Carbonyl Centers. Tetrahedron *30*, 1563-1572.

Burgi, H.B., Dunitz, J.D., and Shefter, E. (1973). Geometrical Reaction Coordinates .2. Nucleophilic Addition to a Carbonyl Group. Journal of the American Chemical Society *95*, 5065-5067.

Calingasan, N.Y., Sheu, K.F.R., Baker, H., Jung, E.H., Paoletti, F., and Gibson, G.E. (1995). Heterogeneous Expression of Transketolase in Rat-Brain. Journal of Neurochemistry *64*, 1034-1044.

Cavazza, C., Contreras-Martel, C., Pieulle, L., Chabriere, E., Hatchikian, E.C., and Fontecilla-Camps, J.C. (2006). Flexibility of thiamine diphosphate revealed by kinetic crystallographic studies of the reaction of pyruvate-ferredoxin oxidoreductase with pyruvate. Structure *14*, 217-224.

Cazares, A., Galman, J.L., Crago, L.G., Smith, M.E.B., Strafford, J., Rios-Solis, L., Lye, G.J., Dalby, P.A., and Hailes, H.C. (2010). Non-alpha-hydroxylated aldehydes with evolved transketolase enzymes. Organic & Biomolecular Chemistry *8*, 1301-1309.

Chabriere, E., Vernede, X., Guigliarelli, B., Charon, M.H., Hatchikian, E.C., and Fontecilla-Camps, J.C. (2001). Crystal structure of the free radical intermediate of pyruvate:ferredoxin oxidoreductase. Science *294*, 2559-2563.

Chakraborty, S., Nemeria, N., Yep, A., McLeish, M.J., Kenyon, G.L., and Jordan, F. (2008). Mechanism of benzaldehyde lyase studied via thiamin diphosphate-bound intermediates and kinetic isotope effects. Biochemistry *47*, 3800-3809.

Chakraborty, S., Nemeria, N.S., Balakrishnan, A., Brandt, G.S., Kneen, M.M., Yep, A., McLeish, M.J., Kenyon, G.L., Petsko, G.A., Ringe, D., *et al.* (2009). Detection and time course of formation of major thiamin diphosphate-bound covalent intermediates derived from a chromophoric substrate analogue on benzoylformate decarboxylase. Biochemistry *48*, 981-994.

Charmantray, F., Helaine, V., Legeret, B., and Hecquet, L. (2009). Preparative scale enzymatic synthesis of D-sedoheptulose-7-phosphate from beta-hydroxypyruvate and D-ribose-5-phosphate. Journal of Molecular Catalysis B-Enzymatic *57*, 6-9.

Cleland, W.W., Frey, P.A., and Gerlt, J.A. (1998). The low barrier hydrogen bond in enzymatic catalysis. Journal of Biological Chemistry *273*, 25529-25532.

Coy, J.F., Dubel, S., Kioschis, P., Thomas, K., Micklem, G., Delius, H., and Poustka, A. (1996). Molecular cloning of tissue-specific transcripts of a transketolase-related gene: Implications for the evolution of new vertebrate genes. Genomics *32*, 309-316.

Crosby, J., and Lienhard, G.E. (1970). Mechanisms of Thiamine-Catalyzed Reactions - a Kinetic Analysis of Decarboxylation of Pyruvate by 3,4-Dimethylthiazolium Ion in Water and Ethanol. Journal of the American Chemical Society *92*, 5707-+.

Davis, I.W., Leaver-Fay, A., Chen, V.B., Block, J.N., Kapral, G.J., Wang, X., Murray, L.W., Arendall, W.B., 3rd, Snoeyink, J., Richardson, J.S., *et al.* (2007). MolProbity: all-atom contacts and structure validation for proteins and nucleic acids. Nucleic acids research *35*, W375-383.

Demmel, F., Doster, W., Petry, W., and Schulte, A. (1997). Vibrational frequency shifts as a probe of hydrogen bonds: thermal expansion and glass transition of myoglobin in mixed solvents. Eur Biophys J *26*, 327-335.

Duke, C.C., Macleod, J.K., and Williams, J.F. (1981). Nuclear Magnetic-Resonance Studies of D-Erythrose 4-Phosphate in Aqueous-Solution - Structures of the Major Contributing Monomeric and Dimeric Forms. Carbohydrate Research *95*, 1-26.

DuPre, D.B., and Wong, J.L. (2005). Topological analysis of the electron density in model azolium systems for thiamin structure-function: sulfur is the electron sink and positively polarized carbanions act as nucleophiles. J Phys Chem A *109*, 7606-7612.

DuPre, D.B., and Wong, J.L. (2007). Thiamin deprotonation mechanism. Carbanion development stabilized by the LUMOs of thiazolium and pyrimidylimine working in tandem and release governed by a H-bond switch. J Phys Chem A *111*, 2172-2181.

Eisenmesser, E.Z., Millet, O., Labeikovsky, W., Korzhnev, D.M., Wolf-Watz, M., Bosco, D.A., Skalicky, J.J., Kay, L.E., and Kern, D. (2005). Intrinsic dynamics of an enzyme underlies catalysis. Nature *438*, 117-121.

Emsley, P., Lohkamp, B., Scott, W.G., and Cowtan, K. (2010). Features and development of Coot. Acta Crystallographica Section D-Biological Crystallography *66*, 486-501.

Enders, D., and Balensiefer, T. (2004). Nucleophilic carbenes in asymmetric organocatalysis. Acc Chem Res *37*, 534-541.

Enders, D., Niemeier, O., and Henseler, A. (2007). Organocatalysis by N-heterocyclic, carbenes. Chemical Reviews *107*, 5606-5655.

Ericsson, U.B., Hallberg, B.M., DeTitta, G.T., Dekker, N., and Nordlund, P. (2006). Thermofluor-based high-throughput stability optimization of proteins for structural studies. Analytical Biochemistry *357*, 289-298.

Fersht, A. (1999). Structure and Mechanism in Protein Science.

Fessner, W.D., and Helaine, V. (2001). Biocatalytic synthesis of hydroxylated natural products using aldolases and related enzymes. Curr Opin Biotechnol *12*, 574-586.

Fiedler, E., Golbik, R., Schneider, G., Tittmann, K., Neef, H., Konig, S., and Hubner, G. (2001). Examination of donor substrate conversion in yeast transketolase. J Biol Chem *276*, 16051-16058.

Fiedler, E., Thorell, S., Sandalova, T., Golbik, R., Konig, S., and Schneider, G. (2002). Snapshot of a key intermediate in enzymatic thiamin catalysis: Crystal structure of the alpha-carbanion of (alpha,beta-dihydroxyethyl)-thiamin diphosphate in the active site of transketolase from Saccharomyces cerevisiae. Proceedings of the National Academy of Sciences of the United States of America *99*, 591-595.

Frank, R.A.W., Leeper, F.J., and Luisi, B.F. (2007). Structure, mechanism and catalytic duality of thiamine-dependent enzymes. Cellular and Molecular Life Sciences *64*, 892-905.

Frank, R.A.W., Titman, C.M., Pratap, J.V., Luisi, B.F., and Perham, R.N. (2004). A molecular switch and proton wire synchronize the active sites in thiamine enzymes. Science *306*, 872-876.

Franke, F.P., Kapuscinski, M., and Lyndon, P. (1985). Synthesis and Nmr Characterization of Intermediates in the L-Type Pentose-Phosphate Cycle. Carbohydrate Research *143*, 69-76.

Frey, P.A. (1989). 2-Acetylthiamin pyrophosphate: an enzyme-bound intermediate in thiamin pyrophosphate-dependent reactions. Biofactors *2*, 1-9.

Freyer, M.W., and Lewis, E.A. (2008). Isothermal titration calorimetry: experimental design, data analysis, and probing macromolecule/ligand binding and kinetic interactions. Methods Cell Biol *84*, 79-113.

Friedemann, R., and Breitkopf, C. (1996). Theoretical studies on the decarboxylation reaction in thiamin catalysis. International Journal of Quantum Chemistry *57*, 943-948.

Galman, J.L., Steadman, D., Bacon, S., Morris, P., Smith, M.E.B., Ward, J.M., Dalby, P.A., and Hailes, H.C. (2010). alpha,alpha '-Dihydroxyketone formation using aromatic and heteroaromatic aldehydes with evolved transketolase enzymes. Chemical Communications *46*, 7608-7610.

Gerhardt, S., Echt, S., Busch, M., Freigang, J., Auerbach, G., Bader, G., Martin, W.F., Bacher, A., Huber, R., and Fischer, M. (2003). Structure and properties of an engineered transketolase from maize. Plant Physiol *132*, 1941-1949.

Golbik, R., Meshalkina, L.E., Sandalova, T., Tittmann, K., Fiedler, E., Neef, H., Konig, S., Kluger, R., Kochetov, G.A., Schneider, G., *et al.* (2005). Effect of coenzyme modification on the structural and catalytic properties of wild-type transketolase and of the variant E418A from Saccharomyces cerevisiae - Contrasting protonation state requirements of thiamin diphosphate in decarboxylases and transketolases. Febs Journal *272*, 1326-1342.

Gouet, P., Courcelle, E., Stuart, D.I., and Metoz, F. (1999). ESPript: analysis of multiple sequence alignments in PostScript. Bioinformatics *15*, 305-308.

Hammes, H.P., Du, X.L., Edelstein, D., Taguchi, T., Matsumura, T., Ju, Q.D., Lin, J.H., Bierhaus, A., Nawroth, P., Hannak, D., *et al.* (2003). Benfotiamine blocks three major pathways of hyperglycemic damage and prevents experimental diabetic retinopathy. Nature Medicine *9*, 294-299.

Heine, A., DeSantis, G., Luz, J.G., Mitchell, M., Wong, C.H., and Wilson, I.A. (2001). Observation of covalent intermediates in an enzyme mechanism at atomic resolution. Science *294*, 369-374.

Henzler-Wildman, K., and Kern, D. (2007). Dynamic personalities of proteins. Nature *450*, 964-972.

Hibbert, E.G., Senussi, T., Costelloe, S.J., Lei, W., Smith, M.E.B., Ward, J.M., Hailes, H.C., and Dalby, P.A. (2007). Directed evolution of transketolase activity on non-phosphorylated substrates. J Biotechnol *131*, 425-432.

Holm, L., and Rosenstrom, P. (2010). Dali server: conservation mapping in 3D. Nucleic Acids Research *38*, W545-W549.

Hsin, K., Sheng, Y., Harding, M.M., Taylor, P., and Walkinshaw, M.D. (2008). MESPEUS: a database of the geometry of metal sites in proteins. Journal of Applied Crystallography *41*, 963-968.

Hübner, G., Tittmann, K., Killenberg-Jabs, M., Schaffner, J., Spinka, M., Neef, H., Kern, D., Kern, G., Schneider, G., Wikner, C., *et al.* (1998). Activation of thiamin diphosphate in enzymes. Biochimica Et Biophysica Acta-Protein Structure and Molecular Enzymology *1385*, 221-228.

Hur, S., and Bruice, T.C. (2003). The near attack conformation approach to the study of the chorismate to prephenate reaction. Proceedings of the National Academy of Sciences of the United States of America *100*, 12015-12020.

Hur, S., Newby, Z.E.R., and Bruice, T.C. (2004). Transition state stabilization by general acid catalysis, water expulsion, and enzyme reorganization in Medicago savita chalcone isomerase. Proceedings of the National Academy of Sciences of the United States of America *101*, 2730-2735.

Inoue, H., Nojima, H., and Okayama, H. (1990). High-Efficiency Transformation of Escherichia-Coli with Plasmids. Gene *96*, 23-28.

Jensen, K.P., and Ryde, U. (2005). How the Co-C bond is cleaved in coenzyme B12 enzymes: a theoretical study. Journal of the American Chemical Society *127*, 9117-9128.

Jordan, F. (2003). Current mechanistic understanding of thiamin diphosphate-dependent enzymatic reactions. Nat Prod Rep *20*, 184-201.

Jordan, F., Nemeria, N.S., Zhang, S., Yan, Y., Arjunan, P., and Furey, W. (2003). Dual catalytic apparatus of the thiamin diphosphate coenzyme: Acid-base via the 1 ',4 '-iminopyrimidine tautomer along with its electrophilic role. Journal of the American Chemical Society *125*, 12732-12738.

Jordan, F., Zhang, Z., and Sergienko, E. (2002). Spectroscopic evidence for participation of the 1',4'-imino tautomer of thiamin diphosphate in catalysis by yeast pyruvate decarboxylase. Bioorganic chemistry *30*, 188-198.

Jung, I.L., Phyo, K.H., and Kim, I.G. (2005). RpoS-mediated growth-dependent expression of the Escherichia coli tkt genes encoding transketolases isoenzymes. Curr Microbiol *50*, 314-318.

Kabsch, W. (2010). Xds. Acta Crystallographica Section D-Biological Crystallography *66*, 125-132.

Kale, S., and Jordan, F. (2009). Conformational ensemble modulates cooperativity in the rate-determining catalytic step in the E1 component of the Escherichia coli pyruvate dehydrogenase multienzyme complex. J Biol Chem *284*, 33122-33129.

Kao, Y.-T., Tan, C., Song, S.-H., Ozturk, N., Li, J., Wang, L., Sancar, A., and Zhong, D. (2008). Ultrafast dynamics and anionic active states of the flavin cofactor in cryptochrome and photolyase. Journal of the American Chemical Society *130*, 7695-7701.

Kaplun, A., Binshtein, E., Vyazmensky, M., Steinmetz, A., Barak, Z., Chipman, D.M., Tittmann, K., and Shaanan, B. (2008). Glyoxylate carboligase lacks the canonical active site glutamate of thiamine-dependent enzymes. Nature Chemical Biology *4*, 113-118.

Katona, G., Wilmouth, R.C., Wright, P.A., Berglund, G.I., Hajdu, J., Neutze, R., and Schofield, C.J. (2002). X-ray structure of a serine protease acyl-enzyme complex at 0.95-angstrom resolution. Journal of Biological Chemistry *277*, 21962-21970.

Kaupp, G., and Boy, J. (1997). Overlong C-C single bonds. Angewandte Chemie-International Edition in English *36*, 48-49.

Kern, D., Kern, G., Neef, H., Tittmann, K., Killenberg-Jabs, M., Wikner, C., Schneider, G., and Hubner, G. (1997). How thiamine diphosphate is activated in enzymes. Science *275*, 67-70.

Kluger, R., and Tittmann, K. (2008). Thiamin diphosphate catalysis: Enzymic and nonenzymic covalent intermediates. Chemical Reviews *108*, 1797-1833.

Koers, E.J. (2010). Determination of Carbanion Intermediates in ThDP-dependent Enzymes.

Kovalevsky, A.Y., Hanson, L., Fisher, S.Z., Mustyakimov, M., Mason, S.A., Forsyth, V.T., Blakeley, M.P., Keen, D.A., Wagner, T., Carrell, H.L., *et al.* (2010). Metal Ion Roles and the Movement of Hydrogen during Reaction Catalyzed by D-Xylose Isomerase: A Joint X-Ray and Neutron Diffraction Study. Structure *18*, 688-699.

Koziol, A.E., and Lis, T. (1991). Structure of Barium Alpha-D-Ribofuranose-5-Phosphate Pentahemihydrate - a Reinvestigation. Acta Crystallographica Section C-Crystal Structure Communications *47*, 2076-2079.

Krockenberger, M., Honig, A., Rieger, L., Coy, J.F., Sutterlin, M., Kapp, M., Horn, E., Dietl, J., and Kammerer, U. (2007). Transketolase-like 1 expression correlates with subtypes of ovarian cancer and the presence of distant metastases. Int J Gynecol Cancer *17*, 101-106.

Kutter, S., Weiss, M.S., Wille, G., Golbik, R., Spinka, M., and Konig, S. (2009). Covalently Bound Substrate at the Regulatory Site of Yeast Pyruvate Decarboxylases Triggers Allosteric Enzyme Activation. Journal of Biological Chemistry *284*, 12136-12144.

Laemmli, U.K. (1970). Cleavage of Structural Proteins during Assembly of Head of Bacteriophage-T4. Nature *227*, 680-&.

Larkin, M.A., Blackshields, G., Brown, N.P., Chenna, R., McGettigan, P.A., McWilliam, H., Valentin, F., Wallace, I.M., Wilm, A., Lopez, R., *et al.* (2007). Clustal W and Clustal X version 2.0. Bioinformatics *23*, 2947-2948.

Le Huerou, Y., Gunawardana, I., Thomas, A.A., Boyd, S.A., de Meese, J., Dewolf, W., Gonzales, S.S., Han, M., Hayter, L., Kaplan, T., *et al.* (2008). Prodrug thiamine analogs as inhibitors of the enzyme transketolase. Bioorganic & Medicinal Chemistry Letters *18*, 505-508.

Leavitt, S., and Freire, E. (2001). Direct measurement of protein binding energetics by isothermal titration calorimetry. Current opinion in structural biology *11*, 560-566.

Lehwess-Litzmann, A., Neumann, P., Parthier, C., Ludtke, S., Golbik, R., Ficner, R., and Tittmann, K. (2011). Twisted Schiff base intermediates and substrate locale revise transaldolase mechanism. Nature Chemical Biology *7*, 678-684.

Levitt, M., and Warshel, A. (1978). Extreme Conformational Flexibility of Furanose Ring in DNA and RNA. Journal of the American Chemical Society *100*, 2607-2613.

Lindqvist, Y., Schneider, G., Ermler, U., and Sundstrom, M. (1992). Three-dimensional structure of transketolase, a thiamine diphosphate dependent enzyme, at 2.5 A resolution. Embo J *11*, 2373-2379.

Littlechild, J., Turner, N., Hobbs, G., Lilly, M., Rawas, A., and Watson, H. (1995). Crystallization and preliminary X-ray crystallographic data with Escherichia coli transketolase. Acta Crystallogr D Biol Crystallogr *51*, 1074-1076.

Liu, S.Q., Sun, M.Z., Tang, J.W., Wang, Z.Q., Sun, C.R., and Greenaway, F.T. (2008). High-performance liquid chromatography/nano-electrospray ionization tandem mass spectrometry, two-dimensional difference in-gel electrophoresis and gene microarray identification of lymphatic metastasis-associated biomarkers. Rapid Communications in Mass Spectrometry *22*, 3172-3178.

Lüdtke, S. (2008). Analyse von Zuckerkonformationen während der enzymatischen Katalyse von Transketolase und Implikationen für die Reaktivität von Intermediaten.

Machius, M., Wynn, R.M., Chuang, J.L., Li, J., Kluger, R., Yu, D., Tomchick, D.R., Brautigam, C.A., and Chuang, D.T. (2006). A versatile conformational switch regulates reactivity in human branched-chain alpha-ketoacid dehydrogenase. Structure *14*, 287-298.

Maslak, P., Chapman, W.H., Vallombroso, T.M., and Watson, B.A. (1995). Mesolytic scission of C-C bonds in radical cations of amino derivatives: Steric and solvent effects. Journal of the American Chemical Society *117*, 12380-12389.

Matosevic, S., Lye, G.J., and Baganz, F. (2010). Design and Characterization of a Prototype Enzyme Microreactor: Quantification of Immobilized Transketolase Kinetics. Biotechnology Progress *26*, 118-126.

Matosevic, S., Lye, G.J., and Baganz, F. (2011). Immobilised enzyme microreactor for screening of multi-step bioconversions: Characterisation of a de novo transketolase-omega-transaminase pathway to synthesise chiral amino alcohols. J Biotechnol *155*, 320-329.

Matthews, B.W. (1968). Solvent content of protein crystals. Journal of molecular biology *33*, 491-497.
Mayer, A., Von Wallbrunn, A., and Vaupel, P. (2010). Glucose metabolism of malignant cells is not regulated by transketolase-like (TKTL)-1. Int J Oncol *37*, 265-271.

McCoy, A.J. (2007). Solving structures of protein complexes by molecular replacement with Phaser. Acta Crystallogr D Biol Crystallogr *63*, 32-41.

Meyer, D. (2009). Kinetische und strukturelle Untersuchung der Katalysemechanismen ausgewählter Kofaktor-abhängiger Enzyme -Implikationen für die Decarboxylierung von α-Ketosäuren durch Thiamindiphosphat-abhängige Enzyme.

Meyer, D., Neumann, P., Parthier, C., Friedemann, R., Nemeria, N., Jordan, F., and Tittmann, K. (2010). Double duty for a conserved glutamate in pyruvate decarboxylase: evidence of the participation in stereoelectronically controlled decarboxylation and in protonation of the nascent carbanion/enamine intermediate. Biochemistry *49*, 8197-8212.

Meyer, D., Neumann, P., Koers E., Sjuts, H., Lüdtke S., Sheldrick, G., Ficner, R., Tittmann, K. (2012). Unexpected tautomeric equilibria of the carbanion-enamine intermediate in pyruvate oxidase highlight unrecognized chemical versatility of the thiamin cofactor. PNAS *under revision*.

Meyer, D., Walter, L., Kolter, G., Pohl, M., Muller, M., and Tittmann, K. (2011). Conversion of pyruvate decarboxylase into an enantioselective carboligase with biosynthetic potential. Journal of the American Chemical Society *133*, 3609-3616.

Milic, D., Demidkina, T.V., Faleev, N.G., Phillips, R.S., Matkovic-Calogovic, D., and Antson, A.A. (2011). Crystallographic snapshots of tyrosine phenol-lyase show that substrate strain plays a role in C-C bond cleavage. Journal of the American Chemical Society *133*, 16468-16476.

Mitschke, L. (2008). Kinetische und strukturelle Charakterisierung humaner Transketolase.

Mitschke, L., Parthier, C., Schroder-Tittmann, K., Coy, J., Ludtke, S., and Tittmann, K. (2010). The crystal structure of human transketolase and new insights into its mode of action. J Biol Chem *285*, 31559-31570.

Moffat, K. (2001). Time-resolved biochemical crystallography: a mechanistic perspective. Chemical reviews *101*, 1569-1581.

Muller, M., Gocke, D., and Pohl, M. (2009). Thiamin diphosphate in biological chemistry: exploitation of diverse thiamin diphosphate-dependent enzymes for asymmetric chemoenzymatic synthesis. Febs Journal *276*, 2894-2904.

Muller, Y.A., Lindqvist, Y., Furey, W., Schulz, G.E., Jordan, F., and Schneider, G. (1993). A Thiamin Diphosphate Binding Fold Revealed by Comparison of the Crystal-Structures of Transketolase, Pyruvate Oxidase and Pyruvate Decarboxylase. Structure *1*, 95-103.

Murshudov, G.N., Vagin, A.A., and Dodson, E.J. (1997). Refinement of macromolecular structures by the maximum-likelihood method. Acta Crystallographica Section D-Biological Crystallography *53*, 240-255.

Naghibi, H., Tamura, A., and Sturtevant, J.M. (1995). Significant discrepancies between van't Hoff and calorimetric enthalpies. Proceedings of the National Academy of Sciences of the United States of America *92*, 5597-5599.

Nemeria, N., Baykal, A., Joseph, E., Zhang, S., Yan, Y., Furey, W., and Jordan, F. (2004). Tetrahedral intermediates in thiamin diphosphate-dependent decarboxylations exist as a 1 ',4 '-imino tautomeric form of the coenzyme, unlike the Michaelis complex or the free coenzyme. Biochemistry *43*, 6565-6575.

Nemeria, N.S., Arjunan, P., Chandrasekhar, K., Mossad, M., Tittmann, K., Furey, W., and Jordan, F. (2010). Communication between Thiamin Cofactors in the Escherichia coli Pyruvate Dehydrogenase Complex E1 Component Active Centers EVIDENCE FOR A "DIRECT PATHWAY" BETWEEN THE 4 '-AMINOPYRIMIDINE N1' ATOMS. Journal of Biological Chemistry *285*, 11197-11209.

Nemeria, N.S., Chakraborty, S., Balakrishnan, A., and Jordan, F. (2009). Reaction mechanisms of thiamin diphosphate enzymes: defining states of ionization and tautomerization of the cofactor at individual steps. Febs J *276*, 2432-2446.

Nilsson, U., Hecquet, L., Gefflaut, T., Guerard, C., and Schneider, G. (1998). Asp477 is a determinant of the enantioselectivity in yeast transketolase. FEBS Lett *424*, 49-52.

Nilsson, U., Meshalkina, L., Lindqvist, Y., and Schneider, G. (1997). Examination of substrate binding in thiamin diphosphate-dependent transketolase by protein crystallography and site-directed mutagenesis. Journal of Biological Chemistry *272*, 1864-1869.

Pace, C.N., Hebert, E.J., Shaw, K.L., Schell, D., Both, V., Krajcikova, D., Sevcik, J., Wilson, K.S., Dauter, Z., Hartley, R.W., *et al.* (1998). Conformational stability and thermodynamics of folding of ribonucleases Sa, Sa2 and Sa3. Journal of Molecular Biology *279*, 271-286.

Paramasivam, S., Balakrishnan, A., Dmitrenko, O., Godert, A., Begley, T.P., Jordan, F., and Polenova, T. (2011). Solid-state NMR and density functional theory studies of ionization states of thiamin. J Phys Chem B *115*, 730-736.

Pearson, A.R., Mozzarelli, A., and Rossi, G.L. (2004). Microspectrophotometry for structural enzymology. Current opinion in structural biology *14*, 656-662.

Pei, X.-Y., Erixon, K.M., Luisi, B.F., and Leeper, F.J. Structural insights into the prereaction state of pyruvate decarboxylase from Zymomonas mobilis. Biochemistry *49*, 1727-1736.

Petsko, G.A., and Ringe, D. (2000). Observation of unstable species in enzyme-catalyzed transformations using protein crystallography. Curr Opin Chem Biol *4*, 89-94.

Petsko, G.A., Ringe, D. (2004). Protein Structure and Function. Primers in Biology.

Pierce, J., Serianni, A.S., and Barker, R. (1985). Anomerization of Furanose Sugars and Sugar Phosphates. Journal of the American Chemical Society *107*, 2448-2456.

Pletcher, J., Blank, G., Wood, M., and Sax, M. (1979). Thiamin Pyrophosphate .4 1/2h2o - 2nd Polymorph of the Neutral Zwitterion. Acta Crystallographica Section B-Structural Science *35*, 1633-1637.

Pohl, M., Sprenger, G.A., and Muller, M. (2004). A new perspective on thiamine catalysis. Curr Opin Biotechnol *15*, 335-342.

Rasmussen, B.F., Stock, A.M., Ringe, D., and Petsko, G.A. (1992). Crystalline ribonuclease A loses function below the dynamical transition at 220 K. Nature *357*, 423-424.

Sax, C.M., Salamon, C., Kays, W.T., Guo, J., Yu, F.S.X., Cuthbertson, R.A., and Piatigorsky, J. (1996). Transketolase is a major protein in the mouse cornea. Journal of Biological Chemistry *271*, 33568-33574.

Schellenberger, A. (1998). Sixty years of thiamin diphosphate biochemistry. Biochimica Et Biophysica Acta-Protein Structure and Molecular Enzymology *1385*, 177-186.

Schenk, G., Duggleby, R.G., and Nixon, P.F. (1998). Properties and functions of the thiamin diphosphate dependent enzyme transketolase. International Journal of Biochemistry & Cell Biology *30*, 1297-1318.

Schenk, G., Layfield, R., Candy, J.M., Duggleby, R.G., and Nixon, P.F. (1997). Molecular evolutionary analysis of the thiamine-diphosphate-dependent enzyme, transketolase. Journal of Molecular Evolution *44*, 552-572.

Schneider, G., and Lindqvist, Y. (1998). Crystallography and mutagenesis of transketolase: mechanistic implications for enzymatic thiamin catalysis. Biochimica Et Biophysica Acta-Protein Structure and Molecular Enzymology *1385*, 387-398.

Schreiner, P.R., Chernish, L.V., Gunchenko, P.A., Tikhonchuk, E.Y., Hausmann, H., Serafin, M., Schlecht, S., Dahl, J.E.P., Carlson, R.M.K., and Fokin, A.A. (2011). Overcoming lability of extremely long alkane carbon-carbon bonds through dispersion forces. Nature *477*, 308-U373.

Schuttelkopf, A.W., and van Aalten, D.M.F. (2004). PRODRG: a tool for high-throughput crystallography of protein-ligand complexes. Acta Crystallographica Section D-Biological Crystallography *60*, 1355-1363.

Schutz, A., Golbik, R., Konig, S., Hubner, G., and Tittmann, K. (2005). Intermediates and transition states in thiamin diphosphate-dependent decarboxylases. A kinetic and NMR study on wild-type indolepyruvate decarboxylase and variants using indolepyruvate, benzoylformate, and pyruvate as substrates. Biochemistry *44*, 6164-6179.

Seifert, F. (2010). Katalyse und Regulation der E1-Komponente des humanen Pyruvat-Dehydrogenase-Komplexes auf molekularer Ebene.

Seifert, F., Golbik, R., Brauer, J., Lilie, H., Schroder-Tittmann, K., Hinze, E., Korotchkina, L.G., Patel, M.S., and Tittmann, K. (2006). Direct kinetic evidence for half-of-the-sites reactivity in the E1 component of the human pyruvate dehydrogenase multienzyme complex through alternating sites cofactor activation. Biochemistry *45*, 12775-12785.

Sheldrick, G.M. (2008). A short history of SHELX. Acta Crystallographica Section A *64*, 112-122.
Soderberg, T. (2005). Biosynthesis of ribose-5-phosphate and erythrose-4-phosphate in archaea: a phylogenetic analysis of archaeal genomes. Archaea *1*, 347-352.

Sprenger, G.A., Schorken, U., Sprenger, G., and Sahm, H. (1995). Transketolase-a of Escherichia-Coli K12 - Purification and Properties of the Enzyme from Recombinant Strains. European Journal of Biochemistry *230*, 525-532.

Steiner, T., and Saenger, W. (1994). Lengthening of the Covalent O-H Bond in O-H...O Hydrogen-Bonds Reexamined from Low-Temperature Neutron-Diffraction Data of Organic-Compounds. Acta Crystallographica Section B-Structural Science *50*, 348-357.

Suzuki, R., Katayama, T., Kim, B.-J., Wakagi, T., Shoun, H., Ashida, H., Yamamoto, K., and Fushinobu, S. (2010). Crystal structures of phosphoketolase: thiamine diphosphate-dependent dehydration mechanism. J Biol Chem *285*, 34279-34287.

Thomas, A.A., De Meese, J., Le Huerou, Y., Boyd, S.A., Romoff, T.T., Gonzales, S.S., Gunawardana, I., Kaplan, T., Sullivan, F., Condroski, K., *et al.* (2008 a). Non-charged thiamine analogs as inhibitors of enzyme transketolase. Bioorganic & Medicinal Chemistry Letters *18*, 509-512.

Thomas, A.A., Le Huerou, Y., De Meese, J., Gunawardana, I., Kaplan, T., Romoff, T.T., Gonzales, S.S., Condroski, K., Boyd, S.A., Ballard, J., *et al.* (2008 b). Synthesis, in vitro and in vivo activity of thiamine antagonist transketolase inhibitors. Bioorganic & Medicinal Chemistry Letters *18*, 2206-2210.

Tittmann, K. (2000). Untersuchungen zu Katalysemechanismen von Flavin- und Thiamindiphosphat-abhängigen Enzmyen. Aktivierung vin Thiamindiphosphate in Enzmyen. Katalysemechanismus der Pyruvateoxidase aus *Lactobacillus plantarum*.

Tittmann, K. (2009). Reaction mechanisms of thiamin diphosphate enzymes: redox reactions. Febs J *276*, 2454-2468.

Tittmann, K., Golbik, R., Uhlemann, K., Khailova, L., Schneider, G., Patel, M., Jordan, F., Chipman, D.M., Duggleby, R.G., and Hubner, G. (2003). NMR analysis of covalent intermediates in thiamin diphosphate enzymes. Biochemistry *42*, 7885-7891.

Tittmann, K., Vyazmensky, M., Hubner, G., Barak, Z., and Chipman, D.M. (2005 a). The carboligation reaction of acetohydroxyacid synthase II: Steady-state intermediate distributions in wild type and mutants by NMR. Proceedings of the National Academy of Sciences of the United States of America *102*, 553-558.

Tittmann, K., and Wille, G. (2009). X-ray crystallographic snapshots of reaction intermediates in pyruvate oxidase and transketolase illustrate common themes in thiamin catalysis. Journal of Molecular Catalysis B-Enzymatic *61*, 93-99.

Tittmann, K., Wille, G., Golbik, R., Weidner, A., Ghisla, S., and Hubner, G. (2005 b). Radical phosphate transfer mechanism for the thiamin diphosphate- and FAD-dependent pyruvate oxidase from Lactobacillus plantarum. Kinetic coupling of intercofactor electron transfer with phosphate transfer to acetyl-thiamin diphosphate via a transient FAD semiquinone/hydroxyethyl-ThDP radical pair. Biochemistry *44*, 13291-13303.

Toda, F. (2000). Naphthocyclobutenes and benzodicyclobutadienes: Synthesis in the solid state and anomalies in the bond lengths. European Journal of Organic Chemistry, 1377-1386.

Tung, W.L., and Chow, K.C. (1995). A Modified Medium for Efficient Electrotransformation of Escherichia-Coli. Trends in Genetics *11*, 128-129.

Turano, A., Furey, W., Pletcher, J., Sax, M., Pike, D., and Kluger, R. (1982). Synthesis and Crystal-Structure of an Analog of 2-(Alpha-Lactyl)Thiamin, Racemic Methyl 2-Hydroxy-2-(2-Thiamin)Ethylphosphonate Chloride Trihydrate - a Conformation for a Least-Motion, Maximum-Overlap Mechanism for Thiamin Catalysis. Journal of the American Chemical Society *104*, 3089-3095.

Turner, N.J. (2000). Applications of transketolases in organic synthesis. Curr Opin Biotechnol *11*, 527-531.

Vagin, A., and Teplyakov, A. (1997). MOLREP: an automated program for molecular replacement. Journal of Applied Crystallography *30*, 1022-1025.

Vazquez, S., and Camps, P. (2005). Chemistry of pyramidalized alkenes. Tetrahedron *61*, 5147-5208.

Versees, W., Spaepen, S., Wood, M.D.H., Leeper, F.J., Vanderleyden, J., and Steyaert, J. (2007). Molecular mechanism of allosteric substrate activation in a thiamine diphosphate-dependent decarboxylase. Journal of Biological Chemistry *282*, 35269-35278.

Voet, D., Voet, J.G., Pratt C.W. (2008). Principles of Biochemistry. WILEY-VCH *Third Edition*.

Volker, H.U., Scheich, M., Schmausser, B., Kammerer, U., and Eck, M. (2007). Overexpression of transketolase TKTL1 is associated with shorter survival in laryngeal squamous cell carcinomas. European Archives of Oto-Rhino-Laryngology *264*, 1431-1436.

Wang, J.J.L., Martin, P.R., and Singleton, C.K. (1997). Aspartate 155 of human transketolase is essential for thiamine diphosphate magnesium binding, and cofactor binding is required for dimer formation. Biochimica Et Biophysica Acta-Protein Structure and Molecular Enzymology *1341*, 165-172.

Warshel, A., Sharma, P.K., Kato, M., Xiang, Y., Liu, H., and Olsson, M.H.M. (2006). Electrostatic basis for enzyme catalysis. Chemical reviews *106*, 3210-3235.

Washabaugh, M.W., and Jencks, W.P. (1988). Thiazolium C(2)-Proton Exchange - Structure Reactivity Correlations and the Pka of Thiamin C(2)-H Revisited. Biochemistry *27*, 5044-5053.

Weber, K., Pringle, J.R., and Osborn, M. (1972). Measurement of molecular weights by electrophoresis on SDS-acrylamide gel. Methods Enzymol *26 PtC*, 3-27.

Weidner, A. (2010). Studien zur Struktur, Funktion und Aktivierung der membran-assoziierten Pyruvatoxidase aus *Escherichia coli*.

Wikner, C., Meshalkina, L., Nilsson, U., Backstrom, S., Lindqvist, Y., and Schneider, G. (1995). His103 in Yeast Transketolase Is Required for Substrate Recognition and Catalysis. European Journal of Biochemistry *233*, 750-755.

Wikner, C., Nilsson, U., Meshalkina, L., Udekwu, C., Lindqvist, Y., and Schneider, G. (1997). Identification of catalytically important residues in yeast transketolase. Biochemistry *36*, 15643-15649.

Wille, G., Meyer, D., Steinmetz, A., Hinze, E., Golbik, R., and Tittmann, K. (2006). The catalytic cycle of a thiamin diphosphate enzyme examined by cryocrystallography. Nature chemical biology *2*, 324-328.

Willige, B.C., Kutzer, M., Tebartz, F., and Bartels, D. (2009). Subcellular localization and enzymatic properties of differentially expressed transketolase genes isolated from the desiccation tolerant resurrection plant Craterostigma plantagineum. Planta *229*, 659-666.

Xu, X., Zur Hausen, A., Coy, J.F., and Lochelt, M. (2009). Transketolase-like protein 1 (TKTL1) is required for rapid cell growth and full viability of human tumor cells. Int J Cancer *124*, 1330-1337.

Xu, Z.P., Wawrousek, E.F., and Piatigorsky, J. (2002). Transketolase haploinsufficiency reduces adipose tissue and female fertility in mice. Molecular and Cellular Biology *22*, 6142-6147.

Yevenes, A., and Frey, P.A. (2008). Cloning, expression, purification, cofactor requirements, and steady state kinetics of phosphoketolase-2 from Lactobacillus plantarum. Bioorganic chemistry *36*, 121-127.

Zahr, N.M., Kaufman, K.L., and Harper, C.G. (2011). Clinical and pathological features of alcohol-related brain damage. Nat Rev Neurol *7*, 284-294.

Zavitsas, A.A. (2003). The relation between bond lengths and dissociation energies of carbon-carbon bonds. Journal of Physical Chemistry A *107*, 897-898.

Zhao, Y.L., Pan, X.L., Zhao, J., Wang, Y., Peng, Y., and Zhong, C.J. (2009). Decreased transketolase activity contributes to impaired hippocampal neurogenesis induced by thiamine deficiency. Journal of Neurochemistry *111*, 537-546.

Curiculum Vitae

Stefan Lüdtke

Georg-August-Universität Goettingen
Department of Bioanalytics
Justus-von-Liebig Weg 11
Goettingen, Germany

Phone: +49 551 3914422
e-mail: sluedtk@gwdg.de

Date of Birth:	October 8th 1982
Place of Birth:	Haldensleben
Nationality:	German

Education

1993-03/2002	Friedrich-Ludwig-Jahn Gymnasium Haldensleben (Abitur: 1.6)
10/2002-06/2003	Military service
10/2003-7/2008	Biochemistry student, Martin-Luther Universität Halle/Wittenberg
08/2005	Intermediate examination: “excellent” (1.1)
07/2007	Diploma examination: „excellent“ (1.0)
10/2007-07/2008	Diploma Thesis, Martin-Luther Universität Halle/Wittenberg, Department of Molecular Enzymology: „Analysis of sugar conformations during enzymatic catalysis of transketolase and implications for the reactivity of intermediates“, “excellent” (1.0) Advisors: Jun. Prof. Dr. Kai Tittmann, Dr. Christoph Parthier
08/2008-05/2012	PhD student, Georg-August-Universität Göttingen, Department of Bioanalytics „Structural and Functional Studies on Vitamin B1-Dependent, Human and Bacterial Transketolases “, “summa cum laude” (1.0) Thesis commitee: Prof. Dr. Kai Tittmann, Prof. Dr. Ralf Ficner, Prof. Dr. Christian Griesinger
05/2012-08/2012	Postdoctoral Fellow with Prof. Kai Tittmann

Practical Experience

10/2005-2/2007	**Institute for Biochemistry and Biotechnology, Department of Technical Biochemisty, University of Halle/Wittenberg** **Research project:** Expression, refolding and biochemical characterization of G-protein coupled receptors and their ligands **Supervision:** Prof. Dr. Rainer Rudolph, Dr. Eva Bosse-Doennicke, Dr. Kathrin Schröder-Tittmann **Methods:** molecular cloning, high-density cell fermentation, protein purification, in-vitro refolding techniques, fluorescence spectroscopy, surface plasmon resonance
10/2007-07/2008	**Intitute for Institute for Biochemistry and Biotechnology, Department of Molecular Enzymology, University of Halle/Wittenberg** **Research project:** Diploma Thesis **Methods:** isothermal titration calorimetry, circular dichroism and fluorescence spectroscopy, basics in NMR-spectroscopy, fast kinetic methods (stopped-flow and quenched-flow techniques)
08/2008-present	**Department of Bioanalytics, Georg-August-Universität Göttingen** X-ray data collection at ESRF (Grenoble), SLS (Villigen) and HZB (Berlin) as well as at different in-house generators, X-ray data analysis (XDS, MOSFLM), Molecular Replacement, SAD and MAD phasing, X-ray structure refinement and deposition, multiangle light scattering, HPLC, basics in organic and chemo-enzymatic synthesis
11/2009-09/2011	**Practical courses within the Goettingen Graduate Schools for Neuroscience, Biophysics and Molecular Biosciences (GGNB):** Electron spin resonance spectroscopy, Supervision: Prof. Dr. Marina Bennati Surface Plasmon Resonance, Supervision: Prof. Dr. Claudia Steinem Mass spectrometry, Supervision: Dr. Henning Urlaub Fluorescence Anisotropy, Supervision: Prof. Dr. Dirk Fasshauer

Teaching Experience

2008 and 2009	Two-day GGNB practical course: "Thermodynamic characterization of biomolecular interactions by ITC"
2008, 2009 and 2010	Tutorials master program "Molecular Biology": "Enzyme Mechanism and Regulation"
11/2008-10/2009	Supervision of a diploma student
02/2011	Lecture course for biology master students: "Circular Dichroism and Microcalorimetry"
06/2012	Lecture course for biology master students: "Enzyme Mechanisms" and "Enzymes-Kinetics, Inhibition and Regulation"
02/2009-04/2009	Supervision of laboratory rotation student
04/2010 -06/2010	Supervision of laboratory rotation student

Skills & Interests

Computer skills	Windows and Linux, Crystallographic software (XDS, MOSFLM, CCP4 suite, PHENIX suite, SHELX, COOT, O, PYMOL), MestreNova, Origin, SigmaPlot, Kaleidagraph, MS Office
Languages	English: advanced in written and spoken French: intermediate in written and spoken German: Mother tongue
Hobbies	Mountain biking, running

Scientific Contribution

Publications

- Mitschke L, Parthier C, Schröder-Tittmann K, Coy J, Lüdtke S, Tittmann K, (2010) Crystal structure of human transketolase and new insights into its mode of action. Journal of Biological Chemistry 285(41):31559-70.
- Lehwess-Litzmann A, Neumann P, Parthier C, Lüdtke S, Golbik R, Ficner R, Tittmann K (2011) Twisted Schiff base intermediates and substrate locale revise transaldolase mechanism. Nature Chemical Biology 7(10):678-684
- Meyer D, Neumann P, Koers E, Sjuts H, Lüdtke S, Sheldrick G, Ficner R, and Tittmann K, (2012) Unexpected tautomeric equilibria of the carbanion-enamine intermediate in pyruvate oxidase highlight unrecognized chemical versatility of the thiamin cofactor. Proceedings of the National Academy of Science, USA 109(27):10867-72
- Schneider S, Lüdtke S, Schröder-Tittmann K, Wechsler C, Sprenger G, Meyer D, and Tittmann K, (2012) A Δ 38 deletion variant of human transketolase as a model of transketolase-like protein 1 exhibits no enzymatic activity, (under revision in Journal of Biological Chemistry)
- Lüdtke S, Neumann P, Kluger R, Ficner R and Tittmann K, (2012) High-resolution observation of a coenzyme-derived intermediate – preservation of reactivity as a principle of catalysis, (under revision in Nature Chemical Biology)
-

Talks

11/2008	"Winkelspannungen, Circe-Effekt, flexible Kofaktoren und reaktive Substrat-Konformere: Neue Einblicke zum Reaktionsmechanismus der Transketolase" Symposium: Homogene Katalyse als biologisches Prinzip, Halle/Germany
08/2009	"Stereoelectronic control, strain and near attack conformers: molecular enzymology of transketolase" Goettingen Center for Molecular bioscience (GZMB) summer retreat, Goettingen/Germany
08/2010	"Molecular catalysis of human transketolase" GGNB retreat: Biomolecules: Structure-Function-Dynamics, Goettingen/Germany

Poster

05/2008	"X-ray crystallographic snapshots of the reaction coordinate of transketolase" Chemical Biology of Thiamin, 7th International Conference on Mechanisms and Physiology of Thiamin, Wittenberg/Germany
12/2008	"Molecular catalysis of human transketolase" GGNB Science day 2008, Goettingen/Germany
12/2011	"Trapping a "hot" intermediate in cofactor catalysis" GGNB Science day 2011, Goettingen/Germany

Awards and Distinctions

03/2008-02/2010	Recipient of a Chemiefonds-Stipend– Fonds der Chemischen Industrie
02/2009-05/2012	Member of the GGNB, Program Biomolecules: Structure-Function-Dynamics
03/2009	Attended MicroCal-ITC Workshop, Milton Keynes/UK
09/2011	Attended the Biacore-MicroCal User Day Conference, Heidelberg/Germany